Chemically-fueled reaction networks to control supramolécular polymers

Serena de Piccoli

UNIVERSITÉ DE STRASBOURG

ÉCOLE DOCTORALE 222

UMR 7140

THÈSE présentée par :

Serena DE PICCOLI

Soutenue le : **17 Juin 2021**

pour obtenir le grade de : **Docteur de l'Université de Strasbourg**

Discipline/ Spécialité : Chimie moléculaire - chimie supramoléculaire

Chemically-fueled reaction networks to control supramolecular polymers

THÈSE dirigée par :

M Hermans Thomas — Professeur, Université de Strasbourg, UMR7140, Strasbourg, France

RAPPORTEURS :

Mme Ghislaine Vantomme — Professeur adjoint, Department of Chemical Engineering and Chemistry (TU), Eindhoven, Pays-bas

M Leonard Prins — Professeur, Department of Chemical Sciences – Université de Padova, Padova, Italie

AUTRES MEMBRES DU JURY :

M Alberto Bianco — Professeur, Université de Strasbourg, IBMC, Strasbourg, France

Table of contents

Acknowledgements

First of all, I would like to thank Prof. Thomas Hermans for giving me the opportunity to pursue my studies in his group of out-of-equilibrium complex systems. It was a pleasure for me to work in such a multidisciplinary environment. I am thankful because I investigated and got passionate to such diverse subjects over these three years. I was just a pharmacist, and you saw some potential in me. Thank you!

Thank you Dr. Ghislaine Vantomme and Prof. Leonard Prins for taking time to read and judge my work, and together with Pr. Alberto Bianco for being part of the jury for my thesis.

First of all, I would like to thank Dr. Nishant Singh and Dr. Georges Formon with whom I shared two works. It was a pleasure for me to take part to scientific discussions, learn from you, and get interested to always new things. I am glad to have worked with you, thank you guys!

I would like to thank also Bruno Lainer, we have spent such good times in and out of the lab. Then, I would like to thank Anastasiia Sharko. Thank you for all the support, you are such a good chemist and a strong woman. I am glad we are sharing a review. I would like also to acknowledge Prof. Kyle Bishop and Dimitri Livitz for the time spent discussing self-assembly, steady states and oscillations. It was such inspiring moments!

Thank you, Dr. Ana Maria Fuentes Caparro. Even if we only shared a few months, it was a pleasure to work with you. I would like to thank also Dr. Ana Maria Garcia for her advice and support during these years.

Grazie, Dr. Alessandra Tassoni! You know I am not good with words and I do not like the ‘blabla’ but without your support I would have not succeeded. During these three years, your presence was essential in the lab, but mostly outside. I am so glad to have shared this experience with you.

I would like also to thank Michi Schicho, thank you for all the support you gave me. You understood what was going on with my life and you knew how to make me feel better. Each time (especially this 2020!).

Also thank you Chunfeng Chen, I am happy we have started together, and now we are almost finishing together. I have spent nice and funny moments with you! Also thank you Alvaro Lopez for the constant support, help and dances.. I do hope more are coming soon!

Thank you Dr. Jennifer Ciesielski, I do not know how I could have managed this thesis without your constant help, support and supervision. And I want to acknowledge Thomas Biellmann for his help with French but mainly for being a good friend, especially, when I needed the most!

I would like also to acknowledge Takuji Adachi (former), Flor, Arvind, Tianheng, Caroline, Lucas, Vincent, Jorge, Reza, Dani, Aleksander, Shana, Victor for being part of this incredible team. Thank you all!

Besides Hermans people, I would like to thank by Dr. Jean-Louis Schmitt, Cyril Antheaume, Dr. Valentin Bauer, Dr. Elise Naudin for the (technical) support and help. I would like to thank all the support staff at ISIS and at the chemistry department of University of Strasbourg. I would like to thank Soumia for her administrative help.

To Annia Bertrand and Dr. Muriel Muzet, thank you! I am glad I have met two women like you during my stay here, in Strasbourg. It was a pleasure for me to spend time with you, organizing events and I am grateful to have received your support, always.

I would like to thank all the people I met these years, particularly: Aline, Maciej, Svetlana, Adeline, Cyprien, Aromal, Alessandra, Etienne, Filippo.

To my 'Italians' friends, I am so happy to have you in my life! Anna, Elisa, Erika, Luca, Marco this 2020 was difficult for all of us, but you always checked on me, you were always by myside ready to hear my drama and support me. I do hope these relationships we have will last forever.

To my family, you are my life! Thank you. I do not have words to describe what you represent for me. Carmen and Sergio, we come from a small village where people talk and judge a lot, but you did not care. You gave me an education, you gave me the opportunity to travel and learn English, you allowed me to study at University, you support me in all my decisions even when I chose to leave my country. That's LOVE. Vi amo di bene.

Direction de la **recherche**
et de la **valorisation**
Collège **doctoral**
Université de Strasbourg

Déclaration sur l'honneur
Declaration of Honour

J'affirme être informé que le plagiat est une faute grave susceptible de mener à des sanctions administratives et disciplinaires pouvant aller jusqu'au renvoi de l'Université de Strasbourg et passible de poursuites devant les tribunaux de la République Française.

Je suis conscient(e) que l'absence de citation claire et transparente d'une source empruntée à un tiers (texte, idée, raisonnement ou autre création) est constitutive de plagiat.

Au vu de ce qui précède, **j'atteste sur l'honneur que le travail décrit dans mon manuscrit de thèse est un travail original et que je n'ai pas eu recours au plagiat ou à toute autre forme de fraude.**

I affirm that I am aware that plagiarism is a serious misconduct that may lead to administrative and disciplinary sanctions up to dismissal from the University of Strasbourg and liable to prosecution in the courts of the French Republic.

I am aware that the absence of a clear and transparent citation of a source borrowed from a third party (text, idea, reasoning or other creation) is constitutive of plagiarism.

In view of the foregoing, ***I hereby certify that the work described in my thesis manuscript is original work and that I have not resorted to plagiarism or any other form of fraud.***

Nom : Prénom : DE PICCOLI SERENA

Ecole doctorale : ED222

Laboratoire : LABORATOIRE DES SYSTEMES COMPLEXES HORS EQUILIBRE

(UMR 7140)

Date : 29/06/2021

Signature :

Résumé

La chimie supramoléculaire vise à développer des systèmes complexes à partir des briques de construction interagissant par des forces non covalentes. Elle a été définie comme la « chimie au-delà de la molécule » par Jean-Marie Lehn.[1] En général, les interactions impliquées dans l'élaboration de ces systèmes sont de type : liaisons hydrogène, effets hydrophobes, interactions van der Waals et électrostatiques.[2] Il est particulièrement important d'étudier les étapes d'auto-assemblage des édifices supramoléculaires pour en comprendre les propriétés mais aussi pour pouvoir développer des systèmes complexes avec des propriétés reproduisant les systèmes naturelles. [3]

L'avantage des polymères supramoléculaires est d'obtenir des systèmes dynamiques à partir d'interactions non covalentes qui permettent aux structures supramoléculaires de s'adapter aux changements de l'environnement, à la réponse aux stimuli et de remplir des fonctions diverses.[4] Les structures supramoléculaires comme, par exemple, les microtubules sont vitales.[5] Les microtubules et les filaments d'actine sont des systèmes supramoléculaires présents dans le cytosquelette des cellules où ils remplissent des fonctions essentielles. En tant que tels, ils permettent la motilité, l'autoreproduction et l'auto-guérison des cellules. Pour accomplir ces fonctions, les microtubules et les filaments d'actine sont maintenus dans des états dissipatifs hors équilibre qui est un état thermodynamique où l'énergie est constamment fournie.[5] Les structures des microtubules oscillent entre l'élongation et l'effondrement à mesure que le carburant est consommé.[6] La chimie des systèmes complexes vise à reproduire ce réseau par le développement de systèmes complexes synthétiques.[3]

Dans cette thèse, nous présentons et discutons principalement deux systèmes. D'une part, nous étudions largement un réseau de réactions enzymatiques alimenté par l'adénosine triphosphate (ATP), et d'autre part, nous montrons un cycle de réaction synthétique pour le contrôle des propriétés mécaniques d'un hydrogel.

Au **Chapitre 2**, nous étudions un réseau enzymatique et démontrons la présence d'états pseudo stationnaires hors équilibré (pNESS) ainsi que le comportement oscillatoire de ce même réseau. Le réseau est basé sur la phosphorylation et la déphosphorylation d'un dérivé peptidique du pérylène-diimide (**PDI**).[7] Le substrat contient une séquence qui est reconnue par deux enzymes, la protéine kinase cAMP-dépendante (PKA) et la Lambda protéine phosphatase (λPP). PKA en présence d'ATP, le carburant, phosphoryle **PDI** entraînant la production d'ADP (adénosine

diphosphate) et de **p2-PDI**. Ensuite, la déphosphorylation est médiée par λPP qui libère du phosphate inorganique et restaure **PDI**. Ce cycle de réactions a fait l'objet d'études approfondies par mes anciens collègues.[7] Cependant, la production de déchets (ADP et phosphate inorganique[8,9]) pendant le cycle de phosphorylation/déphosphorylation a nui à la réalisation de multiples états stationnaires hors équilibrés (NESS). Afin de contourner le problème, ils ont développé une cassette de dialyse où le système (c'est-à-dire **PDI**, PKA et λPP) était confiné et les déchets étaient continuellement retirés. L'ajout de différentes concentrations de carburant a permis d'obtenir quatre NESS. Comme le but final de ce projet est le développement des matériaux supramoléculaires, une troisième réaction est insérée dans le réseau. La réaction, catalysée par une pyruvate kinase PK, facilite la régénération de l'ATP à partir de l'ADP en présence de phosphoénolpyruvate (PEP).[10] Par conséquent, le carburant est généré *in situ* en continu à partir de déchets, car la PEP (pré-carburant) est présente. En effet, la régénération de l'ATP dépend directement de la concentration de pré-carburant utilisée. De cette façon, nous étudions le réseau enzymatique en fonction du pré-carburant ajouté au système. Ainsi, nous obtenons des états pseudo stationnaires hors équilibrés (pNESS) dans un lot fermé non agité en fonction de la concentration de pré-carburant. La durée de pNESS passe de 2 à 7 heures lorsque la concentration de PEP est augmentée (de 0,5 à 2 mM). Le système enzymatique est maintenu sous pNESS en raison de la production continue d'ATP et, par conséquent, de la phosphorylation et de la déphosphorylation constantes de **PDI**. De manière inattendu, l'étude du réseau au aussi permis de montrer que celui-ci présente un comportement oscillatoire. Ces oscillations résultent des cycles de phosphorylation/déphosphorylation.[11–13] Par conséquent, nous supposons que la présence d'un réseau de phosphorylation et déphosphorylation avec le control enzymatique de l'activité du PK induit les oscillations. Ces résultats sont rares et surprenants car les expériences sont effectuées dans un système fermé non agité.

Le **Chapitre 3** montre le contrôle des réactions de (dé)phosphorylation par l'insertion d'une rétroaction négative. Dans la nature, la rétroaction, positive ou négative, sert à calibrer les réactions et à réguler la production des metabolites.[5] Ces deux types de rétroaction agissent en améliorant ou en inhibant les réactions. Le processus d'homéostasie est un exemple clair de régulation de la température par rétroaction positive et négative dans notre corps.[14] Ainsi, un inhibiteur compétitif de **PDI** pour l'interaction avec la protéine kinase cAMP-dépendante PKA est synthétisé. L'inhibiteur contient une séquence peptidique qui présente un constant d'inhibition dans une range nano molaire et agit en rivalisant avec le **PDI** pour l'interaction avec la poche enzymatique.[15,16] En outre,

le dérivé de pérylène-diimide de la séquence inhibitrice est synthétisé pour obtenir un analogue du **PDI**, que nous appelons **PDI-I**. Ensuite, la phosphorylation de **PDI** est effectuée en présence à la fois de l'inhibiteur de peptide et de **PDI-I**. Les résultats confirment un profil cinétique différent pour la réaction de phosphorylation en présence et en absence d'inhibiteurs. Ainsi, nous observons une tendance différente pour les deux inhibiteurs, en particulier il en résulte une inhibition plus élevée de la phosphorylation quand **PDI-I** est ajouté au cycle de réactions. Afin de comprendre si ce comportement est le résultat du co-assemblage entre **PDI-I** et **PDI**/**p2-PDI**, nous étudions l'auto-assemblage du système par diffraction des rayons X (XRD) et des expériences de 'self-sorting'. Plus précisément, le motif obtenu par XRD est similaire pour toutes les espèces et le mélange d'espèces présentes dans le système. En outre, l'effet de l'ajout de la **PDI-I** au réseau complexe (où la (dé)phosphorylation de la **PDI** et la régénération de l'ATP ont lieu) est étudié dans des conditions d'états pseudo stationnaires hors équilibrés (pNESS). La **PDI-I** est ajoutée au réseau complexe lorsque le plateau de pNESS est atteint (après 2 heures) pour étudier l'effet de l'inhibiteur concurrentiel. Cependant, au cours des diverses expériences, la précipitation de fibres de longueur de l'ordre du micromètres est observée. Nous supposons que cela est dû à de fortes π-π interactions entre les substrats **PDI-I** et **PDI**/**p2-PDI** dans le tampon de réaction.

Au **Chapitre 4**, on développe un matériau de synthèse à base de peptide, qui combiné à un réseau enzymatique, présente une fonction métabolique. La séquence LRRASL, reconnue par la protéine kinase cAMP-dépendante PKA et la Lambda protéine phosphatase λPP, est étudiée pour le développement d'hydrogels. En particulier, le dipeptide FF, un hydrogelator bien connu[17], est inséré à différentes positions de la séquence peptidique (C-terminal, N-terminal et les deux terminus).[18] L'ajout du dipeptide augmente l'effet hydrophobe, ce qui entraîne un degré plus élevé d'auto-assemblage. Plus précisément, trois séquences sont étudiées pour comprendre l'effet du dipeptide sur l'auto-assemblage, sur les propriétés mécaniques du matériau et sur l'interaction avec les enzymes lorsqu'ils sont situés à des positions différentes. Après la synthèse des dérivés du LRRASL par synthèse peptidique en phase solide (SPPS), la phosphorylation (en présence de la réaction de régénération de l'ATP) et la déphosphorylation des substrats sont étudiées par étapes. Une fois que le fonctionnement du système enzymatique est confirmé, des expériences rhéologiques sont menées pour étudier les propriétés mécaniques des hydrogels. La gélification en présence et en l'absence de réactions enzymatiques est étudiée en surveillant G' et G'' au fil du temps. Les profils cinétiques sont différents pour toutes les expériences effectuées qui se soient pour la phosphorylation médiée par PKA et ATP, la phosphorylation en présence de la réaction de

régénération ATP et l'ensemble du réseau enzymatique en présence de λPP. Par conséquent, nous supposons que l'ATP joue également un rôle dans l'auto-assemblage et dans les propriétés mécaniques finales de l'hydrogel.[19,20] Néanmoins, d'autres études et techniques complémentaires, telles que la microscopie optique et la spectroscopie par dichroïsme circulaire, sont nécessaires pour mieux comprendre la dynamique de l'auto-assemblage supramoléculaire. En outre, nous envisageons que l'étude des états stables non équilibrés conduirait à la réalisation du pNESS dans un matériau à base de peptides.

Au **Chapitre 5**, un cycle de réaction synthétique pur est exploré pour obtenir un contrôle cinétique et structurel sur un hydrogel. Le système est basé sur un hydrogelateur à base d'un saccharide fonctionnalisé avec un aldéhyde, **SachCHO**.[21] La réaction du **SachCHO** avec la dithionite de sodium ($Na_2S_2O_4$, DT) produit le respectif α-hydroxy-sulfonate, **SachSO$_3^-$**.[22] En raison de la répulsion électrostatique, **SachSO$_3^-$** ne s'auto-assemble pas, de sorte que lorsque de la dithionite de sodium est ajoutée à un hydrogel **SachCHO**, le réseau est détruit en 5 minutes. Pour obtenir le transition gel-sol-gel, le formaldéhyde est utilisé pour régénérer l'aldéhyde d'origine. Cependant, le formaldéhyde et le dithionite de sodium réagissent l'un avec l'autre, de sorte qu'ils ne peuvent pas être ajoutés simultanément. Par conséquent, l'hexamine (HMTA), qui se décompose en formaldéhyde et en ammoniac par hydrolyse catalysée par acide, et la gluconolactone (GdL) sont employés pour atteindre un cycle autonome. Le cycle entraîne la conversion de l'hydrogel **SachCHO** en **SachSO$_3^-$**, une solution translucide, en environ 5 minutes et la régénération du réseau de gel (**SachCHO**) en 30 à 60 minutes. La concentration de gluconolactone influe sur la cinétique du cycle de réaction, et une concentration plus élevée augmente la cinétique de la décomposition du **HMTA**, ce qui accélère le cycle de réaction. En analysant les hydrogels par microscopie confocale et microscopie électronique à balayage, nous observons que la morphologie des fibres **SachCHO** dépend de la méthode de formation de gel. L'hydrogel thermodynamique (formé en chauffant une suspension de **SachCHO** suivie d'un refroidissement) est constitué de fibres longues et droites. Lorsque l'hydrogel est formé par le cycle de réaction, la morphologie dépend de la concentration de gluconolactone. Ainsi, les fibres formées par **SachCHO** sont plus courtes et avec des bords irréguliers, et des fibres en forme d'étoile ou très ramifiées, plus minces et plus longues provenant d'un site de nucléation central sont aussi observées. En outre, la concentration en gluconolactone affecte également les propriétés mécaniques de l'hydrogel. En général, la rigidité du gel augmente avec la concentration de GdL. Enfin, **SachCHO** possède une propriété appelée synerèse, ce qui signifie qu'elle repousse le solvant sous pression mécanique. Cette propriété est explorée pour

éliminer les sous-produits du cycle de réaction permettant la réalisation de cycles de réaction multiples. Ensuite, un gel **SachCHO** est formé dans une seringue équipée de coton dans le moyeu de l'aiguille. Les combustibles chimiques (DT, HMTA, GdL) sont ajoutés et le cycle de réaction se déroule normalement, avec la formation de l'hydrogel après 30 minutes. Le piston de la seringue est pressé, en retirant le solvant avec les déchets. Le cycle de réaction peut être répété jusqu'à 13 fois.

En conclusion, nous avons exploré deux cycles différents de réaction hors équilibre. Tout d'abord, nous avons contrôlé la polymérisation supramoléculaire du substrat **PDI** *via* des modifications covalentes enzymatiquement catalysé. Ensuite, la mise en œuvre du système avec une réaction enzymatique supplémentaire qui convertit les déchets en carburant *in situ*, a permis de réaliser des états pseudo stationnaires hors équilibrés. De plus, l'étude du réseau enzymatique a donné lieu à un comportement oscillatoire inattendu. Afin de mieux contrôler le cycle des réactions, un inhibiteur compétitif a été synthétisé. Malheureusement, la précipitation des fibres a entravé les études approfondies du système. Le but final de ce travail de thèse a été le développement de matériaux capables d'exécuter des fonctions similaires à celles de la nature. Ainsi, le comportement du réseau enzymatique a été étudié dans des matériaux à base de peptides. Enfin, un cycle de réaction synthétique pur a été réalisé dans un hydrogel et nous avons obtenu le contrôle sur la morphologie et les propriétés mécaniques de ce dernier en fonction des paramètres réactionnels.

Les études présentées dans ces travaux de doctorats sont un pas de plus dans le développement des propriétés et fonctions émergentes de synthèses analogues à celles trouvées dans la nature, dans le domaine de la chimie des systèmes complexes. De plus, à notre connaissance, il existe très peu d'exemples où les scientifiques ont poussé leurs systèmes complexes vers des états pseudo stationnaires hors équilibrés ou où des systèmes complexes présentent un comportement oscillatoire. Enfin, la recherche dont il est question dans cette thèse permettra d'approfondir l'étude de ces comportements afin d'obtenir finalement des matériaux imitant les systèmes biologiques.

Summary

Supramolecular chemistry aims at developing complex systems *via* noncovalent forces and it has been defined as the "chemistry beyond the molecule" by Jean-Marie Lehn.[1] Generally, the interactions involved in the development of such systems are hydrogen bonds, hydrophobic effects, van der Waals and electrostatic interactions.[2]

Supramolecular polymers that are held together solely by noncovalent interactions have the advantage of being responsive as they can assemble/disassemble *via* external stimuli.[4] In Nature, supramolecular structures are vital.[5] Microtubules and actin filaments are supramolecular systems present in the cytoskeleton of the eucaryotic cells where they perform essential functions. As such, they permit motility, self-reproduction and self-healing of cells. In order to carry out these functions, microtubules and actin filaments are kept under a dissipative non-equilibrium state (i.e., a thermodynamic state in which energy is constantly supplied).[5] As such, microtubule structures oscillate between growing and shrinkage as fuel gets consumed.[6] Systems Chemistry aims at reproducing these complex networks through the development of synthetic complex systems.[23]

In this thesis, we present and discuss two main systems. On the one hand, we investigated an enzymatic reactions network driven by adenosine triphosphate (ATP), and, on the other, we built a pure synthetic reaction cycle to control the mechanical properties of a hydrogel.

In **Chapter 2**, we achieved pseudo non-equilibrium steady states (pNESS) and an oscillatory behavior in an enzymatic network. The network is based on the phosphorylation and dephosphorylation of a peptide perylene diimide derivate (**PDI**).[7] The substrate contains a consensus sequence that is recognized by two enzymes, cAMP-dependent kinase PKA and Lambda protein phosphatase λPP. PKA, in the presence of ATP, phosphorylates **PDI** resulting in the production of ADP (adenosine diphosphate) and **p2-PDI**. The dephosphorylation is mediated by λPP, which releases an inorganic phosphate and restores **PDI**. This reactions cycle was extensively investigated by my former colleagues.[7] However, the production of waste (ADP and an inorganic phosphate)[8,9] during the phosphorylation/dephosphorylation cycle hindered the achievement of multiple cycles. In order to bypass the issue, they developed a dialysis cassette where the system (that is **PDI**, PKA and λPP) was confined and the waste was continuously removed. By adding different concentration of the fuel, they reached four non-equilibrium steady states (NESS). Nevertheless, the ultimate goal of the project is to develop supramolecular materials, and, to accomplish this, a third reaction was coupled to the network. The reaction, catalyzed by a pyruvate

kinase PK, mediates the regeneration of ATP from ADP in the presence of phosphoenol pyruvate (PEP), the 'pre-fuel'.[10] Here, the fuel in continuously generated *in situ* from the waste. The latter is directly dependent on the concentration of pre-fuel. In this way, we explored the enzymatic network as a function of pre-fuel added to the system. Interestingly, we achieved pseudo non-equilibrium steady states (pNESS) in a non-stirred closed batch as a function of pre-fuel concentration. The duration of pNESS increased from 2 to 7 hours when the concentration of PEP was augmented (from 0.5 to 2 mM). The enzymatic system was kept under pNESS as a result of the continuous production of ATP and consequently the constant phosphorylation and dephosphorylation of **PDI**. Interestingly, after extensively studying this network, we found this system exhibited an oscillatory behavior. Oscillations likely arose from the phosphorylation/dephosphorylation cycles, which has been previously reported in literature.[11–13] Therefore, we assumed that the complex reaction network along with an enzymatic control of the PK activity is inducing this surprising behavior. These results are surprising as the experiments were carried out in a non-stirred closed batch.

Chapter 3 presents the control over the (de)phosphorylation reactions through the addition of a negative feedback. In Nature, positive and negative feedback are used to tune reactions and regulate the production of metabolites.[5] They act by enhancing or inhibiting the reactions. As an example, homeostasis is a physiological regulation process to control our body temperature mediated by positive and/or negative feedback.[14]

In order to introduce this concept into our enzymatic system, we synthesized a competitive **PDI** inhibitor to interact with the kinase PKA. The inhibitor contains a peptide sequence which has an inhibition constant in the nanomolar range and acts by competing with **PDI** for the interaction with the enzymatic pocket.[15,16] Additionally, a perylene diimide derivate of the inhibitor sequence was synthetized to obtain an analog of **PDI**, that we called **PDI-I**. Then, the phosphorylation of **PDI** was carried out in the presence of both the peptide inhibitor and **PDI-I**. The results confirmed a different kinetic profile for the phosphorylation reaction in the presence and absence of inhibitors. Surprisingly, we observed a different trend for the two inhibitors. When **PDI-I** was used, a higher inhibition of phosphorylation was observed. In order to understand if this behavior was the result of the co-assembly between the different species (**PDI**, **p2-PDI** and **PDI-I**), we investigated the self-assembly by Powder X-Ray Diffraction (XRD) and self-sorting experiments. The pattern obtained by XRD are similar for all the species and their 1:1 mixture. The same behavior was observed for self-sorting experiments. Thus, the species self-assembled in a narcissistic regime (i.e., they only self-

assembled with themselves). In addition, the effect of the addition of **PDI-I** to the complex network (where the (de)phosphorylation of **PDI** and the regeneration of ATP are taking place) was studied under pseudo non-equilibrium steady states conditions (pNESS). However, during the experiments, we observed the precipitation of micrometer length fibers. The latter are most probably the results of strong π-π and electrostatic forces between the PDI derivatives.

In **Chapter 4**, we developed a peptide-based material in which we inserted the enzymatic network. The consensus sequence LRRASLG, recognized by cAMP-dependent protein kinase PKA and Lambda protein phosphatase λPP, was investigated for the development of hydrogels. Particularly, the dipeptide FF, a well-known hydrogelator[17], was introduced at various positions of the peptide sequence (C-terminal, N-terminal and both termini).[18] The addition of the dipeptide increased the hydrophobic effect resulting in a higher degree of self-assembly. Specifically, three sequences were investigated to understand the effect of the dipeptide on the self-assembly, the mechanical properties of the material, and the interaction with enzymes when located at different positions. After the synthesis of LRRASLG derivatives by solid phase peptide synthesis (SPPS), the phosphorylation (in the presence of ATP regeneration reaction) and dephosphorylation of the substrates were studied stepwise by LC-MS.

Once the operation of the enzymatic system was confirmed, rheology experiments were conducted to investigate the mechanical properties of the hydrogels. The gelation in the presence and absence of the enzymatic reactions was studied by monitoring G' and G'' over time. The kinetic profiles were different for all the experiments performed that is for the phosphorylation mediated by PKA and ATP, the phosphorylation in the presence of the ATP regeneration reaction, and the entire enzymatic network when also λPP was present. Moreover, we observed an increase in the stiffness of the hydrogel when ATP is present in the network.[19,24] ATP may participate directly to the peptide self-assembly intercalating in the supramolecular structures. Nonetheless, further studies and complementary techniques, i.e., optical microscopy and circular dichroism spectroscopy, are needed to better understand the dynamics of the supramolecular self-assembly. Additionally, we envisage that the study of pseudo non-equilibrium steady states conditions would lead to achieve pNESS in a peptide-based material.

In **Chapter 5**, a pure synthetic reaction cycle was explored to achieve kinetic and structural control over a hydrogel. The system is based on a previously reported saccharide-based, aldehyde-containing, hydrogelator, **SachCHO**.[21] The reaction of **SachCHO** with sodium dithionite ($Na_2S_2O_4$, DT) produced the respective α-hydroxy-sulfonate, **SachSO$_3^-$**.[22] Because of electrostatic repulsion,

SachSO$_3^-$ did not self-assemble, so when sodium dithionite was added to a **SachCHO** hydrogel the network was destroyed within 5 minutes. In order to obtain the transition gel-sol-gel, formaldehyde was used to recover the original aldehyde. However, formaldehyde and sodium dithionite react with each other, so they cannot be added simultaneously. Therefore, hexamine (HMTA), which decomposes into formaldehyde and ammonia through an acid-catalyzed hydrolysis, and gluconolactone (acid) were employed to achieve an autonomous cycle. The cycle resulted in **SachCHO** hydrogel conversion into **SachSO$_3^-$**, a translucent solution, in approximately 5 minutes and the recovery of the gel network (**SachCHO**) in 30-60 minutes. Gluconolactone (GdL) concentration influenced the kinetics of the reaction cycle, with higher concentration increasing the kinetics of HMTA decomposition leading to an overall faster reaction cycle. By analyzing hydrogels by confocal microscopy and scanning electron microscopy, we observed that the morphology of **SachCHO** fibers depends on the method of gel formation. The thermodynamic hydrogel (formed by heating a suspension of **SachCHO** followed by cooling) consisted of long and straight fibers. When the hydrogel was formed by the reaction cycle, the morphology depended on the concentration of gluconolactone. Therefore, the fibers formed by **SachCHO** were shorter and with irregular edges, and star-shaped or highly branched, thinner, and longer fibers originating from a central nucleation site. Additionally, gluconolactone concentration affected the hydrogel mechanical properties. In general, the stiffness of the gel increased with the concentration of GdL. Finally, **SachCHO** has a property called syneresis, meaning that it repels the solvent under mechanical pressure. This property was exploited so that the by-products could be removed to achieve multiple reaction cycles. Then, a **SachCHO** gel was formed in a syringe equipped with cotton in the needle hub. The chemical fuels (DT, HMTA, GdL) were added and the reaction cycle proceeded normally, with the formation of the hydrogel after 30 minutes. The syringe piston was squeezed, removing the solvent together with the waste. The reaction cycle could be repeated up to 13 times.

In conclusion, we explored two different out-of-equilibrium reaction cycles. First, we controlled the supramolecular polymerization *via* covalent modifications of a substrate by enzymatic catalysis. Then, the implementation of the system with an additional enzymatic reaction, which converts waste into fuel *in situ*, allowed us to achieve pseudo non-equilibrium steady states. The ultimate goal of this thesis was to develop materials capable of performing functions similarly to the ones found in Nature (i.e., self-healing, motility, etc.). Thus, the behavior of the enzymatic network was investigated into a peptide-based material. Lastly, a pure synthetic reaction cycle was

presented where we achieved control over the morphology and the mechanical properties of a hydrogel.

The studies presented herein contribute to the ultimate goal of mimicking Nature in Systems Chemistry. Additionally, to the best of our knowledge, there are very few examples where scientists pushed their systems to achieve non-equilibrium steady states and/or where complex systems exhibit oscillatory behavior. To conclude, the research pursued in this thesis will permit further investigation of behaviors that will ultimately help us develop 'life-like' materials.

References

(1) Lehn, J.-M. Toward Self-Organization and Complex Matter. *Science* **2002**, *295* (5564), 2400–2403. https://doi.org/10.1126/science.1071063.

(2) Steed, J. W.; Atwood, J. L. *Supramolecular Chemistry*, 2nd Edition.; Wiley-VCH: New York, NY, 2009.

(3) Ashkenasy, G.; Hermans, T. M.; Otto, S.; Taylor, A. F. Systems Chemistry. *Chem. Soc. Rev.* **2017**, *46* (9), 2543–2554. https://doi.org/10.1039/C7CS00117G.

(4) De Greef, T. F. A.; Smulders, M. M. J.; Wolffs, M.; Schenning, A. P. H. J.; Sijbesma, R. P.; Meijer, E. W. Supramolecular Polymerization. *Chem. Rev.* **2009**, *109* (11), 5687–5754. https://doi.org/10.1021/cr900181u.

(5) Alberts, B. *Molecular Biology of the Cell*, Sixth edition.; Garland Science, Taylor and Francis Group: New York, NY, 2015.

(6) Katrukha, K. A.; Guriya, G. T. Dynamic Instabilities in the Microtubule Cytoskeleton: A State Diagram. *Biophysics* **2006**, *51* (5), 781–788.

(7) Sorrenti, A.; Leira-Iglesias, J.; Sato, A.; Hermans, T. M. Non-Equilibrium Steady States in Supramolecular Polymerization. *Nat. Commun.* **2017**, *8* (1), 15899. https://doi.org/10.1038/ncomms15899.

(8) Reiter, N. J.; White, D. J.; Rusnak, F. Inhibition of Bacteriophage λ Protein Phosphatase by Organic and Oxoanion Inhibitors. *Biochemistry* **2002**, *41* (3), 1051–1059. https://doi.org/10.1021/bi011577b.

(9) Whitehouse, S.; Feramisco, J. R.; Casnellie, J. E.; Krebs, E. G.; Walsh, D. A. Studies on the Kinetic Mechanism of the Catalytic Subunit of the CAMP-Dependent Protein Kinase. *J. Biol. Chem.* **1983**, *258* (6), 3693–3701. https://doi.org/10.1016/S0021-9258(18)32720-0.

(10) Hirschbein, B. L.; Mazenod, F. P.; Whitesides, G. M. Synthesis of Phosphoenolypyruvate and Its Use in ATP Cofactor Regeneration. *J. Org. Chem.* **1982**, *47* (19), 3765–3766. https://doi.org/10.1021/jo00140a036.

(11) Martins, B. M. C.; Swain, P. S. Ultrasensitivity in Phosphorylation-Dephosphorylation Cycles with Little Substrate. *PLoS Comput. Biol.* **2013**, *9* (8), e1003175. https://doi.org/10.1371/journal.pcbi.1003175.

(12) Ferrell, J. E.; Ha, S. H. Ultrasensitivity Part III: Cascades, Bistable Switches, and Oscillators. *Trends Biochem. Sci.* **2014**, *39* (12), 612–618. https://doi.org/10.1016/j.tibs.2014.10.002.

(13) Goldbeter, A.; Koshland, D. E. Ultrasensitivity in Biochemical Systems Controlled by Covalent Modification. *J. Biol. Chem.* **1984**, *259* (23), 14441–14447.

(14) Cannon, W. B. Organization for Physiological Homeostasis. *Physiol. Rev.* **1929**, *9* (3), 399–431. https://doi.org/10.1152/physrev.1929.9.3.399.

(15) Glass, D. B.; Lundquist, L. J.; Katz, B. M.; Walsh, D. A. Protein Kinase Inhibitor-(6-22)-Amide Peptide Analogs with Standard and Nonstandard Amino Acid Substitutions for Phenylalanine 10. *J. Biol. Chem.* **1989**, *264* (24), 14579–14584. https://doi.org/10.1016/S0021-9258(18)71718-3.

(16) Glass, D. B.; Cheng, H.-C.; Mende-Mueller, L.; Reed, J.; Walsh, D. A. Primary Structural Determinants Essential for Potent Inhibition of CAMP-Dependent Protein Kinase by Inhibitory Peptides Corresponding to the Active Portion of the Heat-Stable Inhibitor Protein. *J. Biol. Chem.* **1989**, *264* (15), 8802–8810.

(17) Mahler, A.; Reches, M.; Rechter, M.; Cohen, S.; Gazit, E. Rigid, Self-Assembled Hydrogel Composed of a Modified Aromatic Dipeptide. *Adv. Mater.* **2006**, *18* (11), 1365–1370. https://doi.org/10.1002/adma.200501765.

(18) Frederix, P. W. J. M.; Scott, G. G.; Abul-Haija, Y. M.; Kalafatovic, D.; Pappas, C. G.; Javid, N.; Hunt, N. T.; Ulijn, R. V.; Tuttle, T. Exploring the Sequence Space for (Tri-)Peptide Self-Assembly to Design and Discover New Hydrogels. *Nat. Chem.* **2015**, *7* (1), 30–37. https://doi.org/10.1038/nchem.2122.

(19) Maiti, S.; Fortunati, I.; Ferrante, C.; Scrimin, P.; Prins, L. J. Dissipative Self-Assembly of Vesicular Nanoreactors. *Nat. Chem.* **2016**, *8* (7), 725–731. https://doi.org/10.1038/nchem.2511.

(20) Kumar, M.; Brocorens, P.; Tonnelé, C.; Beljonne, D.; Surin, M.; George, S. J. A Dynamic Supramolecular Polymer with Stimuli-Responsive Handedness for in Situ Probing of Enzymatic ATP Hydrolysis. *Nat. Commun.* **2014**, *5* (1), 5793. https://doi.org/10.1038/ncomms6793.

(21) Chen, Q.; Lv, Y.; Zhang, D.; Zhang, G.; Liu, C.; Zhu, D. Cysteine and PH-Responsive Hydrogel Based on a Saccharide Derivative with an Aldehyde Group. *Langmuir* **2010**, *26* (5), 3165–3168. https://doi.org/10.1021/la903102z.

(22) De Vries, J. G.; Kellogg, R. M. Reduction of Aldehydes and Ketones by Sodium Dithionite. *J. Org. Chem.* **1980**, *45* (21), 4126–4129. https://doi.org/10.1021/jo01309a011.

(23) Mattia, E.; Otto, S. Supramolecular Systems Chemistry. *Nat. Nanotechnol.* **2015**, *10* (2), 111–119. https://doi.org/10.1038/nnano.2014.337.

(24) Kumar, M.; Brocorens, P.; Tonnelé, C.; Beljonne, D.; Surin, M.; George, S. J. A Dynamic Supramolecular Polymer with Stimuli-Responsive Handedness for in Situ Probing of Enzymatic ATP Hydrolysis. *Nat. Commun.* **2014**, *5* (1), 5793. https://doi.org/10.1038/ncomms6793.

List of Abbreviations

%wt	Molecular weight percentage
3-D	Three dimensional
A	Ala – Alanine
A_{504nm}/A_{540nm}	Ratio of absorbances at 504 nm and 540 nm
ADP	Adenosine diphosphate
AMP	Adenosine monophosphate
ATP	Adenosine triphosphate
CD	Circular dichroism spectroscopy
$CHCl_3$	Chloroform
D_2O	Deuterated water
DCM	Dichloromethane
DIPEA	*N,N*-Diisopropylethylamine
DLS	Dynamic Light Scattering
DMF	Dimethylformamide
DMSO	Dimethyl Sulfoxyde
DNA	Deoxyribonucleic acid
DT	Dithionite
ESI-TOF	Electrospray ionization time-of-flight mass spectrometry
F	Phe – Phenylalanine
G	Gly – Glycine
G'	Shear storage modulus
G''	Shear loss modulus
γ_c	Critical strain
GdL	Glucono-δ-lactone
GDP	Guanosine diphosphate
GTP	Guanosine triphosphate
H_2O	Water
HBTU	Hexafluorophosphate Benzotriazole Tetramethyl Uronium
HCl	Hydrochloric acid

HMTA	Hexamethylenetetramine
HOBt	Hydroxybenzotriazole
HPLC	High-performance liquid chromatography
HRMS	High Resolution Mass Spectrometry
I	Ile - Isoleucine
K	Equilibrium constant
k	Kinetic rate constant
k_B	Boltzmann constant
L	Leu – Leucine
LC-MS	Liquid chromatography–mass spectrometry
λPP	Lambda protein phosphatase
LVER	Linear visco-elastic region
MeOH	Methanol
MWCO	Molecular weight cut off
N	Asn – Asparagine
$NaHCO_3$	Sodium hydrogen carbonate
NaOH	Sodium hydroxyde
NMR	Nuclear magnetic resonance
O.D.	Optical density
p-PDI	Monophosphorylated PDI
p2-PDI	Diphosphorylated PDI
PDI	Perylene diimide
PDI-I	PDI inhibitor
PEP	Phosphoenol pyruvate
Pi	Inorganic phosphate
PK	Pyruvate kinase
PKA	c-AMP dependent protein kinase
R	Gas constant
R	Arg – Arginine
R_H	Hydrodynamic radius
S	Ser – Serine
SPPS	Solid phase peptide synthesis

t	Time
T	Temperature
T	Tyr – Tyrosine
TFA	Trifluoroacetic acid
THF	Tetrahydrofuran
TIPS	Triisopropylsylane
T_{m}	Melting temperature (when α = 0.5)
UV/Vis	Ultraviolet/Visible spectroscopy
V	Val - Valine
XRD	X-Ray diffraction
α	Dimensionless degree of aggregation
Γ	Decay rate
ΔG	Gibbs free energy
ΔH	Enthalpy
ΔS	Entropy
τ	Relaxation time (DLS)
$\tau_{1/2}$	Half time of polymerization (when α = 0.5)

Chapter 1.

Non-equilibrium Supramolecular Reactions Cycles

Abstract

Self-assembly systems are ubiquitous in living organisms performing complex functions. Supramolecular chemistry aims to develop complex functional materials through non-covalent interactions. Up to now, supramolecular chemists have developed systems that can self-assemble into distinct structures in their most stable configuration (thermodynamic equilibrium). As a step further, supramolecular chemists have developed different dissipative supramolecular systems that can perform transient self-assembly upon addition of a chemical fuel mimicking the self-assembly processes in the cell. In this chapter, we introduce various chemically-fueled systems present in literature.

Parts of this chapter have been published in:

Singh, N.†; Formon, G. J. M.†; De Piccoli, S.†; and Hermans, T. M. Devising Synthetic Reaction Cycles for Dissipative Nonequilibrium Self-Assembly. *Adv. Mater.* **2020,** 32 (20), 1906834. https://doi.org/10.1002/adma.201906834

† Authors contributed equally

1.1. General Introduction

Supramolecular chemistry has been defined by Jean-Marie Lehn as "the chemistry beyond the molecule".[1] It aims at developing highly complex chemical systems from components interacting through noncovalent intermolecular forces (i.e., hydrogen bonding, π-π stacking, van der Waals interactions, etc.).[1] Thus, supramolecular self-assembly is highly dynamic and reversible, which makes these materials structurally different from synthetic polymers built up of covalent bonding.[2]

Living organisms use supramolecular self-assembly to perform important functions such as replication, growing, signaling, and cellular transport.[3] Examples are microtubules and actin filaments which are part of the cytoskeleton of cells, DNA, ribosomes, etc.[3]

Up to now, supramolecular chemists have designed and engineered self-assembled supramolecular polymers capable of responding to various stimuli like pH, light, etc.[4–10] The exploration of those interactions over the past decade has led to the emerging field of Systems Chemistry.[11] However, most of the supramolecular polymers synthesized exist at the thermodynamic equilibrium while in Nature, supramolecular structures perform their function out-of-equilibrium.

In this Chapter, we discuss the mechanisms of supramolecular polymerization and the pathway complexity behind the supramolecular polymerization.[12] Next, we give examples of dissipative non-equilibrium structures present in Nature and the state-of-the-art on chemically-fueled self-assembling systems and materials.

1.2. Thermodynamic States

Molecular self-assembly dynamics arise from the continuous reversible exchange of non-covalent bonds. The supramolecular structures eventually find their most stable configuration[13], the thermodynamic equilibrium (#1 in Figure 1.1).[14] Nevertheless, when the self-assembly is controlled by the kinetics of the system, the final morphology depends on the conditions at which the sample has been prepared and it will be localized at the local energy minima (states #2 and #3 in Figure 1.1).[15] Thus, the methodologies used to obtain the supramolecular self-assembly permit the location of the system in a metastable or kinetically trapped state, as well as the development of different structures and materials. In contrast, living systems perform their function out-of-equilibrium (state #4 in Figure 1.1); they continuously consume energy to maintain their structures.

Hermans and co-workers provided a general classification and description of the four different supramolecular thermodynamic states (#1, #2, #3 and #4 in Figure 1.1): [12]

- *Thermodynamic equilibrium*: the system resides in the global minimum of the free energy landscape (state #1 in Figure 1.1). No external energy inputs are required to maintain the system and no changes are observed with time. The structures at equilibrium are still dynamic as the monomers continuously exchange with the solution. However, once the state is reached no further dissipation occurs. This reversibility is necessary for the self-assembly to reach its most stable configuration.

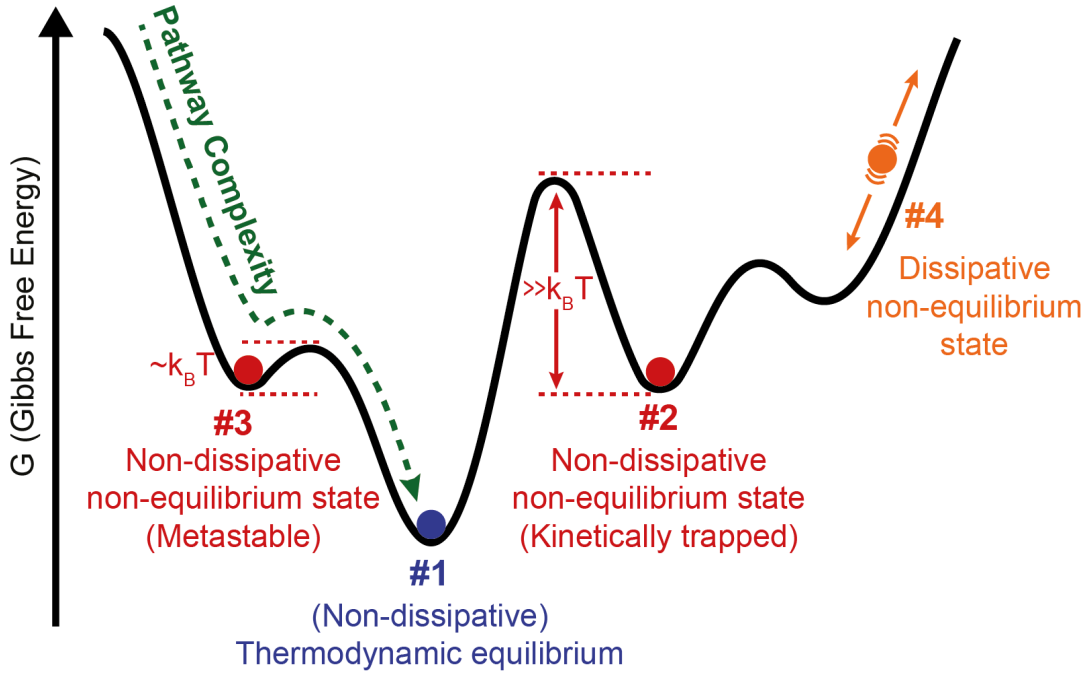

Figure 1.1. The Thermodynamic States. Schematic Gibbs free energy landscape. Reproduced from Ref.[12]

- *Non-dissipative non-equilibrium states* (*kinetically trapped* and *metastable states*): the self-assembled system is confined in a local minimum of the energy landscape (states #2 and #3 in Figure 1.1). The time evolution of the self-assembly depends on the shape of the energy landscape around the minimum. If the energy barrier leading to the thermodynamic equilibrium is low enough, that is on the same order as $k_B T$ (where k_B is the Boltzmann constant and T is the temperature), the system will relax to the most stable state. The state is referred as the metastable state (state #3 in Figure 1.1). However, when the energy barrier is

much higher than k_BT, the system will be kept in the local minimum for a time longer than the experimental observation. That is the so-called kinetically trapped state (state #2 in Fig.1.1).

- *Dissipative non-equilibrium state*: the system requires the continuous flux of energy or matter, and the removal of the waste products, to be steadily maintained (state #4 in Figure 1.1). If the energy supply stops, dissipative self-assembled systems will relax spontaneously to the thermodynamic equilibrium or they will get trapped in one of the non-dissipative non-equilibrium states. The dissipative self-assembly represents a new exciting direction[16–20] where obtaining non-equilibrium steady-states (NESS) and oscillations are still challenging.

1.3. Supramolecular Polymerization

Supramolecular polymerization can be described as the stepwise reversible assembly of monomers at the thermodynamic equilibrium, where each step is characterized by the decrease/increase of Gibbs free energy.[14] Here, we discuss two major growth mechanisms, isodesmic and cooperative. The isodesmic model is defined by the growth of the supramolecular polymer through a single equilibrium constant (k_e) for the entire process (Figure 1.2A). The latter depends on the monomer, the temperature and the solvent. On the contrary, in the cooperative supramolecular polymerization the assembly of the monomer passes by two association constants, k_a and k_e. The first process is the formation of a nucleus, described by k_a. The addition of a second monomer to the nucleus occurs with a higher association constant, k_e (Figure 1.2A). The initial stage of the cooperative supramolecular polymerization is then characterized by a higher Gibbs free energy barrier (nucleation); it proceeds by an elongation phase that is a linear isodesmic polymerization, i.e., constant decrease in the free energy (Figure 1.2B).

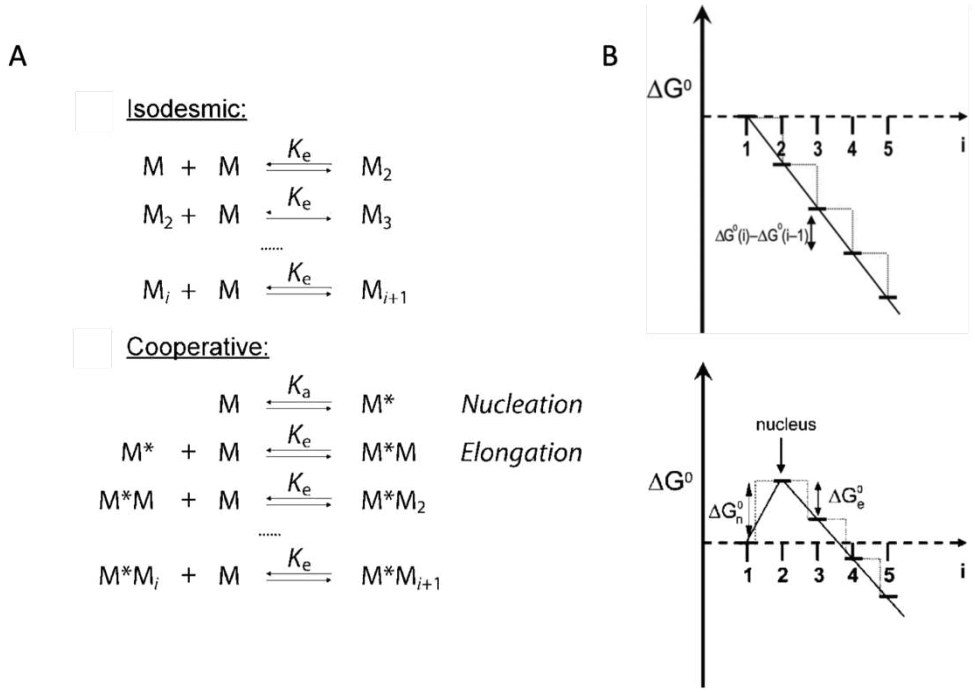

Figure 1.2. Supramolecular Polymerization Mechanisms. (A) Schematic representation of the isodesmic and the cooperative models for the monomer M. (B) Schematic energy diagrams of an isodesmic supramolecular polymerization and a cooperative nucleated supramolecular polymerization. The abscissa in the plots represents the size of the oligomer (i), whereas the ordinate measures the free energy ΔG° in arbitrary units. Reproduced from Ref.[14]

Understanding the process that leads to self-assembled structures can be accomplished *via* spectroscopic techniques, such us UV-Vis, circular dichroism (CD) or fluorescence spectroscopy.[21,22,23] Recent studies have focused on temperature-dependent experiments more than concentration-dependent studies because the measurements in the latter case are limited to the number of data points.[21] As reported by Meijer and co-workers, a thermodynamic model can be used to elucidate the self-assembly pathways that will lead to two different aggregate morphologies.[21] Here, we can clearly see that the free energy landscape offers different thermodynamic equilibria (with different morphologies) depending on the monomer, temperature, solvent composition or ionic strength.[15]

The kinetics of the supramolecular polymerization can be measured by heating-cooling studies, in which the different aggregation states are monitored with temperature. In some cases, heating and cooling do not coincide, which is often referred to as hysteresis.[14] This effect is due to the presence of large kinetic barriers in the assembly and disassembly process (state #2 in Figure 1.1). Therefore, thermodynamic parameters as well as kinetic parameters are the key to understanding supramolecular polymerization.

Supramolecular chemists have used various protocols to localize their systems in different states of the energy landscape. As mentioned in section 1.1., supramolecular structures can be confined in non-dissipative non-equilibrium states (#2 and #3 in Figure 1.1). The confinement can be done by using the same substrate at the same conditions (e.g., pH, solvent, temperature, etc.)[12] and varying the protocol procedures.

Molecular self-assembly, in a non-aqueous solution, happens spontaneously and is an exothermic process that is favored at lower temperatures. The cooling rate to reach the same final temperature can be, then, regulated to obtain different self-assemblies. Meijer and co-workers reported an interesting example where they show the chirality of the assemblies can be controlled adjusting the temperature profile.[24–26] The monomeric solution of *S*-chiral oligo(*p*-phenylenevinylene) (SOPV) at 70°C was cooled down to 0°C (cooling rate 1°C min^{-1}) resulting in the most stable left-handed helical configuration (state #1 in Figure 1.1). However, when the system was quickly cooled down, right-handed assemblies were obtained (state #2 in Figure 1.1). Interestingly, the chirality was reverted when the solution was heated at 25°C, showing metastable assemblies at this temperature (state #3 in Figure 1.1.). Additionally, the pathway complexity in molecular self-assembly can be regulated by changing the order of addition of the different components[27,28] or by multi-step non-covalent synthesis.[29,30]

So far, we have discussed the mechanisms of supramolecular polymerization (isodesmic and cooperative) and how various self-assembly morphologies can be achieved by localizing the system in different thermodynamic states (states #1, #2 and #3 in Figure 1.1). Thermodynamic and kinetic studies are important tools for understanding the pathway of supramolecular assembly. In the next section, we focus on examples of dissipative non-equilibrium natural systems (state #4 in Figure 1.1).

1.4. Dissipative Non-equilibrium State

In Nature, different structures work under dissipative non-equilibrium conditions, such as microtubules and actin filaments.[11] The latter are supramolecular polymers present in our cells, where, together with the intermediate filaments, they form the cytoskeleton.[3] The cells need to rearrange their internal components to grow, divide and adapt to their surroundings. Thus, cell's varied functions depend on the behavior of the three components of the cytoskeleton.[31] Microtubules, actin filaments, and intermediate filaments are dynamic and adaptable well-

organized structures. The spatiotemporal control is organized by the flux of chemical fuels, the reactions network and feedback loops, which regulates the molecular self-assembly of these supramolecular polymers. These features allow the structural rearrangement of cells in a wide range of different structures requiring a continuous supply of energy.[32]

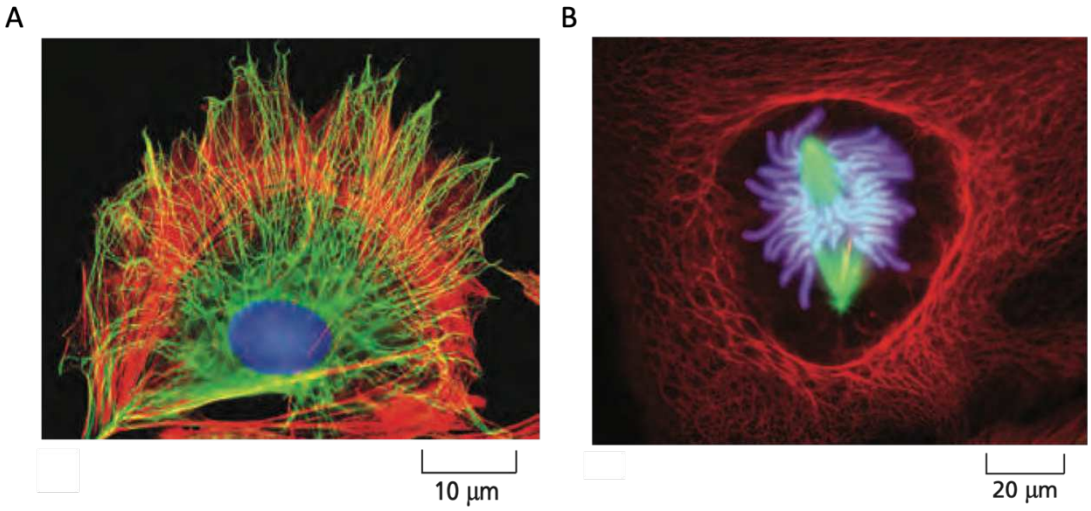

Figure 1.3. The cytoskeleton. (A) A cell in culture has been fixed. Microtubules are shown in green and actin filaments in red. (B) The dividing cell shows its spindle microtubules (green) and surrounding cage of intermediate filaments (red). The DNA in both figures is labeled in blue. Reproduced from Ref.[3]

Microtubules are highly dynamic polymers of the protein tubulin (Figure 1.4).[33] Tubulin is a heterodimer composed of α-tubulin and β-tubulin, bound together by non-covalent bonds. Each subunit can bind one molecule of GTP (guanosine triphosphate). The nucleotide on the β-tubulin can be either GTP or GDP (guanosine diphosphate). Microtubule assembly generates a hollow cylindrical structure of 13 protofilaments, each composed of heterodimers stacked head to tail and folded in a tube (Figure 1.4).[3] Microtubules are the largest and the stiffest structure present in most animal cells, as a result of the multiple interactions between the subunits.[3]

The polymerization is driven by an exchange of GDP for GTP in free tubulin. GTP-tubulin polymerization is a thermodynamically favored process.[34] The activation, inside the microtubule structure, of a catalytic cleavage side leads to the hydrolysis of GTP into GDP and Pi (inorganic phosphate). Then, GDP-tubulin causes the microtubules to shrink (Figure 1.4B). Nevertheless, GDP-tubulin by itself does not polymerize. The hydrolysis of GTP happens only on the assembled structures resulting in a high-energy assembly composed of GDP-tubulin. However, the exchange GDP-GTP occurs only with the free tubulin and not the assembly.

Microtubules are dynamically unstable as they undergo rapid conversion between growing state and shrinking state.[35] This switching behavior is essential for microtubules to perform vital cell functions. These functions rely on out-of-equilibrium states. Dissipative states cannot be sustained if the energy supply (GTP) stops. Thus, if GTP is consumed, the system will relax to the thermodynamic state.

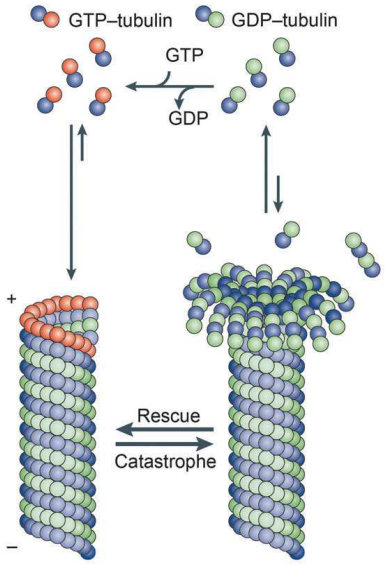

Figure 1.4. Microtubules. Schematic representation of dynamic instabilities during microtubule polymerization. Reproduced from Ref.[36]

Similarly to tubulin, actin binds and hydrolyzes the nucleoside triphosphate, ATP (adenosine triphosphate).[3] Actin filaments are right-handed helices of actin subunits assembled head-to-tail (Figure 1.5A).[37] In the presence of ATP, ATP binds to the filaments, which leads to polymerization. When ATP is hydrolyzed to ADP (adenosine diphosphate), the energy of the phosphate bond cleavage is kept inside the structure, as in GDP-tubulin assembly. Then, when the filament binds to ADP, it depolymerizes. At a certain subunit concentration, the filament cycles between growing and shrinking (Figure 1.5B), while the total length remains unchanged. In this so-called 'steady state' the system is constantly consuming ATP to remain out-of-equilibrium.

The vital functions expressed by eucaryote cells (i.e., motility, self-reproduction, signaling) are performed out-of-equilibrium and require a continuous supply of energy (fuel). In addition, chemical fuels are controlling the spatiotemporal self-assembly of these supramolecular polymers. Microtubules and actin filaments are only two examples of the complex supramolecular network present in Nature.

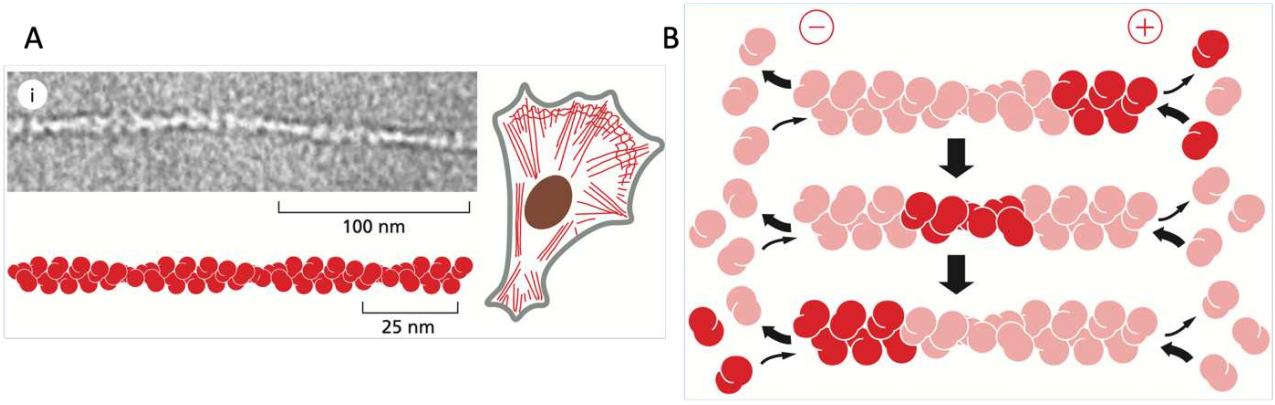

Figure 1.5. Actin Filaments. (A) Actin filaments are helical polymers of the protein actin. They are flexible structures organized into a variety of linear bundles. In (i) a single actin filament is shown. (B) The actin filaments maintain constant their length by a continuous net flux of subunits through the polymer, known as treadmilling. Reproduced from Ref.[3]

Nature is a source of inspiration for systems chemists. However, synthesizing networks that are capable of reproducing functions similar to those found in Nature is nontrivial. In the following sections, we describe a few examples of chemically-fueled systems and highlight the issues scientists are currently facing.

1.5. ATP-Fueled Systems

ATP is essential for many cell functions including transport work, mechanical work (i.e., muscle contraction) and chemical work (i.e., synthesis of macromolecules).[38,39] ATP contains the purine base adenine and the sugar ribose, which together form the nucleoside adenosine, and a tail consisting of three phosphates (PO_4).[3] The phosphates are well-known high-energy molecules meaning that the energy released during the hydrolysis of ATP (30.5 kJ mol^{-1}) makes it the primary energy currency for cells.[40] Humans turn over the mass of their body weight in ATP every day, as a result of a very efficient ADP/ATP recycling system.[3]

ATP is essential in cell signaling (Figure 1.6).[3] The communication network requires phosphorylation/dephosphorylation processes, where the phosphate group can be transferred from ATP to a molecule or an enzyme, causing the modification of its shape and the production of a signal. At the same time, the phosphate group can be cleaved (by a phosphatase) restoring the initial state. Thus, ATP can be used as a trigger or a chemical fuel for the control of the self-assembly of supramolecular polymers and the development of complex reactions networks. Figure 1.6 shows only part of the enzymatic reactions and human diseases ATP is involved in.

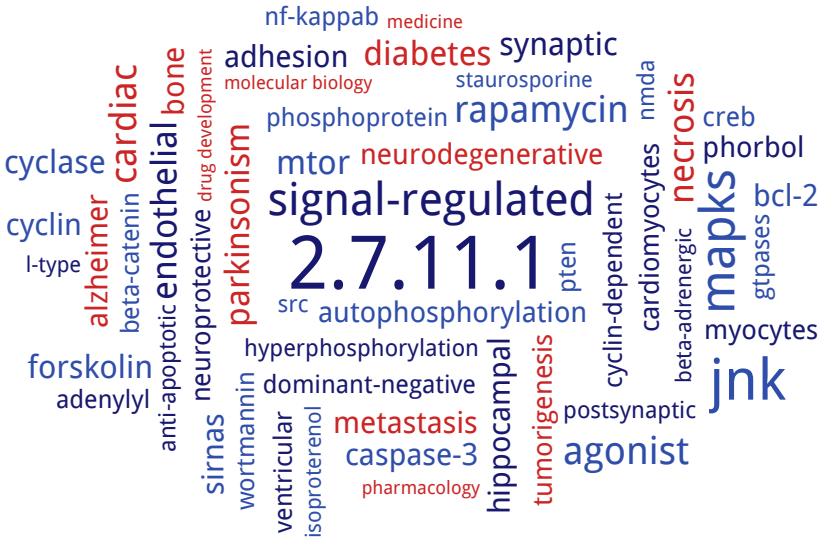

Figure 1.6. ATP Word Map. This is part of the wide signaling network where ATP play a fundamental role. ATP is the target of various drugs, as it is involved in many enzymatic cascades. Reproduced from Ref.[41]

Recently, Walther and co-workers published an extensive overview on ATP-fueled self-assembling systems and materials reported so far in Systems Chemistry.[42] Here, we report examples where ATP triggers the self-assembly and is consumed during reactions to push the system out-of-equilibrium.

One of the first points they highlighted was the lack of nucleotide recognition, for instance between ATP, GTP, ADP and GDP in order to reach orthogonal responses in multicomponent mixtures. This type of selectivity could be achieved in systems with multiple binding-sites, such as RNA or DNA aptamers.[43–47] In this direction, Szostak and co-workers developed a RNA-based aptamer capable of distinguishing ATP from ADP, AMP or adenosine.[48] However, extremely sensitive systems are still a challenge. Therefore, ATP-fueled enzymatic systems (i.e., protein kinases) are the best method to reach control and selectivity over reactions.

The first example is an insightful work by Stupp and co-workers.[49] They developed a peptide-based system where the self-assembly was controlled by two enzymes, a protein kinase A (PKA) and an alkaline phosphatase (AP) (Figure 1.7A). The enzymes triggered the phosphorylation and the dephosphorylation, respectively, of the serine residue present in the peptide sequence (KRRASVAGK[C_{12}]–NH_2). The peptide formed a hydrogel resulting from the formation of intermolecular β-sheet. When PKA was added the phosphorylation of the structure induced the disassembly of the supramolecular nanofibers and, consequently, disrupted the hydrogel (Figure 1.7B). Upon treatment with the phosphatase, the filamentous nanostructures were restored as a result of the dephosphorylation of the peptide sequence (Figure 1.7B). The use of a

kinase/phosphatase system was previously reported for the control of a supramolecular hydrogel.[50] And it represents a very useful approach to obtain selectivity and control over the supramolecular assembly. In addition, the authors included a therapeutical application where the supramolecular polymerization and depolymerization was used to control the release of drugs, specifically, doxorubicin (DOX).[49]

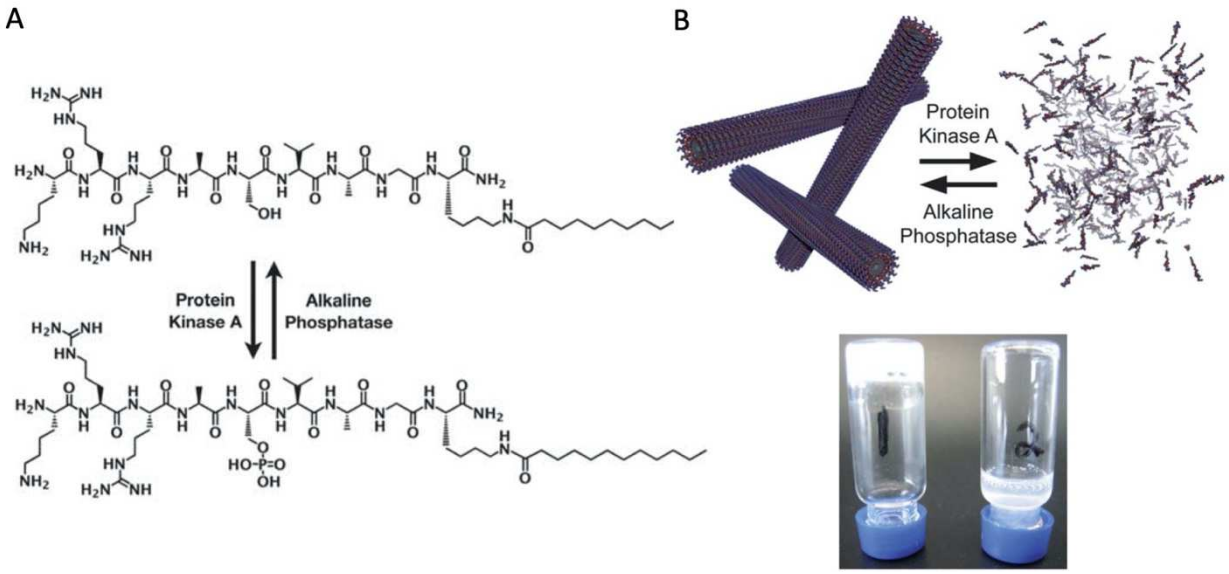

Figure 1.7. Self-assembly of a Peptide-based Phosphorylation and the Dephosphorylation System. (A) Reaction scheme for the conversion of the peptide derivative into the phosphorylated analog by protein kinase A and the restore of the initial structure mediated by alkaline phosphatase. (B) Disassembly upon treatment with PKA and its reassembly upon treatment with AP. The vial inversion test shows the formation of a hydrogel of the peptide derivative without exposure to PKA (1) and after exposure to PKA (2). Reproduced from Ref.[49]

Another interesting system was reported by Aida and co-workers where they described protein-based nanocarriers, resulting from the self-assembly of chaperonin GroEL mutant. [51] The chaperonin, in living systems, releases proteins after refolding them by a conformational change fueled by the hydrolysis of ATP. The polymerization of the monomer units of $GroEL_{Cys}$, appended with zwitterionic merocyanine (MC), to form $GroEL_{MC}$ (Figure 1.8) was previously described by the group.[52] Next, the incubation of ATP for 30 minutes resulted in a mixture of monomer, dimer and trimer of $GroEL_{MC}$.

Additionally, the ATP-responsive system was used for intracellular drug delivery; the surface was functionalized with a boronic acid derivative, which facilitated entry in the cells. When inside, the hydrolysis of ATP led the disassembly of the nanotubes and released the drug. This example points out the importance in the design of some sort of sensitivity in the supramolecular structures. Particularly, biological sensing capability is key attribute to achieve materials that can mimic the

ones observed in Nature. The latter is a key point to obtain 'life-like' materials able to perform such processes and interact with biological systems.

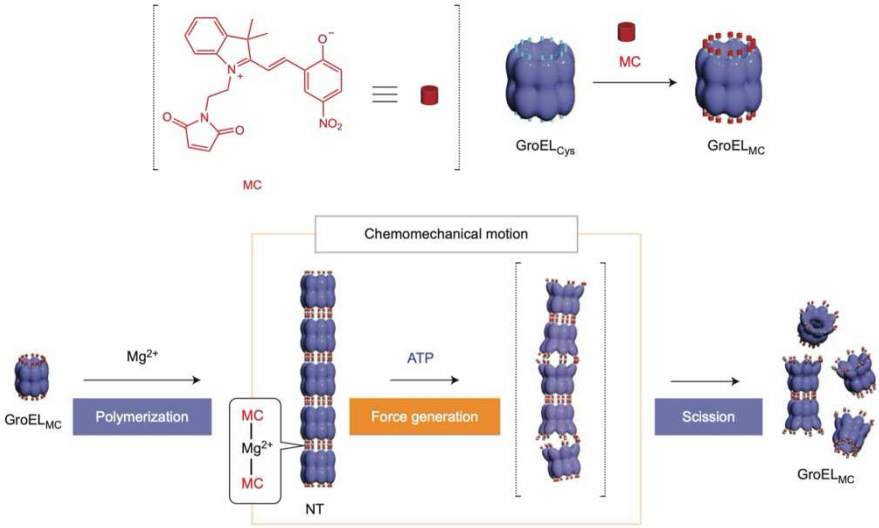

Figure 1.8. Protein-based Nanocarriers. Representation of the preparation from mutant GroEL$_{Cys}$ and Mg^{2+}–mediated supramolecular polymerization of GroEL$_{MC}$, forming a nanotube (NT), and its ATP-fueled scission. Reproduced from Ref.[51]

Another approach for the investigation of ATP-fueled systems was developed by George and co-workers.[53] The system was based on helical assemblies of naphthalenediimide (NDI) chromophores functionalized with zinc coordinated dipicolylethylenediamine (NDPA). First, they investigated the interaction of the supramolecular building block with different adenosine phosphates (APs). The binding with AMP (adenosine monophosphate) or ADP or ATP induced a change in the chirality of the supramolecular polymer (Figure 1.9A). The different assemblies of NDPA with APs were studied by circular dichroism (CD) spectroscopy, and showed that the interactions were stronger in the presence of ATP compared to ADP and AMP (Figure 1.9B). Additionally, a change in the supramolecular chirality was observed. Specifically, AMP and ADP formed left-handed helices while ATP imparted the formation of right-handed helices. Interestingly, the assemblies displayed a competitive replacement of AMP or ADP by ATP. The behavior of NDPA-ATP stacks was analyzed in the presence of a phosphatase, which dissociates ATP into adenosine and inorganic phosphates. ATP was first converted to ADP and then, AMP. This resulted in a reverse CD signal followed by a loss of the supramolecular chirality (CD signal equal to zero) (Figure 1.9B).

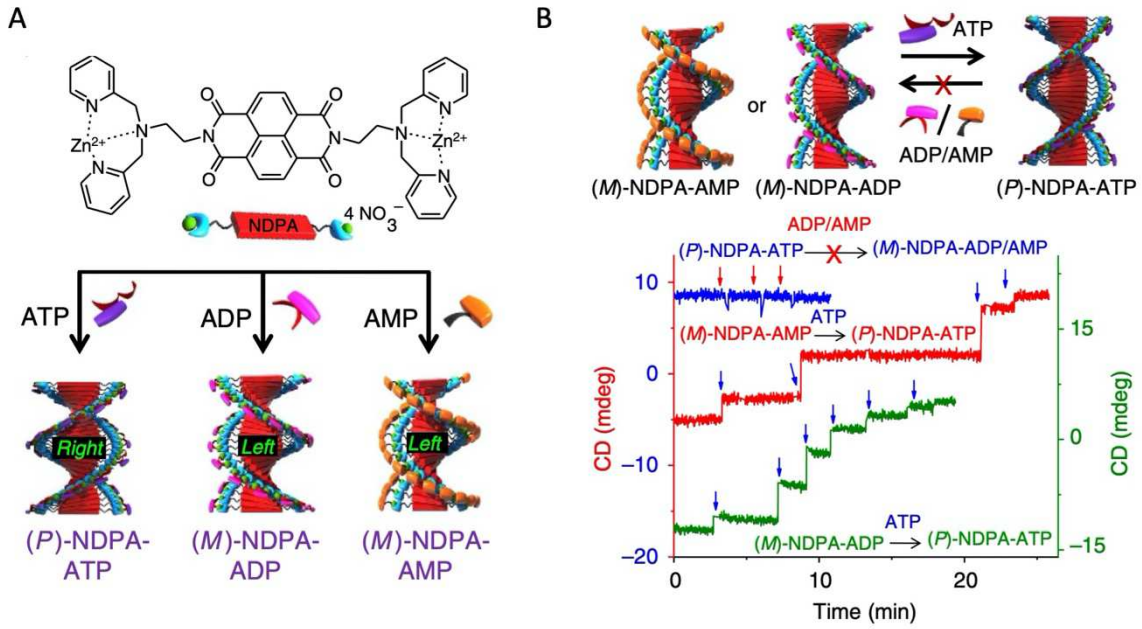

Figure 1.9. Helical chiral-induced assemblies of NDPA with adenosine phosphates. (A) Molecular structure of naphthalenediimide (NDI) chromophores functionalized with zinc coordinated dipicolylethylenediamine (NDPA) and the representation of the supramolecular helices in the presence of ATP, ADP and AMP. (B) Representation of helicity reversal in NDPA assembly *via* competitive binding of multivalent adenosine phosphates. Stepwise dynamic helix reversal experiments performed by sequential addition of ATP to NDPA-AMP (red) and NDPA-ADP (green) assemblies. Reproduced from Ref.[53]

In 2017, George and co-workers[54] implemented the helical system with the use of two complementary enzymes, a hexokinase (HK) and a creatine phosphokinase (CPK). The hexokinase consumes ATP while the creatine phosphokinase restores ATP (Figure 1.10). As previously described, the self-assembly of the supramolecular building block with ATP rather than ADP exhibits a change in the supramolecular chirality. Thus, they achieved temporal changing in the helical conformation as a function of concentration of enzymes and substrates.

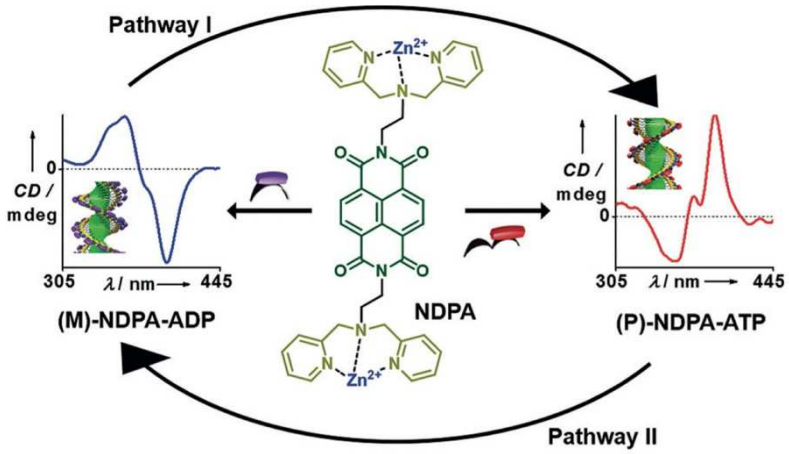

Figure 1.10. Enzyme-responsive Helical handedness of supramolecular polymer. Molecular structure of NDPA and CD spectra of the opposite helical conformations formed by NDPA upon interaction with ATP and ADP. Enzymatic reaction pathways I and II are controlled by creatinine phosphokinase (CPK) and hexokinase (HK), respectively. Reproduced from Ref.[54]

Maiti *et al.*[20] described the formation of vesicles by the stabilization of C_{16}TACN·Zn^{2+} surfactant aggregates with ATP. The surfactant was composed by a polar chain C_{16} and a head group of 1,4,7-triazacyclononane·Zn^{2+} (TACN·Zn^{2+}) and it aggregated into micelles. In the presence of ATP, the self-assembly was favored; thereby, yielding bigger aggregates (vesicles) with higher stability. In order to reach a dissipative state, the authors examined the system in the presence of potato apyrase. The enzyme hydrolyzed ATP into AMP and inorganic phosphates, releasing the chemical energy stored in the molecule. Therefore, the hydrolysis of the fuel (ATP) leads to the destabilization of the vesicles. In Figure 1.11 the transient formation of vesicles is represented.

In this system, the lifetime of the self-assembled structures was control by the hydrolysis rate of ATP. As such, transient behavior of the supramolecular structures was achieved, which is determined by the fuel present in the system. Indeed, the non-equilibrium self-assembled state can be maintained as long as ATP was not consumed.

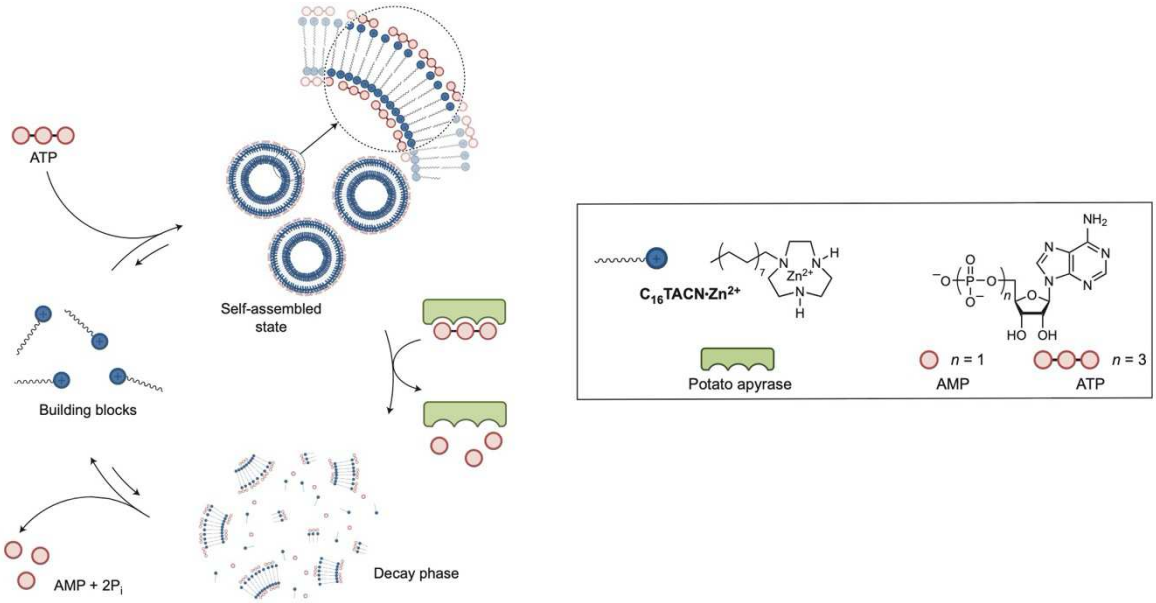

Figure 1.11. Transient Formation of Vesicles by the Stabilization with ATP. Schematic representation of the dissipative self-assembly of vesicles**.** Reproduced from Ref.[20]

As previously stated, cells reach spatial organization by localizing molecules and reactions at the surface of compartments.[3] The compartmentalization is a powerful tool that Nature uses to discriminate reaction cycles and avoid cross-reactivity between undesired molecules.[55] Thus, many synthetic systems are now confined into vesicles, droplets, etc., but pushing these processes out-of-equilibrium remains challenging.

Mann and co-workers reported a model for novel bioreactors and synthetic cells by using peptide-based coacervate droplets as membrane-free organelles.[56] In 2018, Spruijt and co-workers developed a coacervate droplets system based on an enzymatic reaction network.[57] The coacervates were formed by liquid-liquid phase separation of Poly-$_L$-lysine (pLys). Two enzymes were present in the system, a hexokinase and a pyruvate kinase. The enzymes controlled the turnover of ATP by regulating the concentration of the substrates, D-glucose and pyruvate, respectively. D-glucose was necessary for the production of ATP while pyruvate was produced and converted by the hexokinase. Thus, the assembly and the disassembly of the system was governed by the presence of ATP/pLys (coacervate droplets) or ADP/pLys (droplets dissolution). Interestingly, the switch between condensation and dissolution was governed by the concentration of the enzymes and substrates concentration. They reported six transition cycles for the system after which the system was inhibited by the accumulation of waste. This work represents an elegant way to reach spatiotemporal organization of supramolecular systems.

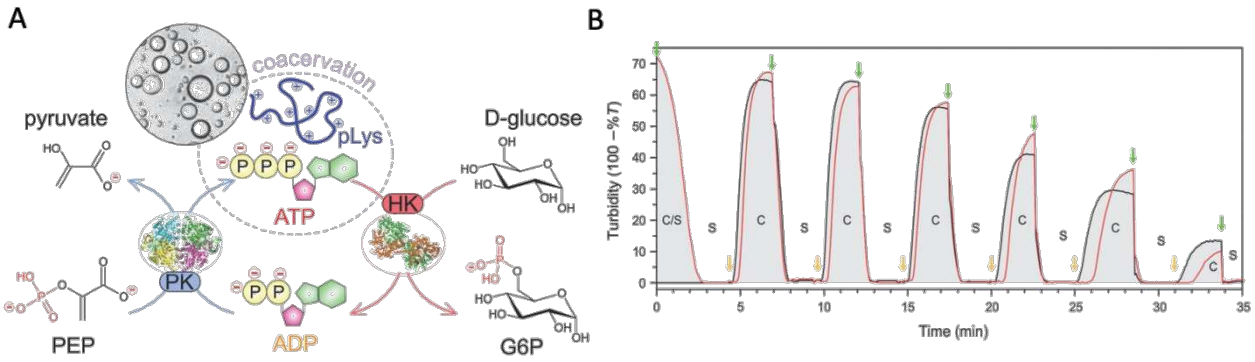

Figure 1.12. Coacervate Droplets system based on an Enzymatic Reaction Network. (A) Schematic illustration of the enzymatic reaction network. (B) Repeating additions of phosphoenolpyruvate and D-glucose show that the system can switch multiple times between condensation and dissolution states. Reproduced from Ref.[57]

So far, we have discussed several examples of ATP-fueled systems and materials present in the literature. ATP is used as a template to induce the self-assembly of supramolecular structures. In addition, under dissipative conditions, ATP represents a tool to control the lifetime of self-assembled structures.

In the following section, chemically-fueled synthetic systems are presented and we discuss challenges that are still open in the field of Systems Chemistry.

1.6. Chemically-Fueled Dissipative Systems

Recently, we reviewed chemically-fueled dissipative self-assemblies reported so far in literature.[58] We focused on systems where no biological elements were involved, such as DNA[44,45,59,60], enzymes[5,7,19,20,61–63] or where no pH change[4,64,65] or redox reaction[66–68] were employed. We discussed only synthetic reaction cycles where bonds are made or broken *via* synthetic means. The desired reaction cycles were divided into:

- Cat (1): spontaneous deactivation of the self-assembly by the solvent (i.e., hydrolysis by water);[17,18,69–78]
- Cat (2): the same chemistry was used to activate and deactivate the self-assembling molecules;[79–81]
- Cat (3): a catalyst acted on one specific step of the reaction cycle.[82–85]

The synthetic chemically fueled systems from 2010 until now will be presented and discussed in a chronological order.

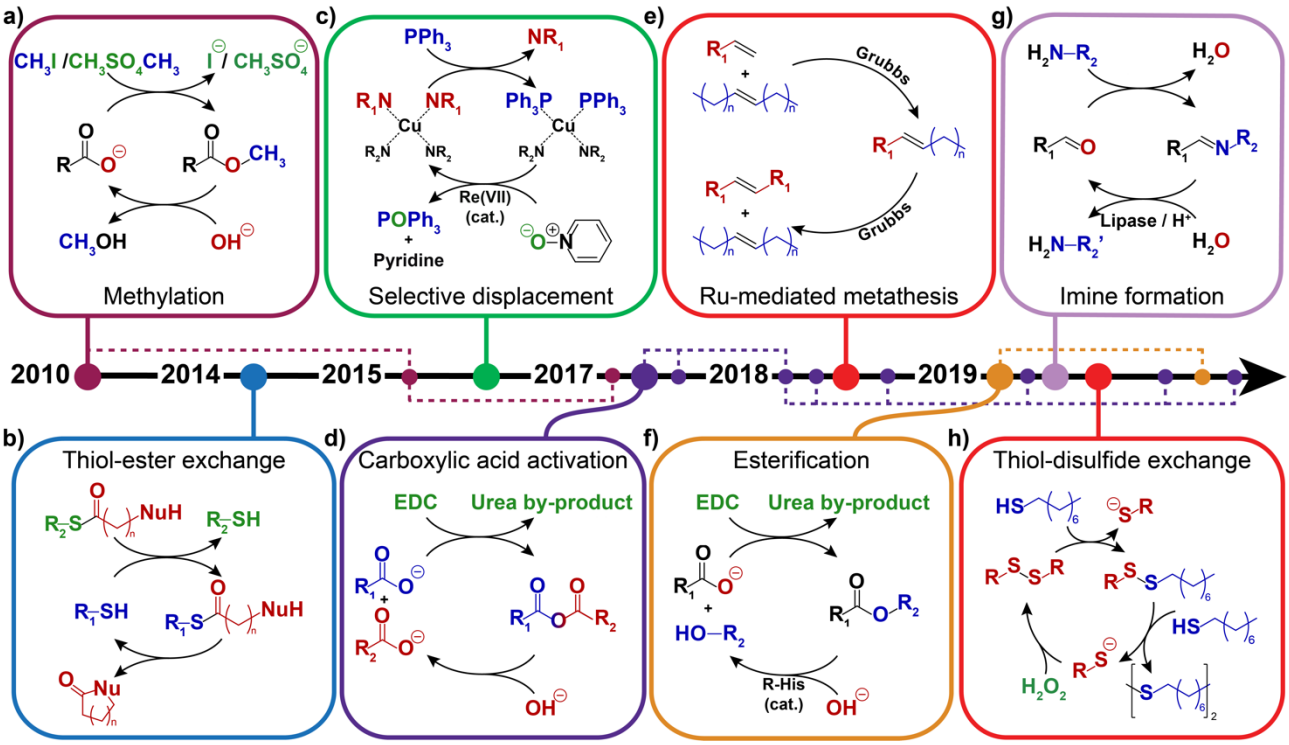

Figure 1.13. Timeline of Chemical Reaction Cycles. See description a-h) in the main text. Reproduced from Ref.[58]

In 2010, van Esch and co-workers performed the first synthetic example of chemically-fueled supramolecular system using a methylation reaction to activate a small molecule building block (Figure 1.13a, Cat. 1).[17] Dibenzoyl-(L)-cystine (DBC), which is soluble in aqueous media at a pH above its pKa (c.a. 4.5), was used as substrate. The carboxylic acids of DBC were converted by methyl iodide (MeI) to the corresponding methyl esters, which reduced the electrostatic repulsion and lead to fiber self-assembly. The hydrolysis of the esters back to the acid form caused disassembly of the fibers and regenerated DBC. The cycle was repeated by addition of multiple aliquots of fuel (MeI). However, over time, the production of waste hampered the reaction cycle.

In 2015, the reaction cycle was improved by the use of dimethyl sulfate (DMS) as methylating agent (Figure 1.14A), and the transient gelation could be obtained (Figure 1.14B).[18] The lifetime of the resulting gels could be controlled by the amount of fuel added. The same reaction cycle was later used to control the clustering of carboxylic acid-decorated colloids.[69] This methylation/hydrolysis approach demonstrated the first chemically fueled transient formation of a molecular hydrogelator between assembling and non-assembling states.

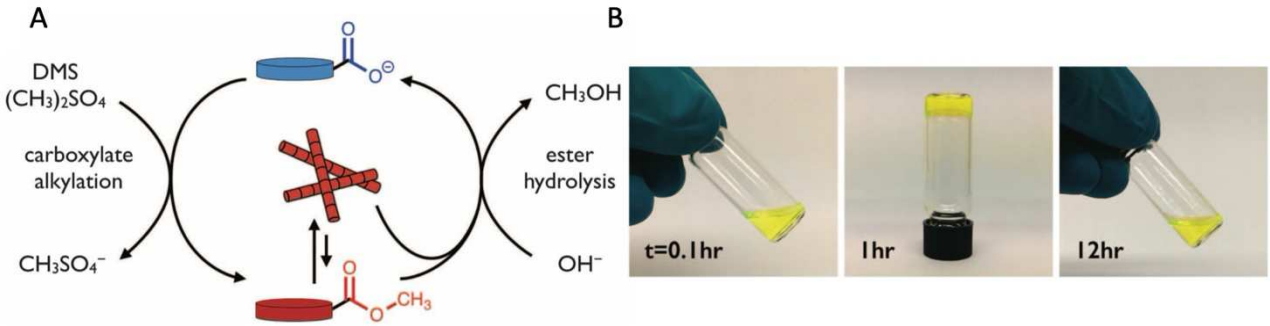

Figure 1.14. Chemically fueled transient self-assembly. (A) Representation of the reaction cycle. The carboxylate groups on the inactive monomer react with the fuel, DMS, to produce methyl esters, active structures that self-assemble. (B) The reaction cycle at pH 11 showing the transition sol-gel-sol of the system. Reproduced from Ref.[18]

In 2014, Fyles and co-authors reported a chemically fueled transport membrane system.[79] The dissipative assembly of the transport system involved a thiol-thioester exchange to activate a mercaptan precursor (Figure 1.13b, Cat. 2). The resulting thioester product formed conducting channels within bilayer membranes. The activity was studied and proved by voltage-clamp experiments, which showed the flow of ions through the transport system. The system was elegantly designed in such a way that the inactive precursor was reestablished *via* intramolecular lactam formation through the nucleophilic attack of the amine to the thioester.

One year later, Nitschke and co-workers reported a chemically fueled metal-templated self-assembly of supramolecular structures (Figure 1.13c, Cat. 3).[82] They studied the disassembly of a Cu-based pseudorotaxane, by selective displacement of bipyridine after addition of triphenylphosphine (PPh_3). Then, the initial substrate was restored *via* an oxidation-reduction reaction involving pyridine n-oxide and a rhenium catalyst to generate triphenylphosphine oxide ($O=PPh_3$). Thus, they demonstrated the uptake and release of fullerene from a macrocyclic host. Interestingly, the rate of disassembly was easily controlled due to its catalytic nature and the authors were able to repeat the cycle up to six times.

Boekhoven and co-authors, in 2017, described a chemical reaction network driven by dicarboxylic acid activation to obtain a transient anhydride (Figure 1.13d, Cat. 1), using the common coupling agent EDC (1-Ethyl-3-(3-dimethylaminopropyl)carbodiimide).[70] The experiments were performed in aqueous media where the anhydride was hydrolyzed to recover the starting non-activated building block. The transiently formed anhydride self-assembled into hydrogels forming fibers and colloids. The phase separation was achieved one year later from the same group by applying the same chemistry to fatty acids.[72] The anhydride product (linking together two fatty

acids) phase separated into droplets and consequently, as the anhydride was protected from the surrounding aqueous environment, the hydrolysis rate of the anhydride was delayed.[73].

Recently, Grötsch *et al.*[76] extended the application of carboxylic acid activation to gold and iron oxide nanoparticles (Figure 1.15). The EDC system has been used in different examples and applications thanks to its broadly applicable functional group and the easily purchased fuels.[71,74,75,77,78]

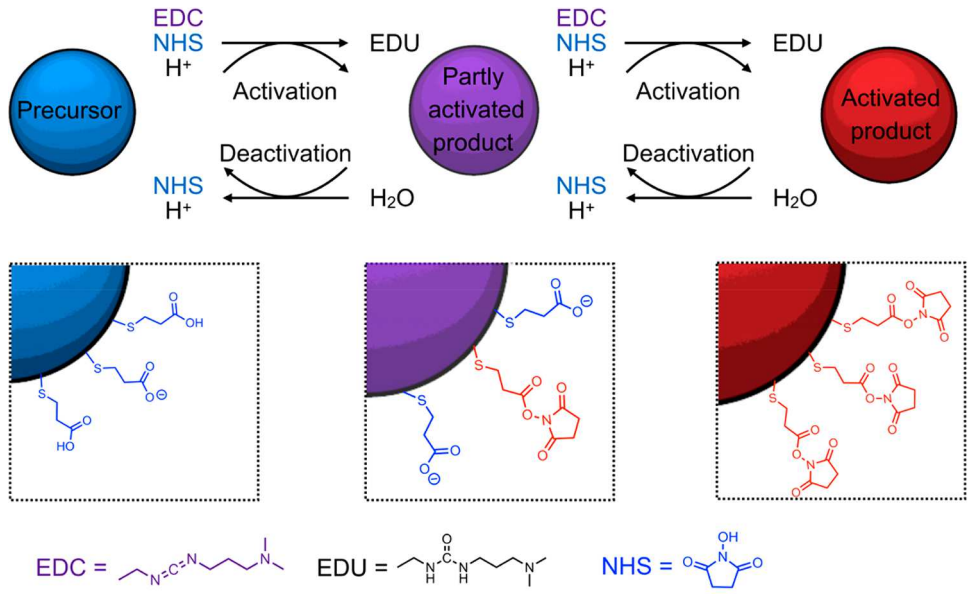

Figure 1.15. Chemical Reaction Cycle driven by the Hydrolysis of EDC. The carboxylates on a gold nanoparticle (precursor) react with EDC and NHS to form the corresponding esters (activated product). Depending on the amount of EDC added, the precursor is partly or fully activated. Reproduced from Ref.[76]

In 2018, Fletcher and co-workers developed a transient self-replicating system employing a catalytic metathesis reaction (Figure 1.13e, Cat. 2).[80] In a bi-phasic system, a water-soluble alkene reacted with a hydrophobic alkene through metathesis using the second–generation Grubbs catalyst. The product self-assembled into micelles, which physically enhanced the reactivity between the hydrophobic and hydrophilic substrates in an autocatalytic fashion by increasing the contact area between the immiscible part. The surfactant then reacted with itself through cross-metathesis, to form the water-soluble/inactive thermodynamic product. It's important to note that the transient cycle could be repeated.

Recently, Das and co-workers[83] presented a chemically fueled system where an amphiphile (C18H) containing a eighteen-carbon chain (C18) coupled to a histidine residue (H) was used as a substrate for the esterification in the presence of 4-nitrophenol (Figure 1.13f, Cat. 3). This

esterification step led to the transient formation of a hydrogel. The ester hydrolysis, catalyzed by the vicinal histidine, yielded the soluble molecules. Thus, the self-assembled structures were catalyzing their own disassembly, analogous to microtubule structures. To study the system further, Das and co-workers used the C18H molecule for the co-assembly with a similar amphiphile with C18 stearoyl and L-phenylalanine amino acid appended with nitrophenol (C18-FNP).[84] The co-assembly of C18H and C18-FNP occurred in the reaction media and gave helical structures (Figure 1.16). The vicinity of pendant phenylalanine-nitro groups linked by ester bonds (in C18-FNP) to the histidine (in C18H), allowed for the cleavage of the ester linkage by histidine causing the subsequent disassembly of the helices. The lifetime of the assemblies could be controlled by various substituents of the phenol group.

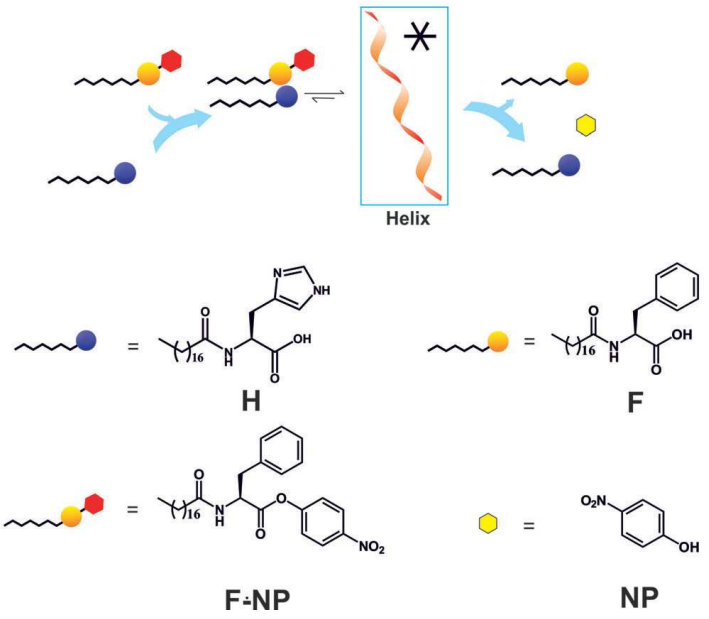

Figure 1.16. Representation of the substrate F-NP induces the co-assembly driving the formation of helical nanostructures (marked with an asterisk). The presence of histidine in the molecular structure augments the catalytic rates and the disassembly leading to the release of NP. Reproduced from Ref.[84]

Recently, George and co-workers used a dynamic imine bond to form a charge-transfer surfactant that self-assembled into fibers (Figure 1.13g, Cat. 3).[85] Upon the addition of an aliphatic primary amine (fuel), the substrate was activated leading to an amphiphile. The deactivation of the monomer was regulated by a lipase (enzymatically) and by pH variation (tuning imine stability and reactivity). The equilibrium of the imine bond towards the inactive substrates could be shifted by using various hydrolysable esters (e.g., γ-butyrolactone, β-butyrolactone or ε-caprolactone), as the pH of the solution is decreased with a time delay. By substituting the fully aliphatic tail of primary amine with an ester-containing alkyl chain, the ester bond could be hydrolyzed in the presence of a

lipase; thereby, rendering the building block inactive and generating a transient system. In both cases, the lifetime of the assembled state could be controlled by the lipase concentration, changing the amount and/or nature of the hydrolysable ester.

In 2019, Fletcher and co-workers showed a chemically fueled bi-phasic self-replicator.[81] The chemistry relied on a disulfide exchange between a water-soluble disulfide and octanethiol (Figure 1.13h, Cat. 2). The thiol reacted with the amphiphile, giving a hydrophobic disulfide and inactive hydrophilic thiolate. This system showed (physical) autocatalytic and transient behavior due to the surface-active properties of the transient amphiphile. The cycle could be repeated when hydrogen peroxide was added to the solution causing reactivation of the thiolates into water-soluble disulfides. Steady states of the assemblies was sustained by continuously suppling the oxidizing agent.

In 2020, Singh *et al.*[86] described a new out-of-equilibrium system based on a sugar-based aldehyde-containing hydrogelator. This system will be discussed in detail in Chapter 5.

Overall, systems chemists have a plethora of reactions that can be explored for the development of new synthetic chemically-fueled systems. There are several limitations that currently plague Systems Chemistry.[58] One of the biggest problems is waste, which halts the reaction cycle. In most systems, multiple reaction cycles cannot be achieved due to the inhibition of side-products. Over the past 10 years, only a few solutions to this impending issue have been proposed, such as the use of a dialysis membrane[61] or the precipitation of waste[86,87].

In the same way, an elegant system has been recently developed by Kim and co-workers.[6] They reported a pH-responsive transient self-assembly process driven by a gaseous mixture composed of CO_2 (the fuel) and argon (or compressed air) as the carrier gas. The monomer (the organic dye methyl orange MO) was activated *via* the formation of carbonic acid in solution from the mixed flow of CO_2 and argon. The activation induced the self-assembly of transient microstructures. The initial monomer was recovered with time. The authors demonstrated that multiple cycles could be obtained *via* sequential additions of the fuel. In this case, the waste was a gas, which leaves the system and does not inhibit subsequent reaction cycles. Nevertheless, the system *per se* is more a switch than an actual transient assembly. Because CO_2 was flowed for about 2 minutes in order to permeate the solution. Based on the amount of fuel added, the 'switch' (disassembly/assembly) could last 2, 4 or 6 minutes. Moreover, CO_2 was leaving the system as gas,

thus the microstructures became inactive as soon as the fuel was completely evaporated, and this was directly proportional to the amount of CO_2 injected at the start of the reaction.

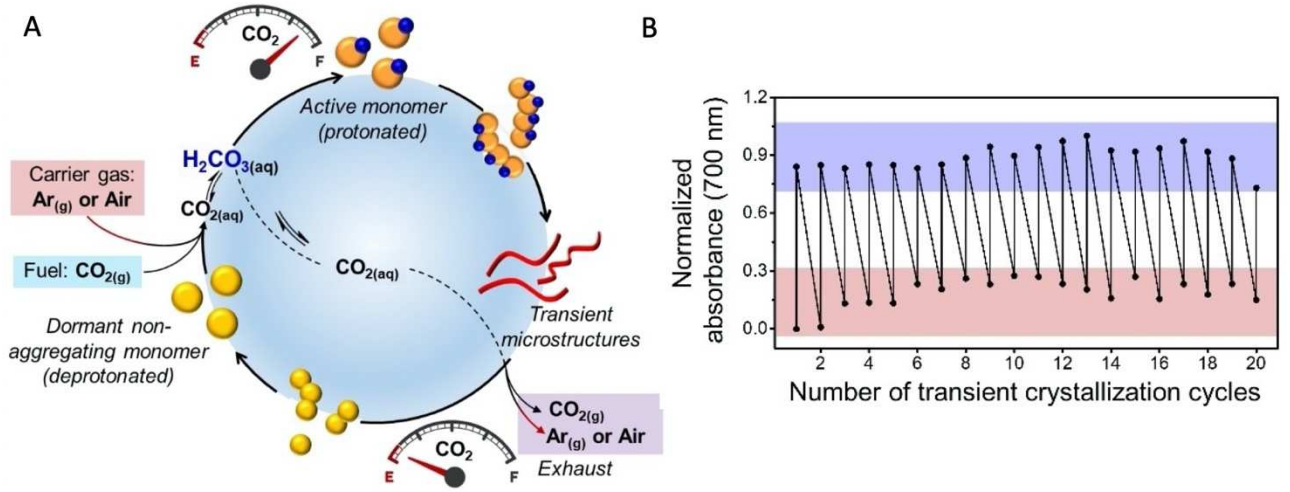

Figure 1.14. Transient self-assembly driven by gaseous fuels. (A) Schematic representation of a pH-responsive transient self-assembly process. (B) Gas flow controlled transient microstructures formation over repeated cycles without significant loss of efficiency. Reproduced from Ref.[6]

Contrary, in the same work, a transient self-assembly was achieved by pH change in the presence of trichloroacetic acid (TCA) and triethylamine (TEA). TCA activated the monomer MO leading to the protonation and the formation of microcrystals. With time, TEA catalyzed the deprotonation and the recovery of the initial inactivated monomer. The lifetime of the self-assembled structures depended on the ratio between TCA and TEA.

Secondly, the chemical fuels themselves can be improved as they are quite reactive and degrade slowly under the conditions.[17,18,70,72] The use of an unreactive 'pre-fuel' that can be converted *in situ* into a more reactive species is definitely an approach that chemists are investigating more and more. This transformation would be done catalytically or by reacting with a second pre-fuel or directly with waste. Another approach would be using a catalyst that brings the substrate and fuel together to achieve high selectivity. Examples of recycling waste and/or use of a pre-fuel are described in Chapter 2 and 5.

The third important point is the control over the kinetics of the involved reaction(s). In most of the cycles designed so far, the deactivation reaction rate was solvent-mediated, and therefore, difficult to control.[17,18,70,72] This drawback of spontaneous deactivation is also observed in systems

with carefully synthesized fuels that drive the assembly (or disassembly).[79] The use of catalysts, such as Ruthenium[80] and Grubbs[82] catalysts, is a good approach to control cycles at each reaction step.

1.7. Energy Costs of Chemically-fueled Self-assembly

Up to now, the systems previously described are transient systems. This transient behavior can be described as: i) activation of the monomer and polymerization into defined structures, ii) a short plateau and iii) deactivation and disassembly of the supramolecular structures. The transient self-assembly can be associated to a disassembly-assembly-disassembly transition. However, in a few systems the assembly gets transiently deactivated. Therefore, we observe a transient disassembly.[67,68]

Recently, a great effort has been made to classify these systems into well-defined cases in order to understand how fuels can be used to control the self-assembly.[88,89] Four classes have been identified[89]:

- *Templated self-assembly*: the fuel activates the monomer inducing self-assembly into a more thermodynamically stable structure. Then, the polymer dissociates restoring the initial monomer. In the chemical conversion of fuel to waste, no energy is dissipated;
- *Templated self-assembly under dissipative conditions*: the fuel templates the energetically favored self-assembly process. However, compared to the first class, the fuel is slowly degraded by external conditions (i.e., reactants, enzymes) and converted into waste. The waste is no longer templating the assembly, which leads to the disassembly of the structure. The fuel to waste transition leads to a temporary alteration of the energy landscape;
- *Dissipative assembly* (*kinetic symmetry*): compared to the previous two classes, in this case, the self-assembly process and the fuel consumption are coupled. That is, the energy stored in the fuel is used to shift the equilibrium (disassembled to assembled structure). In this class, kinetic symmetry is installed, thus the main species present is the thermodynamically most stable one, i.e., the assembled structure.[88] Energy is continuously being dissipated, as long as fuel is not fully consumed, but overall, the system is governed by thermodynamic stabilities.

- *Driven self-assembly* (*kinetic asymmetry*): in this class, the species in the system preferentially drive the cycle in one direction, that is fuel to waste conversion.[88] The fuel activates the monomer, and the deactivation is kinetically favored in the assembled state. The stationary concentrations reached in kinetic asymmetry are different from those at thermodynamic equilibrium. Therefore, as for microtubule structures, waste formation maintains the stationary non-equilibrium composition of the network.

This classification goes from thermodynamic controlled templated self-assembly to non-equilibrium systems. Nature performs spatiotemporal dynamic functions with the use of complex structures and dissipative processes. This organization is not possible at thermodynamic equilibrium and requires a continuous flow of energy. The comprehension of dissipative processes is essential and it has recently attracted more and more systems chemists.[88–91] In the process of designing similar functions in synthetic systems, it is crucial to assess the kinetic asymmetry. As such, the energy released by the consumption of fuel can drive the cycle towards a specific direction, inducing (dis)assembly of supramolecular structures.[88,92] A review of the literature clearly shows a lack of kinetic studies, which is crucial to understanding these systems. Specifically, systems chemists tend not to separate the kinetics of the self-assembly from the ones of the reactions network. The latter are essential for understanding the full complexity of these systems.

1.8. Aim and Outline of the Thesis

In this introduction we described the work that has been achieved so far in Systems Chemistry. Particularly, we stressed the role of ATP as trigger to control the assembly of supramolecular polymers and develop dissipative complex systems. Next, we discussed chemically driven synthetic systems focusing on what has been reported until now and the issues that are still present in the field.

In **Chapter 2**, we implement a previously reported enzymatic cycle[61] with the addition of an enzymatic reaction. The latter permits the continuous regeneration of fuel (ATP) *in situ* from waste. The investigation of the system lead to non-equilibrium pseudo steady states where the network was constantly pushed out-of-equilibrium as the fuel was regenerated. Interestingly, we observed an oscillatory behavior due to the multisite phosphorylation network.

Each reaction cycle released side-products, which affected the system. In Nature, by-products are used to control reactions and the production of metabolites. These processes are known as positive/negative feedback. In **Chapter 3**, we envisaged the regulation of the enzymatic activity using a competitive inhibitor. The inhibitor competed with the substrate for the interaction with the enzyme resulting in a negative feedback. Moreover, the inhibitor was designed to reach co-assembly between the different species present in the system. The formation of these supramolecular polymers will allow amplification of signals when a local stimulus is applied. Indeed, the self-assembly of the inhibitor with the substrate results in a negative and positive regulation of the enzymes present in the network, augmenting the communication inside the net.

The ultimate goal of this thesis is the development of 'life-like' materials. In **Chapter 4**, we designed and synthesized hydrogelators based on the peptide consensus sequence recognized by the enzymes present in the network. Then, the insertion of the reactions cycle in the material was investigated. In order to understand how the mechanical properties of the gel are affected by the enzymatic system, rheology experiments were carried out.

Finally, in **Chapter 5** a non-equilibrium reaction cycle was explored to achieve kinetic and structural control over a hydrogel. Treating the hydrogel, a sugar-based aldehyde-containing substrate, with sodium dithionite, a formaldehyde releasing molecule and a hydrolysable lactone led to its complete dissolution within a few minutes and its re-formation in less than one hour. The final material properties could be controlled by the amount of catalyst added.

Lastly, **Chapter 6** summarizes the results obtained and an outlook for further research on the development of non-equilibrium reaction cycles.

1.9. References

(1) Lehn, J.-M. Toward Self-Organization and Complex Matter. *Science* **2002**, *295* (5564), 2400–2403. https://doi.org/10.1126/science.1071063.

(2) Aida, T.; Meijer, E. W.; Stupp, S. I. Functional Supramolecular Polymers. *Science* **2012**, *335* (6070), 813–817. https://doi.org/10.1126/science.1205962.

(3) Alberts, B. *Molecular Biology of the Cell*, Sixth edition.; Garland Science, Taylor and Francis Group: New York, NY, 2015.

(4) Panja, S.; Patterson, C.; Adams, D. J. Temporally-Programmed Transient Supramolecular Gels. *Macromol. Rapid Commun.* **2019**, 40 (15), e1900251. https://doi.org/10.1002/marc.201900251.

(5) Angulo-Pachón, C. A.; Miravet, J. F. Sucrose-Fueled, Energy Dissipative, Transient Formation of Molecular Hydrogels Mediated by Yeast Activity. *Chem. Commun.* **2016**, *52* (31), 5398–5401. https://doi.org/10.1039/C6CC01183G.

(6) Mukhopadhyay, R. D.; Choi, S.; Sen, S. K.; Hwang, I.; Kim, K. Transient Self-assembly Processes Operated by Gaseous Fuels under Out-of-Equilibrium Conditions. *Chem Asian J* **2020**, *15* (23), 4118-4123. https://doi.org/10.1002/asia.202001183.

(7) Spitzer, D.; Rodrigues, L. L.; Straßburger, D.; Mezger, M.; Besenius, P. Tuneable Transient Thermogels Mediated by a PH- and Redox-Regulated Supramolecular Polymerization. *Angew. Chem. Int. Ed.* **2017**, *56* (48), 15461–15465. https://doi.org/10.1002/anie.201708857.

(8) Li, F.; Jiang, Y.; Zhang, B.; Huang, F.; Gao, Y.; Sun, L. Towards A Solar Fuel Device: Light-Driven Water Oxidation Catalyzed by a Supramolecular Assembly. *Angew. Chem. Int. Ed.* **2012**, *51* (10), 2417–2420. https://doi.org/10.1002/anie.201108051.

(9) Salzano de Luna, M.; Marturano, V.; Manganelli, M.; Santillo, C.; Ambrogi, V.; Filippone, G.; Cerruti, P. Light-Responsive and Self-Healing Behavior of Azobenzene-Based Supramolecular Hydrogels. *J. Colloid Interface Sci.* **2020**, *568*, 16–24. https://doi.org/10.1016/j.jcis.2020.02.038.

(10) Yin, Z.; Song, G.; Jiao, Y.; Zheng, P.; Xu, J.-F.; Zhang, X. Dissipative Supramolecular Polymerization Powered by Light. *CCS Chem.* **2019**, *1* (4), 335–342. https://doi.org/10.31635/ccschem.019.20190013.

(11) Ashkenasy, G.; Hermans, T. M.; Otto, S.; Taylor, A. F. Systems Chemistry. *Chem. Soc. Rev.* **2017**, *46* (9), 2543–2554. https://doi.org/10.1039/C7CS00117G.

(12) Sorrenti, A.; Leira-Iglesias, J.; Markvoort, A. J.; de Greef, T. F. A.; Hermans, T. M. Non-Equilibrium Supramolecular Polymerization. *Chem. Soc. Rev.* **2017**, *46* (18), 5476–5490. https://doi.org/10.1039/C7CS00121E.

(13) Lehn, J.-M. Toward Complex Matter: Supramolecular Chemistry and Self-Organization. *Proc. Natl. Acad. Sci.* **2002**, *99* (8), 4763–4768. https://doi.org/10.1073/pnas.072065599.

(14) De Greef, T. F. A.; Smulders, M. M. J.; Wolffs, M.; Schenning, A. P. H. J.; Sijbesma, R. P.; Meijer, E. W. Supramolecular Polymerization. *Chem. Rev.* **2009**, *109* (11), 5687–5754. https://doi.org/10.1021/cr900181u.

(15) Tantakitti, F.; Boekhoven, J.; Wang, X.; Kazantsev, R. V.; Yu, T.; Li, J.; Zhuang, E.; Zandi, R.; Ortony, J. H.; Newcomb, C. J.; Palmer, L. C.; Shekhawat, G. S.; de la Cruz, M. O.; Schatz, G. C.; Stupp, S. I. Energy Landscapes and Functions of Supramolecular Systems. *Nat. Mater.* **2016**, *15* (4), 469–476. https://doi.org/10.1038/nmat4538.

(16) Mattia, E.; Otto, S. Supramolecular Systems Chemistry. *Nat. Nanotechnol.* **2015**, *10* (2), 111–119. https://doi.org/10.1038/nnano.2014.337.

(17) Boekhoven, J.; Brizard, A. M.; Kowlgi, K. N. K.; Koper, G. J. M.; Eelkema, R.; van Esch, J. H. Dissipative Self-Assembly of a Molecular Gelator by Using a Chemical Fuel. *Angew. Chem. Int. Ed.* **2010**, *49* (28), 4825–4828. https://doi.org/10.1002/anie.201001511.

(18) Boekhoven, J.; Hendriksen, W. E.; Koper, G. J. M.; Eelkema, R.; van Esch, J. H. Transient Assembly of Active Materials Fueled by a Chemical Reaction. *Science* **2015**, *349* (6252), 1075–1079. https://doi.org/10.1126/science.aac6103.

(19) Debnath, S.; Roy, S.; Ulijn, R. V. Peptide Nanofibers with Dynamic Instability through Nonequilibrium Biocatalytic Assembly. *J. Am. Chem. Soc.* **2013**, *135* (45), 16789–16792. https://doi.org/10.1021/ja4086353.

(20) Maiti, S.; Fortunati, I.; Ferrante, C.; Scrimin, P.; Prins, L. J. Dissipative Self-Assembly of Vesicular Nanoreactors. *Nat. Chem.* **2016**, *8* (7), 725–731. https://doi.org/10.1038/nchem.2511.

(21) Smulders, M. J.; Nieuwenhuizen, M. L.; de Greef, T. A.; van der Schoot, P.; Schenning, A. H. J.; Meijer, E. W. How to Distinguish Isodesmic from Cooperative Supramolecular Polymerisation. *Chem. - Eur. J.* **2010**, *16* (1), 362–367. https://doi.org/10.1002/chem.200902415.

(22) Korevaar, P. A.; de Greef, T. F. A.; Meijer, E. W. Pathway Complexity in π-Conjugated Materials. *Chem. Mater.* **2014**, *26* (1), 576–586. https://doi.org/10.1021/cm4021172.

(23) Jonkheijm, P.; van der Schoot, P.; Schenning, A. P. H. J.; Meijer, E. W. Probing the Solvent-Assisted Nucleation Pathway in Chemical Self-Assembly. *Science* **2006**, *313* (5783), 80–83. https://doi.org/10.1126/science.1127884.

(24) Korevaar, P. A.; George, S. J.; Markvoort, A. J.; Smulders, M. M. J.; Hilbers, P. A. J.; Schenning, A. P. H. J.; De Greef, T. F. A.; Meijer, E. W. Pathway Complexity in Supramolecular Polymerization. *Nature* **2012**, *481* (7382), 492–496. https://doi.org/10.1038/nature10720.
(25) Markvoort, A. J.; Eikelder, H. M. M. ten; Hilbers, P. A. J.; de Greef, T. F. A. Fragmentation and Coagulation in Supramolecular (Co)Polymerization Kinetics. *ACS Cent. Sci.* **2016**, *2* (4), 232–241. https://doi.org/10.1021/acscentsci.6b00009.
(26) van der Zwaag, D.; Pieters, P. A.; Korevaar, P. A.; Markvoort, A. J.; Spiering, A. J. H.; de Greef, T. F. A.; Meijer, E. W. Kinetic Analysis as a Tool to Distinguish Pathway Complexity in Molecular Assembly: An Unexpected Outcome of Structures in Competition. *J. Am. Chem. Soc.* **2015**, *137* (39), 12677–12688. https://doi.org/10.1021/jacs.5b08138.
(27) Escudero, C.; D'Urso, A.; Lauceri, R.; Bonaccorso, C.; Sciotto, D.; Di Bella, S.; El-Hachemi, Z.; Crusats, J.; Ribó, J. M.; Purrello, R. Hierarchical Dependence of Porphyrin Self-Aggregation: Controlling and Exploiting the Complexity. *J. Porphyr. Phthalocyanines* **2010**, *14* (08), 708–712. https://doi.org/10.1142/S1088424610002525.
(28) El-Hachemi, Z.; Mancini, G.; Ribó, J. M.; Sorrenti, A. Role of the Hydrophobic Effect in the Transfer of Chirality from Molecules to Complex Systems: From Chiral Surfactants to Porphyrin/Surfactant Aggregates. *J. Am. Chem. Soc.* **2008**, *130* (45), 15176–15184. https://doi.org/10.1021/ja805669v.
(29) Hermans, T. M.; Broeren, M. A. C.; Gomopoulos, N.; Smeijers, A. F.; Mezari, B.; Van Leeuwen, E. N. M.; Vos, M. R. J.; Magusin, P. C. M. M.; Hilbers, P. A. J.; Van Genderen, M. H. P.; Sommerdijk, N. A. J. M.; Fytas, G.; Meijer. Stepwise Noncovalent Synthesis Leading to Dendrimer-Based Assemblies in Water. *J. Am. Chem. Soc.* **2007**, *129* (50), 15631–15638. https://doi.org/10.1021/ja074991t.
(30) Hermans, T. M.; Broeren, M. A. C.; Gomopoulos, N.; van der Schoot, P.; van Genderen, M. H. P.; Sommerdijk, N. A. J. M.; Fytas, G.; Meijer, E. W. Self-Assembly of Soft Nanoparticles with Tunable Patchiness. *Nat. Nanotechnol.* **2009**, *4* (11), 721–726. https://doi.org/10.1038/nnano.2009.232.
(31) Ferrier, D. R. *Biochemistry*, 6th ed.; Lippincott's illustrated reviews; Wolters Kluwer Health/Lippincott Williams & Wilkins: Philadelphia, 2014.
(32) Heinen, L.; Walther, A. Celebrating Soft Matter's 10th Anniversary: Approaches to Program the Time Domain of Self-Assemblies. *Soft Matter* **2015**, *11* (40), 7857–7866. https://doi.org/10.1039/C5SM01660F.
(33) Brouhard, G. J.; Rice, L. M. Microtubule Dynamics: An Interplay of Biochemistry and Mechanics. *Nat. Rev. Mol. Cell Biol.* **2018**, *19* (7), 451–463. https://doi.org/10.1038/s41580-018-0009-y.
(34) Arai, T.; Kaziro, Y. Effect of Guanine Nucleotides on the Assembly of Brain Microtubules: Ability of 5'-Guanylyl Imidodiphosphate to Replace GTP in Promoting the Polymerization of Microtubules in Vitro. *Biochem. Biophys. Res. Commun.* **1976**, *69* (2), 369–376. https://doi.org/10.1016/0006-291X(76)90531-3.
(35) Katrukha, K. A.; Guriya, G. T. Dynamic Instabilities in the Microtubule Cytoskeleton: A State Diagram. *Biophysics* **2006**, *51* (5), 781–788.
(36) Merindol, R.; Walther, A. Materials Learning from Life: Concepts for Active, Adaptive and Autonomous Molecular Systems. *Chem. Soc. Rev.* **2017**, *46* (18), 5588–5619. https://doi.org/10.1039/C6CS00738D.
(37) Blanchoin, L.; Boujemaa-Paterski, R.; Sykes, C.; Plastino, J. Actin Dynamics, Architecture, and Mechanics in Cell Motility. *Physiol. Rev.* **2014**, *94* (1), 235–263. https://doi.org/10.1152/physrev.00018.2013.
(38) Bergman, J. ATP: The Perfect Energy Currency for the Cell. *Creat. Res. Soc.* **1999**, *36* (1), 15.
(39) Boyer, P. D. Energy, Life, and ATP (Nobel Lecture). *Angew Chem Int Ed* **1998**, *37*, 2296–2307.
(40) Davies, P. C. W.; Rieper, E.; Tuszynski, J. A. Self-Organization and Entropy Reduction in a Living Cell. *Biosystems* **2013**, *111* (1), 1–10. https://doi.org/10.1016/j.biosystems.2012.10.005.
(41) Jeske, L.; Placzek, S.; Schomburg, I.; Chang, A.; Schomburg, D. BRENDA in 2019: A European ELIXIR Core Data Resource. *Nucleic Acids Res.* **2019**, *47* (D1), D542–D549. https://doi.org/10.1093/nar/gky1048.
(42) Deng, J.; Walther, A. ATP-Responsive and ATP-Fueled Self-Assembling Systems and Materials. *Adv Mater* **2020**, 32 (42), 2002629.
(43) Huizenga, D. E.; Szostak, J. W. A DNA Aptamer That Binds Adenosine and ATP. *Biochemistry* **1995**, *34* (2), 656–665. https://doi.org/10.1021/bi00002a033.
(44) Del Grosso, E.; Amodio, A.; Ragazzon, G.; Prins, L. J.; Ricci, F. Dissipative Synthetic DNA-Based Receptors for the Transient Loading and Release of Molecular Cargo. *Angew. Chem. Int. Ed.* **2018**, *57* (33), 10489–10493. https://doi.org/10.1002/anie.201801318.
(45) Del Grosso, E.; Ragazzon, G.; Prins, L. J.; Ricci, F. Fuel-Responsive Allosteric DNA-Based Aptamers for the Transient Release of ATP and Cocaine. *Angew. Chem. Int. Ed.* **2019**, *58* (17), 5582–5586. https://doi.org/10.1002/anie.201812885.
(46) Merindol, R.; Loescher, S.; Samanta, A.; Walther, A. Pathway-Controlled Formation of Mesostructured All-DNA Colloids and Superstructures. *Nat. Nanotechnol.* **2018**, *13* (8), 730–738. https://doi.org/10.1038/s41565-018-0168-1.
(47) Deng, J.; Walther, A. Pathway Complexity in Fuel-Driven DNA Nanostructures with Autonomous Reconfiguration

of Multiple Dynamic Steady States. *J. Am. Chem. Soc.* **2020**, *142* (2), 685–689. https://doi.org/10.1021/jacs.9b11598.

(48) Sazani, P. L.; Larralde, R.; Szostak, J. W. A Small Aptamer with Strong and Specific Recognition of the Triphosphate of ATP. *J Am Chem Soc* **2004**, *126* (27), 8370–8371.

(49) Webber, M. J.; Newcomb, C. J.; Bitton, R.; Stupp, S. I. Switching of Self-Assembly in a Peptide Nanostructure with a Specific Enzyme. *Soft Matter* **2011**, *7* (20), 9665. https://doi.org/10.1039/c1sm05610g.

(50) Yang, Z.; Liang, G.; Wang, L.; Xu, B. Using a Kinase/Phosphatase Switch to Regulate a Supramolecular Hydrogel and Forming the Supramolecular Hydrogel in Vivo. *J. Am. Chem. Soc.* **2006**, *128* (9), 3038–3043. https://doi.org/10.1021/ja057412y.

(51) Biswas, S.; Kinbara, K.; Niwa, T.; Taguchi, H.; Ishii, N.; Watanabe, S.; Miyata, K.; Kataoka, K.; Aida, T. Biomolecular Robotics for Chemomechanically Driven Guest Delivery Fuelled by Intracellular ATP. *Nat. Chem.* **2013**, *5* (7), 613–620. https://doi.org/10.1038/nchem.1681.

(52) Biswas, S.; Kinbara, K.; Oya, N.; Ishii, N.; Taguchi, H.; Aida, T. A Tubular Biocontainer: Metal Ion-Induced 1D Assembly of a Molecularly Engineered Chaperonin. *J Am Chem Soc* **2009**, *131* (22), 7556–7557.

(53) Kumar, M.; Brocorens, P.; Tonnelé, C.; Beljonne, D.; Surin, M.; George, S. J. A Dynamic Supramolecular Polymer with Stimuli-Responsive Handedness for in Situ Probing of Enzymatic ATP Hydrolysis. *Nat. Commun.* **2014**, *5* (1), 5793. https://doi.org/10.1038/ncomms6793.

(54) Dhiman, S.; Jain, A.; George, S. J. Transient Helicity: Fuel-Driven Temporal Control over Conformational Switching in a Supramolecular Polymer. *Angew. Chem. Int. Ed.* **2017**, *56* (5), 1329–1333. https://doi.org/10.1002/anie.201610946.

(55) Grzybowski, B. A.; Huck, W. T. S. The Nanotechnology of Life-Inspired Systems. *Nat. Nanotechnol.* **2016**, *11* (7), 585–592. https://doi.org/10.1038/nnano.2016.116.

(56) Koga, S.; Williams, D. S.; Perriman, A. W.; Mann, S. Peptide–Nucleotide Microdroplets as a Step towards a Membrane-Free Protocell Model. *Nat. Chem.* **2011**, *3* (9), 720–724. https://doi.org/10.1038/nchem.1110.

(57) Nakashima, K. K.; Baaij, J. F.; Spruijt, E. Reversible Generation of Coacervate Droplets in an Enzymatic Network. *Soft Matter* **2018**, *14* (3), 361–367. https://doi.org/10.1039/C7SM01897E.

(58) Singh, N.; Formon, G. J. M.; De Piccoli, S.; Hermans, T. M. Devising Synthetic Reaction Cycles for Dissipative Nonequilibrium Self-Assembly. *Adv. Mater.* **2020**, *32* (20), 1906834. https://doi.org/10.1002/adma.201906834.

(59) Montagne, K.; Plasson, R.; Sakai, Y.; Fujii, T.; Rondelez, Y. Programming an *in Vitro* DNA Oscillator Using a Molecular Networking Strategy. *Mol. Syst. Biol.* **2011**, *7* (1), 466. https://doi.org/10.1038/msb.2010.120.

(60) Green, L. N.; Subramanian, H. K. K.; Mardanlou, V.; Kim, J.; Hariadi, R. F.; Franco, E. Autonomous Dynamic Control of DNA Nanostructure Self-Assembly. *Nat. Chem.* **2019**, *11* (6), 510–520. https://doi.org/10.1038/s41557-019-0251-8.

(61) Sorrenti, A.; Leira-Iglesias, J.; Sato, A.; Hermans, T. M. Non-Equilibrium Steady States in Supramolecular Polymerization. *Nat. Commun.* **2017**, *8* (1), 15899. https://doi.org/10.1038/ncomms15899.

(62) Mishra, A.; Korlepara, D. B.; Kumar, M.; Jain, A.; Jonnalagadda, N.; Bejagam, K. K.; Balasubramanian, S.; George, S. J. Biomimetic Temporal Self-Assembly via Fuel-Driven Controlled Supramolecular Polymerization. *Nat. Commun.* **2018**, *9* (1), 1295. https://doi.org/10.1038/s41467-018-03542-z.

(63) Heinen, L.; Walther, A. Programmable Dynamic Steady States in ATP-Driven Nonequilibrium DNA Systems. *Sci. Adv.* **2019**, 5 (7), eaaw0590.

(64) Heuser, T.; Steppert, A.-K.; Molano Lopez, C.; Zhu, B.; Walther, A. Generic Concept to Program the Time Domain of Self-Assemblies with a Self-Regulation Mechanism. *Nano Lett.* **2015**, *15* (4), 2213–2219. https://doi.org/10.1021/nl5039506.

(65) Panzarasa, G.; Sai, T.; Torzynski, A. L.; Smith-Mannschott, K.; Dufresne, E. R. Supramolecular Assembly by Time-Programmed Acid Autocatalysis. *Mol. Syst. Des. Eng.* **2020**, *5* (2), 445–448. https://doi.org/10.1039/C9ME00139E.

(66) Wojciechowski, J. P.; Martin, A. D.; Thordarson, P. Kinetically Controlled Lifetimes in Redox-Responsive Transient Supramolecular Hydrogels. *J. Am. Chem. Soc.* **2018**, *140* (8), 2869–2874. https://doi.org/10.1021/jacs.7b12198.

(67) Leira-Iglesias, J.; Sorrenti, A.; Sato, A.; Dunne, P. A.; Hermans, T. M. Supramolecular Pathway Selection of Perylenediimides Mediated by Chemical Fuels. *Chem. Commun.* **2016**, *52* (58), 9009–9012. https://doi.org/10.1039/C6CC01192F.

(68) Leira-Iglesias, J.; Tassoni, A.; Adachi, T.; Stich, M.; Hermans, T. M. Oscillations, Travelling Fronts and Patterns in a Supramolecular System. *Nat. Nanotechnol.* **2018**, *13* (11), 1021–1027. https://doi.org/10.1038/s41565-018-0270-4.

(69) van Ravensteijn, B. G. P.; Hendriksen, W. E.; Eelkema, R.; van Esch, J. H.; Kegel, W. K. Fuel-Mediated Transient Clustering of Colloidal Building Blocks. *J. Am. Chem. Soc.* **2017**, *139* (29), 9763–9766. https://doi.org/10.1021/jacs.7b03263.

(70) Tena-Solsona, M.; Rieß, B.; Grötsch, R. K.; Löhrer, F. C.; Wanzke, C.; Käsdorf, B.; Bausch, A. R.; Müller-Buschbaum,

P.; Lieleg, O.; Boekhoven, J. Non-Equilibrium Dissipative Supramolecular Materials with a Tunable Lifetime. *Nat. Commun.* **2017**, *8* (1), 15895. https://doi.org/10.1038/ncomms15895.

(71) Kariyawasam, L. S.; Hartley, C. S. Dissipative Assembly of Aqueous Carboxylic Acid Anhydrides Fueled by Carbodiimides. *J. Am. Chem. Soc.* **2017**, *139* (34), 11949–11955. https://doi.org/10.1021/jacs.7b06099.

(72) Tena-Solsona, M.; Wanzke, C.; Riess, B.; Bausch, A. R.; Boekhoven, J. Self-Selection of Dissipative Assemblies Driven by Primitive Chemical Reaction Networks. *Nat. Commun.* **2018**, *9* (1), 2044. https://doi.org/10.1038/s41467-018-04488-y.

(73) Rieß, B.; Wanzke, C.; Tena-Solsona, M.; Grötsch, R. K.; Maity, C.; Boekhoven, J. Dissipative Assemblies That Inhibit Their Deactivation. *Soft Matter* **2018**, *14* (23), 4852–4859. https://doi.org/10.1039/C8SM00822A.

(74) Grötsch, R. K.; Angı, A.; Mideksa, Y. G.; Wanzke, C.; Tena-Solsona, M.; Feige, M. J.; Rieger, B.; Boekhoven, J. Dissipative Self-Assembly of Photoluminescent Silicon Nanocrystals. *Angew. Chem. Int. Ed.* **2018**, *57* (44), 14608–14612. https://doi.org/10.1002/anie.201807937.

(75) Zhang, B.; Jayalath, I. M.; Ke, J.; Sparks, J. L.; Hartley, C. S.; Konkolewicz, D. Chemically Fueled Covalent Crosslinking of Polymer Materials. *Chem. Commun.* **2019**, *55* (14), 2086–2089. https://doi.org/10.1039/C8CC09823A.

(76) Grötsch, R. K.; Wanzke, C.; Speckbacher, M.; Angı, A.; Rieger, B.; Boekhoven, J. Pathway Dependence in the Fuel-Driven Dissipative Self-Assembly of Nanoparticles. *J. Am. Chem. Soc.* **2019**, *141* (25), 9872–9878. https://doi.org/10.1021/jacs.9b02004.

(77) Wanzke, C.; Jussupow, A.; Kohler, F.; Dietz, H.; Kaila, V. R. I.; Boekhoven, J. Dynamic Vesicles Formed By Dissipative Self-Assembly. *ChemSystemsChem* **2020**, *2* (1), e1900044. https://doi.org/10.1002/syst.201900044.

(78) Panja, S.; Dietrich, B.; Adams, D. J. Chemically Fuelled Self-Regulating Gel-to-Gel Transition. *ChemSystemsChem* **2020**, *2* (1), e1900038. https://doi.org/10.1002/syst.201900038.

(79) Dambenieks, A. K.; Vu, P. H. Q.; Fyles, T. M. Dissipative Assembly of a Membrane Transport System. *Chem Sci* **2014**, *5* (9), 3396–3403. https://doi.org/10.1039/C4SC01258E.

(80) Colomer, I.; Morrow, S. M.; Fletcher, S. P. A Transient Self-Assembling Self-Replicator. *Nat. Commun.* **2018**, *9* (1), 2239. https://doi.org/10.1038/s41467-018-04670-2.

(81) Morrow, S. M.; Colomer, I.; Fletcher, S. P. A Chemically Fuelled Self-Replicator. *Nat. Commun.* **2019**, *10* (1), 1011. https://doi.org/10.1038/s41467-019-08885-9.

(82) Wood, C. S.; Browne, C.; Wood, D. M.; Nitschke, J. R. Fuel-Controlled Reassembly of Metal–Organic Architectures. *ACS Cent. Sci.* **2015**, *1* (9), 504–509. https://doi.org/10.1021/acscentsci.5b00279.

(83) Bal, S.; Das, K.; Ahmed, S.; Das, D. Chemically Fueled Dissipative Self-Assembly That Exploits Cooperative Catalysis. *Angew. Chem. Int. Ed.* **2019**, *58* (1), 244–247. https://doi.org/10.1002/anie.201811749.

(84) Afrose, S. P.; Bal, S.; Chatterjee, A.; Das, K.; Das, D. Designed Negative Feedback from Transiently Formed Catalytic Nanostructures. *Angew. Chem. Int. Ed.* **2019**, *58* (44), 15783–15787. https://doi.org/10.1002/anie.201910280.

(85) Jain, A.; Dhiman, S.; Dhayani, A.; Vemula, P. K.; George, S. J. Chemical Fuel-Driven Living and Transient Supramolecular Polymerization. *Nat. Commun.* **2019**, *10* (1), 450. https://doi.org/10.1038/s41467-019-08308-9.

(86) Singh, N.; Lainer, B.; Formon, G. J. M.; De Piccoli, S.; Hermans, T. M. Re-Programming Hydrogel Properties Using a Fuel-Driven Reaction Cycle. *J. Am. Chem. Soc.* **2020**, *142* (9), 4083–4087. https://doi.org/10.1021/jacs.9b11503.

(87) Wang, H.; Wang, Y.; Shen, B.; Liu, X.; Lee, M. Substrate-Driven Transient Self-Assembly and Spontaneous Disassembly Directed by Chemical Reaction with Product Release. *J. Am. Chem. Soc.* **2019**, *141* (10), 4182–4185. https://doi.org/10.1021/jacs.8b12777.

(88) Ragazzon, G.; Prins, L. J. Energy Consumption in Chemical Fuel-Driven Self-Assembly. *Nat. Nanotechnol.* **2018**, *13* (10), 882–889. https://doi.org/10.1038/s41565-018-0250-8.

(89) Das, K.; Gabrielli, L.; Prins, L. J. Chemically-fueled Self-assembly in Biology and Chemistry. *Angew. Chem. Int. Ed.* **2021**, anie.202100274. https://doi.org/10.1002/anie.202100274.

(90) Dou, Y.; Dhatt-Gauthier, K.; Bishop, K. J. M. Thermodynamic Costs of Dynamic Function in Active Soft Matter. *Curr. Opin. Solid State Mater. Sci.* **2019**, *23* (1), 28–40. https://doi.org/10.1016/j.cossms.2018.11.002.

(91) van der Helm, M. P.; de Beun, T.; Eelkema, R. On the Use of Catalysis to Bias Reaction Pathways in Out-of-Equilibrium Systems. *Chem. Sci.* **2021**, 12, 4484-4493. 10.1039.D0SC06406H. https://doi.org/10.1039/D0SC06406H.

(92) Astumian, R. D. Kinetic Asymmetry Allows Macromolecular Catalysts to Drive an Information Ratchet. *Nat. Commun.* **2019**, *10* (1), 3837. https://doi.org/10.1038/s41467-019-11402-7.

Chapter 2.

Pseudo Steady States and Oscillations in a Complex Enzymatic Network under batch conditions

Abstract

In this Chapter, we show that long-lived (pseudo) steady states of up to 7 hours can be achieved in a chemically fueled phosphorylation/dephosphorylation network. We build on a previously reported enzymatic system and incorporate a new step that turns a waste product (ADP) back into a chemical fuel (ATP) by using a 'pre-fuel'. This approach has resulted in non-equilibrium steady states by varying the concentration of pre-fuel added to the system. The amount of pre-fuel is correlated to the production of fuel and the dynamics of the phosphorylation and dephosphorylation network. Additionally, we report the emergence of batch oscillations arising from the network, which surprisingly persist even under non-stirred conditions.

2.1. Introduction

In Chapter 1 we have discussed important steps that have been achieved in the past years in the field of Systems Chemistry. Much of the work that has been reported so far is inspired by Nature and the delicate balance of complex networks. Such networks in our cells are crucial for signaling, motion, self-reproduction and many other vital functions.[1,2] Adenosine triphosphate (ATP) is a crucial source of energy to keep and sustained all the dynamics in the cell. The consumption of ATP, its hydrolysis to ADP and an inorganic phosphate and its recycling are central for the control of basic processes of life.[3] Enzymes are macromolecules of crucial importance for biological functions and they regulate signal transduction by coupling unfavorable processes with the hydrolysis of ATP (energetically favorable).[4] For cell regulation, for example, enzymes as kinases or phosphates are used for the phosphorylation or dephosphorylation, respectively, of substrates or enzymes.[5] These processes permit the communication between different parts of the cell and the transmitting of the signal from one cell to the other. Additionally, enzymes are involved in the regulation of different dissipative supramolecular structures, such as microtubules or actin filaments that are sustained by constant addition of chemical fuels (GTP and ATP, see Chapter 1). Indeed, microtubules are kept steadily under non-equilibrium by guanosine triphosphate (GTP) turnover, allowing the simultaneous formation and shrinkage of tubules structure.[6] Therefore, microtubules result into a stiff material capable of changing its mechanical properties and adapting to environment changes. This adaptation is important, among others, for the motility and self-reproduction of cells.[1] Understanding these processes (i.e., cell's signaling, self-organization and reproduction) is essential for the engineering of new synthetic supramolecular systems.[7]

In our group, an enzymatic reaction network has been previously developed.[8] The system is based on the phosphorylation and the dephosphorylation of a symmetric peptide derivative of 3,4,9,10-perylenediimide (**PDI** in Figure 2.1, half of the molecule is presented). The core of the substrate is a widely used building block in supramolecular chemistry; the perylene diimide derivative derives from perylene-3,4,9,10-tetracarboxylic acid diimide (PDI). The scaffold self-assembly can be controlled through π-π stacking, electrostatic interactions and the hydrophobic effect.[9] The substrate **PDI** contains the consensus sequence LRRASLG which is recognized by the cAMP-dependent protein kinase A (PKA) and the lambda phosphatase (λPP).[10] The two enzymes operate at the serine residue of the peptide sequence. In the presence of ATP (fuel), PKA can transfer one phosphate group from the adenosine phosphate to the serine residue causing the phosphorylation of the substrate and leading to, first **p-PDI** (monophosphorylated) and,

consequently, to **p2-PDI** (diphosphorylated). The phosphate groups are, then, cleaved by λPP recovering the initial dephosphorylated substrate. The dephosphorylation **p2-PDI→PDI** passes through the formation of the monophosphorylated **p-PDI**. Each phosphorylation and dephosphorylation cycle produces ADP and an inorganic phosphate Pi, from the hydrolysis of ATP.

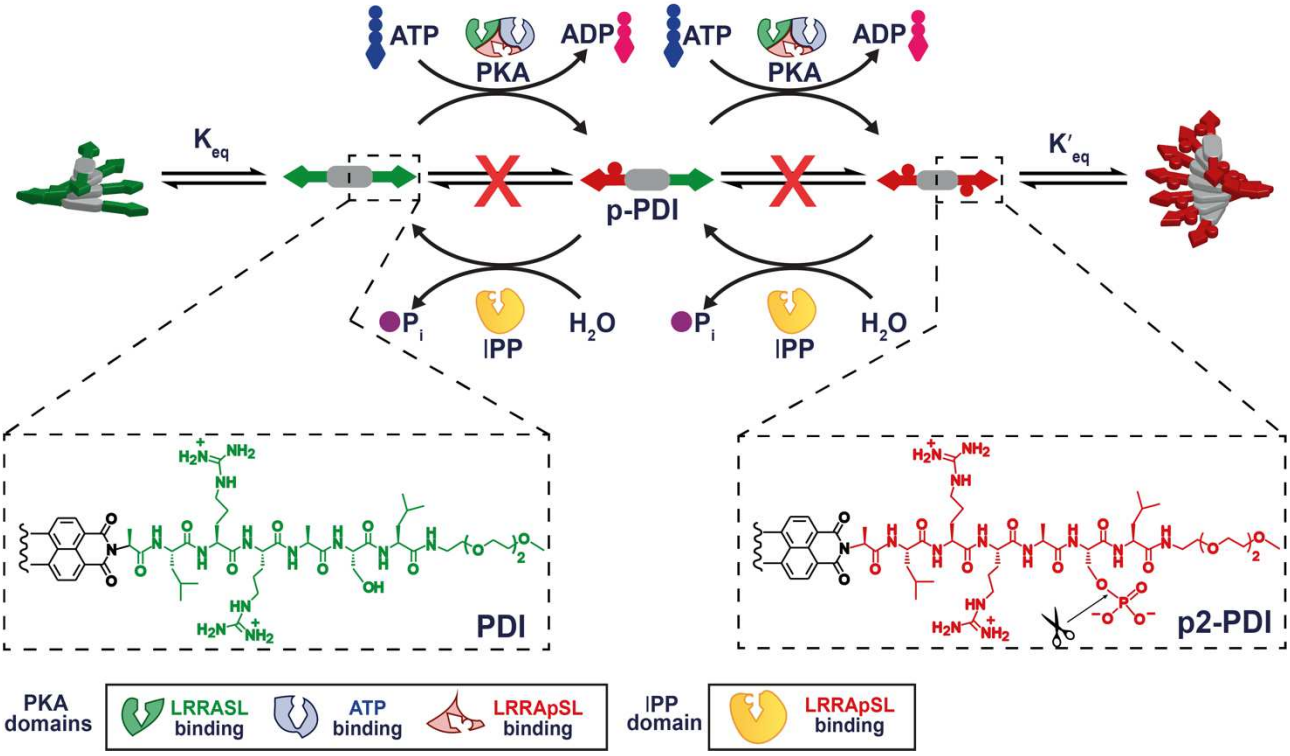

Figure 2.1. Enzyme-controlled Supramolecular Polymerization. PDI (half is shown) is phosphorylated at the serine residue of the peptide sequence by a protein kinase A (PKA) in the presence of ATP (fuel), leading to **p-PDI** (monophosphorylated) and **p2-PDI** (diphosphorylated). ATP is hydrolyzed to ADP. The dephosphorylation is performed by the λPP (scissors) yielding inorganic phosphate Pi and restoring **PDI**. PKA has three binding sites: for the LRRASL (green), the ATP (blue) and for LRRApSL (red). Reproduced from Ref.[8]

The phosphorylation of the substrate **PDI** introduces negative charges onto the molecule; 4^+ for **PDI** (electrostatic interactions) and nearly zwitterionic $4^+/3.3^-$ for **p2-PDI**. The resulting stability and structure of the supramolecular polymer is affected. Besides that, the self-assembly of the derivative **PDI** is driven by the presence of a core of perylene diimide. The latter consists of a rigid polycyclic scaffold substituted with two amide groups at the 3,4- and 9,10- positions, creating a flat and rigid π-conjugated system. The substrate is prone to self-assemble in aqueous media *via* π-π stacking and hydrophobic effect.[9,11] Overall, we can reach the control of supramolecular polymerization by (de)phosphorylation of **PDI**.

2.2. Previous Studies from our group

The effect of the phosphorylation on the self-assembly of **PDI** was first studied by UV-Vis spectroscopy. **PDI** dissolves in the reaction buffer at mM concentrations, giving a pink solution that remains stable over time. UV-Vis spectra of **PDI** shows a wide absorption in the range between 400 to 620 nm due to the S0→S1 electronic transitions of the core with maxima at 504 and 540 nm (A_{504nm} and A_{540nm}). The variation between the 0-0 and 0-1 transitions ($A_{0\text{-}1}/A_{0\text{-}0}$) was used to elucidate the self-assembly process (an increase of the ratio indicates further aggregation of assemblies; the value for monomeric species in solution is about 0.65).[9] Specifically, the lack of vibronic progression of monomeric PDIs and the ratio A_{504nm}/A_{540nm} of 1.46 indicate that **PDI** self-assembles into helical stacks through π–π stacking (H-aggregation).[9,11,12] Upon addition of PKA and ATP, a decrease of the two maxima (Figure 2.2A) and an increase of the ratio A_{504nm}/A_{540nm} to 1.65 (Figure 2.2B) were observed. The overall increase of the ratio suggested that **p2-PDI** assemblies grow into bigger structures.

In the second place, the system was studied by circular dichroism (CD) spectroscopy. **PDI** displays an asymmetric positive couplet at the main absorption band of the chromophore (black line in Figure 2.2C) characteristic of right-handed P-helical assemblies. Surprisingly, the phosphorylation to **p2-PDI** induces the inversion of the CD signal to a negative couplet (red line in Figure 2.2C) indicating the formation of left-handed M-helical assemblies.[13–15]

The UV-Vis and CD spectroscopy studies revealed that the phosphorylation of the substrate **PDI** to **p2-PDI**, not only induces further aggregation but it shows also the inversion of the supramolecular chirality of the assembly.

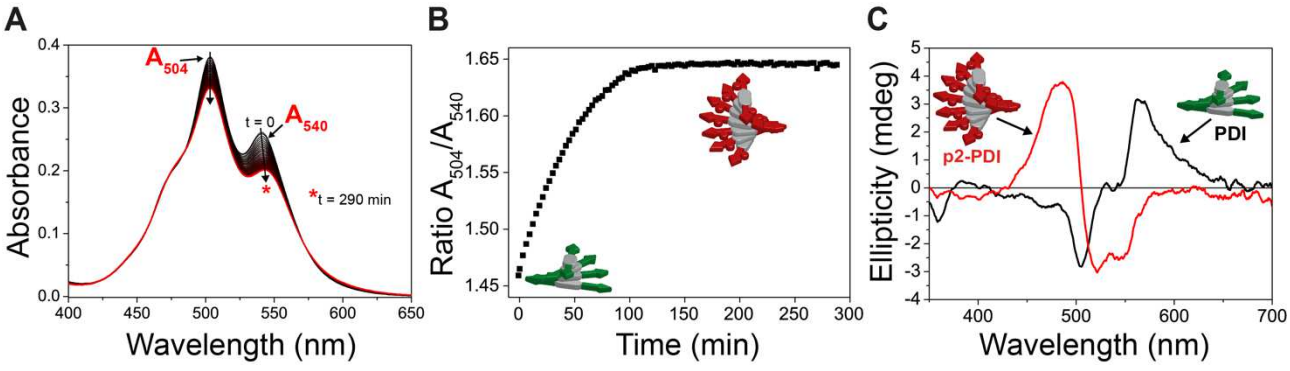

Figure 2.2. Phosphorylation induces Changes in the Supramolecular Polymerization. (A) UV-Vis spectrum of a 200 μM **PDI** solution (optical path 1 mm) during phosphorylation triggered by PKA (0.13 μM) and ATP (400 μM), showing the evolution of the two maxima at 504 and 540 nm. (B) Time course ratio A_{504nm}/A_{540nm} during phosphorylation; the data are extracted from the spectrum A. (C) CD spectrum of 200 μM **PDI** (black line) and **p2-PDI** (red line) solutions (optical path 1 mm). Reproduced from Ref.[8]

My former colleagues showed three different types of experiments outlined in Figure 2.3: A) a stimuli-responsive experiment where the phosphorylation and dephosphorylation are completely decoupled, B) a transient self-assembly experiment, where a single shot of fuel leads to enhanced assembly followed by disassembly, and C) different non-equilibrium steady states (NESS) that depend on the concentration of ATP maintained in a membrane reactor. I will now briefly describe each of these three types of experiments.

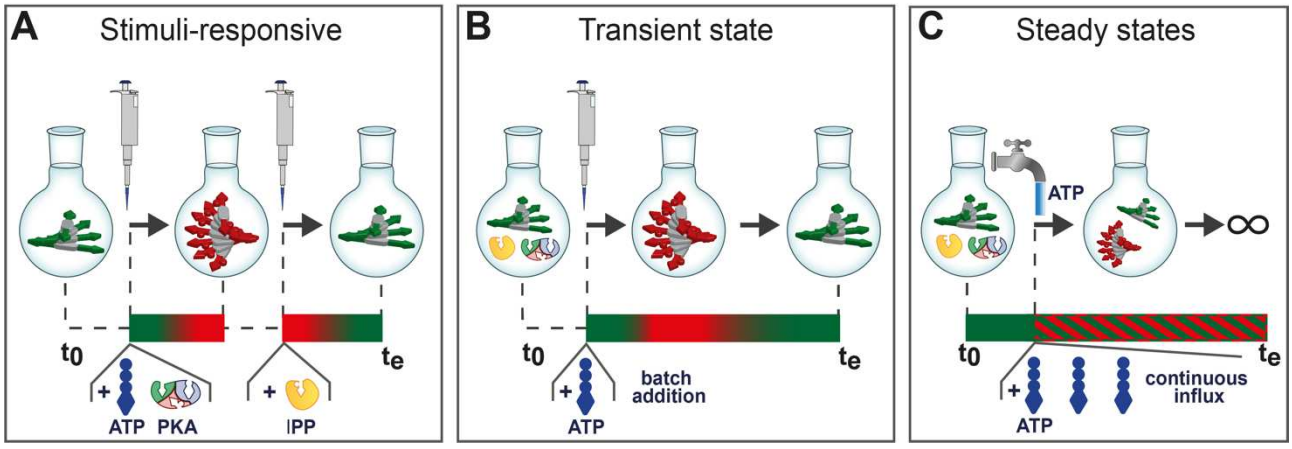

Figure 2.3. From Stimuli-responsive to NESS conditions. (A) Stimuli-responsiveness: the addition of ATP and PKA to a solution of **PDI** results in **p2-PDI** and a change in the supramolecular structure. A second stimulus is needed to recover the initial non-phosphorylated structure (i.e., the addition of λPP). (B) Transient state: the addition of ATP to a batch containing PKA and λPP, leads to a transient change of the supramolecular assembly. (C) Supramolecular non-equilibrium steady states (NESS): the system is kept in a dissipative steady state by continuous influx of ATP. Reproduced from Ref.[8]

Stimuli-responsive. The differences in the CD spectra between **PDI** and **p2-PDI** assemblies allowed to track the wavelength in time in the range between 475 to 500 nm. Phosphorylation and dephosphorylation were studied separately; as shown in Figure 2.4, the addition of ATP and PKA to a **PDI** solution induced a progressive change in the CD signal. The spectrum shows that a plateau can be reached over time, indicating the conversion of **PDI** to **p2-PDI**. The latter was also verified by LC-MS. Then, λPP is added to **p2-PDI** solution causing a fast decrease of the ellipticity to the initial value in agreement with full dephosphorylation and recovery of **PDI**.

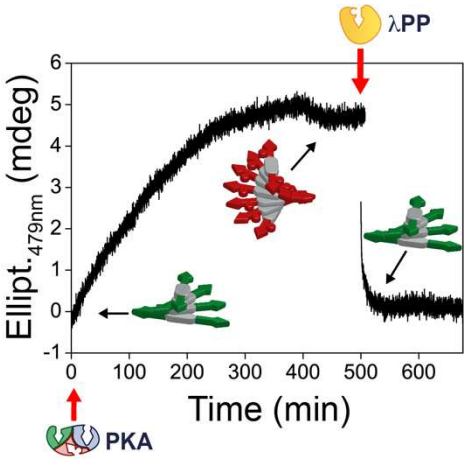

Figure 2.4. Stepwise Phosphorylation/Dephosphorylation. Time course CD measurements of a 200 μM **PDI** solution during stepwise phosphorylation/dephosphorylation (optical path 1 mm, 400 μM ATP, 0.13 μM PKA, followed by 0.3 μM λPP). Reproduced from Ref.[8]

Transient Self-assembly. After establishing the stepwise phosphorylation and dephosphorylation of the substrate **PDI**, ATP was added to a **PDI** solution, containing PKA and λPP. The addition of fuel to the system led to the full cycle **PDI** → **p2-PDI** → **PDI**, as shown in Figure 2.5A. A fast increase followed by a slower decrease in the ellipticity occurs upon addition of a shot of ATP, indicating the transient formation of the supramolecular polymer (transient formation of the species **p-PDI** and **p2-PDI**). The increase in the ellipticity is driven by ATP and, as the fuel is consumed, the system relaxes back to its thermodynamic state **PDI**. The transient self-assembly of **p2-PDI** is controlled by the rates of phosphorylation and dephosphorylation, which are dictated by the dynamics of the network (as we will describe in more detail below).

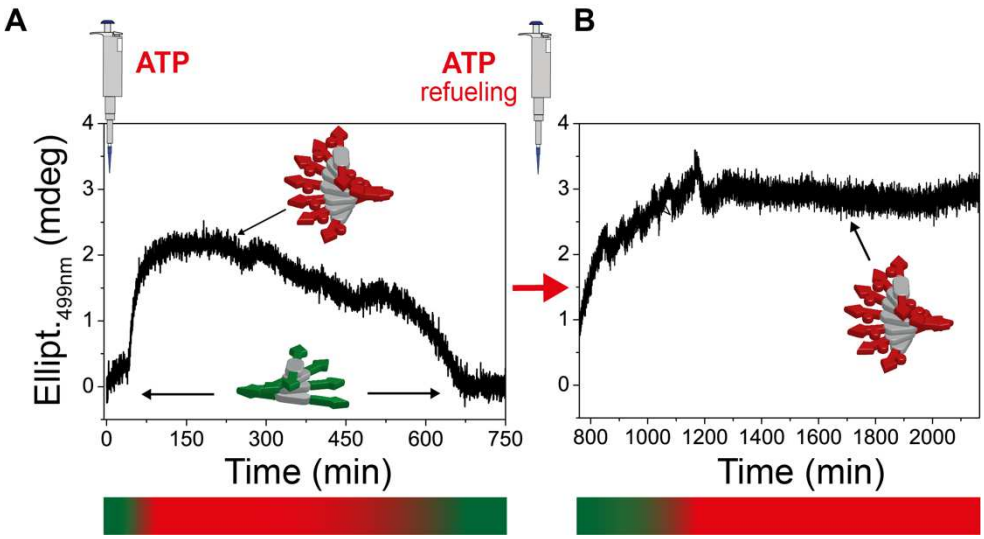

Figure 2.5. Transient state and Refueling. (A) Time course CD measurement (λ = 499 nm, optical path 1 mm) following the batch addition of ATP (2 mM) to a 200 μM **PDI** solution containing PKA (0.13 μM) and λPP (0.2 μM). (B) Time course CD measurement (λ = 499 nm, optical path 1 mm) after refueling the system with a second shot of ATP (2 mM). The plateau represents the accumulation of **p2-PDI**. Reproduced from Ref.[8]

Non-equilibrium Steady States (NESS). Others have shown the possibility of obtaining multiple transient self-assembly cycles by refueling the system.[16–19] Moreover, to achieve non-equilibrium steady states (NESS, Figure 2.3C) each **PDI** molecule needs to go through many phosphorylation/dephosphorylation cycles. Thus, a second aliquot of ATP was added to the same solution. Unfortunately, only the phosphorylation to **p2-PDI** was obtained without any recovery of the initial **PDI** structure (Figure 2.5B). By looking at the enzymatic cycle, we can observe that from each phosphorylation and dephosphorylation, 2 molecules of ADP and Pi are produced as waste by the consumption of two equivalents of ATP. As noted before, the inorganic phosphate Pi is an inhibitor of λPP[20], hampering the dephosphorylation of **p2-PDI** and poisoning the system. The latter is a general issue in supramolecular fueled systems when they are studied in (semi)batch reactors (see Chapter 1).

In the current system, the problem was solved by using a dialysis membrane to flow fuel and remove waste. A continuous flow device was developed to compartmentalize the system into a dialysis cassette (Figure 2.6A); the dialysis membrane (MCWO = 2kD) was chosen to allow the passage of ATP, ADP and Pi. In this way, it was possible to remove waste (ADP and Pi) and to refuel the system by flowing fresh ATP solution.

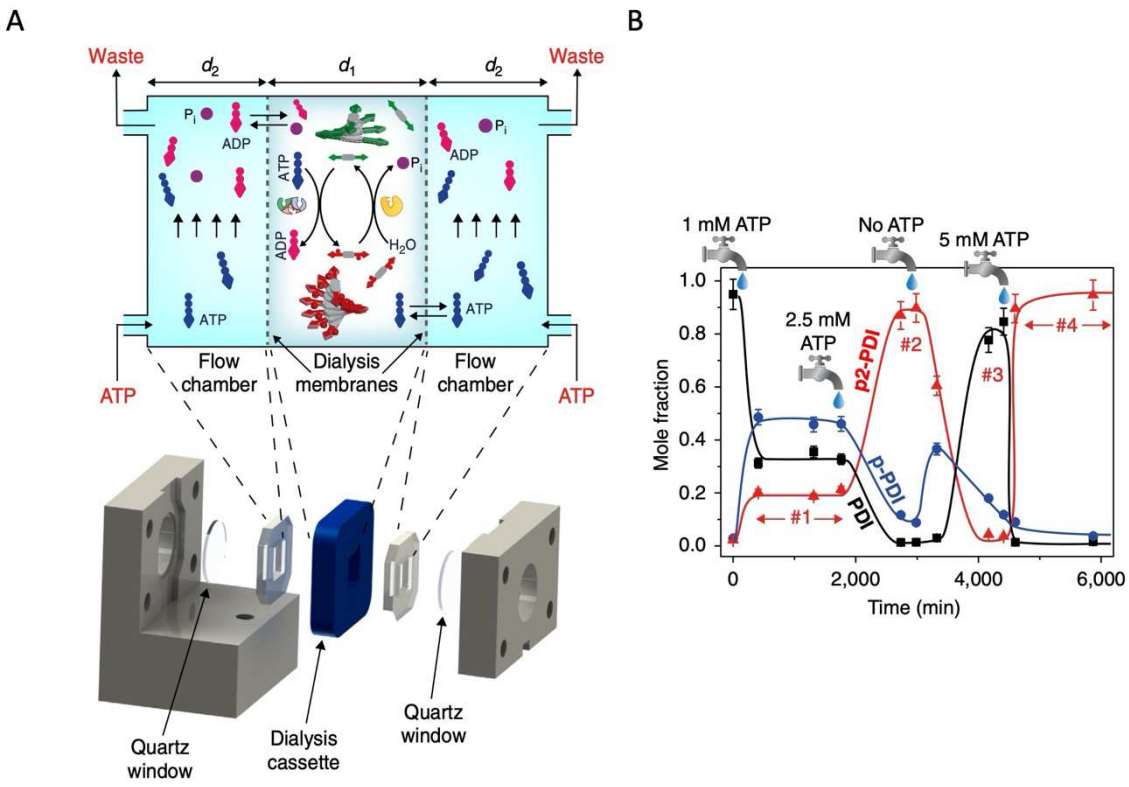

Figure 2.6. Continuous Flow device and Non-equilibrium Steady States. (A) CAD design of the continuous flow device based on a clamped dialysis cassette. The average gap between the membranes d_1 is 1.9 mm, the width of the flow chambers d_2 is 5.1 mm. (B) Different non-equilibrium steady states (plateau regions, #1-4), characterized by different molar fractions of the three species **PDI**, **p-PDI**, **p2-PDI** (by LC-MS analysis) were obtained by flowing different concentration of ATP, fuel. Reproduced from Ref.[8]

In Nature, dissipative supramolecular systems (i.e., actin filaments) are kept under non-equilibrium conditions by constant fuel/waste exchange. Here, by flowing different concentrations of ATP solution, various non-equilibrium steady states (NESS) were reached (Figure 2.6B). Specifically, **PDI** was injected into the central chamber and aliquots were taken in time to track by LC-MS the evolution of the system. A flow of 1 mM ATP in chambers flanking the dialysis cassette led to the first NESS (#1 in Figure 2.6B) in which all three species (**PDI**, **p-PDI**, **p2-PDI**) are present. It is important to highlight that while ATP is consumed, the phosphorylation and dephosphorylation reactions are continuously occurring. The constant flow of ATP kept the NESS for 20 hours. Interestingly, a second NESS was reached by increasing the concentration of ATP to 2.5 mM (#2 in Figure 2.6B). In this case, the mole fraction is composed almost exclusively by **p2-PDI**. Then, the third state (#3 in Figure 2.6B) was attained by flowing fresh buffer restoring the initial **PDI**. The latter is actually the nearly reaching the thermodynamic equilibrium, since no fuel is present. Finally, by flowing 5 mM solution of ATP, a new NESS was reached (#4 in Figure 2.6B); in the central chamber the main species is **p2-PDI**.

The NESS conditions cannot be explained as simple shifting chemical equilibria as described by Le Chatelier's principle. Indeed, the three species in the system are not in equilibrium and can only interconvert in the presence of the two enzymes and ATP. Le Chatelier can be applied in the self-assembly of **PDI** to **PDI** polymers and, equally for the polymerization of **p2-PDI**. Nevertheless, in the network, the chemical reactions between **PDI** and **p2-PDI** are irreversible and therefore the system does not equilibrate. Thus, the principle cannot be applied to our system.

So far, we have presented the system developed in our laboratory by Sorrenti *et al.*[8] and they have shown for the first time non-equilibrium steady states (NESS) in an artificial supramolecular system. The system is based on the phosphorylation and dephosphorylation of the substrate **PDI**. This work represented the starting point of this thesis where the final objective is the achievement of 'life-like' materials, capable of exhibiting new behaviors such as the ones found in Nature. Specifically, we envisaged the development of a metabolic hydrogel based on the previously described enzymatic network; the possibility of reaching different non-equilibrium steady states (NESS) would likely lead to interesting properties and functions.

2.3. Model system: Synthesis and Supramolecular Polymerization

From this point onwards, the work performed during the current PhD project is described. In the first place, we synthetized a new batch of the substrate **PDI**, following the procedure of the previous work (detailed description is reported in Experimental section 2.13).[8] The supramolecular behavior of the synthetized substrate was studied by UV-Vis, DLS and CD spectroscopy; these values were then compared to the ones of the previous work.

Temperature-dependent UV-Vis experiments were performed to compare the supramolecular polymerization of the synthesized **PDI** with the one of the substrate previously reported. A decrease of the ratio A_{504nm}/A_{540nm} was observed upon heating from 283 to 368 K, indicating partial disassembly of the polymer (Figure 2.7A). In addition, consecutive heating/cooling runs of 230 μM solutions (5 consecutive heating/cooling measurements at 1 K/min) were completely reversible. As previously shown, the ratio A_{504nm}/A_{540nm} can be described with a *T*-isodesmic (equal-K_{eq}) polymerization model. The following equation can be derived from the model[21]:

$$R_{obs}\,(T) = \frac{(R_{pol}-R_{mon})^2}{1+e^{-0.908\Delta H\frac{T-T_m}{RT_m^2}}} + R_{mon} \qquad \text{Eq. 1}$$

where $R_{obs}\,(T)$ = A_{504nm}/A_{540nm} at a given temperature (T), R_{pol} corresponds to the ratio $(A_{504nm}/A_{540nm})_{pol}$ for the fully polymerized **PDI** (value that we get from the fitting), R_{mon} corresponds to the ratio $(A_{504nm}/A_{540nm})_{mon}$ for monomeric **PDI** (set to 0.65) and R is the gas constant (8.314 J·mol^{-1}·K^{-1}). Equation 1 was used to fit the data (Figure 2.7B) and obtain the ΔH (the molar enthalpy related to the formation of the non-covalent interactions in the supramolecular polymerization) and the T_m (concentration dependent melting temperature, defined as the temperature for which the degree of polymerization α is 0.5), see Table 2.1.

Table 2.1. Thermodynamics parameters for PDI. Thermodynamics parameters for **PDI** supramolecular polymerization in reaction buffer compared to the previously reported values for the substrate.

Sample	ΔH (kJ·mol^{-1})	T_m (K)	DP_N (298 K)	K_{eq} (10^4 M^{-1})
PDI (230 μM)	-38.72 ± 0.18	346.9 ± 0.11	2.48	1.59
PDI (*previously reported 230 μM*[8])	-36.96 ± 0.23	358.5 ± 0.11	2.77	2.14

In addition, the degree of aggregation can be calculated using the following equation:

$$\alpha = \frac{R_{obs}- R_{mon}}{R_{pol}-R_{mon}} \qquad \text{Eq. 2}$$

Equation 2 was then used to calculate the degree of aggregation (Figure 2.7C). The latter can be used to obtain DP_N (average stack length) and the equilibrium constant (K_{eq}) at 298 K:

$$DP_N\,(T) = \frac{1}{\sqrt{1-\alpha(T)}} \qquad \text{Eq. 3}$$

$$K_{eq}(T) = \frac{[(2DPn-1)^2-1]}{4C_T} \qquad \text{Eq. 4}$$

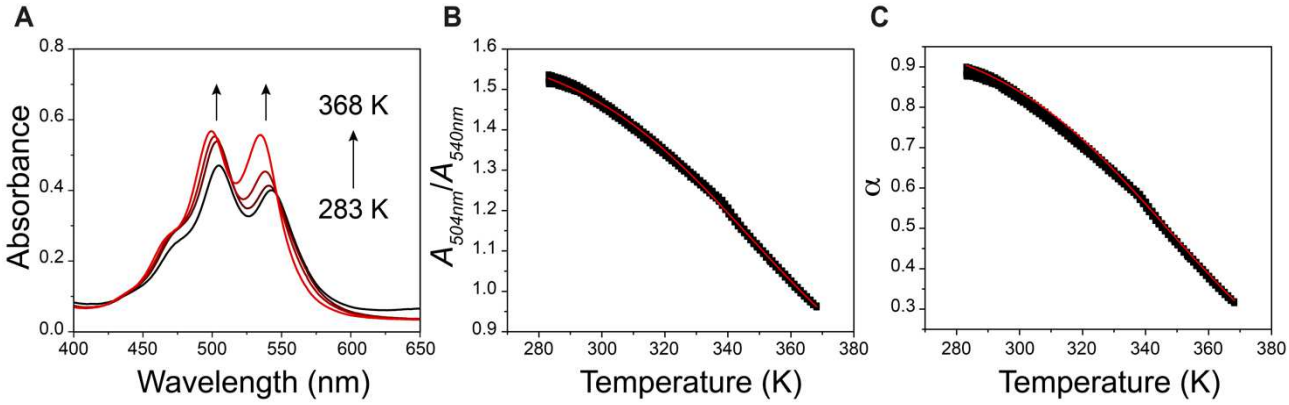

Figure 2.7. Thermodynamics of Supramolecular Polymerization. (A) Temperature dependent UV-Vis spectra of a 230 μM **PDI** solution in the reaction buffer in the presence of ATP (920 μM, 4 eq.) recorded at 283, 298, 323 and 363 K (quartz cuvette, optical path 1 mm). The arrows indicate the evolution of the two peaks (A_{504nm}, A_{540nm}). (B) Ratio A_{504nm}/A_{540nm} as a function of temperature calculated over five consecutive heating/cooling runs recorded between 283 and 368 K at 1 K interval (heating rate 1 K min^{-1}, optical path 1 mm). The red solid line corresponds to the fitting. (C) Temperature-dependent degree of aggregation, $\alpha(T)$, of **PDI** corresponding to the curve in panel B, calculated by using equation 2. The red line represents the theoretical $\alpha(T)$ for the isodesmic model calculated by using the values of ΔH and T_m obtained by the previous fitting.

The results obtained (Table 2.1) indicate that **PDI** polymer synthesized in this batch behaves similarly to the previous reported one. Moreover, dynamic light scattering (DLS) was used to assess the dimension of the polymer. The experiment was performed for 230 μM **PDI** solution in the reaction buffer; the resulting slope D (Figure 2.8) of the linear fitting of the correlation Γ q^2 was used to obtain the final radius (R_H) of the assembly by following the equation:

$$R_H = \frac{k_B \cdot T}{6 \cdot \pi \cdot \mu \cdot D} \qquad \text{Eq. 5}$$

where k_B indicates the Boltzmann constant (1.380688·10^{-23} m^2 kg s^{-2} K^{-1}), T is the temperature (293 K) and μ is the viscosity of the solvent (buffer, 0.001 Pa)[22]. The resulting value is R_H = 511 ± 15 nm; the latter is comparable to the one found in the previous work (R_H = 440 nm ± 10 nm).

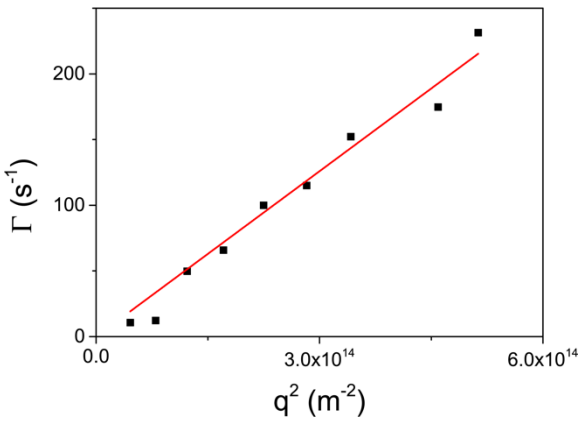

Figure 2.8. Dynamic Light Scattering (DLS) of PDI polymer. DLS measurement: relaxation Γ versus the square of the scattering vector q^2 for 230 μM PDI solution in the reaction buffer at 293 K. The corresponding slope D, resulting from the linear fitting (red line) is apply to equation 5. R_H for **PDI** assembly is calculated to be 511 ± 15 nm.

So far, we have shown that the new synthesized batch of **PDI** behaves similarly to one previously described. The supramolecular polymerization was studied in the first place. However, we also wanted to validate that the phosphorylation and dephosphorylation of the substrate was reproducible.

2.4. Stepwise Phosphorylation and Dephosphorylation

We performed a stepwise phosphorylation and dephosphorylation of **PDI** in the presence of the enzymes PKA and λPP. The composition of the network was studied by LC-MS. Firstly, the phosphorylation of **PDI** to **p2-PDI** was performed in the presence of PKA and ATP and secondly, an aliquot of λPP was added to recover the initial substrate **PDI**. The LC-MS spectra showed the conversion to **p2-PDI** upon phosphorylation (Figure 2.9A) and the dephosphorylation to **PDI** after the addition of λPP (Figure 2.9B). These results confirmed that the new batch of **PDI** could indeed be phosphorylated and dephosphorylated. The phosphorylation occurs in about 2 hours when 2 equivalents of ATP are added (similarly to what reported in the previous work[8]) while the dephosphorylation takes place within minutes.

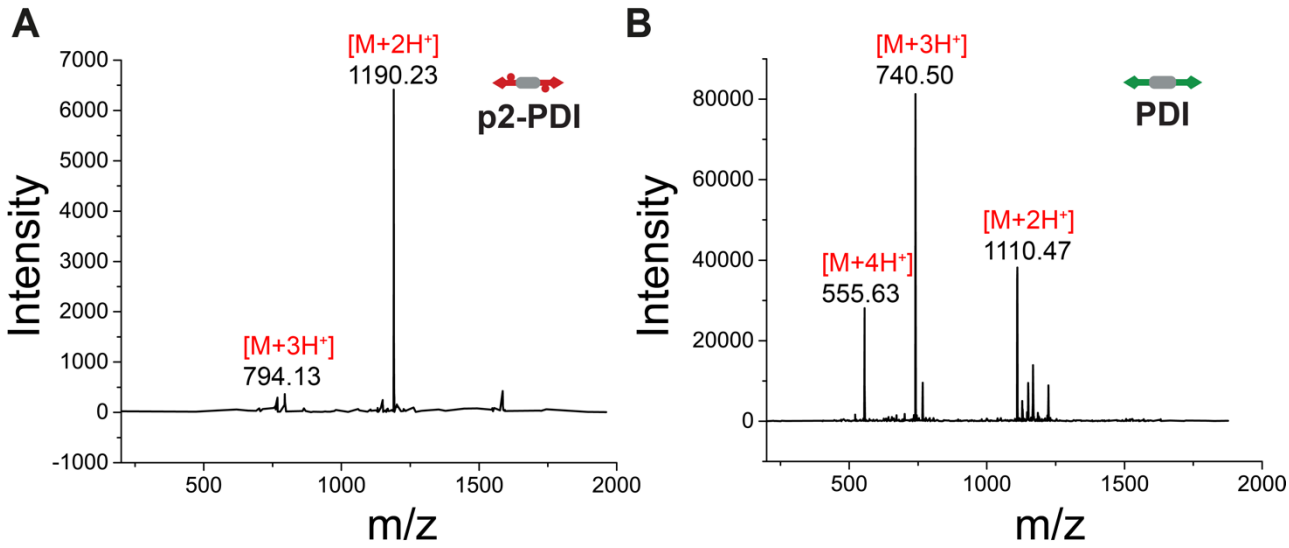

Figure 2.9. Phosphorylation and Dephosphorylation of PDI. LC-MS spectra of a 200 μM **PDI** solution in the presence of ATP (400 μM, 2 eq.), (A) after complete phosphorylation to **p2-PDI** triggered by the addition of 0.13 μM PKA and (B) after dephosphorylation to **PDI** triggered by the addition of λPP (0.06 μM).

Lastly, we studied the system by CD spectroscopy. As shown in Figure 2.10, upon phosphorylation of **PDI** to **p2-PDI** (red line) we observed the inversion of the CD signal, indicating the change in the chirality of the supramolecular assembly, which is again in line with our previous report.[8]

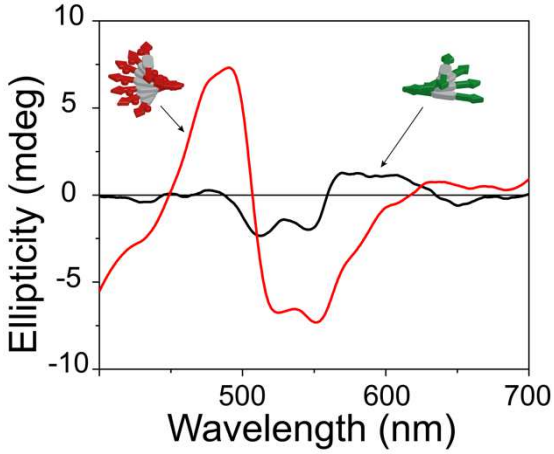

Figure 2.10. CD spectra of PDI and p2-PDI. CD spectra of 200 μM **PDI** (black line) and **p2-PDI** (red line) solutions (optical path 1 mm). The phosphorylation to **p2-PDI** is triggered by the addition of PKA (0.13 μM) and ATP (400 μM, 2 eq.).

So far, we have studied and demonstrated the supramolecular polymerization of the new synthesized batch of **PDI** and its behavior in the enzymatic network by performing stepwise

phosphorylation and dephosphorylation of the substrate. The results were found to be reproducible, and therefore we could continue to build on this system.

2.5. Fuel (ATP) Regeneration *in situ* from Waste (ADP)

In section 2.2, we discussed about non-equilibrium steady states (NESS) in an artificial supramolecular polymer. Moreover, we presented an elegant way to solve the waste problem; 2 molecules of ADP and inorganic phosphate Pi are produced after each phosphorylation/dephosphorylation causing the inhibition of further cycles. The confinement of the system inside a dialysis membrane reactor allowed the continuous flow of ATP and removal of waste. The latter permits the achievement of four different non-equilibrium steady states. However, to make a free-standing NESS gel, the latter approach would not work, since the diffusion times (and formation of internal gradients) would be prohibitive. Thus, we had to make a step back and find a different solution to be able to reach different NESS by varying the influx of fuel.

In the first place, we studied the effect of ADP and Pi to the phosphorylation and dephosphorylation reactions, respectively. Until now, the latter were assumed from the literature[20,23], but they had not been experimentally investigated in the **PDI** system. Generally, in Nature many enzymatic systems use their products as a negative and/or positive feedback to reach a better control over the specific reactions. This subject will be explored in more detail in Chapter 3. For now, we just need to consider simple competitive inhibition. In this case, ADP can interact with one of the pockets of PKA and act as a competitive inhibitor for ATP, causing the inhibition of the phosphorylation. In the same way, Pi is competing with **p2-PDI** for the interaction with λPP. To study the effect, we run simple tests through LC-MS by adding 10 equivalents of ADP (Figure 2.11A) and Pi (Figure 2.11B) during the phosphorylation and dephosphorylation of the substrate **PDI** and follow the evolution of the mole fraction of **p2-PDI** over time.

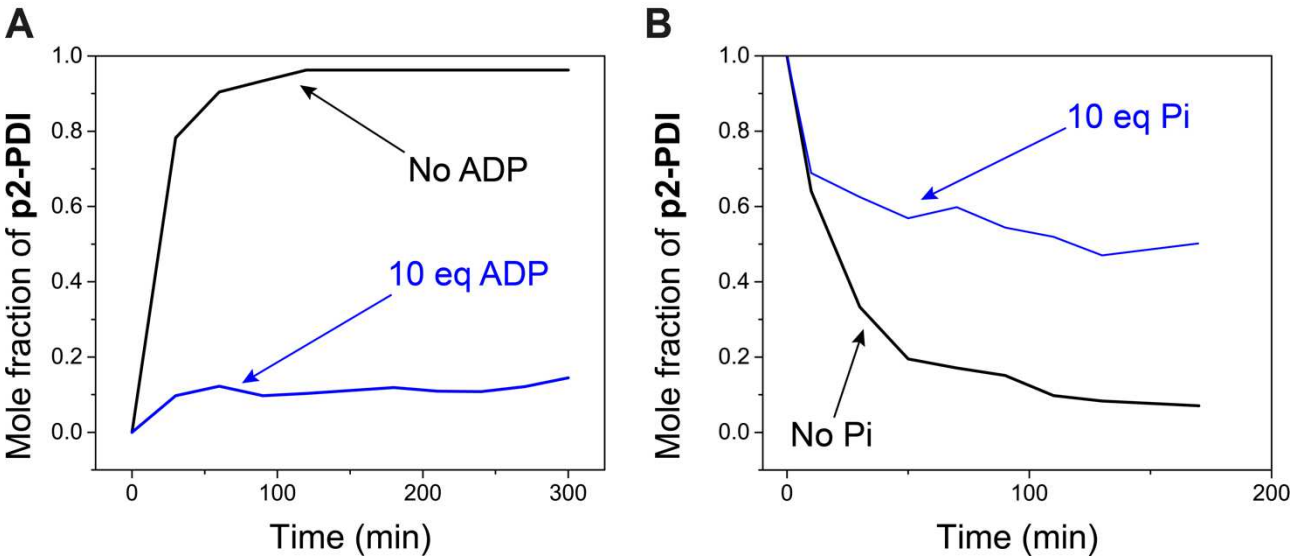

Figure 2.11. ADP and Pi Inhibition. (A) LC-MS spectrum evolution of the phosphorylation of a 200 μM **PDI** solution containing 400 μM ATP and 0.13 μM PKA (black line) and with further addition of 10 eq. of ADP (blue line). (B) LC-MS spectrum of the dephosphorylation of a 200 μM **p2-PDI** solution containing 0.065 μM λPP (black line) and with further 10 eq. of Na_3PO_4 (Pi).

Interestingly, the effect of a 10-fold excess of ADP is much larger to the overall phosphorylation compared to the one of Pi to the dephosphorylation. These experiments were carried out to qualitatively investigate the inhibition of by-products of the reactions cycle. Generally, in the presence of 10 equivalents of ATP the phosphorylation takes place in 1 hour (black line in Figure 2.11A). The further addition (blue line in Figure 2.11A) of 10 equivalents of ADP impedes the conversion to **p2-PDI**. However, comparing the effect on the dephosphorylation we can observe that **PDI** is quickly restored (half-life = 25 min.). The presence of an excess of Pi (10 eq.) is leading to the 0.5 conversion to the dephosphorylated substrate and after 100 minutes the values are reaching a plateau as no further dephosphorylation is occurring.

In both cases, the data confirmed the inhibition of the phosphorylation and dephosphorylation by respectively the ADP and the inorganic phosphate. One possible solution we explored was to use a phosphate-specific resin PiBind (Novus Biologicals), which is commonly used in removing phosphate contaminants in buffer. Unfortunately, upon addition of PiBind to a solution of **PDI**, a pink precipitate formed instantaneously. As we do not know the exact composition of the resin, we can only assume this is due to electrostatic interactions between our substrate and the resin. Since there are very few other approaches to scavenge or recycle Pi, we focused more on the removal of ADP.

As already discussed in Chapter 1, ATP is the main source of energy in our body and its recycling is vital for cell's functions. Glycolysis is a metabolic pathway where glucose is consumed over a series of reactions with the overall production of two molecules of pyruvate and two molecules of ATP.[1] Specifically, in the last reaction, a molecule of phosphoenolpyruvate (PEP) serves as the substrate for the conversion of ADP to ATP. The reaction is catalyzed by pyruvate kinase and it requires one K^+ and 2 Mg^{2+} cations as cofactors.[24] The first step is the nucleophilic attack of the PEP phosphorus atom by β-phosphoryl oxygen of ADP. In this step, enolpyruvate is released while ATP is formed. In the second step, enolpyruvate tautomerizes to pyruvate (Py). The synthesis of ATP is due to phosphate transfer and the consequently conversion to enol-ketone. In our study, we decided to couple this specific ATP regeneration pathway to the existing phosphorylation/dephosphorylation network (Figure 2.12). Therefore, ATP (fuel) will be produced *in situ* from the ADP (waste), by catalytically consuming 'pre-fuel' (PEP).

The ADP + PEP → ATP + Py reaction has been already reported for protein synthesis[25–29], supramolecular assemblies[30,31] and the formation of coacervates[32].

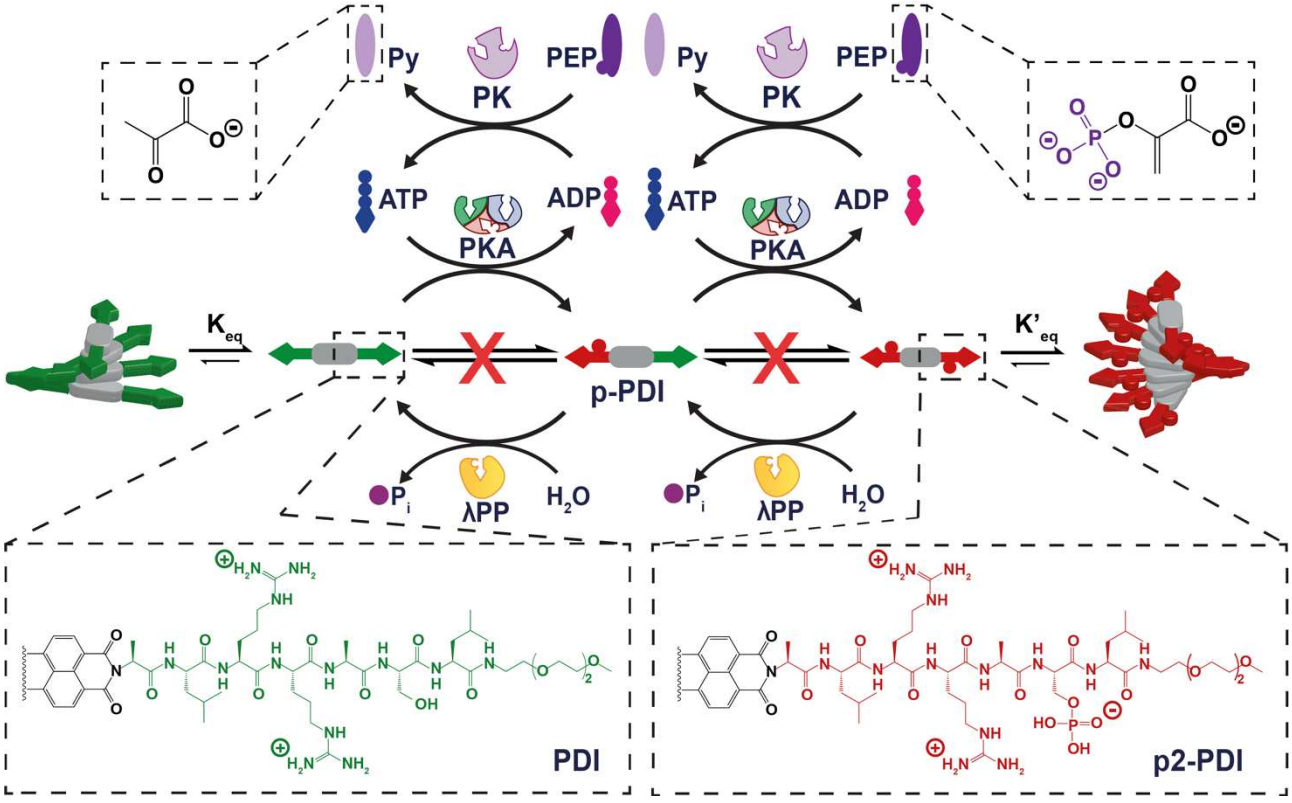

Figure 2.12. Enzymatic Network implemented with ATP Regeneration. PDI (green) is phosphorylated to **p2-PDI** (red) by a protein kinase (PKA) in the presence of ATP. ATP is produced by the transfer of a phosphate group (purple) from phosphoenolpyruvate (PEP) to ADP, releasing pyruvate (Py). The reaction is catalyzed by a pyruvate kinase PK. **p2-PDI** is dephosphorylated by Lambda phosphatase (λPP), recovering the initial structure **PDI**.

The ATP regeneration reaction was firstly studied in the reaction buffer by ^{31}P NMR. The production of ATP was followed by the formation of peaks at -5.0, -10.0 and -18.0 ppm, characteristics of the respective phosphates γ, α, β of ATP.[33] The NMR spectra were recorded for ADP (Figure 2.26 in Appendix 2.16), ADP and PEP (Figure 2.27 in Appendix) and after addition of the enzyme pyruvate kinase PK (Figure 2.28 in Appendix). The ATP formation was confirmed after the addition of PK to the substrates at 25°C in the reaction condition. For the NMR measurements, the buffer was prepared without the further addition of Mn^{2+} to avoid the paramagnetic effect of the ion. Indeed, many attempts were made as lowering the [Mn^{2+}] and/or augmenting the [EDTA] to take advantage of the NMR for the enzyme kinetics study. However, by changing the buffer concentration we ended up changing the kinetics of PKA and λPP. Therefore, NMR spectroscopy was not the most appropriate technique to explore the ATP regeneration reaction kinetics.

2.6. ATP Regeneration Kinetics

In order to obtain the enzyme kinetics for the ADP to ATP conversion catalyzed by pyruvate kinase PK, we used an assay kit (Sigma Aldrich). The latter provides a direct procedure for measuring the pyruvate kinase activity. Specifically, a coupled reaction with a fluorescent peroxidase substrate yields a colorimetric product (λ = 570 nm) when interacting with pyruvate, released as side product during the reaction ADP to ATP. Thus, the absorbance value at 570 nm is directly proportional to the pyruvate produced. However, for our purpose, the protocol was modified and adapted to our working conditions. The detailed procedure is described in the Experimental section 2.13.

Firstly, a calibration curve was made for a direct correlation between the absorbance at 570 nm and the pyruvate concentration, generating 0 (blank), 2, 4, 6, 8 and 10 nmole/cuvette standards (Figure 2.29 in Appendix 2.16). Once the calibration was done, we proceeded with sample preparation for the assay reaction. In order to measure the pyruvate kinase activity, we operated at conditions that were the closest to the ones of the complex system (that are the reaction buffer pH 7.5 at 25 °C, pyruvate kinase, ADP and PEP purchased from Sigma).

Velocity measurements were made to determine the apparent Michaelis constants (K_M) for ADP and PEP. The experiments were performed by tracking the change in the absorbance at 570 nm over 40 minutes, that corresponds to the amount of pyruvate produced. The Michaelis-Menten kinetics were obtained assuming that after mixing the enzyme and the substrate, a steady state is reached in which the concentration of the complex enzyme-substrate remains constant. K_M for PEP

and ADP were determined at saturating concentrations of one of the two substrates ([enzyme]<<[substrate]). In Figure 2.13, the Michaelis-Menten kinetics are reported; the enzyme activity over different concentrations of PEP and ADP is correlated by the function:

$$v = v_{max} \frac{S}{S + K_M} \qquad \text{Eq. 6}$$

where v is the reaction rate (rate of formation of product), S is the concentration of a substrate, v_{max} represents the maximum rate achieved by the system, happening at saturating substrate concentration, K_M is numerically equal to the substrate concentration at which the reaction rate is half of v_{max}.

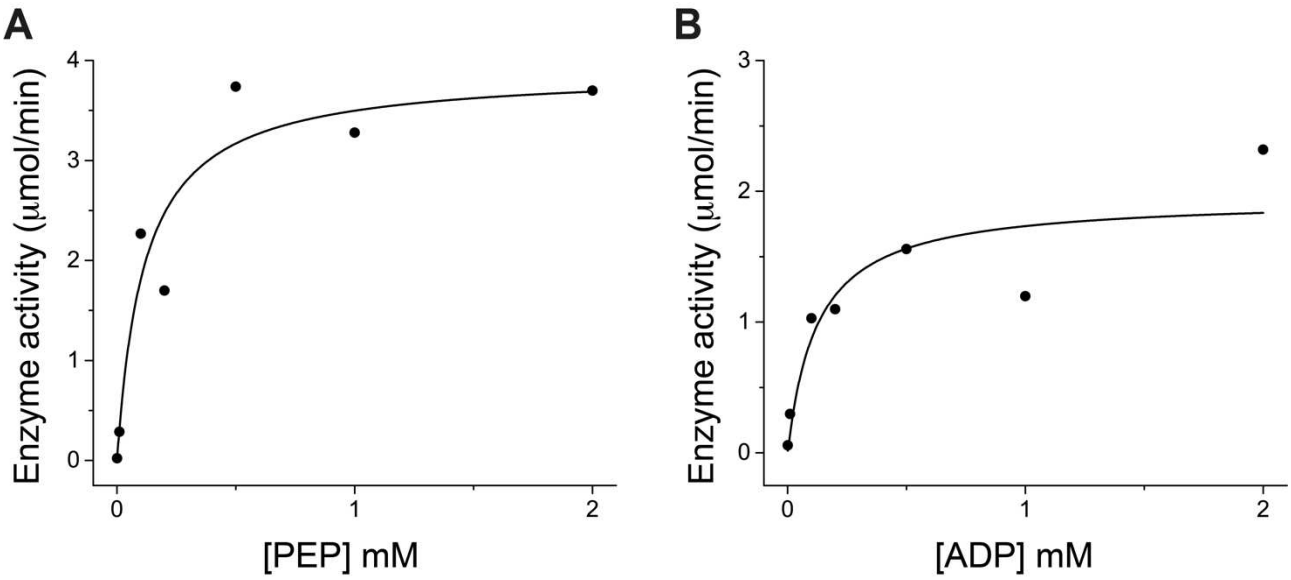

Figure 2.13. Enzyme Kinetics study for Pyruvate Kinase. (A) Variation of the activity of pyruvate kinase with PEP concentration in the presence of 2 mM ADP. (B) Variation of the activity of pyruvate kinase with ADP concentration in the presence of 2 mM PEP. All the data were recorded by UV-Vis spectroscopy in a quartz cuvette (optical path 1 mm).

From the fit of Equation 6 to our experimental data, we obtained the values of K_M for ADP and PEP, $1.24 \cdot 10^{-5}$ M and $1.15 \cdot 10^{-4}$ M respectively. Comparison of kinetically determined constants with literature is difficult as each study is conducted at different pH in specific buffer reaction conditions.[34] The K_M values found are in agreement with most of the range reported in literature.[34–36] Reynard *et al.*[35] for instance, extracted K_M for ADP and PEP, as $2.1 \cdot 10^{-4}$ M and $3.2 \cdot 10^{-5}$ M, from the corresponding Lineweaver-Burk plot. However, the experiments were carried out in a different reaction buffer (varying pH from 8 to 9, with an excess of K^+, 0.1 M) and using lower and various concentrations of saturating substrate (from 0.5 to 0.8 mM).[35]

The goal of these measurements was to get the enzymatic activity of pyruvate kinase using our specific experimental conditions. It has been reported how the changing in pH is affecting the K_M values for both substrates (i.e., the augmentation in the apparent K_M for PEP from 0.3 mM at pH 5.9 to 2.3 mM at pH 8.35).[37] Moreover, the concentrations of K^+ and Mg^{2+} are vital for the optimal activity. It has been demonstrated the optimal activity of PK for [K^+] = 50 mM and [Mg^{2+}] = 13.5 mM.[34,36] In our case, the buffer contains 10 mM Mg^{2+} (from $MgCl_2$) and K^+ is present in the form of phosphoelnolpyruvate monopotassium salt. K^+ is directly involved in the acquisition of the active conformation of the enzyme, enhancing the affinity for PEP and ADP.

The kinetics study of pyruvate kinase in the reaction conditions resulted in the determination of Michaelis-Menten parameters. Nonetheless, we must stress that the final enzyme activity is affected by tiny changes in the environment conditions. So far, we have shown that ADP can be recycled to ATP; the latter would solve our waste inhibition problem (Figure 2.11). In addition, the enzyme activity was explored in the working buffer conditions, confirming the Michaelis constants values as reported in literature. Next, we study the phosphorylation/dephosphorylation of **PDI** in the presence of the ADP to ATP conversion catalyzed by the pyruvate kinase.

2.7. Stimuli-responsive Phosphorylation/Dephosphorylation

The stimuli-responsive phosphorylation/dephosphorylation of the substrate **PDI** was done by stepwise addition of PKA and λPP, respectively. Firstly, the system was studied by LC-MS. The first spectrum was obtained (Figure 2.14A) for a 100 μM **PDI** solution, containing 1 mM PEP and 0.06 μM PK. The peaks at 555.68 and 740.45 represent the [M + $4H^+$] and [M + $3H^+$] of **PDI** molecule. This shows that neither PK nor PEP react with **PDI**, as expected. Secondly, the addition of 200 μM ADP and 0.13 μM PKA led to the phosphorylation of **PDI** to **p2-PDI**. As shown in Figure 2.14B, the peaks at 595.88, 793.85 and 1190.04 represent the [M + $4H^+$], [M + $3H^+$] and [M + $2H^+$] of the phosphorylated substrate **p2-PDI**. That means there was successful conversion of ADP to ATP in the presence of pre-fuel PEP followed by phosphorylation of **PDI** to **p2-PDI**. Ultimately, the dephosphorylation back to **PDI** was done by the addition of 0.5 μM λPP. The spectrum (Figure 2.14C) shows the recovery of the initial substrate with peaks at 555.68 [M + $4H^+$] and 740.45 [M + $3H^+$].

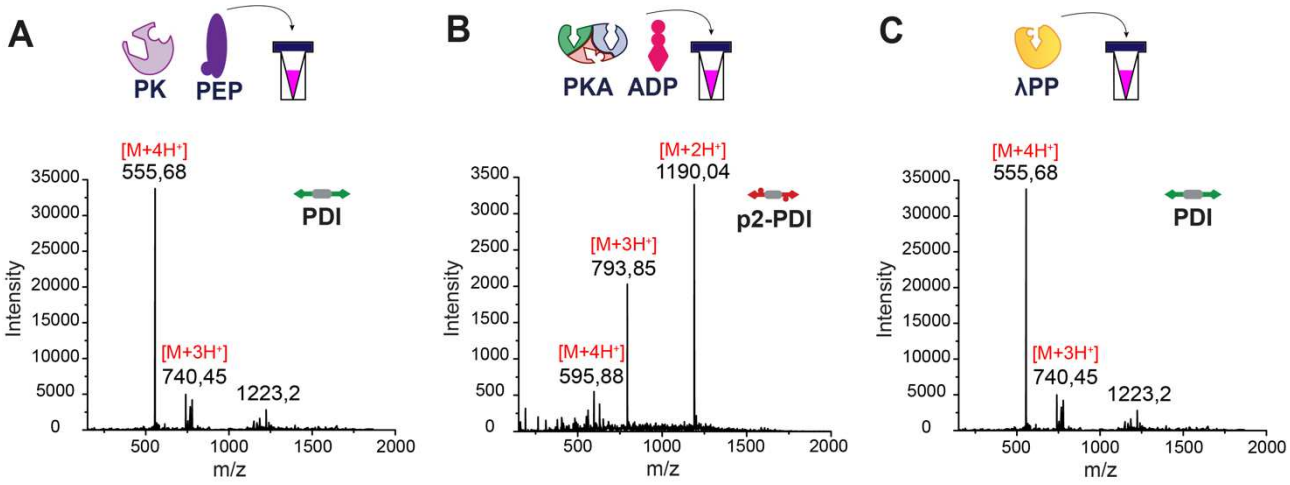

Figure 2.14. Stimuli-responsive Phosphorylation/Dephosphorylation. (A) LC-MS spectrum of 100 μM **PDI** solution in the presence of PEP (1 mM) and PK (0.06 μM). (B) LC-MS spectrum after addition to (A) of ADP (200 μM) and PKA (0.13 μM). The generation *in situ* of ATP is leading to the phosphorylation of **PDI**, and its conversion to **p2-PDI**. (C) After addition of λPP (0.13 μM), **PDI** is restored. All the spectra were recorded in the reaction buffer at 25°C in a LC-MS glass vial with a 400 μL glass insertion.

These results confirmed the stepwise phosphorylation/dephosphorylation of the substrate **PDI** and, in particular, they demonstrate the integration of the new enzymatic reaction with the previous described network. Interestingly, in our body the pyruvate kinase is regulated by a protein kinase A; glucagon and epinephrine activate the protein kinase which causes the phosphorylation and the deactivation of the pyruvate kinase. Nevertheless, among our studies we did not observe any interference between PKA and PK, although they were present in the same batch.

Additionally, we analyzed the system by CD spectroscopy. In the first place, we excluded any effect of the pyruvate, that is released during the ATP regeneration reaction, on the CD signal. The control was run for a 200 μM **PDI** solution containing an excess of pyruvate (10 mM) and the effect of pyruvate was checked at 499 nm for few hours (as shown in Figure 2.30, Appendix 2.16). Overall, we did not observe any change in the CD spectrum. Then, we proceeded the investigation of the network with stimuli-responsive experiments followed by CD spectroscopy.

As previously discussed, the phosphorylation induces a change in the supramolecular chirality of the assembly, from right-handed to left-handed helices, indicative of phosphorylation/dephosphorylation. Thus, the ellipticity at 499 nm was followed by time course CD measurements (Figure 2.15). In the first example (Figure 2.15A), PKA was added to the system, containing **PDI**, PEP, PK and ADP after 3 h, causing the increase of the CD signal due to formation of **p2-PDI**. In the second experiment (Figure 2.15B), PKA was added to the batch **PDI** solution

containing PEP, ADP and PK at time zero. The augmented CD signal due to the phosphorylation of the substrate **PDI** to **p2-PDI** is slightly different compare to Figure 2.15A. This difference is the result of the concurrent ADP to ATP conversion and the phosphorylation of the substrate, consuming ATP while for the first experiment PKA is added when ATP is already present in the solution. Ultimately, the dephosphorylation was investigated (Figure 2.15C). The λPP was added when the ellipticity value reached a plateau, that means **PDI** has been converted to **p2-PDI**. The addition of the phosphatase caused a rapid decrease of the signal, confirming the dephosphorylation of **p2-PDI** back to **PDI**. However, as shown in Figure 2.15C, the CD signal cannot be completely restored because of the continuously regeneration of ATP, which in time permits further phosphorylation of the substrate. For all the experiments, an aliquot was taken to validate the (de)phosphorylation of **PDI** by LC-MS.

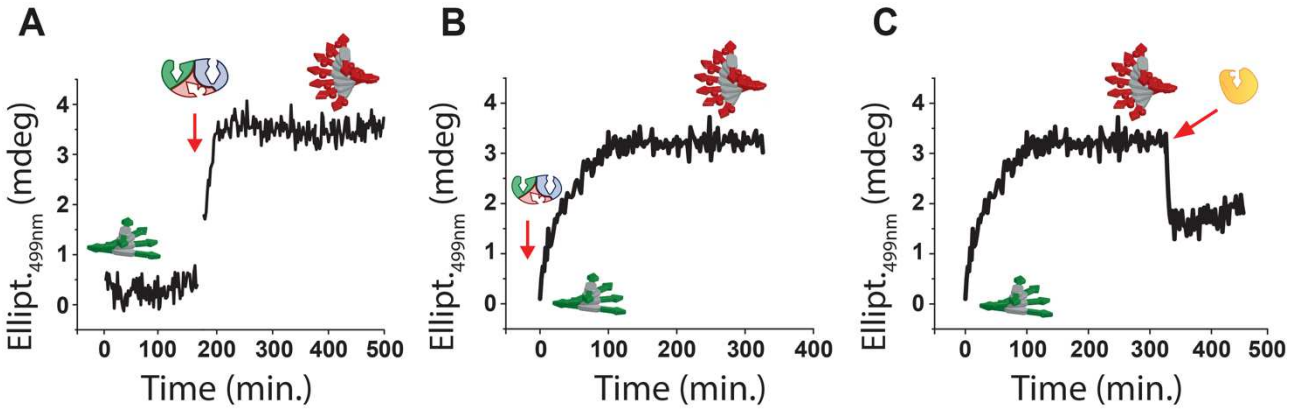

Figure 2.15. Stimuli-responsive studies by Circular Dichroism spectroscopy. (A) Time-course CD measurement of 100 μM **PDI** solution in the presence of PEP (500 μM), ADP (200 μM), PK (0.1 μM). After 1h PKA (0.13 μM) is added leading to the formation of **p2-PDI**. (B) Time-course CD measurement of 100 μM **PDI** solution in the presence of PEP (500 μM), ADP (200 μM), PK (0.1 μM) and PKA (0.13 μM). (C) Time-course CD measurement upon addition of λPP (0.13 μM) at t = 300 min. to the **p2-PDI** solution recovering the initial **PDI** structure.

2.8. Non-Equilibrium Pseudo Steady States

So far, we have investigated the complex enzymatic network by stepwise phosphorylation/dephosphorylation of **PDI**. Specifically, we reported the ATP regeneration reaction coupled to the previously studied network. In this manner, we demonstrated the generation of fuel directly in the system. Also, we showed that the three enzymes (PKA, λPP and PK) can work together. In this complex network while **PDI** is phosphorylated and dephosphorylated by PKA and λPP, respectively, ATP is consumed and regenerated by a pyruvate kinase in the presence of phoshoenolpyruvate, PEP. It is for that reason we have been referring to PEP as 'pre-fuel' because

is used indirectly. The PEP concentration is identical to the maximum amount of ADP that can be converted to ATP. And so, PEP concentration is also limiting the phosphorylation of **PDI**. Therefore, we can suppose that by varying the concentration of PEP, different non-equilibrium steady states will be reached.

The study of out-of-equilibrium steady states is particularly interesting as there are only few systems reported to our knowledge that have shown non-equilibrium steady states (NESS) and it would be a fascinating behavior to study in materials. For instance, many systems were described where the transient gel-sol-gel is achieved but until now there are very few examples where systems are pushed far enough to reach NESS.[8,38] Recently, Deng *et al.*[38] described multiple transient dynamic steady states (DySSs) in fuel-driven DNA nanostructures. The system is based on a previously engineered ATP-driven DNA polymerization.[39] Interestingly, DySSs result from the autonomous switching of multiple building blocks (DNA polymers with different lengths) and the lifetime is controlled by the ATP fuel concentration. This is an important step in programming reaction networks in Systems Chemistry. Nevertheless, we investigated conditions to achieve non-equilibrium steady states in our synthetic system. This study will permit the implementation of NESS into materials, in order to reach higher levels of complexity and programmability.

First, the out-of-equilibrium steady states were studied by CD spectroscopy and we will refer to them as pseudo steady states, since the experiments were performed under closed unstirred batch conditions (quartz cuvette, optical path 1 mm).

In Figure 2.16 three different non-equilibrium pseudo steady states (pNESS) are shown. For each spectrum the only parameter we are varying is the concentration of 'pre-fuel' PEP. The increase of PEP concentration is indeed leading to a longer plateau that means, with time, more ATP is regenerated in the system and the phosphorylation reaction is still competing with the dephosphorylation. Specifically, to a 100 μM **PDI** solution containing PEP, PKA (0.13 μM), λPP (0.06 μM), and PK (0.014 μM), we added 100 μM ADP after 1 hour. In the three experiments, the difference we want to highlight is the amount of PEP present in the solution; we worked at 0.5 (Figure 2.16A), 1 (Figure 2.16B) and 2 mM (Figure 2.16C). These conditions were chosen because we wanted to push the system out-of-equilibrium by constantly regenerating ATP and promoting the phosphorylation of **PDI**.

The three pNESS are the result of the conversion ADP to ATP. After the addition of ADP, the phosphorylation of **PDI** to **p2-PDI** takes place; ADP is converted to ATP by the pyruvate kinase and ATP is consumed by PKA to phosphorylate the substrate. ATP is hydrolyzed to ADP that is again

converted to ATP by PK. The latter reaction is strictly dependent on the presence in the solution of PEP. Hence, once the CD signal reaches a plateau, the ATP regeneration is still working, and it will take place until PEP is present in the batch. Once PEP is consumed, the dephosphorylation dominates over the phosphorylation and **PDI** is restored (decrease of the CD signal). Note that for these experiments the concentration of λPP was drastically decreased (as compared to stimuli-responsive experiments, see Figure 2.14 & 2.15) as the dephosphorylation reaction is faster ($k_{\lambda PP}$ = $4.95 \cdot 10^{1}$ s^{-1}) than the phosphorylation (k_{PKA} = 2.93 s^{-1}); this was a necessary balance to achieve pNESS conditions.

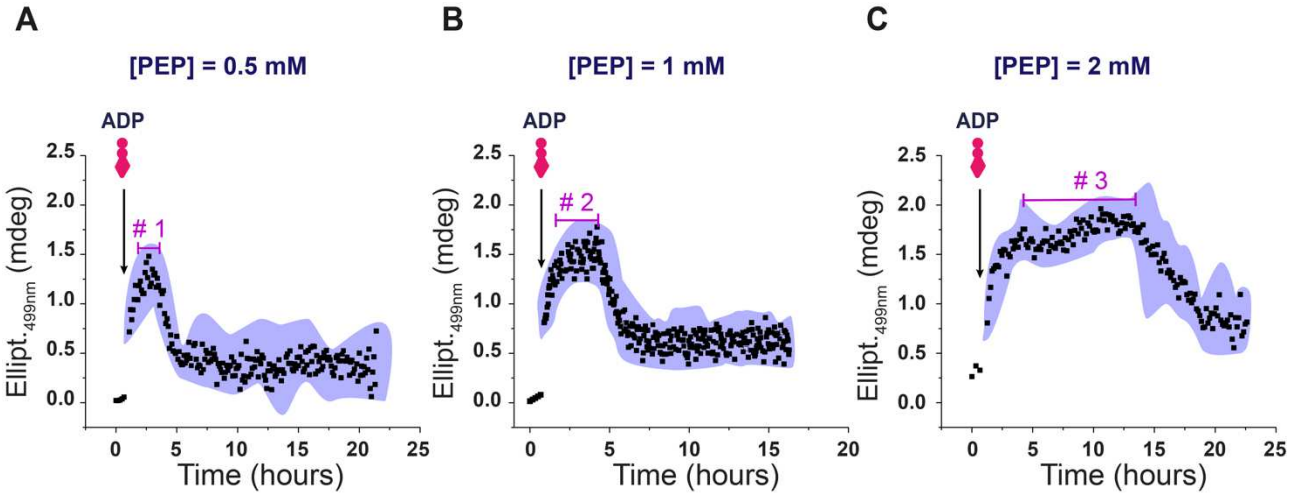

Figure 2.16. Supramolecular Pseudo Non-Equilibrium Steady States. (A) Time-course CD measurement (optical path 1 mm) of a 100 μM **PDI** solution containing PKA (0.13 μM), PK (0.014 μM), λPP (0.006 μM), PEP (0.5 mM). (B) Time-course CD measurement (optical path 1 mm) of a 100 μM **PDI** solution containing PKA (0.13 μM), PK (0.014 μM), λPP (0.006 μM), PEP (1 mM). (C) Time-course CD measurement (optical path 1 mm) of a 100 μM **PDI** solution containing PKA (0.13 μM), PK (0.014 μM), λPP (0.006 μM), PEP (2 mM). In the CD spectra we can observe three different pseudo non-equilibrium steady states (plateau regions, #1-3). For all the experiments, ADP (100 μM) is added to the reaction mixture after 1h. The data reported in the figure represents the mean of 3 independent experiments where the ellipticity is monitored at 499 nm each 2 minutes (points show averages; the shaded violet area shows the standard deviation).

Next, we investigated the pNESS conditions in more detail by LC-MS. The latter permits to follow the formation of the three species (**PDI**, **p-PDI** and **p2-PDI**) over time. Solutions were prepared using the same reaction conditions as for the CD experiments and again the pNESS were studied at different concentrations of PEP (0.5, 1 and 2 mM). The LC-MS samples were prepared in a glass vial with a glass insertion (V_T = 300 μL) and the mass spectra were tracked each hour. From each experiment, we deconvoluted the mass to obtain a qualitative result of the mole fraction of each species presents in the system. We could confirm the three pNESS, similarly to the ones obtained by CD spectroscopy, by studying the mole fraction of **p2-PDI** over time.

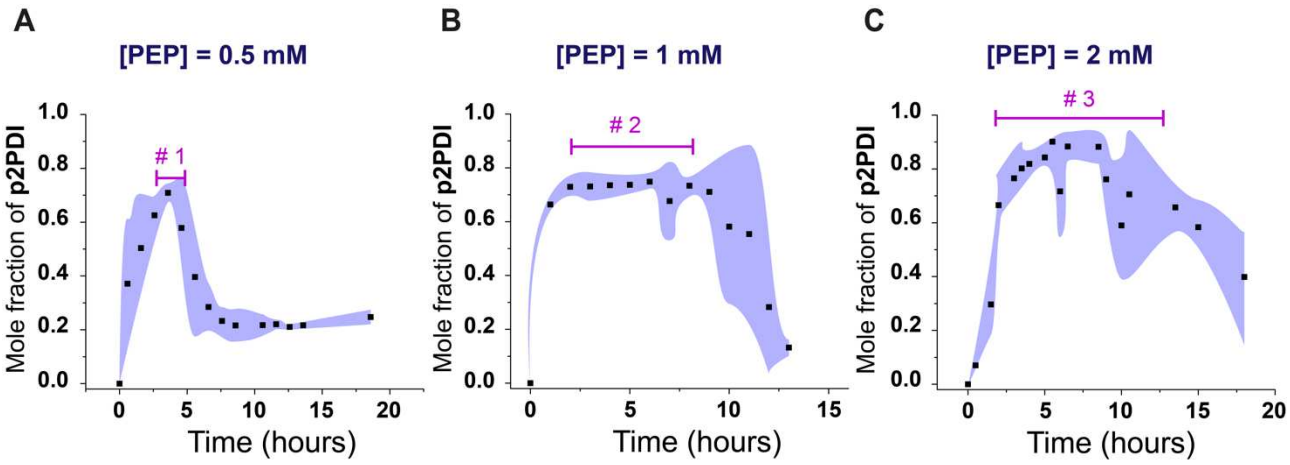

Figure 2.17. Supramolecular Pseudo Non-Equilibrium Steady States. LC-MS spectra of a 100 μM **PDI** solution containing PKA (0.13 μM), PK (0.014 μM), λPP (0.006 μM), ADP (100 μM) at different concentration of PEP 0.5 mM (A); 1 mM (B) and 2mM (C). In the LC-MS spectra we can observe three different pseudo non-equilibrium steady states (plateau regions, #1-3). The **p2-PDI** mass area is deconvoluted to obtain the mole fractions of the species over time. The data reported in the figure represents the mean of 3 independent experiments (points show averages; the shaded violet area shows the standard deviation).

Overall, pNESS were observed both using CD spectroscopy and LC-MS; in both cases, we found three different pseudo non-equilibrium steady states (#1-3). The duration of the plateau (pNESS) is directly correlated to the concentration of pre-fuel, PEP. The latter dictates also the production of ATP and thus the phosphorylation of **PDI** to **p2-PDI**. The decrease of the CD signal, meaning dephosphorylation of **p2-PDI** (decrease of **p2-PDI** mole fraction) to **PDI**, occurs when PEP is consumed. To confirm that what we observed is the actual dephosphorylation of the substrate and it is not the result of any denaturation of the enzymes (PKA and PK), we ran a control experiment. To the NESS solutions, after 40 hours, a shot of ADP (20 eq.) and PEP was added and an increase of the CD signal was observed, confirming the activity of both enzymes, PKA and PK (Figure 2.31 in Appendix 2.16).

Once we established and integrated the ATP regeneration reaction in the enzymatic network, we hypothesized and envisaged the achievement of NESS. However, finding the optimal experimental conditions was not-trivial. We hope that our approach will be adopted in other ATP-fueled systems.[19,39,40] Additionally, the investigation of NESS conditions opens the door to chemically-fueled network that are contained within materials resembling an artificial metabolism.

2.9. Oscillatory behavior of the Enzymatic Network

In Chapter 1, we underlined the objective in Systems Chemistry to reproduce emergent behaviors using reaction networks.[41,42] So far in this chapter, we described and investigated an enzymatic network capable of achieving different NESS by mean of pre-fuel concentration. Nevertheless, the system, which involves a phosphorylation/dephosphorylation cycle, is more complex than expected.

Biochemical systems, like our cells, are generally seen as systems at a steady state, maintained by a continuous flux of intermediates. That means that cells change their states only as a response to external stimuli. However, the molecular processes are intrinsically rhythmic or periodic.

The majority of cellular regulatory processes are enzymatic and the phosphorylation/dephosphorylation reactions are essential for the cell signaling, motility, and reproduction. These covalent modifications affect directly proteins, changing their enzymatic activity or their binding affinity. These cycles have been predicted to exhibit 'ultrasensitivity'.[43,44] In the complex network of our cells, the activity of the molecular processes is regulated by internal and external signals. Therefore, the sensitivity of these processes to the regulation of such signals is an important function for the system. Specifically, with the term 'ultrasensitivity' we describe a sensitivity greater or less that to be expected from the Michaelis-Menten response (hyperbolic). This behavior is interesting as it is a pre-requisite for biochemical networks to generate oscillations or show bistability.[45,46] Ultrasensitivity occurs for cascades of phosphorylation cycles, for multiple phosphorylation sites or in case of product inhibition of the kinase or the phosphatase. Remarkably ultrasensitivity can be generated by multisite phosphorylation; it has been demonstrated that an oscillatory network can arise from a dual-phosphorylated cycle coupled with a feedback.[47]

Multi-site phosphorylation is a widely studied process.[48–51] The chemical modification mediated by a kinase and a phosphatase are typically assumed to be processive or nonprocessive. In a processive catalysis, before releasing the product, the enzymes carry out two phosphorylations and two dephosphorylations. Instead for nonprocessive catalysis, the enzymes release the monophosphorylated substrate, and a new interaction is needed to proceed with the fully (de)phosphorylation. Oscillatory dynamics can arise when these processes are installed, typically when the two enzymes operate with opposite mechanisms (processive or nonprocessive).[50] This behavior is ubiquitous in cell biology as in signaling cascades involving feedback loops.

Surprisingly, while exploring various pNESS conditions we stumbled upon oscillatory behavior (Figure 2.18). The oscillations arise from periodic phosphorylation and dephosphorylation reactions.

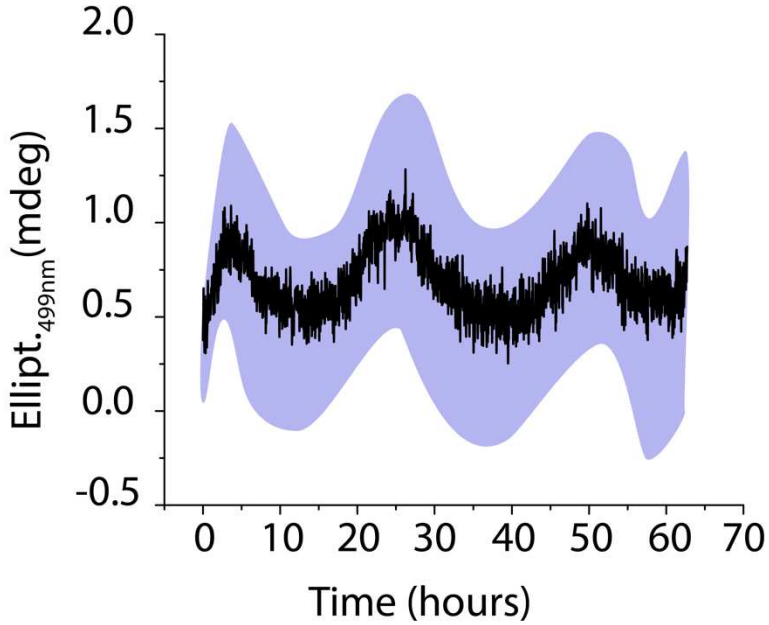

Figure 2.18. Oscillations of the Reactions Network. Time-course CD measurement at λ = 499 nm exhibiting oscillatory behavior. Conditions: **PDI** (100 μM), PEP (1 mM), PKA (0.3 μM), λPP (0.006 μM), PK (0.14 μM), ADP (0.1 μM). The data reported in the figure represents the mean of 3 independent experiments (black line shows averages; the shaded violet area shows the standard deviation).

The experiments were carried out by time-course CD spectroscopy (Figure 2.18). In particular, we noted that the system was sensitive to the variation of the concentration of Lambda phosphatase and ADP. Indeed, by decreasing the ADP concentration by 3 orders of magnitude we increasingly observed oscillations.

The first experiments were performed under closed unstirred batch conditions as before (quartz cuvette, optical path 1 mm). This made us worry that the changes in the CD signal were due to inhomogeneities in the cuvette. Therefore, we implemented various stirring mechanisms inside the cuvette to actively mixed the solution during the experiments. In a first attempt, we utilized a peristaltic pump: a needle was insert into the quartz cuvette and small bubbles were pumped from the bottom to the top of the cuvette, enabling a continuous mixing of the solution. However, we suspected that constant bubbling of air over many hours would have affected the result of the experiments (i.e., interaction and interference of enzymes activity, or drying of the solution). Thus, we decided to use a paper clip as stirrer for such narrow environment. A tiny piece of paper clip was coated with silver or gold (by sputter coating). The exact same oscillations conditions were repeated; and remarkably, the oscillatory behavior was again observed for all the reported experiments (i.e., unstirred, mixed with a peristaltic pump, stirred with Ag or Au coated paper clips). Figure 2.18 shows the periodical oscillation of the system, measured by CD spectroscopy; each

reported value (black) represents the mean of the different experiments performed, and the area (violet) the standard deviation.

This emergent behavior is still quite surprising as a batch oscillator in non-stirred conditions is very rare. Rondelez and co-workers programmed oscillations in a DNA network.[52] They used small DNA templates in which they encoded the network, and they obtained the expected behavior. This approach highlights the programmability of DNA strains and the difficulty in reproducing complex biochemical reactions in synthetic systems.

From previous work in our group, we knew that self-assembly can play an important role to achieve positive and/or negative feedback in a chemically-fueled reaction cycle.[53] Specifically, in the latter work, we found that cooperative self-assembly can lead to positive feedback, whereas formation of micron-sized colloids can lead to negative feedback. It was therefore not unreasonable to assume such a coupling in the current system. As a negative control experiments, we repeated the oscillating experimental conditions with 'kemptide', that is, the peptide sequence LRRASLG found it the two 'arms' of **PDI** recognized by the enzymes PKA and λPP. Surprisingly, oscillations were also observed for the kemptide experiments (Fig. 2.19).

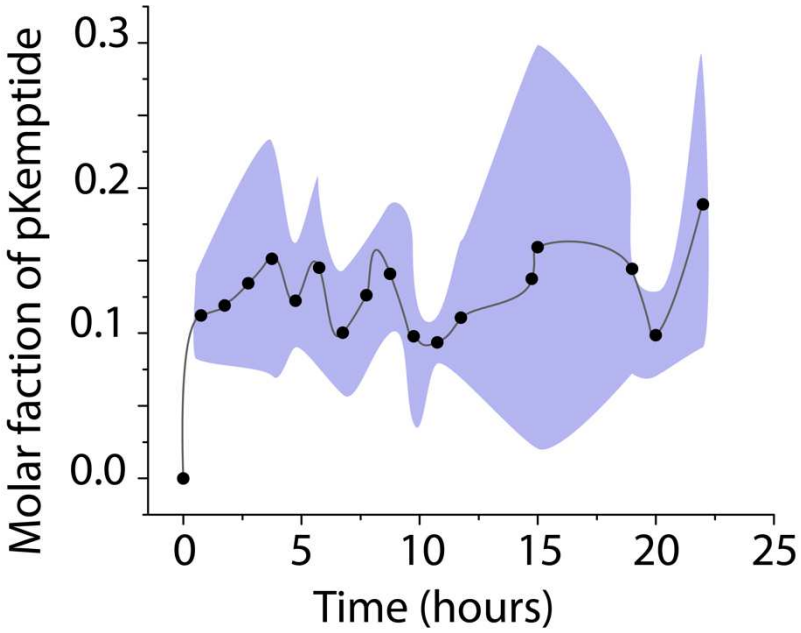

Figure 2.19. Oscillations of the Reactions Network. Mole fraction of pkemptide over 23 hours measured by LC-MS spectrometry. Conditions: kemptide (100 μM), PEP (1 mM), PKA (0.3 μM), λPP (0.006 μM), PK (0.14 μM), ADP (0.1 μM). The experiments were performed in a glass vial with a glass insert and run in triplicates. The data reported in the figure represents the mean of 3 independent experiments (points show averages; the shaded violet area shows the standard deviation).

The oscillatory behavior arises from a very complex network. Initially, we explained such behavior as a result of multi-site phosphorylation. However, the experiments conducted with the 'one arm' kemptide (LRRASLG) demonstrated that the system is more complex than expected. The periodic oscillation of the network can be the consequence of an internal regulation of the activity of pyruvate kinase by the kinase and the phosphatase. The phosphorylation of pyruvate kinase catalyzed by PKA could possibly act as a negative feedback on the ATP regeneration reaction. The phosphorylation is inhibiting the enzymatic activity of PK. Then, λPP dephosphorylates PK restoring the enzymatic activity. This regulatory process is well-known in the glycolysis pathway.[54]

During the stepwise and pNESS experiments, we did not observe the inhibition of PK activity. This might be due to the higher concentration of ADP, which is a substrate for PK and, thus, is competing with PKA. Nevertheless, the exhaustive comprehension of an oscillatory behavior is non-trivial. The system presents cycles of phosphorylation and dephosphorylation where substrates can negatively and/or positively controlled the enzymatic activity and where the enzymes themselves cause a negative loop.

2.10. Mathematical Modelling of the Enzymatic Network

In the previous publication from our group, we reported a mathematical model based on a set of ordinary differential equation ODEs describing the network formed by the enzymes PKA and λPP using mass action kinetics. The model resulted in a network of 55 chemical species, including free substrates, enzymes and products and the different enzyme-substrate complexes. The set of 55 ODEs was implemented in MATLAB to obtain the temporal evolution of the concentrations of all the species. However, the model took into account all the binding and inhibition arising from the different interactions with a total of 103 reactions happening in the network.

In order to describe the pNESS and the oscillatory behavior of the network, containing the ATP regeneration reaction, we decided to start from this model. In a first attempt, we tried to simplify it by studying all the reactions involved, removing the inhibition of ADP (as the ADP to ATP conversion reaction is present in the system) and by considering the inhibition of inorganic phosphate Pi null (as the concentration of λPP is decreased by one order magnitude). Nevertheless, the outcome started to be more complex than expected.

We therefore introduced several simplifications. Firstly, we only consider the phosphorylation of **PDI** (P) as **PDI→p2-PDI**. Therefore, we did not take into account the formation of the

monophosphorylated **p-PDI**. Secondly, we assumed that the three enzymes PKA, PK and λPP are operating at rate constants k_1, k_2 and k_3, therefore discarding their true (more complicated) mechanism. And additionally, the enzyme function and concentration were used implicit in the rate constants. In Figure 2.20 the species and the simplification of the enzymatic network are illustrated and the set of ordinary differential equations ODEs resulting from the network are reported in Table 2.2.

Table 2.2. Differential Equations. Overview of the differential equations describing the concentration versus time of the species depicted in Figure 2.20.

Differential equations (ODEs)
$\frac{d[P]}{dt} = -k_1 * [A] * [P] + k_2 * [PP]$
$\frac{d[PP]}{dt} = -k_2 * [PP] + k_1 * [A] * [P]$
$\frac{d[A]}{dt} = -k_1 * [A] * [P] + k_3 * [D] * [E]$
$\frac{d[D]}{dt} = k_1 * [A] * [P] - k_3 * [D] * [E]$
$\frac{d[E]}{dt} = -k_3 * [D] * [E]$
$\frac{d[Y]}{dt} = k_3 * [D] * [E]$

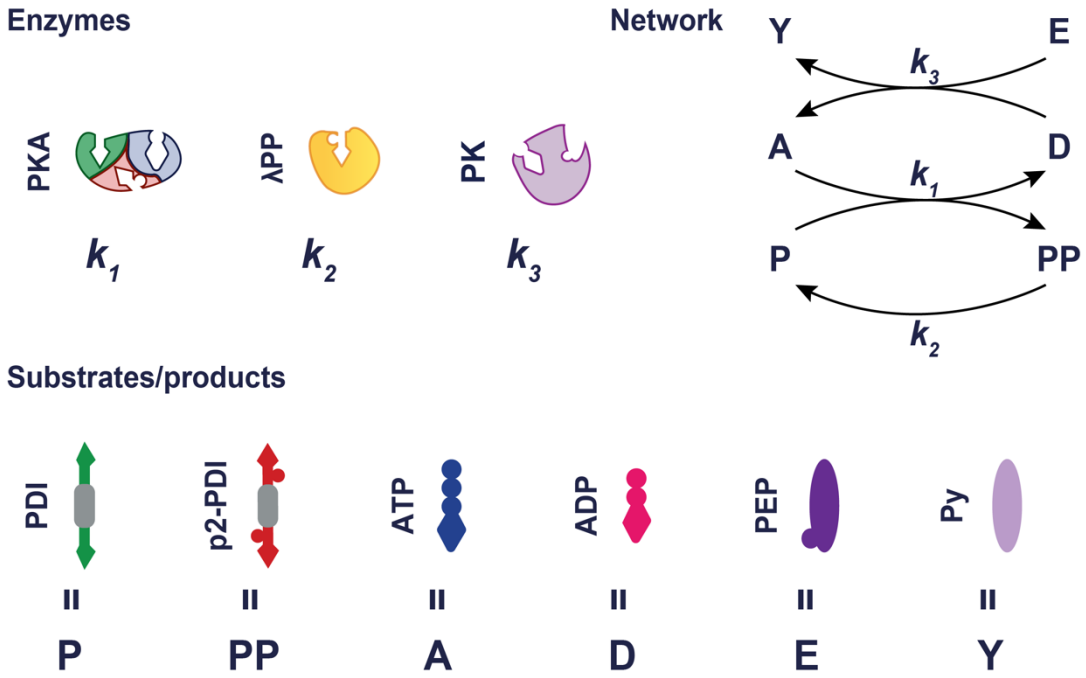

Figure 2.20. Overview of the Species present in the Enzymatic Network.

The ODEs were implemented in Python to obtain the variation in concentration of the species over time. Specifically, the model was implemented in Jupyter Notebook; the latter permits the study of the behavior of the network by a simultaneous change of the parameters k_1, k_2 and k_3 using 'sliders'. Thus, by entering the initial concentrations of the species, we could slide the parameters values to reach a behavior which was the closest to the pNESS experimentally observed. In Figure 2.21, the pNESS were obtained as a function of different concentrations of phosphoenolpyruvate, PEP. The graphs show the variation of the PP concentration over time, that is the total concentration of **p2-PDI** produced by the system. Three pseudo non-equilibrium steady states were reached at [PEP] 0.5 mM (Figure 2.21A), 1 mM (Figure 2.21B) and 2 mM (Figure 2.21C). These results are in agreement with the experimental data obtained during CD spectroscopy and LC-MS spectrometry measurements.

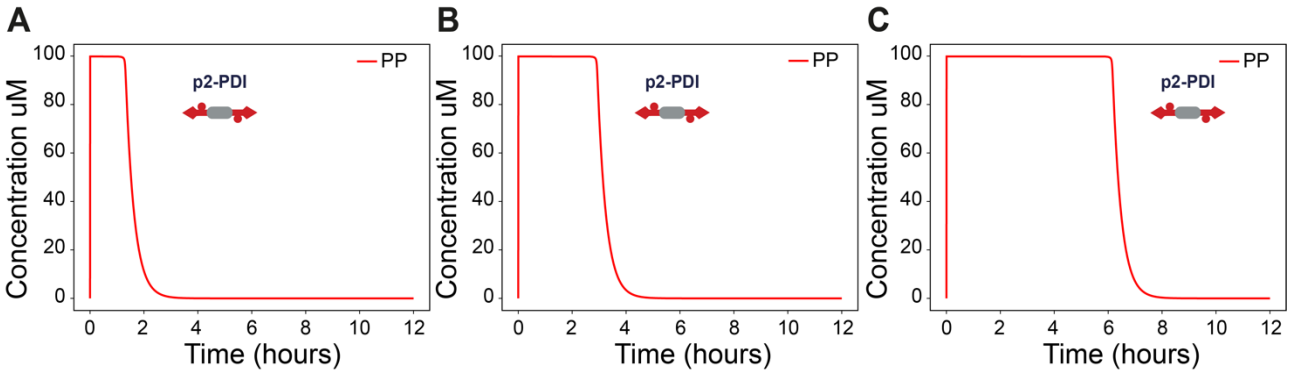

Figure 2.21. NESS described with a Mathematical Model. The graphs represent the change in concentration of **p2-PDI** (μM) over time (hours). The variation in concentration of PEP, 0.5 mM (A), 1 mM (B), 2 mM (C), leads to three different non-equilibrium steady states (plateau regions). The initial conditions were set at: [P] = 100 μM; [PP] = 0 μM; [A] = 0 μM; [D] = 100 μM; [E] = 500, 1000 or 2000 μM; [Y] = 0 μM; k_1 = 20; k_2 = 3.10; k_3 = 14.80.

Our simplified model can indeed explain the duration of the plateau depending on the PEP concentration as seen experimentally. However, this simple representation would not allow for oscillations to arise. Finding the exact origin of the observed oscillations (Figure 2.18) would be very interesting, but beyond the scope of this thesis.

2.11. Conclusions

We have presented a phosphorylation/dephosphorylation network where a peptide derivative **PDI** can be phosphorylated by a kinase (PKA) in the presence of ATP. The phosphorylated molecule **p2-PDI** undergoes dephosphorylation by a phosphatase (λPP), recovering the initial substrate. The hydrolysis of ATP during phosphorylation leads to the formation of ADP while the dephosphorylation produces a molecule of inorganic phosphate Pi. In this chapter, we have shown how waste (ADP, Pi) is affecting the network; a reaction for the recycling of ADP and the regeneration of fuel, ATP, mediated by a pyruvate kinase in the presence of phosphoenolpyruvate PEP has been investigated. The ATP regeneration reaction was coupled to the phosphorylation/dephosphorylation cycle. The enzymatic network has been explored by stimuli-responsive studies and interestingly the optimal conditions to reach non-equilibrium steady states were achieved. Specifically, the concentration of PEP ('pre-fuel') is directly related to production of ATP and thus, to the phosphorylation of **PDI** to **p2-PDI**. The variation of [PEP] induces the observation of different pseudo NESS (we refer to pseudo NESS as we worked in a close not stirred batch). These exciting results were confirmed by circular dichroism spectroscopy and LC-MS spectrometry. Surprisingly, the exploration of NESS conditions has driven the system to exhibit an

oscillatory behavior. The latter can be explained as a result of the phosphorylation/dephosphorylation cycle; indeed, it has been reported that multisite phosphorylation networks are prone to show such oscillatory behavior. Additionally, a mathematical modelling of the system was developed, which was suitable for rationalizing the pseudo NESS experiments, but not to understand the observed oscillations.

To conclude, in this chapter we have investigated non-equilibrium steady states under batch conditions, which we have used to develop life-like materials (see Chapter 4). In addition, we have found oscillations in the fraction of phosphorylated substrate due to a complex network of three enzymes.

2.12. Acknowledgements

Dr. Alessandro Sorrenti developed the phosphorylation/dephosphorylation reaction cycle and designed the **PDI** molecule. Serena De Piccoli synthesized **PDI**, studied the supramolecular polymerization, conceptualized the ATP regeneration *in situ* and integrated the enzymatic network, performed all the CD spectroscopy and LC-MS measurements, studied the kinetics via UV-Vis spectroscopy, studied the conditions for pNESS and oscillations and performed the mathematical modelling of the network. Prof. Thomas Hermans supervised the research.

2.13. Experimental section

General. The detailed synthesis and characterization of **PDI** and intermediates is shown in section 2.3 and Appendix 2.16 (HRMS spectra). ^{31}P NMR for the ATP regeneration, the calibration curve for the kinetics of the pyruvate kinase activity and control tests are provided in the Appendix 2.16.

Experimental conditions. The enzymatic reactions were performed, when not differently specified, in 50 mM Tris-HCl buffer (pH 7.5) containing 10 mM $MgCl_2$, 1 mM $MnCl_2$, 2 mM dithiothreitol (DTT) and 0.1 mM EDTA, at 25°C. The addition of $MnCl_2$ was required for the activity of λPP that is a Mn^{2+}-dependent phosphatase. We refer to this buffer as the reaction buffer. Typically, stock 1 mM **PDI** solutions, in freshly prepared reaction buffer, were prepared by accurate weighing, and used to obtain the diluted 100-200 μM **PDI** solutions used in the experiments. The stock solutions were freshly prepared the same day of the experiment.

Phosphorylation/dephosphorylation. In a typical phosphorylation experiment, an aliquot of freshly prepared ATP (1-4 μL from 20-50 mM solution in the reaction buffer) was added to the **PDI** solution (30-60 μL from 1 mM solution in the reaction buffer), followed by the addition of PKA (1-3 μL of the supplied 13 μM solution) and gentle shaking. The equivalents of ATP are with respect to **PDI** molecules (i.e., 2 eq. of ATP correspond to 1 eq. per phosphorylation site). The dephosphorylation was triggered by the addition of an aliquot of λPP (1 μL of the supplied 20 μM solution) to a **p2-PDI** solution, prepared as described above, in the absence of unreacted ATP. The enzymatic reactions were performed in screw cap sample vial equipped with a glass insert (when

followed by LC-MS), or in a 1 mm quartz cuvette (when followed spectroscopically by UV-Vis or CD spectroscopy).

UV-Vis measurements. UV-Vis spectroscopy was used to follow (in time) the evolution in aggregation upon phosphorylation as well as to study the thermodynamics of the supramolecular polymerization by heating/cooling cycles. To this end, we recorded the absorption spectra of **PDI** solution versus time or temperature, from which we calculated the ratio of the two maxima at 504 and 540 nm (A_{504nm} and A_{540nm}).

CD measurements. CD spectroscopy was used to study the changes in supramolecular chirality upon (de)phosphorylation both in stepwise and batch experiments. For the time-course CD measurements, the phosphorylation was triggered by the addition of PKA and ATP solutions to 300 μL of a **PDI** solution contained in 1 mm quartz cuvette, followed by gentle shaking. Afterwards the CD signal at a fixed wavelength was monitored versus time. Along with those experiments, steady states were studied. PK (0.1 μL of the supplied 43 μM solution), PKA (3 μL of the supplied 13 μM solution) and λPP (1 μL of the supplied 20 μM solution) were added to a **PDI** solution (30 μL of 1 mM solution in the reaction buffer) containing PEP (3-12 μL of 50 mM solution in the reaction buffer). The mixture was gentle shaking. The ADP (6 μL of 5 mM solution in the reaction buffer) was added after 1h and gentle mixed. The oscillatory behavior of the system was studied in the same experimental conditions. To achieve the homogenous stirring of the solution, firstly, a peristaltic pump was employed; a tube was inserted into the 1 mm quartz cuvette and air bubbles were gentle pump from the bottom to the top of the cuvette allowing the continuous mix. To avoid any possible interference of air with the enzymatic network, paper clips were employed. 1 mm piece of paper clip was cut, and sputter coated with a 10 nm gold layer (Emitech K575X) and silver.

LC-MS measurements. Liquid chromatography mass spectrometry (ESI-Ion trap) was used both to check qualitatively the (de)phosphorylation, as well as to calculate the fraction of the three species **PDI**, **p-PDI** and **p2-PDI** in the batch and steady state experiments (Figure 2.14 and Figure 2.17). For the latter, the reconstructed ion chromatogram (RIC) was obtained for the three species taking account their characteristic ions (m/z ± 2), from which their relative mole fractions were calculated. Additionally, liquid chromatography mass spectrometry (ESI-Ion trap) was used to calculate the fraction of kemptide (LRRSAL) (de)phosphorylated for the oscillation studies (Figure 2.19).

Dynamic Light Scattering (DLS) measurements. A 1 mM **PDI** solution was freshly prepared in the reaction buffer and diluted to obtain a 230 μM solution. The sample was measured on a home-built light scattering setup. The diffusion coefficient D was calculated with the slope of Γ/q^2 obtained from the experimental data. Hydrodynamic radius RH was then calculated using the Stokes-Einstein relation (Equation 5). The experiment was carried out at 293K.

Kinetics of ATP generation reaction. The pyruvate kinase (PK) activity has been studied with the use of the Pyruvate Kinase Assay Kit (MAK072, Sigma Aldrich, Germany). Pyruvate (product release with the generation of ATP) concentration is detected as a function of the colorimetric formation of the product in the presence of fluorescence peroxidase substrate. All the experiments were performed in a quartz cuvette (optical path 1 mm) following the absorbance at 570 nm. The kit contains: Pyruvate Kinase Assay Buffer, Pyruvate Standard, Fluorescent Peroxidase Substrate in DMSO, Pyruvate Kinase Enzyme Mix and Pyruvate Kinase Substrate Mix. All the components were prepared following the protocol given within the Kit. The calibration curve was obtained by measuring pyruvate standard solution in pyruvate kinase assay buffer (final volume = 50 μL) at concentrations: 0; 2; 4; 6; 8 and 10 nmol/cuvette (Figure 2.29 In Appendix 2.16).

The reaction has been studied at E >> S, that is 2mM ADP (4 μL of 50 mM solution in the reaction buffer), at different concentration of PEP (0.01, 0.1, 0.5, 1 and 2 mM). The same has been repeated for the measurement of K_M for ADP at [PEP] at 2 mM. For the final and total volume of 100 μL, Pyruvate Kinase Mix (2 μL), Fluorescent Peroxidase (2 μL), Pyruvate Kinase (0.1 μL of the supplied 43 μM solution) and the reaction buffer were added. The UV-Vis spectra were recorded each 2 minutes for 60 total cycles in a quartz cuvette, optical path 1 mm.

2.14. Synthesis of PDI

Synthesis of the perylene-L-alanine core, [N,N'-di(L-alanine)-perylene-3,4,9,10-tetracarboxylic acid diimide], 1

Perylene-3,4,9,10-tetracarboxylic acid bisanhydride (700 mg, 1.78 mmol), L-alanine (380 mg, 4.27 mmol, 2.4 eq.) and imidazole (5 g, 73 mmol, 41 eq.) were purged with N_2 in a 250 mL double neck round-bottom flask for 15 min. Then, the reaction mixture was heated up to 130°C and left stirring 30 min under N_2 atm. Afterwards, the mixture was cooled down to 90°C and 100 mL of water was added. The resulting solution was filtered, and the filtrate was added dropwise to 300 mL of isopropanol giving a red precipitate. The red solid was collected by filtration and dried under vacuum affording compound **1** (800 mg, 85%). ^{1}H NMR (400 MHz, DMSO-d6): δ 8.07 (s, 8H), δ 5.56 (dd, *J* = 7.0 Hz, 2H), δ 1.68 (d, *J* = 7.0 Hz, 6H).

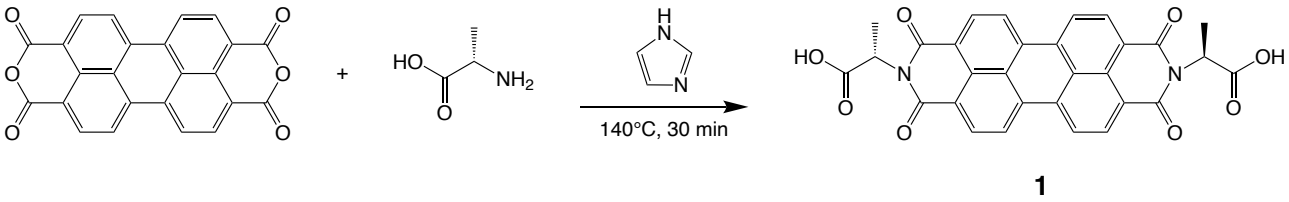

Figure 2.22. Synthesis of the core. Preparation of the perylene-L-alanine core.

Synthesis of Fmoc-LR(Pbf)R(Pbf)AS(tBu)L-OH peptide, 2

Peptide **2** was prepared by manual Fmoc solid phase peptide synthesis, SPPS, starting from 2-chlorotrityl resin loaded with L-leucine (200-400 mesh, 0.79 mmol/g capacity, typically 1 g). This is a highly acid labile resin that requires mild conditions for the final cleavage, which allowed to obtain fully protected **2**. The protocol involved: a) swelling of the resin (DMF); b) activation of the new amino acid at the carboxylate (with HBTU, 1 eq., HOBt, 1 eq., in the presence of DIPEA, 2 eq. for 10 min); c) coupling reaction (3 eq. of activate amino acid with respect to resin capacity); d) Fmoc deprotection to liberate the *N*-terminus of the growing peptide (piperidine/DMF 1:4, 2 x 20 min) plus 10 washes with DMF. The synthesis cycle b – d was repeated for the different amino acids. Fmoc deprotection was not performed in the last cycle. The activation step b was not performed in the case of arginine, to avoid the possible formation of an intermolecular δ-lactame that would decrease the coupling yield.[55] Finally, the fully protected target peptide 2 was cleaved off the resin

by treatment with 1% TFA in dichloromethane for 1h. Then 2 was dissolved in dichloromethane and washed with 1 M aqueous HCl to remove traces of piperidine coming from SPPS. The latter was a necessary step in order to avoid the formation of unwanted acyl-piperidine derivatives in the next coupling reaction. HRMS (ESI+) Calculated Mass for $C_{75}H_{109}N_{12}O_{16}S_2$ [M+H$^+$]: 1497.7520. Found: 1497.7368.

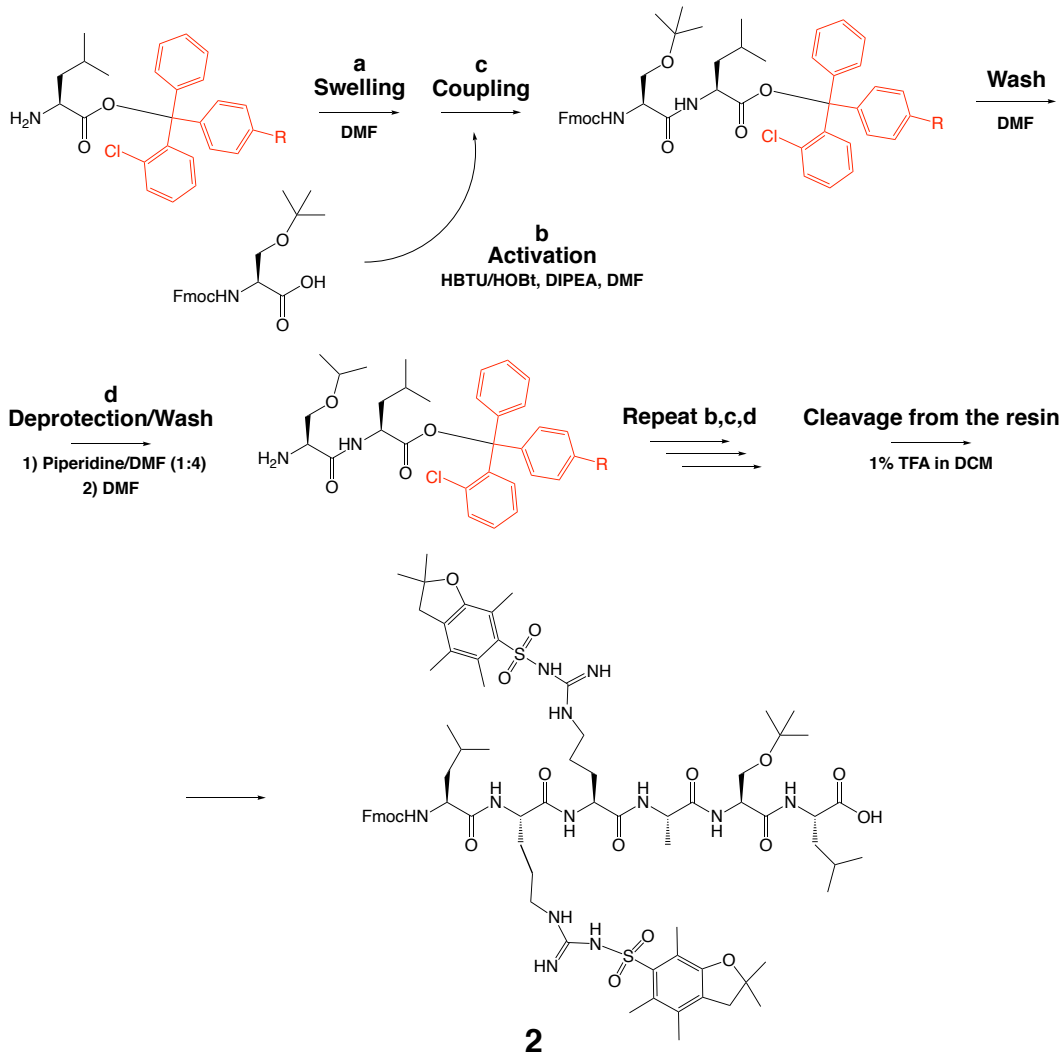

Figure 2.23. Solid phase synthesis. Fmoc solid phase peptide synthesis using the acid labile 2-chlorotrityl resin.

Synthesis of H-LR(Pbf)R(Pbf)AS(tBu)L-TEG, 5

HBTU (407 mg, 1.1 mmol, 1.2 eq.) and DIPEA (500 μL, 2.7 mmol, 3 eq.) were added to a solution of peptide **2** (1.34 g, 0.9 mmol, 1 eq.) in 8 mL DMF under N_2 atm. After 5 min, TEG-amine **3** (175.9 mg, 1.1 mmol, 1.2 eq.) dissolved in 4 mL DMF was added to this solution and the mixture was left stirring for 3 hours.[56] Then, the reaction was quenched by the addition of 100 mL dichloromethane, and the organic phase was washed with saturated $NaHCO_3$ and brine, dried over anhydrous $MgSO_4$ and concentrated to give **4**. Afterwards, the Fmoc protecting group was removed by treating compound **4** with 5 mL of a piperidine/DMF 1:4 mixture during 30 min. After this time, the solvent was evaporated and the crude re-dissolved in 100 mL MeOH. The obtained solution was washed with heptane (5x100 mL) and concentrate to afford **5** (1.19 g, 90% yield) as a sticky solid. HRMS (ESI+) Calculated Mass for $C_{67}H_{114}N_{13}O_{16}S_2$ [M+H$^+$]: 1420.7942. Found: 1420.7786.

Synthesis of PDI

HBTU (170 mg, 0.5 mmol, 2.4 eq.) and DIPEA (300 μL, 1.7 mmol, 9 eq.) were added to a solution of **1** (100 mg, 0.2 mmol, 1 eq.) in 8 mL DMF under N_2 atm. After 10 min, **5** (584.8 mg, 0.4, 2.2 eq.) dissolved in 4 mL DMF was added and the reaction mixture was left stirring for 4 hours. The reaction was quenched by the addition of 50 mL dichloromethane, and the organic phase was washed with saturated $NaHCO_3$ and brine, dried over anhydrous $MgSO_4$ and concentrated. The reaction crude was purified by flash chromatography using CH_2Cl_2/MeOH (gradient from 100:0 to 94:6) as eluent to give 6. Finally, the deprotection of the side chain protecting groups were carried out under strong acid conditions by treatment with TFA/H_2O, 9/1 (4 mL) for 4h. The latter solution was poured into 70 mL of diethyl ether resulting in the precipitation of a red solid, that was filtered, washed with diethyl ether, and dried affording **PDI** (47 mg, 11%). ^{1H}NMR (400 MHz, D_2O): δ 8.14 (m, 6H), 5.65 (s,2H), 4.36 (m,10H), 4.00-3.51 (m, 24H), 3.38 (m, 18H), 1.62 (m, 48H), 0.91 (m, 28H), 0.46 (s, 4H). HRMS (ESI+) Calculated Mass for $C_{104}H_{164}N_{28}O_{26}$ [M+4H$^+$]: 555.3087; found: 555.3115. [M+3H$^+$]: 740.0759; found: 740.0778. [M+2H$^+$]: 1109.6102; found: 1109.6053.

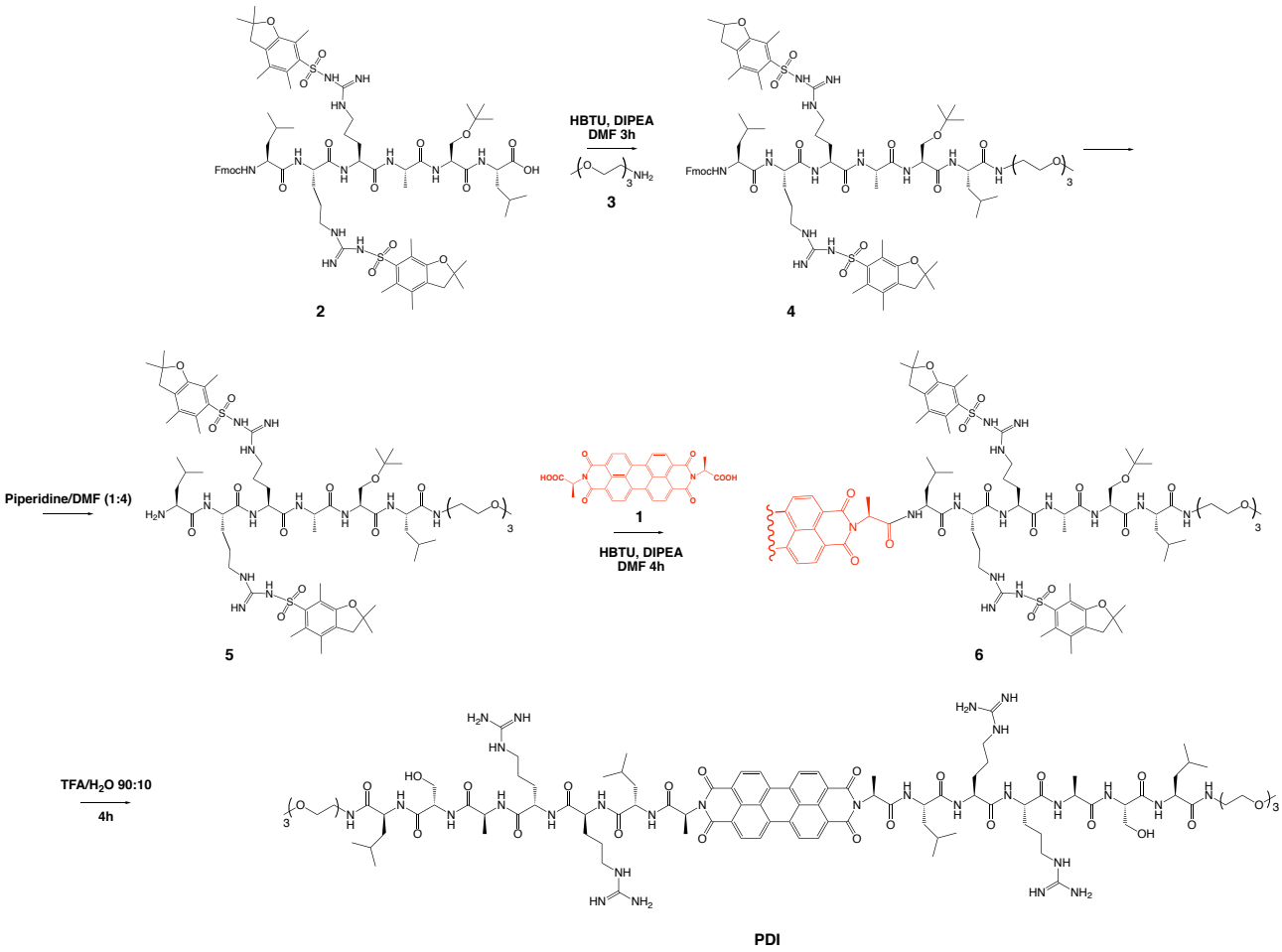

Figure 2.24. Target molecule PDI. Preparation of the final target **PDI**.

2.15. References

(1) Alberts, B. *Molecular Biology of the Cell*, Sixth edition.; Garland Science, Taylor and Francis Group: New York, NY, 2015.

(2) Dogterom, M.; Koenderink, G. H. Actin–Microtubule Crosstalk in Cell Biology. *Nat. Rev. Mol. Cell Biol.* **2019**, *20* (1), 38–54. https://doi.org/10.1038/s41580-018-0067-1.

(3) Bergman, J. ATP: The Perfect Energy Currency for the Cell. *Creat. Res. Soc.* **1999**, *36* (1), 15.

(4) Das, K.; Gabrielli, L.; Prins, L. J. Chemically-fueled Self-assembly in Biology and Chemistry. *Angew. Chem. Int. Ed.* **2021**, anie.202100274. https://doi.org/10.1002/anie.202100274.

(5) Shacter, E.; Chock, P. B.; Stadtman, E. R. Regulation through Phosphorylation/Dephosphorylation Cascade Systems. *J. Biol. Chem.* **1984**, *259* (19), 12252–12259. https://doi.org/10.1016/S0021-9258(20)71347-5.

(6) Brouhard, G. J.; Rice, L. M. Microtubule Dynamics: An Interplay of Biochemistry and Mechanics. *Nat. Rev. Mol. Cell Biol.* **2018**, *19* (7), 451–463. https://doi.org/10.1038/s41580-018-0009-y.

(7) Grzybowski, B. A.; Huck, W. T. S. The Nanotechnology of Life-Inspired Systems. *Nat. Nanotechnol.* **2016**, *11* (7), 585–592. https://doi.org/10.1038/nnano.2016.116.

(8) Sorrenti, A.; Leira-Iglesias, J.; Sato, A.; Hermans, T. M. Non-Equilibrium Steady States in Supramolecular Polymerization. *Nat. Commun.* **2017**, *8* (1), 15899. https://doi.org/10.1038/ncomms15899.

(9) Würthner, F.; Saha-Möller, C. R.; Fimmel, B.; Ogi, S.; Leowanawat, P.; Schmidt, D. Perylene Bisimide Dye Assemblies as Archetype Functional Supramolecular Materials. *Chem. Rev.* **2016**, *116* (3), 962–1052. https://doi.org/10.1021/acs.chemrev.5b00188.

(10) Kemp, B. E.; Pearson, R. B. Protein Kinase Recognition Sequence Motifs. *Trends Biochem. Sci.* **1990**, *15* (9), 342–346. https://doi.org/10.1016/0968-0004(90)90073-K.

(11) Görl, D.; Zhang, X.; Würthner, F. Molecular Assemblies of Perylene Bisimide Dyes in Water. *Angew. Chem. Int. Ed.* **2012**, *51* (26), 6328–6348. https://doi.org/10.1002/anie.201108690.

(12) Seibt, J.; Marquetand, P.; Engel, V.; Chen, Z.; Dehm, V.; Würthner, F. On the Geometry Dependence of Molecular Dimer Spectra with an Application to Aggregates of Perylene Bisimide. *Chem. Phys.* **2006**, *328* (1–3), 354–362. https://doi.org/10.1016/j.chemphys.2006.07.023.

(13) Würthner, F.; Chen, Z.; Hoeben, F. J. M.; Osswald, P.; You, C.-C.; Jonkheijm, P.; Herrikhuyzen, J. v.; Schenning, A. P. H. J.; van der Schoot, P. P. A. M.; Meijer, E. W.; Beckers, E. H. A.; Meskers, S. C. J.; Janssen, R. A. J. Supramolecular P−n-Heterojunctions by Co-Self-Organization of Oligo(*p* -Phenylene Vinylene) and Perylene Bisimide Dyes. *J. Am. Chem. Soc.* **2004**, *126* (34), 10611–10618. https://doi.org/10.1021/ja0475353.

(14) Rehm, T. H.; Stojković, M. R.; Rehm, S.; Škugor, M.; Piantanida, I.; Würthner, F. Interaction of Spermine-Alanine Functionalized Perylene Bisimide Dye Aggregates with Ds-DNA/RNA Secondary Structure. *Chem. Sci.* **2012**, *3* (12), 3393. https://doi.org/10.1039/c2sc20825c.

(15) Berova, N.; Nakanishi, K.; Woody, R. *Circular Dichroism: Principles and Applications*; John Wiley & Sons, 2000.

(16) Boekhoven, J.; Brizard, A. M.; Kowlgi, K. N. K.; Koper, G. J. M.; Eelkema, R.; van Esch, J. H. Dissipative Self-Assembly of a Molecular Gelator by Using a Chemical Fuel. *Angew. Chem. Int. Ed.* **2010**, *49* (28), 4825–4828. https://doi.org/10.1002/anie.201001511.

(17) Debnath, S.; Roy, S.; Ulijn, R. V. Peptide Nanofibers with Dynamic Instability through Nonequilibrium Biocatalytic Assembly. *J. Am. Chem. Soc.* **2013**, *135* (45), 16789–16792. https://doi.org/10.1021/ja4086353.

(18) Pezzato, C.; Prins, L. J. Transient Signal Generation in a Self-Assembled Nanosystem Fueled by ATP. *Nat. Commun.* **2015**, *6* (1), 7790. https://doi.org/10.1038/ncomms8790.

(19) Maiti, S.; Fortunati, I.; Ferrante, C.; Scrimin, P.; Prins, L. J. Dissipative Self-Assembly of Vesicular Nanoreactors. *Nat. Chem.* **2016**, *8* (7), 725–731. https://doi.org/10.1038/nchem.2511.

(20) Reiter, N. J.; White, D. J.; Rusnak, F. Inhibition of Bacteriophage λ Protein Phosphatase by Organic and Oxoanion Inhibitors. *Biochemistry* **2002**, *41* (3), 1051–1059. https://doi.org/10.1021/bi011577b.

(21) Smulders, M. J.; Nieuwenhuizen, M. L.; de Greef, T. A.; van der Schoot, P.; Schenning, A. H. J..; Meijer, E. W. How to Distinguish Isodesmic from Cooperative Supramolecular Polymerisation. *Chem. - Eur. J.* **2010**, *16* (1), 362–367. https://doi.org/10.1002/chem.200902415.

(22) Santos, F. J. V.; Nieto de Castro, C. A.; Dymond, J. H.; Dalaouti, N. K.; Assael, M. J.; Nagashima, A. Standard Reference Data for the Viscosity of Toluene. *J. Phys. Chem. Ref. Data* **2006**, *35* (1), 1–8. https://doi.org/10.1063/1.1928233.

(23) Whitehouse, S.; Feramisco, J. R.; Casnellie, J. E.; Krebs, E. G.; Walsh, D. A. Studies on the Kinetic Mechanism of the Catalytic Subunit of the CAMP-Dependent Protein Kinase. *J. Biol. Chem.* **1983**, *258* (6), 3693–3701. https://doi.org/10.1016/S0021-9258(18)32720-0.

(24) Scrutton, M. C.; Utter, M. F. The Regulation of Glycolysis and Gluconeogenesis in Animal Tissues. *Annu. Rev. Biochem.* **1968**, *37* (1), 249–302. https://doi.org/10.1146/annurev.bi.37.070168.001341.

(25) Andexer, J. N.; Richter, M. Emerging Enzymes for ATP Regeneration in Biocatalytic Processes. *ChemBioChem* **2015**, *16* (3), 380–386. https://doi.org/10.1002/cbic.201402550.
(26) Krimsky, I. Phosphorylation of Pyruvate by the Pyruvate Kinase Reaction and Reversal of Glycolysis in a Reconstructed System. *J. Biol Chem.* **1959**, *234* (2), 232-236.
(27) Kim, D.-M.; Swartz, J. R. Prolonging Cell-free Protein Synthesis with a Novel ATP Regeneration System. *Biotechnol. Bioeng.* **1999**, *66* (3), 180-188.
(28) Kim, D.-M.; Swartz, J. R. Regeneration of Adenosine Triphosphate from Glycolytic Intermediates for Cell-Free Protein Synthesis. *Biotechnol. Bioeng.* **2001**, *74* (4), 309–316. https://doi.org/10.1002/bit.1121.
(29) Nakajima, H.; Kondo, H.; Tsurutani, R.; Dombou, M.; Tomioka, I.; Tomita, K. Industrial Application of Adenosine 5′-Triphosphate Regeneration to Synthesis of Sugar Phosphates. In *Enzymes in Carbohydrate Synthesis*; Bednarski, M. D., Simon, E. S., Eds.; ACS Symposium Series; American Chemical Society: Washington, DC, 1991; Vol. 466, pp 111–120. https://doi.org/10.1021/bk-1991-0466.ch009.
(30) Dhiman, S.; Jain, A.; George, S. J. Transient Helicity: Fuel-Driven Temporal Control over Conformational Switching in a Supramolecular Polymer. *Angew. Chem. Int. Ed.* **2017**, *56* (5), 1329–1333. https://doi.org/10.1002/anie.201610946.
(31) Dhiman, S.; Jain, A.; Kumar, M.; George, S. J. Adenosine-Phosphate-Fueled, Temporally Programmed Supramolecular Polymers with Multiple Transient States. *J. Am. Chem. Soc.* **2017**, *139* (46), 16568–16575. https://doi.org/10.1021/jacs.7b07469.
(32) Nakashima, K. K.; Baaij, J. F.; Spruijt, E. Reversible Generation of Coacervate Droplets in an Enzymatic Network. *Soft Matter* **2018**, *14* (3), 361–367. https://doi.org/10.1039/C7SM01897E.
(33) Vogel, H. J.; Bridger, W. A. Phosphorus-31 Nuclear Magnetic Resonance Studies of the Methylene and Fluoro Analogs of Adenine Nucleotides. Effects of PH and Magnesium Ion Binding. *Biochemistry* **1982**, *21* (2), 394–401. https://doi.org/10.1021/bi00531a029.
(34) Ainsworth, S.; Macfarlane, N. A Kinetic Study of Rabbit Muscle Pyruvate Kinase. *Biochem. J.* **1973**, *131* (2), 223–236. https://doi.org/10.1042/bj1310223.
(35) Reynard, A. M.; Hass, L. F.; Jacobsen, D. D.; Boyer, P. D. The Correlation of Reaction Kinetics and Substrate Binding with the Mechanism of Pyruvate Kinase. *J. Biol. Chem.* **1961**, *236* (8), 2277–2283. https://doi.org/10.1016/S0021-9258(18)64071-2.
(36) Ekman, P.; Dahlqvist, U.; Humble, E.; Engström, L. Comparative Kinetic Studies on the L-Type Pyruvate Kinase from Rat Liver and the Enzyme Phosphorylated by Cyclic 3′,5′-AMP-Stimulated Protein Kinase. *Biochim. Biophys. Acta BBA - Enzymol.* **1976**, *429* (2), 374–382. https://doi.org/10.1016/0005-2744(76)90285-0.
(37) Rozengurt, E.; Jinénez De Asúa, L.; Carminatti, H. Some Kinetic Properties of Liver Pyruvate Kinase. *J. Biol. Chem.* **1969**, *244* (12), 3142–3147.
(38) Deng, J.; Walther, A. Pathway Complexity in Fuel-Driven DNA Nanostructures with Autonomous Reconfiguration of Multiple Dynamic Steady States. *J. Am. Chem. Soc.* **2020**, *142* (2), 685–689. https://doi.org/10.1021/jacs.9b11598.
(39) Heinen, L.; Walther, A. Programmable Dynamic Steady States in ATP-Driven Nonequilibrium DNA Systems. *Sci. Adv.* **2019**, 5 (7), eaaw0590.
(40) Kumar, M.; Brocorens, P.; Tonnelé, C.; Beljonne, D.; Surin, M.; George, S. J. A Dynamic Supramolecular Polymer with Stimuli-Responsive Handedness for in Situ Probing of Enzymatic ATP Hydrolysis. *Nat. Commun.* **2014**, *5* (1), 5793. https://doi.org/10.1038/ncomms6793.
(41) Nijemeisland, M.; Abdelmohsen, L. K. E. A.; Huck, W. T. S.; Wilson, D. A.; van Hest, J. C. M. A Compartmentalized Out-of-Equilibrium Enzymatic Reaction Network for Sustained Autonomous Movement. *ACS Cent. Sci.* **2016**, *2* (11), 843–849. https://doi.org/10.1021/acscentsci.6b00254.
(42) Helwig, B.; van Sluijs, B.; Pogodaev, A. A.; Postma, S. G. J.; Huck, W. T. S. Bottom-Up Construction of an Adaptive Enzymatic Reaction Network. *Angew. Chem. Int. Ed.* **2018**, *57* (43), 14065–14069. https://doi.org/10.1002/anie.201806944.
(43) Goldbeter, A.; Koshland, D. E. Ultrasensitivity in Biochemical Systems Controlled by Covalent Modification. *J. Biol. Chem.* **1984**, *259* (23), 14441–14447.
(44) Martins, B. M. C.; Swain, P. S. Ultrasensitivity in Phosphorylation-Dephosphorylation Cycles with Little Substrate. *PLoS Comput. Biol.* **2013**, *9* (8), e1003175. https://doi.org/10.1371/journal.pcbi.1003175.
(45) Ferrell, J. E.; Ha, S. H. Ultrasensitivity Part I: Michaelian Responses and Zero-Order Ultrasensitivity. *Trends Biochem. Sci.* **2014**, *39* (10), 496–503. https://doi.org/10.1016/j.tibs.2014.08.003.
(46) Ferrell, J. E.; Ha, S. H. Ultrasensitivity Part III: Cascades, Bistable Switches, and Oscillators. *Trends Biochem. Sci.* **2014**, *39* (12), 612–618. https://doi.org/10.1016/j.tibs.2014.10.002.
(47) Kholodenko, B. N. Negative Feedback and Ultrasensitivity Can Bring about Oscillations in the Mitogen-activated Protein Kinase Cascades. *Eur. J. Biochem.* **2000**, *263*, 1583–1588.
(48) Suwanmajo, T.; Krishnan, J. Mixed Mechanisms of Multi-Site Phosphorylation. *J. R. Soc. Interface* **2015**, *12* (107),

20141405. https://doi.org/10.1098/rsif.2014.1405.
(49) Markevich, N. I.; Hoek, J. B.; Kholodenko, B. N. Signaling Switches and Bistability Arising from Multisite Phosphorylation in Protein Kinase Cascades. *J. Cell Biol.* **2004**, *164* (3), 353–359. https://doi.org/10.1083/jcb.200308060.
(50) Chickarmane, V.; Kholodenko, B. N.; Sauro, H. M. Oscillatory Dynamics Arising from Competitive Inhibition and Multisite Phosphorylation. *J. Theor. Biol.* **2007**, *244* (1), 68–76. https://doi.org/10.1016/j.jtbi.2006.05.013.
(51) Conradi, C.; Mincheva, M.; Shiu, A. Emergence of Oscillations in a Mixed-Mechanism Phosphorylation System. *Bull. Math. Biol.* **2019**, *81* (6), 1829–1852. https://doi.org/10.1007/s11538-019-00580-6.
(52) Montagne, K.; Plasson, R.; Sakai, Y.; Fujii, T.; Rondelez, Y. Programming an *in Vitro* DNA Oscillator Using a Molecular Networking Strategy. *Mol. Syst. Biol.* **2011**, *7* (1), 466. https://doi.org/10.1038/msb.2010.120.
(53) Leira-Iglesias, J.; Tassoni, A.; Adachi, T.; Stich, M.; Hermans, T. M. Oscillations, Travelling Fronts and Patterns in a Supramolecular System. *Nat. Nanotechnol.* **2018**, *13* (11), 1021–1027. https://doi.org/10.1038/s41565-018-0270-4.
(54) Hers, H. G.; Hue, L. Gluconeogenesis and Related Aspects of Glycolysis. *Annu. Rev. Biochem.* **1983**, *52* (1), 617–653. https://doi.org/10.1146/annurev.bi.52.070183.003153.
(55) Isidro-Llobet, A.; Álvarez, M.; Albericio, F. Amino Acid-Protecting Groups. *Chem. Rev.* **2009**, *109* (6), 2455–2504. https://doi.org/10.1021/cr800323s.
(56) Scherman, O. A.; Ligthart, G. B. W. L.; Ohkawa, H.; Sijbesma, R. P.; Meijer, E. W. Olefin Metathesis and Quadruple Hydrogen Bonding: A Powerful Combination in Multistep Supramolecular Synthesis. *Proc. Natl. Acad. Sci.* **2006**, *103* (32), 11850–11855. https://doi.org/10.1073/pnas.0602413103.

2.16. Appendix

2.16.1. HRMS of final target PDI

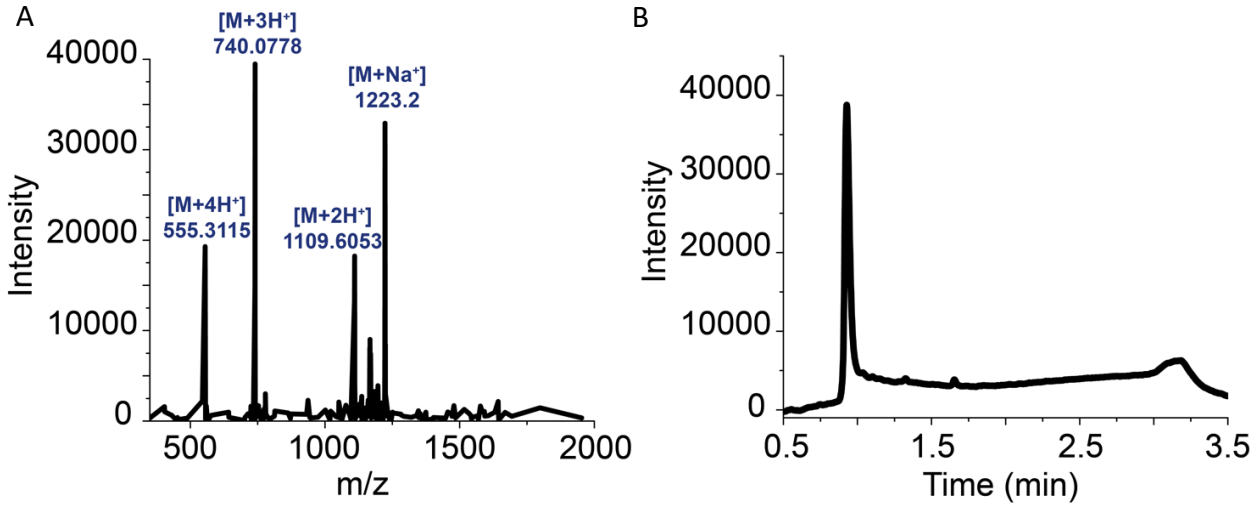

Figure 2.25. HRMS of the final target PDI. (A) Mass spectrum of the final molecule **PDI** in the reaction buffer. (B) Chromatogram of the final target **PDI** in the reaction buffer.

2.16.2. ^{31}P-nuclear magnetic resonance studies of the ATP generation reaction

^{31}P NMR spectra of the different species present in the reaction buffer were recorded: ADP, ADP and PEP, ATP formation upon addition of pyruvate kinase (PK). The solutions were prepared in the reaction buffer, described in the session 2.13 (Experimental conditions), 20% D_2O. The buffer was prepared without Mn^{2+}. ADP and PEP solutions were diluted to a final concentration of 1 mM (from freshly prepared 50 mM solutions in the reaction buffer).

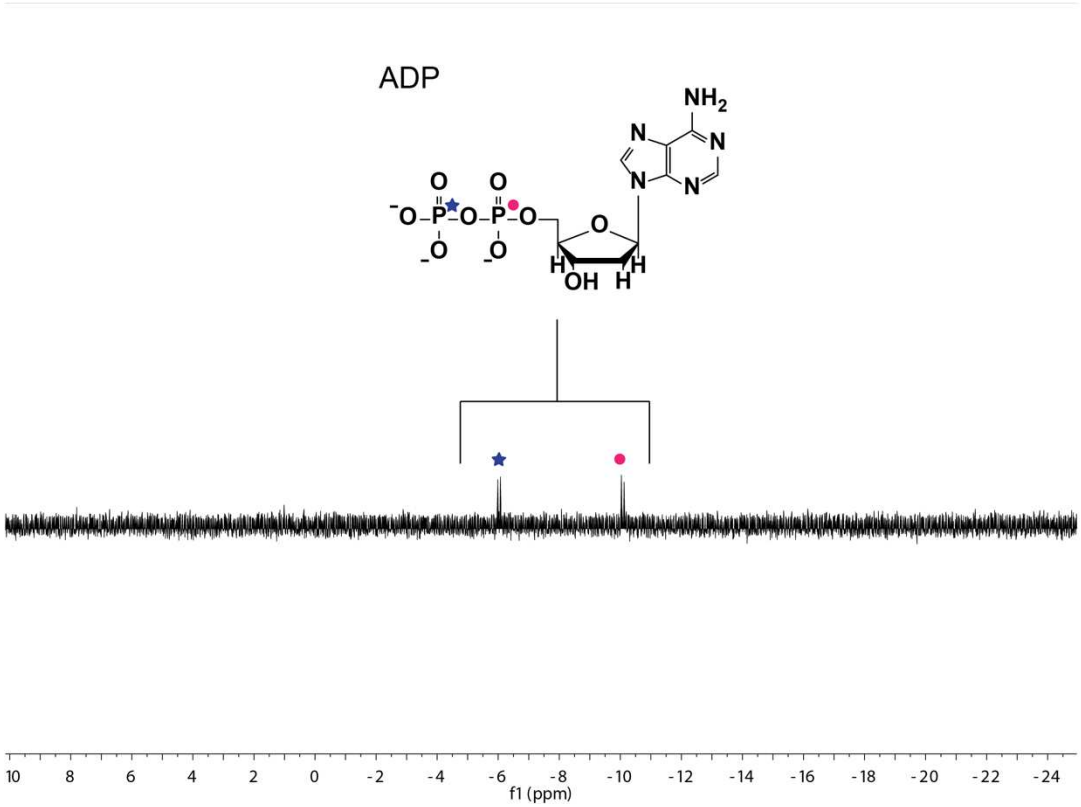

Figure 2.26. ^{31}P NMR spectrum of ADP. The peaks at -10 ppm and -6 ppm are respectively the phosphorus α (pink dot) and the β (blue star) of 1 mM ADP solution.

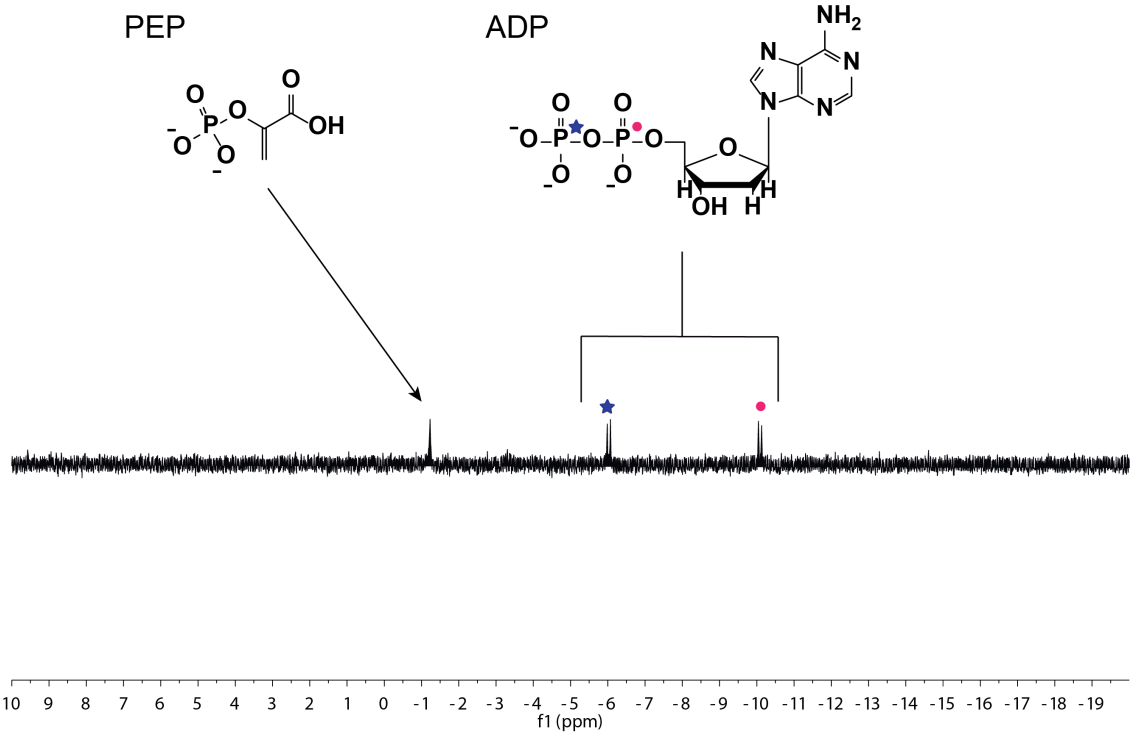

Figure 2.27. ^{31}P NMR spectrum of ADP and PEP. The peaks at -10 ppm and -6 ppm are respectively the phosphorus α (pink dot) and the β (blue star) of 1 mM ADP and 1 mM PEP solutions. The peak at -1.4 ppm corresponds to the phosphorous of phosphoenolpyruvate (PEP).

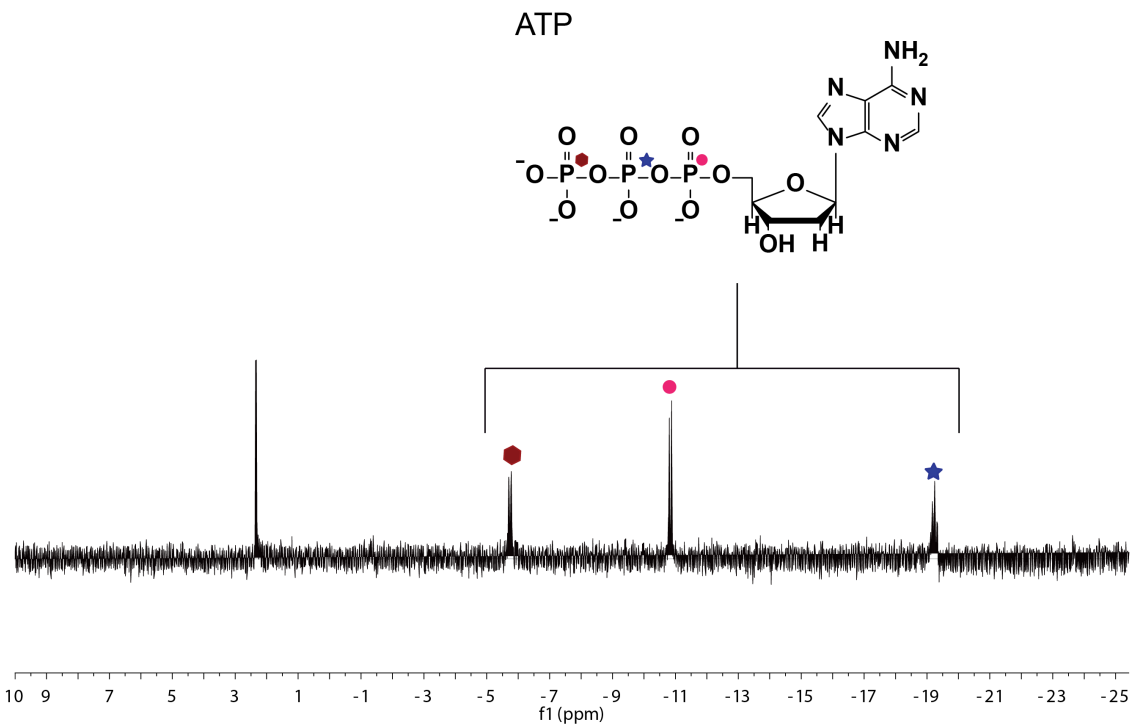

Figure 2.28. ^{31}P NMR spectrum after the addition of Pyruvate Kinase (PK) to the mixture. The peaks at -20 ppm, -11 ppm and -6 ppm are respectively the phosphorus β (blue star), α (pink dot) and γ (red hexagon) of ATP. The peak at 2 ppm is inorganic phosphate produced among the reaction.

2.16.3. Kinetics of ATP generation reaction

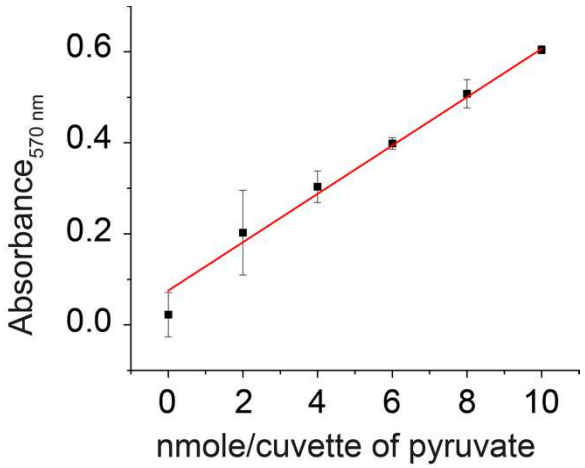

Figure 2.29. Calibration curve of the Pyruvate Standards for the Colorimetric Detection. 1 nmole/μL standard solution has been prepared by diluting 10 μL of 100 nmole/μL Pyruvate Standard with 990 μL of the Pyruvate Kinase Assay Buffer. To generate the 0 (blank), 2, 4, 6, 8, 10 nmole/cuvette solutions, to the Assay Buffer (50 μL) 0, 2, 4, 6, 8, 10 μL, respectively, of standard solution has been added.

2.16.4. Control tests

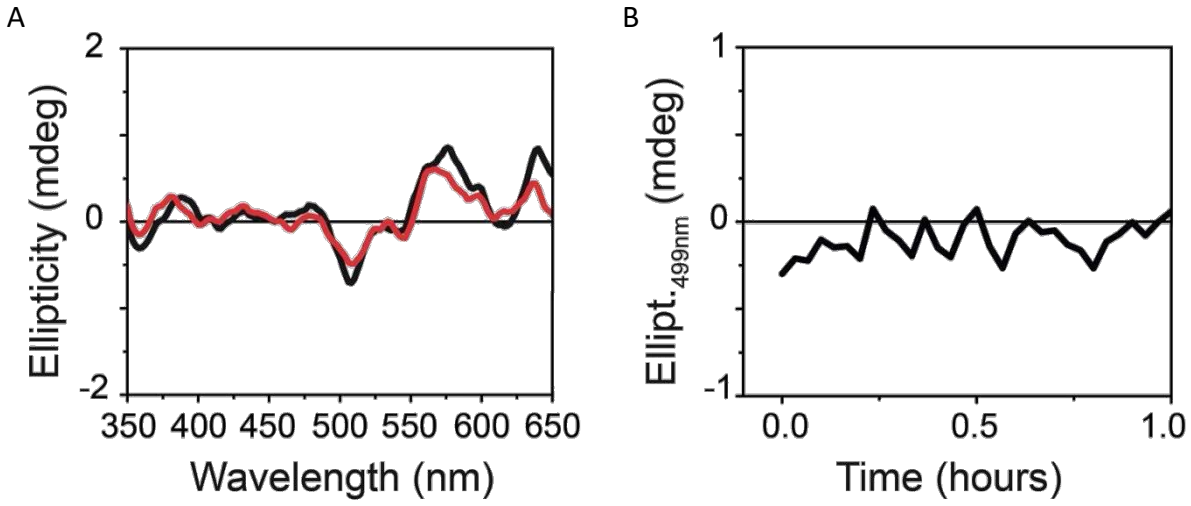

Figure 2.30. Control tests for Pyruvate CD signal. (A) CD spectrum of a 100 μM **PDI** solution in the reaction buffer without (black) and with a 100 μM pyruvate solution (red). (B) Time-course CD measurement of a 100 μM **PDI** solution in the presence of pyruvate (100 μM) at 25°C.

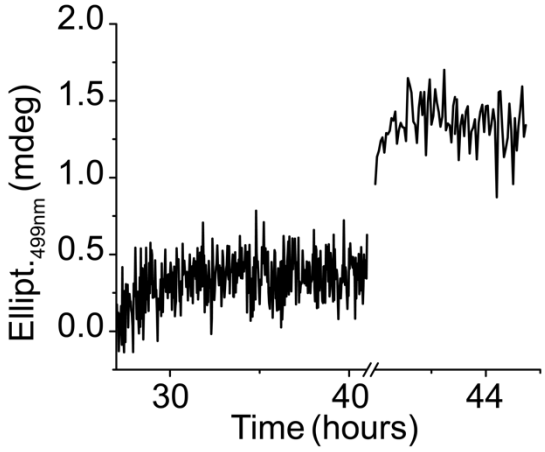

Figure 2.31. Control test for Enzymes Activity. To prove that the decrease of the signals during the non-equilibrium steady states is actually done by Lambda phosphatase and not by a decrease of the activity of PKA or PK, a shot of ADP (2 mM) has been added. After the addition of ADP, we could observe a fast increase of the CD signal meaning the phosphorylation of **PDI**. Over 45 hours no denaturation or loss of the enzymatic activity has been reported.

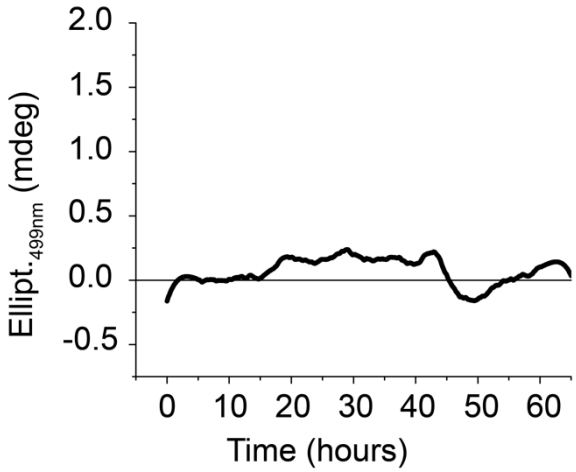

Figure 2.32. Control tests for the Oscillation studies. CD spectrum of 100 μM **PDI** solution in the reaction buffer at the oscillatory conditions without ADP. The CD signal has been recorded over 65 hours at 25°C.

2.16.4. Mathematical Modelling of the Enzymatic Network

```
#!/usr/bin/env python3
# -*- coding: utf-8 -*-
"""
Created on Mon Feb 24 17:59:52 2020

@author: serenadepiccoli
"""

import numpy as np
from scipy.integrate import odeint
import matplotlib.pyplot as plt

global k1,k2,k3
k1 = 20
k2 = 3.10
k3 = 14.80

def model (C,t):
    P = C[0]
    PP = C[1]
    A = C[2]
    D = C[3]
    E = C[4]
    Y = C[5]
    dPdt = -k1*A*P + k2*PP
    dPPdt = -k2*PP + k1*A*P
    dAdt = -k1*A*P + k3*D*E
    dDdt = k1*A*P - k3*D*E
    dEdt = -k3*D*E
    dYdt = k3*D*E
    return [dPdt, dPPdt, dAdt, dDdt, dEdt, dYdt]

#initial concentration uM
C0 = [100,0,0,100,500,0]

#time points
t = np.linspace (0,12,10000)

#solve ODE
Cint = odeint (model,C0,t)
#Cint = odeint (model,C0,t,rtol = 1*(10**-15), atol=1*(10**-15), mxstep=10000)

#simple plot results
plt.figure()
#plt.plot(t,Cint[:,0],label=r'P')
plt.plot(t,Cint[:,1],label=r'[PP]',color='navy')
#plt.loglog(t,Cint[:,2],label=r'A')
#plt.loglog(t,Cint[:,3],label=r'D')
#plt.loglog(t,Cint[:,4],label=r'E')
#plt.loglog(t,Cint[:,5],label=r'Y')
plt.ylabel ('Concentration uM')
plt.xlabel ('Time (hours)')
plt.legend (loc='best')
plt.show()

```

Chapter 3.

Self-assembling Inhibitor to Engineer Negative Feedback in an Enzymatic Reaction Cycle

Abstract

In this Chapter, we present preliminary results on a self-assembling inhibitor, designed to obtain negative feedback in the enzymatic network of Chapter 2. To this end, we have synthesized a known peptide inhibitor sequence GRTGRRNAI that is recognized by the cAMP-dependent protein kinase PKA and that acts as competitive inhibitor. The latter sequence was coupled to a perylene diimide core to create bivalent inhibitor analog **PDI-I**. We show that **PDI-I** self-sorts from **PDI**, thus forming separate self-assembled structures, whereas co-assembly was predicted *a priori*. Unexpected precipitation of micrometers length fibers in experiments with the overall enzymatic reaction cycle hampered the use of **PDI-I** as originally designed.

3.1. Introduction

In Chapter 2, we have reported and investigated a complex enzymatic network where fuel ATP is regenerated from waste ADP and where we explored different concentrations of pre-fuel PEP to achieve pseudo non-equilibrium steady states (pNESS). Additionally, the system exhibited an unexpected oscillatory behavior. Generally, biological oscillators arise from circuits containing positive and negative feedback or ones containing only negative feedback.[1] Therefore, adding additional positive and/or negative feedback in an enzymatic network could lead to a better control over the (de)phosphorylation reactions.[2]

When we talk about feedback we refer to processes that connect output signals to their inputs.[3] The concept of feedback becomes useful when describing physiological homeostasis[4], product inhibition[5] or metabolic oscillations[6], and many other biological processes. The presence of feedback loops in those systems provides fine control over cellular behavior by tuning the cellular signaling and the production of metabolites. To give an example, the endoplasmic reticulum (ER) Ca^{2+}-sensing protein STIM2 (stromal interaction molecule 2) maintains basal levels of Ca^{2+} through a negative feedback.[7] STIM2 is a transmembrane protein that mediates the influx of extracellular Ca^{2+} (Figure 3.1). When ER Ca^{2+} concentration become elevated STIM2 is inhibited, and this (indirectly) stops the influx of new Ca^{2+}. The latter represents a negative feedback loop that controls the variation of Ca^{2+} levels in a narrow range. As many biological processes are regulated by Ca^{2+}, the conservation of Ca^{2+} levels is vital.

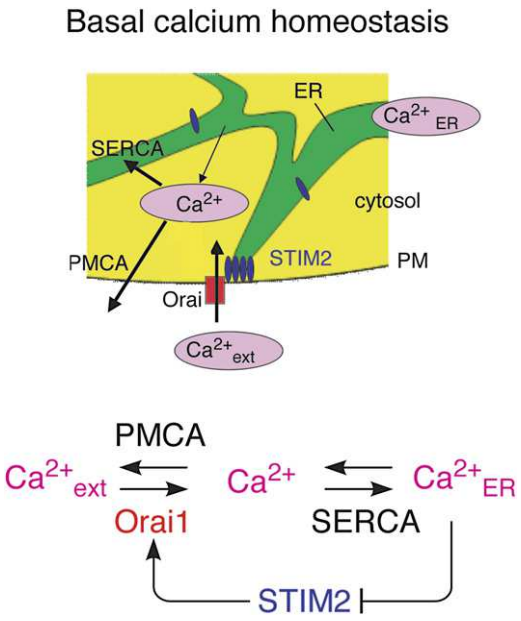

Figure 3.1. Model for STIM2 Function in Basal Ca^{2+} Homeostasis. Schematic representations of the conservation of basal ER Ca^{2+} level by negative feedback. Reproduced from Ref.[7]

An elegant example of feedback mechanisms in synthetic systems comes from Semenov *et al.*[2], where they built an adaptive enzymatic reaction network, in which positive and negative feedback enabled an adaptive output in response to a persistent input. Overall, positive and negative feedback led to robust oscillations in a wide range of experimental conditions.[2]

In order to assess some of the properties found in Nature (i.e., signaling, self-healing), our general idea was to develop a material consisting of chemically-fueled supramolecular polymers whose dynamics could be controlled using a reaction network. Specifically, the engineering of inhibitors that co-assemble with the substrates (**PDI** and **p2-PDI**) could lead to a better control over the amplification of the signal. For instance, if a stimulus is locally applied to the material it could possibly induce some supramolecular polymer rupture, resulting in a local release of inhibitor. The overall increased concentration of inhibitor would induce increased disassembly of the supramolecular fibers (since it is a PKA inhibitor preventing phosphorylations), and thus more release of inhibitor. Since, the latter process would be auto-amplifying, a wave of disassembly could propagate throughout the entire gel. Therefore, a single local input could lead to a global destruction of the gel. For the latter to work, we first need to show that we can make a co-assembling PKA inhibitor. Here, have looked at the self-assembly and inhibitory properties of a new inhibitor **PDI-I**—a bivalent self-assembling inhibitor.

3.2. Inhibitors: Design, Synthesis and Supramolecular Polymerization

The study of positive/negative feedback in the enzymatic network started with preliminary attempts on the competitive inhibition of cAMP-dependent protein kinase (PKA). Specifically, we investigated the heat-stable inhibitor protein of PKA.[8,9] The latter inhibits the catalytic subunit of PKA in the nanomolar range and acts as competitive inhibitor with respect to the phosphoryl-acceptor substrate, in our case, **PDI**. Glass *et al.*[8] investigated the entire 75 amino acid sequence to identify the active part needed for the inhibition. Based on the latter work, we selected sequence (14-22) Gly-Arg-Thr-Gly-Arg-Arg-Asn-Ala-Ile-NH_2 (GRTGRRNAI) for our experiments, which should have an inhibition constant (K_i) of 36 nM with respect to the kemptide peptide sequence LRRASLG (i.e., the phosphoryl-acceptor substrate).[8]

The peptide sequence GRTGRRNAI was synthesized as well as **PDI-I**, an analog of **PDI** where a perylene diimide core is coupled to the peptide inhibitor sequence (Figure 3.2B). The peptide

substrates were synthesized, in both cases, by Fmoc-solid phase peptide synthesis (SPPS). The detailed syntheses are reported in the section 3.9.

The peptide inhibitor and **PDI-I** allowed a comparative study of the inhibition of the phosphorylation reaction. As shown in Figure 3.2A, we envisaged the co-assembly between **PDI**/**p2-PDI** and **PDI-I**. The co-assembly will impact the enzymatic network as the inhibitor lowers the PKA activity, reducing the amount of **p2-PDI** produced and promoting the less assembled **PDI**. Overall, we will observe the inhibition of the phosphorylation reaction and the enhance of the dephosphorylation reaction.

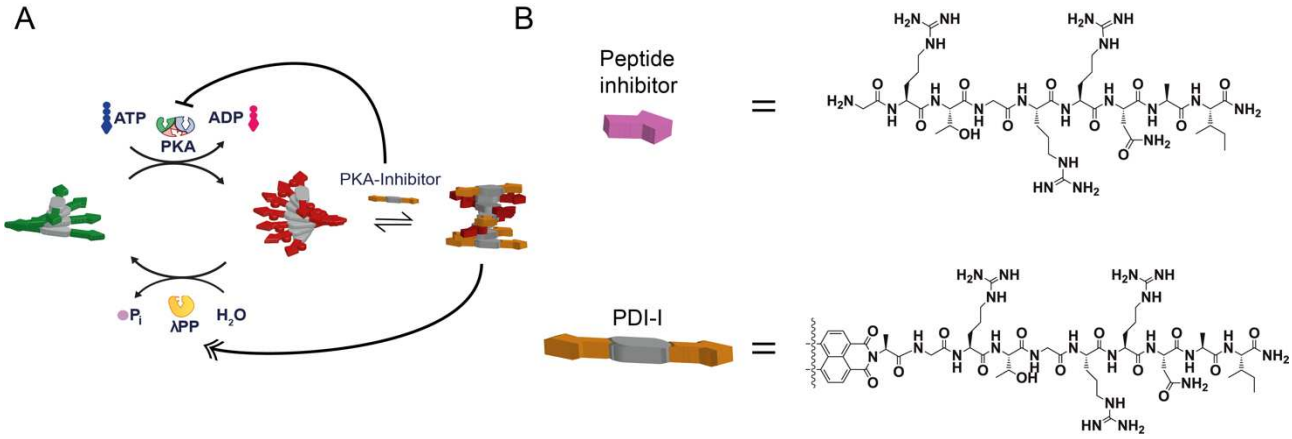

Figure 3.2. Negative Feedback. (A) The enzymatic network is represented: the inhibitor (orange) triggers the inhibition of the kinase (PKA), acting as a competitive inhibitor for the substrate **PDI**. The simultaneously co-assembly with **PDI**/**p2-PDI** is enhancing the dephosphorylation reaction. (B) Inhibitor peptide sequence GRTGRRNAI (pink) and **PDI-I** (orange), inhibitor sequence coupled to a perylene diimide core (half molecule is shown).

Temperature-dependent UV-Vis experiments were performed to compare the supramolecular polymerization of the synthesized **PDI-I** with the substrate **PDI**. A decrease of the ratio A_{504nm}/A_{540nm} was observed upon heating from 283 to 368 K, indicating partial disassembly of the polymer (Figure 3.3A). In addition, consecutive heating/cooling runs of 230 μM solutions (4 consecutive heating/cooling measurements at 1 K/min) were completely reversible. As previously shown, the ratio A_{504nm}/A_{540nm} can be described with an isodesmic (equal-K_{eq}) polymerization model. The following equation can be derived from the model[10]:

$$R_{obs}\,(T) = \frac{\left(R_{pol} - R_{mon}\right)^2}{1 + e^{-0.908\Delta H\frac{T - T_m}{RT_m^2}}} + R_{mon} \qquad \text{Eq. 1}$$

where $R_{obs}\,(T)$ = A_{504nm}/A_{540nm} at a given temperature (T), R_{pol} corresponds to the ratio $(A_{504nm}/A_{540nm})_{pol}$ for the fully polymerized **PDI-I** (value that we get from the fitting), R_{mon} corresponds to the ratio $(A_{504nm}/A_{540nm})_{mon}$ for monomeric **PDI-I** (set to 0.65) and R is the gas constant (8.314 J·mol^{-1}·K^{-1}). Equation 1 was used to fit the data (Figure 3.3B) and obtain the ΔH (the molar enthalpy related to the formation of the non-covalent interactions in the supramolecular polymerization) and the T_m (concentration dependent melting temperature, defined as the temperature for which the degree of polymerization α is 0.5), see Table 3.1.

Table 3.1. Thermodynamics parameters for PDI-I. Thermodynamics parameters for **PDI-I** supramolecular polymerization in reaction buffer compared to the substrate **PDI** (see Chapter 2).

Sample	ΔH (kJ·mol^{-1})	T_m (K)	DP_N (298 K)	K_{eq} (10^4 M^{-1})
PDI-I (230 μM)	-26.27 ± 0.58	338.2 ± 0.94	2.21	1.16
PDI (230 μM)	-38.72 ± 0.18	346.9 ± 0.11	2.48	1.59

In addition, the degree of aggregation (α) can be calculated using the following equation:

$$\alpha = \frac{R_{obs} - R_{mon}}{R_{pol} - R_{mon}} \qquad \text{Eq. 2}$$

Equation 2 was then used to calculate the degree of aggregation (Figure 3.3C). The latter can be used to obtain DP_N (average stack length) and the equilibrium constant (K_{eq}) at 298 K:

$$DP_N\,(T) = \frac{1}{\sqrt{1-\alpha(T)}} \qquad \text{Eq. 3}$$

$$K_{eq}(T) = \frac{\left[(2DPn-1)^2-1\right]}{4C_T} \qquad \text{Eq. 4}$$

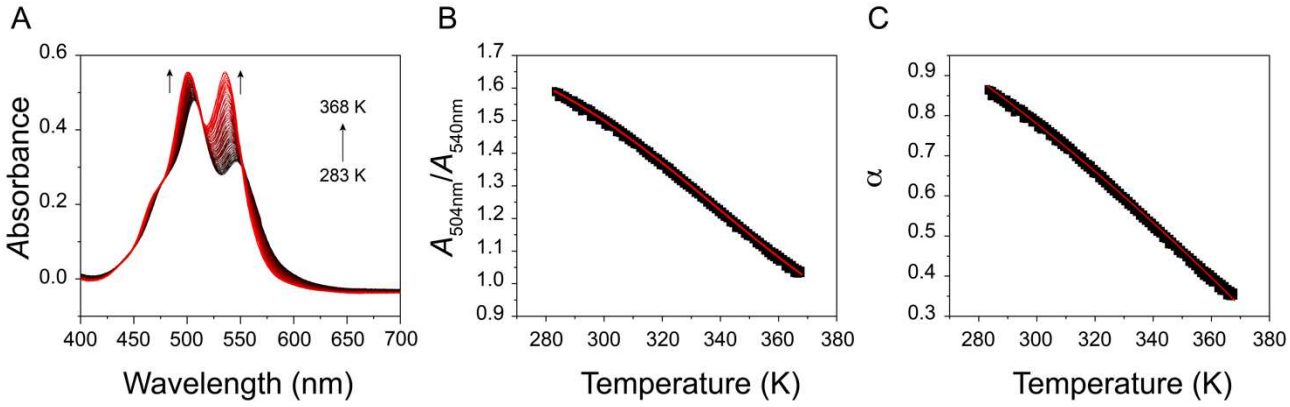

Figure 3.3. Thermodynamics of Supramolecular Polymerization. (A) Temperature dependent UV-Vis spectra of a 230 μM **PDI-I** solution in the reaction buffer in the presence of ATP (920 μM, 4 eq.) recorded at 283 to 368 K (quartz cuvette, optical path 1 mm). The arrows indicate the evolution of the two peaks (A_{504nm}, A_{540nm}). (B) Ratio A_{504nm}/A_{540nm} as a function of temperature calculated over four consecutive heating/cooling runs recorded between 283 and 368 K at 1 K interval (heating rate 1 K min^{-1}, optical path 1 mm). The red solid line corresponds to the fitting. (C) Temperature-dependent degree of aggregation, $\alpha(T)$, of **PDI-I** corresponding to the curve in panel B, calculated by using equation 2. The red line represents the theoretical $\alpha(T)$ for the isodesmic model calculated by using the values of ΔH and T_m obtained by the previous fitting.

Dynamic light scattering (DLS) was used to assess the dimension of the polymer. The experiment was performed for 230 μM **PDI-I** solution in the reaction buffer; the resulting slope D (Figure 3.4) of the linear fitting of the correlation Γ q^2 was used to obtain the final radius (R_H) of the assembly by following the equation:

$$R_H = \frac{k_B \cdot T}{6 \cdot \pi \cdot \mu \cdot D} \qquad \text{Eq. 5}$$

where k_B is the Boltzmann constant ($1.38 \cdot 10^{-23}$ m^2 kg s^{-2} K^{-1}), T is the temperature (293 K) and μ is the viscosity of the solvent (buffer, 0.001 Pa)[11]. The resulting value is R_H = 906 ± 82 nm. Thus, **PDI-I** self-assembles into larger polymers compared to the substrate **PDI** (note: the latter has a R_H of 511 ± 15 nm).

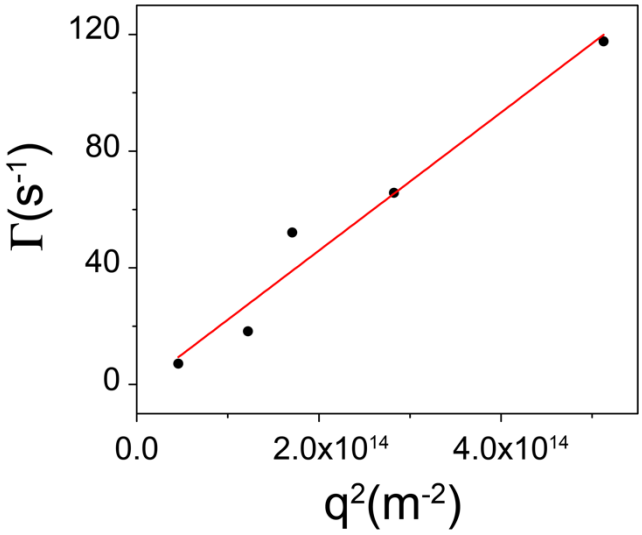

Figure 3.4. Dynamic Light Scattering (DLS) of PDI-I polymer. DLS measurement: relaxation Γ versus the square of the scattering vector q^2 for 230 μM **PDI-I** solution in the reaction buffer at 293 K. The corresponding slope D, resulting from the linear fitting (red line) is apply to equation 5. R_H for **PDI-I** assembly is calculated to be 906 ± 82 nm.

3.3. Preliminary studies of PKA-Inhibitors

After the synthesis of the two PKA-inhibitors and the study of the supramolecular polymerization of **PDI-I**, we investigated the effect on the phosphorylation reaction in the presence of inhibitors. First, we analyzed by circular dichroism (CD) spectroscopy the inhibition of the phosphorylation reaction in the presence of the peptide sequence GRTGRRNAI. The latter should have a K_i of 36 nM as reported in literature.[8,9] Time-course CD measurements were performed by following the wavelength at 499 nm. The increase of the CD signal at this specific wavelength is directly related to the inversion of the supramolecular chirality of the self-assembly due to the phosphorylation of **PDI** to **p2-PDI** (see Chapter 2).

In Figure 3.5, we observe the phosphorylation in absence (black) and presence of two different concentrations of peptide inhibitor, 0.036 and 100 μM. The phosphorylation of substrate **PDI** in the presence of PKA and ATP (black) reaches a plateau within 1.5 hours. That is, **PDI** is converted to **p2-PDI**. However, if we add the peptide inhibitor at 36 nM (purple), we observe a different kinetic profile. Specifically, the CD signal increases until it reaches a plateau after 8 hours that corresponds to the ~30% conversion of **PDI** into **p2-PDI** (as shown in Figure 3.5, the ellipticity value reaches a plateau around 2 mdeg while in absence of inhibitor the plateau is at 6 mdeg). Surprisingly, the addition of a higher concentration of peptide inhibitor (100 μM) resulted in less inhibition. We assume that this is due to the self-assembly of the peptide at higher concentration and, thus, resulting in a decreased interaction with the kinase.

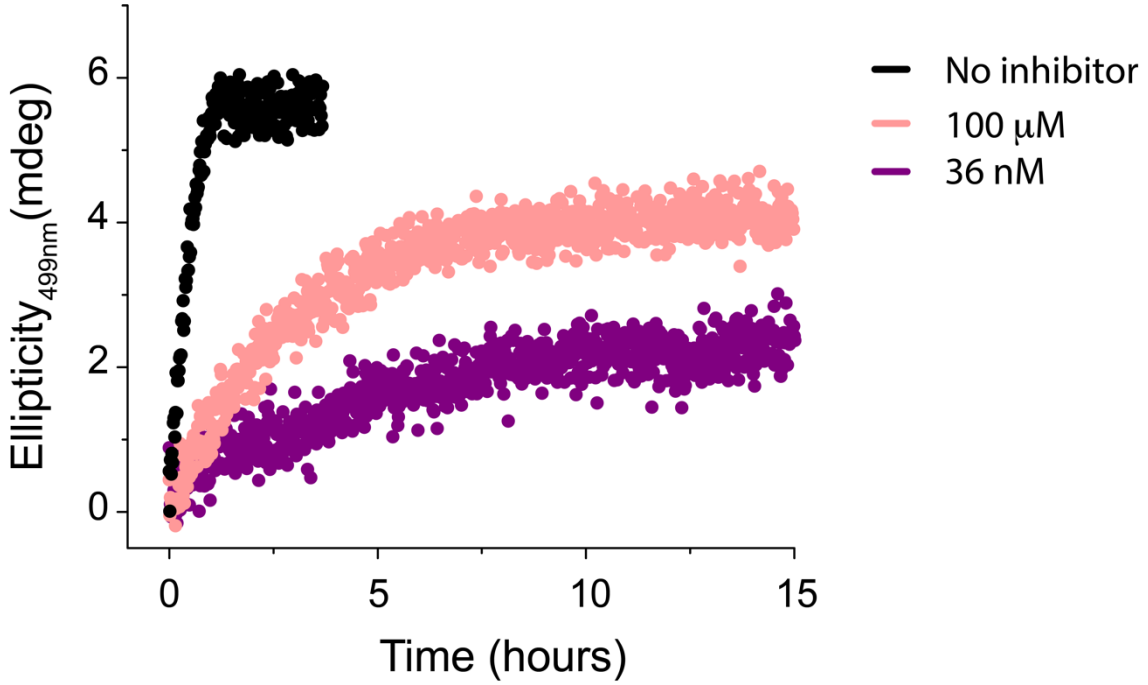

Figure 3.5. Phosphorylation of PDI in the presence of GRTGRRNAI. Time-course CD measurements of a 100 μM **PDI** solution containing PKA (0.13 μM) and ATP (1 mM, 10 eq.) in the absence (black) and presence of peptide inhibitor GRTGRRNAI at 36 nM (purple) and 100 μM (pink). The experiments were carried out in a quartz cuvette (optical path 1 mm) at 25 °C.

Despite the unexpected inhibitory behavior or GRTGRRNAI, we continued the comparison with **PDI-I** (Figure 3.6). The experiment was carried out for a **PDI** solution containing PKA and ATP, similarly to the experiments presented in Figure 3.6. Surprisingly, a behavior analogous to the one of peptide inhibitor at 36 nM was observed. The CD signal (orange in Figure 3.6) slowly increases until a plateau is reached at about 7.5 hours. Additionally, the ellipticity value reached does not correspond to the fully converted **PDI** into **p2-PDI**. Figure 3.6 shows also the comparison between the inhibition in the presence of the peptide inhibitor (pink) and the **PDI-I** (orange) at 100 μM. The higher inhibition observed in the case of **PDI-I** could be the result of an interaction between the inhibitor with **PDI** and/or **p2-PDI** and therefore a considerable impact on the phosphorylation reaction.

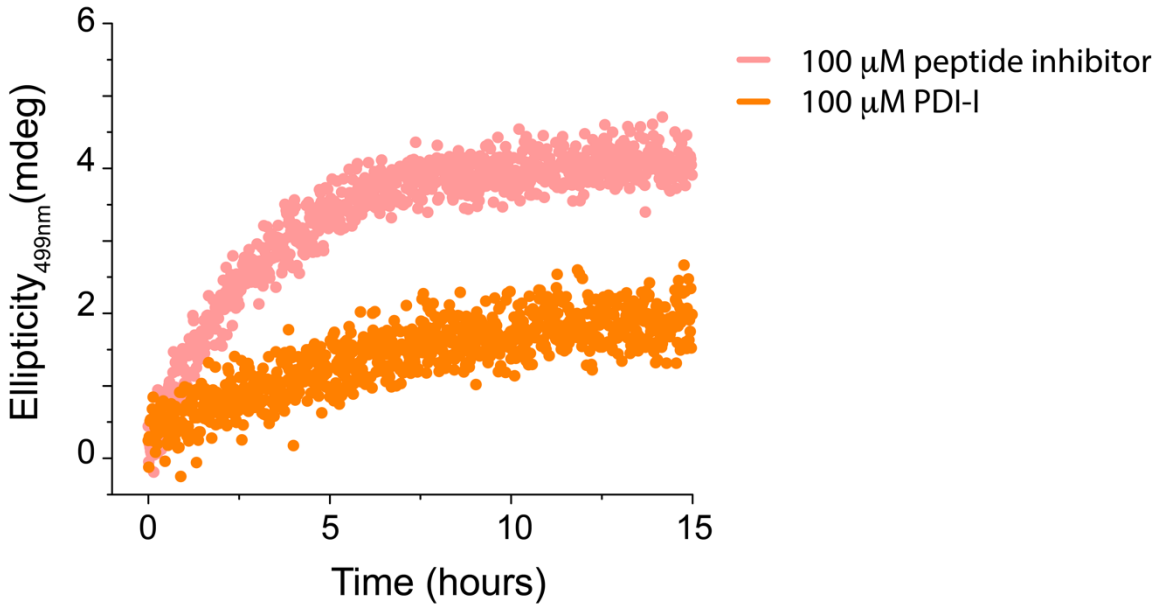

Figure 3.6. Phosphorylation of PDI in the presence of PDI-I. Time-course CD measurements of a 100 μM **PDI** solution containing PKA (0.13 μM) and ATP (1 mM, 10 eq.) in the presence of 100 μM peptide inhibitor GRTGRRNAI (pink) and 100 μM **PDI-I** (orange). The experiments were carried out in a quartz cuvette (optical path 1 mm) at 25 °C.

3.4. Co-assembly studies

In order to study the interaction between the three species **PDI**, **p2-PDI** and **PDI-I**, we performed self-sorting experiments. Self-sorting can be defined as recognition between molecules within complex mixtures.[12] Two regimes can be identified: i) "narcissistic", where molecules only self-assemble with themselves, or ii) "social", where there is an affinity for other types of molecules as well. Thus, the analysis of mixtures of the different species by CD spectroscopy could possibly reveal the tendency of the molecules to assemble with themselves or with others. To this end, we characterized the assembly of **PDI**/**PDI-I** and of **p2-PDI**/**PDI-I** at a total final concentration of 200 μM; 11 solutions were prepared for both mixtures, with decreasing concentration of **PDI** or **p2-PDI** and increasing concentration of **PDI-I** (detailed description is reported in the Experimental section 3.8). However, the experiments showed a linear increase as the fraction of **PDI-I** increases, going from 0 to 1 (Figure 3.7). For the species **PDI** and **p2-PDI**, it was previously demonstrated that they showed narcissistic self-sorting.[13] The same narcissistic behavior was observed for both cases when we studied the self-assembly of the species **PDI** and **PDI-I** (Figure 3.7A), and for **p2-PDI** and **PDI-I** (Figure 3.7B).

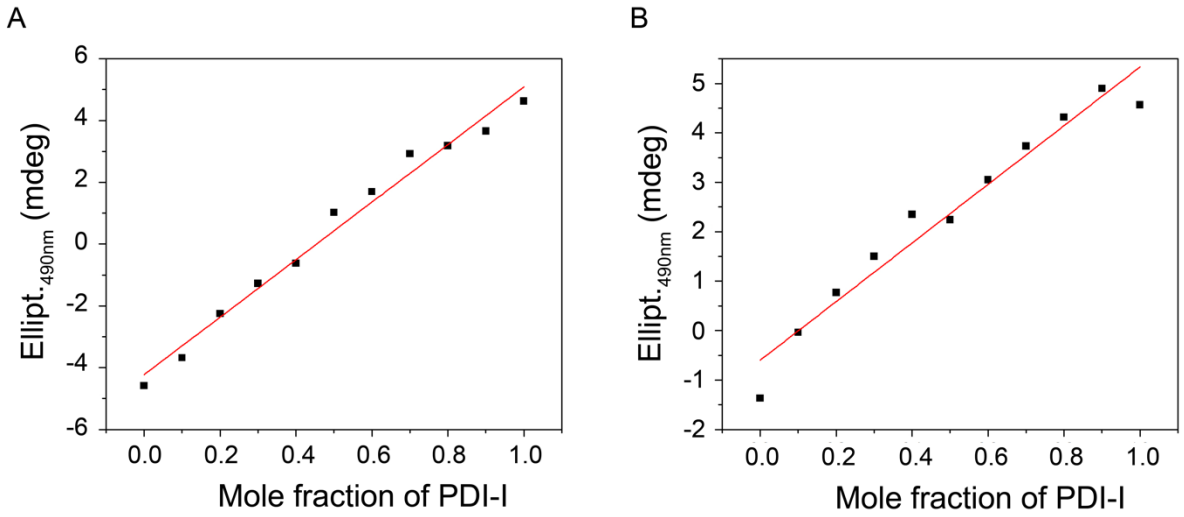

Figure 3.7. Self-sorting Experiments. (A) Self-sorting measurement of the assembly **PDI/PDI-I**. (B) Self-sorting measurement of the assembly **p2-PDI/PDI-I**. Ellipticity values measured at 490 nm (quartz cuvette, optical path 1 mm) plotted versus the increasing concentration of **PDI-I**.

To investigate the self-sorting behavior in more detail, we resorted to Powder X-Ray diffraction (XRD) to obtain the patterns for all the species and their mixtures. This approach was successfully used by Singh *et al.*[14] where a mixture of molecules showed a different pattern of packing compared to the individual hydrogelators, as a result of a co-assembled network. First, we performed the XRD analysis by drop casting **PDI-I** onto a silicon wafer. However, we could not drop cast **p2-PDI** as it was obtained by phosphorylation of **PDI** in the presence of ATP and PKA in the reaction buffer. In order to perform the experiments, the **p2-PDI** solution was, after the phosphorylation was completed, dialyzed using a dialysis membrane (MWCO = 0.5-1k Da) to remove the buffer. A drop cast solution of the reaction buffer would have merely revealed the diffraction pattern for the buffer (salts). After the dialysis, the **p2-PDI** solution was lyophilized. Thus, we repeated the same procedure, that is dialysis and lyophilization, for **PDI-I** and a 1:1 mixture of **p2-PDI** and **PDI-I** to obtain consistent results. The patterns we obtained were not entirely clear; Figure 3.8 shows the patterns for **p2-PDI** (black), **PDI-I** (orange) and the 1:1 mixture (red). As we can observe, the pattern resulting from the mixture derives mainly from the sum of the single **PDI-I** and **p2-PDI** patterns. However, a very small peak appears at 17.1° (dashed line in Figure 3.8) that is not present in either the two patterns and there are very few changes in the shape of the mixture pattern compare to the others. From these results, we can conclude that for the most part each species self-assembles with themselves, in a narcissistic regime.

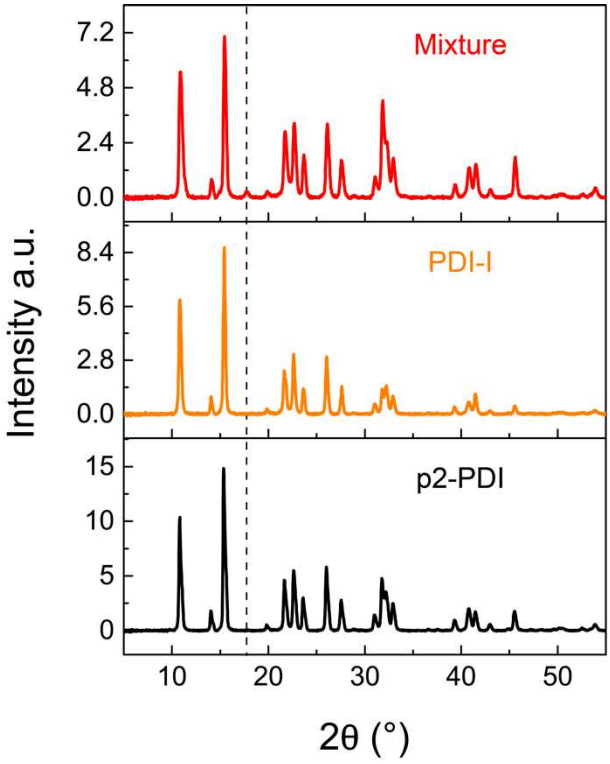

Figure 3.8. XRD Patterns. XRD patterns obtained from lyophilized powder of **p2-PDI** (black), **PDI-I** (orange) and a mixture 1:1 solution (red). The black dashed line at 17.1° indicates the peak emerged by the mixture of the two species.

3.5. Perturbation of pNESS

Finally, we investigated the influence of the **PDI-I** molecule during pseudo non-equilibrium steady states (pNESS). As described in Chapter 2, a third reaction was coupled to the (de)phosphorylation reactions in order to regenerate ATP from adenosine diphosphate (ADP) and phosphoenol pyruvate (PEP). The reaction is catalyzed by a pyruvate kinase PK. The continuous regeneration of fuel (ATP) *in situ* permitted to reach three different pNESS by varying the concentration of pre-fuel (PEP) added to the network.

In a first attempt, we reproduced the same pNESS conditions studied in Chapter 2 and we followed the evolution of the ellipticity at 499 nm over time. In Figure 3.9A, we observe the CD spectrum when we used 0.5 mM of PEP. In this case, a 100 μM **PDI-I** solution was added after 1 hour. We did not observe any pNESS, the CD signal increases after 8 hours and it is maintained (Figure 3.9A). Then, we investigate pNESS when [PEP] is 2 mM (Figure 3.9B) and the pNESS is maintained for about 7 hours. As for 0.5 mM PEP, a 100 μM **PDI-I** solution was added to the network after 1 hour from the beginning of the analysis. However, in this case we could not reach a pseudo non-equilibrium steady state with similar behavior as reported in Chapter 2 (Figure 3.9B). On the contrary, during the different experiments in the presence of **PDI-I**, we observed precipitates at the

bottom of the quartz cuvette (Figure 3.9C). The latter was noticed after pNESS studies with **PDI-I**. The precipitate was analyzed by optical microscopy (Figure 3.9C). From the images taken we can observe micrometers length fibers, from 100 up to 600 μm length. These fibers were stable over days and resisted gentle shacking of the cuvette. Additionally, during dialysis of **PDI-I** and the mixture 1:1 with **p2-PDI** for the preparation of XRD samples we already reported the observation of fibers onto the dialysis membrane (Figure 3.12 in Appendix 3.11).

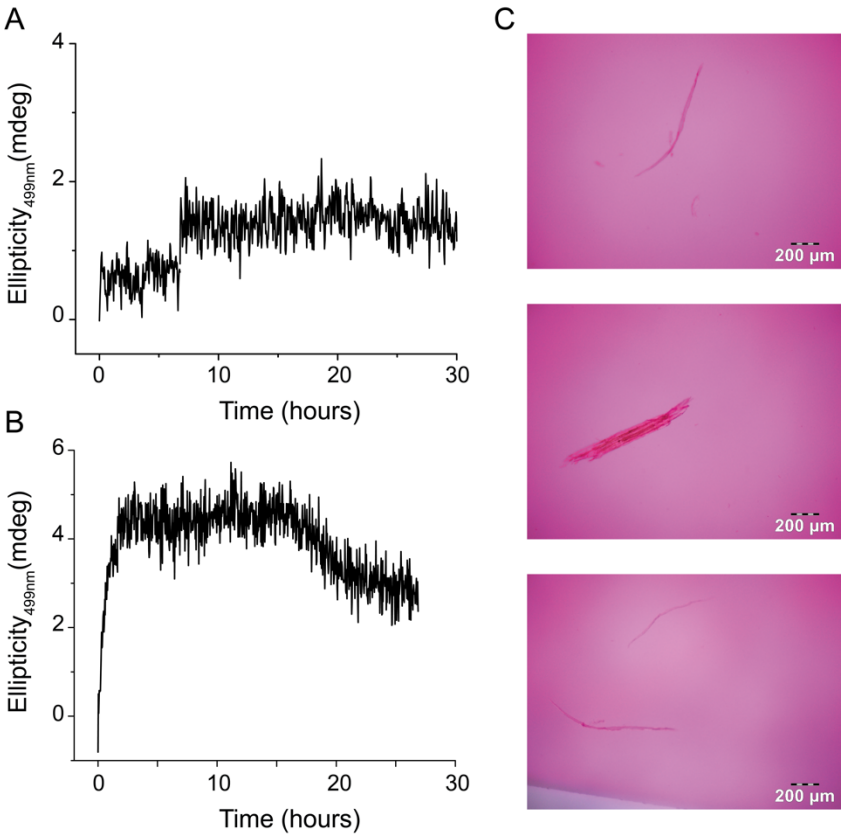

Figure 3.9. Pseudo Non-equilibrium Steady States. Time-course CD measurements at 499 nm (quartz cuvette, optical path 1 mm) of a 100 μM **PDI** solution containing PKA (0.014 μM), ADP (100 μM), PK (0.014 μM), λPP (0.06 μM), **PDI-I** (100 μM) and PEP at (A) 0.5 mM and at (B) 2 mM. (C) Optical microscopy pictures of the precipitate obtained during various experiments with **PDI-I**.

The same type of aggregates (micrometers order) was measured during dynamic light scattering experiments (Figure 3.13 in Appendix 3.11). Specifically, a solution containing a 1:1 mixture of **p2-PDI** and **PDI-I** was analyzed ~4 hours after the preparation of the sample. The R_H obtained is 1009 ± 90 nm. Thus, we hypothesized that with time the substrate **PDI-I** precipitates leading to the loss of the inhibitory activity. Indeed, **p2-PDI** behaves like a zwitterionic molecule as the four arginine are positively charged at pH 7.5 (4^+) and the phosphorylation reaction introduces negative charges (3.3^-).[13] **PDI-I** in its structure has six arginine positively charged in the reaction

buffer. Therefore, we can assume that charges are playing an important role in the formation and the precipitation of bigger aggregates.

3.6. Conclusions

In Chapter 3, we have investigated a competitive inhibitor of the substrate **PDI** for the activity of PKA. Two molecules were synthesized: the peptide sequence GRTGRRNAI and the sequence coupled to a perylene diimide core, **PDI-I**. The latter was designed to create a correspondent substrate for **PDI** as we envisaged a possible co-assembly **PDI-I** and **p2-PDI**/**PDI**. Interestingly, the study of PKA-inhibitors on the phosphorylation reaction showed a major effect coming from the PDI derivative (**PDI-I**) when added to the system, compared to the peptide inhibitor. Self-sorting experiments were conducted to understand the behavior, narcissistic or social, of the three (**PDI-I**, **PDI** and **p2-PDI**) self-assemblies. Together with XRD analysis, we concluded a narcissistic behavior as the three species self-assembled preferentially with themselves. Afterwards, we explored the perturbance of pNESS when **PDI-I** is added to the network. Despite many attempts, we were always observing the precipitation of micrometers length fibers at the bottom of the cuvette.

These studies were important as we envisioned the integration of positive/negative feedback loops in materials. However, the precipitation of these fibers needs further insights. Indeed, the precipitation of aggregates sequestrates inhibitor and, most probably, **p2-PDI**. This is exactly what we were looking at in the very beginning of this project. As such, the decreased concentration of two species in the enzymatic system may have consequences in the dynamics of the entire network.

3.7. Acknowledgements

Serena De Piccoli synthesized **PDI**, peptide inhibitor and **PDI-I** substrates and studied the supramolecular polymerization of **PDI-I**. She performed CD spectroscopy measurements, self-sorting experiments, analyzed the samples by Powder X-Ray diffraction and optical microscopy. Prof. Thomas Hermans supervised the work.

3.8. Experimental section

General. The detailed synthesis and characterization of peptide inhibitor and **PDI-I** is shown in section 3.9.

Experimental conditions. The enzymatic reactions were performed, when not differently specified, in 50 mM Tris-HCl buffer (pH 7.5) containing 10 mM $MgCl_2$, 1 mM $MnCl_2$, 2 mM dithiothreitol (DTT) and 0.1 mM EDTA, at 25°C. The addition of $MnCl_2$ was required for the activity of λPP that is a Mn^{2+}-dependent phosphatase. We refer to this buffer as the reaction buffer. Typically, stock 1 mM **PDI**/GRTGRRNAI/**PDI-I** solutions, in freshly prepared reaction buffer, were prepared by accurate weighing, and used to obtain the respective diluted 100-200 μM solutions used in the experiments. The stock solutions were freshly prepared the same day of the experiment.

Phosphorylation. In a typical phosphorylation experiment, an aliquot of freshly prepared ATP (1-4 μL from 20-50 mM solution in the reaction buffer) was added to the **PDI** solution (30-60 μL from 1 mM solution in the reaction buffer), followed by the addition of PKA (1-3 μL of the supplied 13 μM solution) and gentle shaking. The equivalents of ATP are with respect to **PDI** molecules (i.e., 2 eq. of ATP correspond to 1 eq. per phosphorylation site). The enzymatic reactions were performed in screw cap sample vial equipped with a glass insert (when followed by LC-MS), or in a 1 mm quartz cuvette (when followed spectroscopically by UV-Vis or CD spectroscopy).

CD measurements. CD spectroscopy was used to study the change in supramolecular chirality upon phosphorylation. For the time-course CD measurements, the phosphorylation was triggered by the addition of PKA and ATP solutions to 300 μL of a **PDI** solution contained in 1 mm quartz cuvette, followed by gentle shaking. Afterwards the CD signal at a fixed wavelength was monitored

versus time. For both experiments, with peptide inhibitor and **PDI-I**, 60 and 30 μL respectively of 1 mM solutions were added at the batch solution, containing **PDI**, PKA and ATP.

Along with those experiments, the perturbance of steady states caused by **PDI-I** was studied. PK (0.1 μL of the supplied 43 μM solution), PKA (3 μL of the supplied 13 μM solution) and λPP (1 μL of the supplied 20 μM solution) were added to a **PDI** solution (30 μL of 1 mM solution in the reaction buffer) containing PEP (3-12 μL of 50 mM solution in the reaction buffer). The mixture was gentle shaking. The ADP (6 μL of 5 mM solution in the reaction buffer) was added after 1h and gentle mixed. After 2 hours, when the NESS was reached by the system, a 100 μM **PDI-I** solution was added to the solution.

Powder X-Ray Diffraction. Powder X-ray diffraction measurements were performed on a Bruker D2 Phaser diffractometer (Source: Standard ceramic sealed tube CuKa 1.54184 Å. Detector: Bruker 1D-LYNXEYE). The samples were dop casted onto the surface (silicon wafer) after dialysis to remove the reaction buffer from the solutions. The measurements were done at 25°C.

Self-sorting experiments. The samples for the self-sorting experiments were prepared by mixing different volumes of 200 μM **PDI/PDI-I** and **p2-PDI/ PDI-I** solutions in the reaction buffer. **p2-PDI** was previously prepared by phosphorylation triggered by ATP (400 μM, 2 eq.) and PKA (0.065 μM). The mixed samples were incubated for 10 min at room temperature before the CD measurements. The experiments were performed in a 1 mm quartz cuvette.

3.9. Synthesis of the inhibitors

3.9.1. Synthesis of PDI

PDI was synthesized as reported in Chapter 2.

3.9.2. Synthesis of peptide GRTGRRNAI, 1

The peptide **GRTGRRNAI** was synthesized following the Fmoc solid phase peptide synthesis (Fmoc-SPPS) procedure. The resin used for GRTGRRNAI is the Rink Amide Resin (purchased by IRIS Biotech GMBH), loading 0.72 mmol/g. SPPS was performed in a sintered column where the influx of N_2 allowed the continuous stirring of the reaction. Firstly, the resin was placed in the reaction vessel and washed twice with DMF; DMF was then added to cover all the beads and let it swell for about 1 hour. After removing DMF by vacuum filtration, we proceeded by removing the Fmoc-protecting group of the resin with a solution of 4-methyl piperidine (20%) in DMF. The solution was let it react for 20 minutes and then removed. The resin was rinsed and washed with DMF.

The first Fmoc-protected amino acid (4 eq. with respects to the resin) was activated by the addition of a solution of 0.38 M HBTU in DMF (1ml for 0.1 mmol scale) and DIPEA (6 eq.); the reaction mixture was vortex and let it react for 2 minutes. The solution was poured onto the beads and let it react for 30 minutes and continuously mixed by gentle N_2 bubbling. The mixture was then rinse and washed with DMF. To control that all the free amino group reacted, we performed the Kaiser test. Few beads were washed with EtOH (to remove DMF and avoid a false positive) and transferred in a small glass tube. 100 μL ninhydrin solution (0.5 g in 10 mL of EtOH) and 100 μL KCN solution (0.4 mL of 1 mM $KCN_{(aq.)}$ in 20 mL of pyridine) were added to the beads. The tube was placed at 115°C for 5 minutes. Afterwards, 1 mL of ethanol and 1 mL of water were added. If the solution turns blue (or does the beads), free amino groups are still present and there is a need of a second coupling; if the solution remains colorless the test is negative, and we proceeded with the Fmoc deprotection, as described above.

A series of coupling-deprotection were repeated to obtain the final peptide sequence. After the final deprotection, the resin was washed several times with DCM in order to remove all the DMF. DCM was then removed by vacuum filtration and the resin was let it dry for 1-2 hours. The resin was weighted and transfer to a round bottom flask, and the reagent cocktail (95% TFA, 2.5% TIPS, 2.5% H_2O) was poured (~1 mL per 100 mg of resin). The mixture was let it react for 2 hours. After the cleavage, -20°C diethyl ether was added (~40 mL of Et_2O for 2 mL of cocktail) to the

reaction mixture leading to the precipitation of the peptide in several centrifuge tubes. The precipitation was followed by centrifugation at 4500 rpm for 3 minutes at 4°C and the precipitated was let in the freezer for few hours. The tubes were centrifuged again (4500 rpm for 3 minutes at 4°C) and the supernatant was discarded. The peptide was dissolved in a solution of ACN/H_2O (1:1) 0.1% TFA and filtered to get rid of the beads. The solution was then lyophilized, and the peptide was obtained as white powder. HRMS (ESI+) Calculated Mass for $C_{39}H_{74}N_{20}O_{11}$ [M+H^+]: 999.15. Found: 999.5881

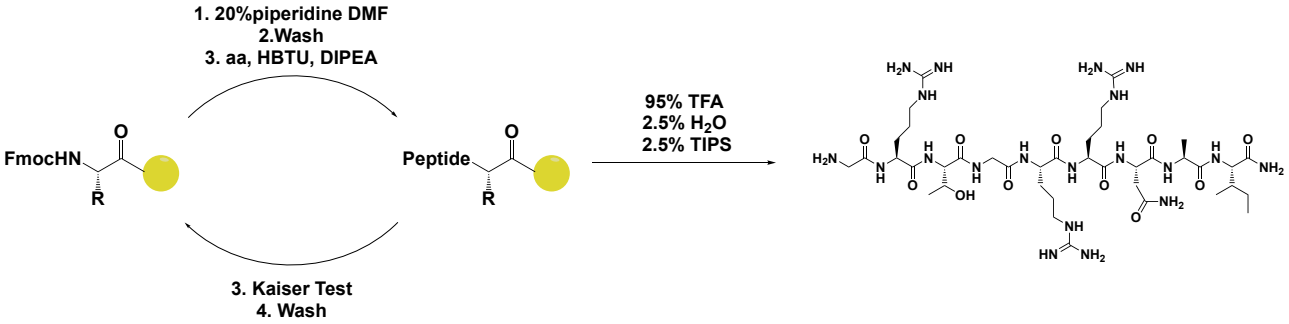

Figure 3.10. Solid Phase Peptide Synthesis of GRTGRRNAI-NH_2. Fmoc-solid phase peptide synthesis using the acid labile Fmoc-Rink amide resin.

3.9.3. Synthesis of PDI-I

Synthesis of the perylene-L-alanine core, [N,N'-di(L-alanine)-perylene-3,4,9,10-tetracarboxylic acid diimide], 2

Perylene-L-alanine core was synthesized as reported in Chapter 2.

Synthesis of GR(Pbf)T(tBu)GR(Pbf)R(Pbf)N(Trt)AI-NH_2 peptide, 3

Peptide **3** was prepared by manual Fmoc solid phase peptide synthesis, SPPS, starting from Fmoc-Sieber resin (purchased by IRIS Biotech GMBH), loading 0.59 mmol/g. This is a highly acid labile resin that requires mild conditions for the final cleavage, which allowed to obtain fully protected **3**. The protocol followed for the coupling and the deprotection was the same as the one described for compound **1**.

The fully protected target peptide **3** was cleaved off the resin by treatment with 1% TFA in dichloromethane for 1h. Then, **2** was dissolved in dichloromethane and washed with 1 M aqueous HCl to remove traces of piperidine coming from SPPS. HRMS (ESI+) Calculated Mass for $C_{101}H_{144}N_{20}O_{20}S_3$ [M+H$^+$]: 2054.56. Found: 417.22 [M+5$^+$], 686.73 [M+3$^+$].

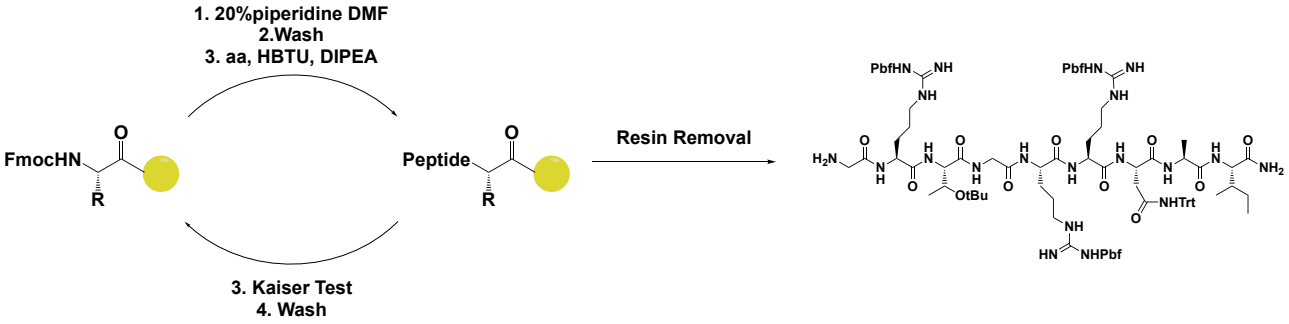

Figure 3.11. Solid Phase Peptide Synthesis. Fmoc-solid phase peptide synthesis using the acid labile Fmoc-sieber resin.

Synthesis of PDI-I

HBTU (67 mg, 0.17 mmol, 2.4 eq.) and DIPEA (115 μL, 0.66 mmol, 9 eq.) were added to a solution of **2** (39.5 mg, 0.07 mmol, 1 eq.) in 8 mL DMF under N_2 atm. After 10 min, **3** (334 mg, 0.16 mmol 2.2 eq.) dissolved in 4 mL DMF was added and the reaction mixture was left stirring for 4 hours. The reaction was quenched by the addition of 50 mL dichloromethane, and the organic phase was washed with saturated $NaHCO_3$ and brine, dried over anhydrous $MgSO_4$ and concentrated. The reaction crude was purified by flash chromatography using CH_2Cl_2/MeOH (gradient from 100:0 to 94:6) as eluent to give 6. Finally, the deprotection of the side chain protecting groups were carried out under strong acid conditions by treatment with 95% TFA, 2.5% H_2O and 2.5% TIPS for 2 hours. The latter solution was poured into 70 mL of diethyl ether resulting in the precipitation of a red solid, that was filtered, washed with diethyl ether, and dried affording **PDI-I**. HRMS (ESI+) Calculated Mass for $C_{108}H_{164}N_{42}O_{28}$ [M+3H$^+$]: 833.25; found: 832.7590 [M+2H$^+$]: 1249.375; found: 1248.1338.

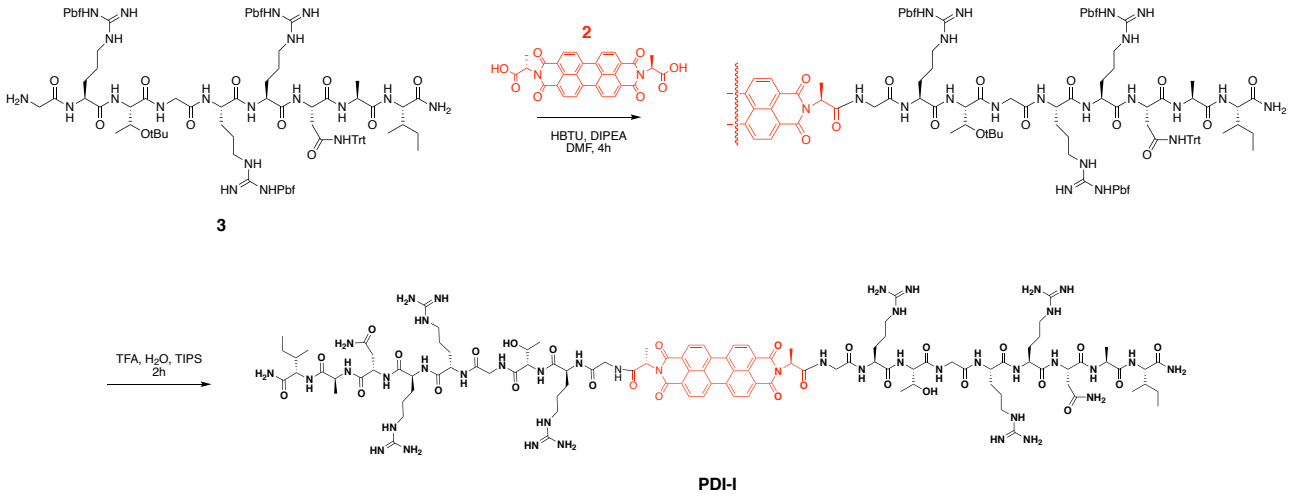

Figure 3.12. Synthesis of PDI-I.

3.10. References

(1) Tsai, T. Y.-C.; Choi, Y. S.; Ma, W.; Pomerening, J. R.; Tang, C.; Ferrell, J. E. Robust, Tunable Biological Oscillations from Interlinked Positive and Negative Feedback Loops. *Science* **2008**, *321* (5885), 126–129. https://doi.org/10.1126/science.1156951.

(2) Semenov, S. N.; Wong, A. S. Y.; van der Made, R. M.; Postma, S. G. J.; Groen, J.; van Roekel, H. W. H.; de Greef, T. F. A.; Huck, W. T. S. Rational Design of Functional and Tunable Oscillating Enzymatic Networks. *Nat. Chem.* **2015**, *7* (2), 160–165. https://doi.org/10.1038/nchem.2142.

(3) Brandman, O.; Meyer, T. Feedback Loops Shape Cellular Signals in Space and Time. *Science* **2008**, *322* (5900), 390–395.

(4) Cannon, W. B. Organization for Physiological Homeostasis. *Physiol. Rev.* **1929**, *9* (3), 399–431. https://doi.org/10.1152/physrev.1929.9.3.399.

(5) Umbarger, H. E. Evidence for a Negative-Feedback Mechanism in the Biosynthesis of Isoleucine. *Science* **1956**, *123* (3202), 848–848. https://doi.org/10.1126/science.123.3202.848.

(6) Chanche, B.; Estabrook, R. W.; Ghosh, A. Damped Sinusoidal Oscillations of Cytoplasmatic Reduced Pyridine Nucleotide in Yeast Cells. *Proc Natl Acad Sci USA* **1964**, *51* (6), 1244–1251.

(7) Brandman, O.; Liou, J.; Park, W. S.; Meyer, T. STIM2 Is a Feedback Regulator That Stabilizes Basal Cytosolic and Endoplasmic Reticulum Ca2+ Levels. *Cell* **2007**, *131*, 1327–1339.

(8) Glass, D. B.; Cheng, H.-C.; Mende-Mueller, L.; Reed, J.; Walsh, D. A. Primary Structural Determinants Essential for Potent Inhibition of CAMP-Dependent Protein Kinase by Inhibitory Peptides Corresponding to the Active Portion of the Heat-Stable Inhibitor Protein. *J. Biol. Chem.* **1989**, *264* (15), 8802–8810.

(9) Glass, D. B.; Lundquist, L. J.; Katz, B. M.; Walsh, D. A. Protein Kinase Inhibitor-(6-22)-Amide Peptide Analogs with Standard and Nonstandard Amino Acid Substitutions for Phenylalanine 10. *J. Biol. Chem.* **1989**, *264* (24), 14579–14584. https://doi.org/10.1016/S0021-9258(18)71718-3.

(10) Smulders, M. J.; Nieuwenhuizen, M. L.; de Greef, T. A.; van der Schoot, P.; Schenning, A. H. J.; Meijer, E. W. How to Distinguish Isodesmic from Cooperative Supramolecular Polymerisation. *Chem. - Eur. J.* **2010**, *16* (1), 362–367. https://doi.org/10.1002/chem.200902415.

(11) Santos, F. J. V.; Nieto de Castro, C. A.; Dymond, J. H.; Dalaouti, N. K.; Assael, M. J.; Nagashima, A. Standard Reference Data for the Viscosity of Toluene. *J. Phys. Chem. Ref. Data* **2006**, *35* (1), 1–8. https://doi.org/10.1063/1.1928233.

(12) Safont-Sempere, M. M.; Fernández, G.; Würthner, F. Self-Sorting Phenomena in Complex Supramolecular Systems. *Chem. Rev.* **2011**, *111* (9), 5784–5814. https://doi.org/10.1021/cr100357h.

(13) Sorrenti, A.; Leira-Iglesias, J.; Sato, A.; Hermans, T. M. Non-Equilibrium Steady States in Supramolecular Polymerization. *Nat. Commun.* **2017**, *8* (1), 15899. https://doi.org/10.1038/ncomms15899.

(14) Singh, N.; Zhang, K.; Angulo-Pachón, C. A.; Mendes, E.; van Esch, J. H.; Escuder, B. Tandem Reactions in Self-Sorted Catalytic Molecular Hydrogels. *Chem. Sci.* **2016**, *7* (8), 5568–5572. https://doi.org/10.1039/C6SC01268J.

3.11. Appendix

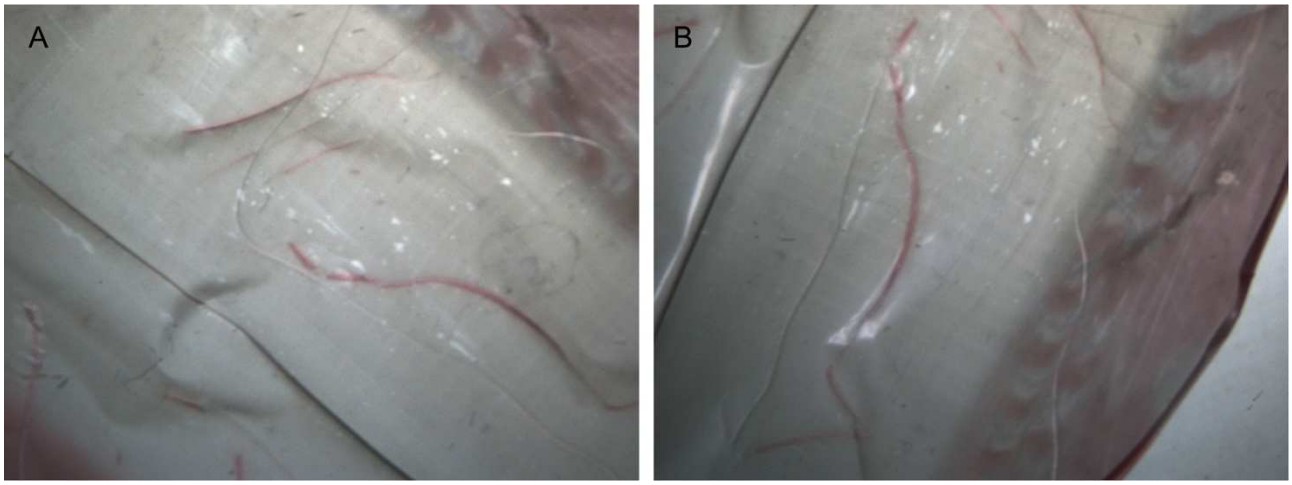

Figure 3.13. Fibers in a dialysis membrane. (A) and (B) are pictures of fibers obtained onto the dialysis membrane after the dialysis of a solution of a 1:1 mixture **p2-PDI** and **PDI-I** at 100 μM.

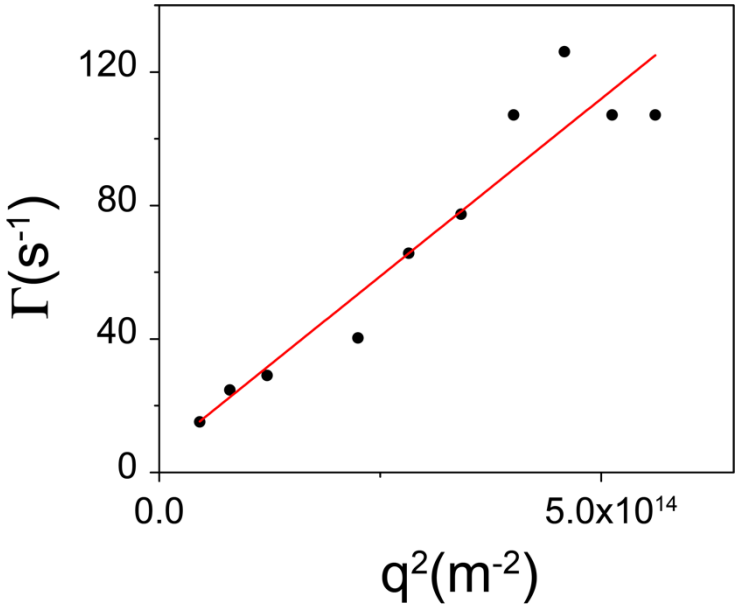

Figure 3.14. Dynamic Light Scattering of a 1:1 mixture of p2-PDI and PDI-I. DLS measurement: relaxation Γ versus the square of the scattering vector q^2 for a 1:1 mixture of **p2-PDI** and **PDI-I** in the reaction buffer (at a final concentration of 200 μM) at 293 K. The corresponding slope D, resulting from the linear fitting (red line) is apply to equation 5. R_H is calculated to be 1009 ± 90 nm.

Chapter 4.

Towards Homeostatic Supramolecular Materials based on an Internal Enzymatic Network

Abstract

In this chapter, we develop peptide-based hydrogels where the insertion of an enzymatic network creates an elementary 'metabolism' inside the material. The peptide LRRASLG sequence recognized by both kinase and phosphatase, is incorporated in the design of 3 new hydrogelators. Specifically, a known di-peptide self-assembling motif (FF, phenylalanine-phenylalanine) is attached either to the leading side or tailing end of the LRRASLG sequence to promote assembly. The enzymatic reaction network presented in Chapter 2 is integrated into the hydrogel network in order to achieve different fuel-mediated mechanical behavior. The final goal is achieving pseudo non-equilibrium steady states (pNESS) by the variation of concentration of pre-fuel (PEP) and consequently controlling the *in situ* production of fuel (ATP), as a means to obtain time-programmable materials properties.

4.1. Introduction

In Chapter 2 and 3, we reported and discussed the (de)phosphorylation enzymatic network in solution. As a reminder, we had solved the waste issue due to ADP inhibition by coupling the phosphorylation/dephosphorylation cycle to a fuel regenerating enzymatic reaction (i.e., pyruvate kinase mediated conversion of ADP to ATP in the presence of phosphoenol pyruvate). We were able to achieve pseudo non-equilibrium steady states of well-defined duration and found an unexpected oscillatory behavior. In addition, we had shown in Chapter 3 a competitive inhibitor that was envisioned for use in hydrogel materials. In addition, based past and ongoing research in our laboratory, we found that many perylenediimide (PDI) derivatives do not easily form hydrogels with favorable mechanical properties, and their synthesis can be quite lengthy. The development of materials based on PDI derivatives, therefore, was abandoned. Before going into the detailed peptide design and behavior of the system that we use in this chapter, it would be good to briefly present some key elements of the field of peptide nanomaterials.

Supramolecular hydrogels are a very interesting and important class of materials as their properties can be regulated by the design of the constituents, being their assembly dynamic and reversible.[1,2] Particularly attractive are soft materials based on amino acids or peptides as those molecules are biocompatible and biodegradable;[3] our bodily functions are mainly carried out by the expression of 20 gene encoded amino acids.[4,5] Synthetic peptides can be designed using a range of charged, hydrophilic, hydrophobic and aromatic amino acids controlling the self-assembly and the secondary structure of the engineered peptides (i.e., α-helix, coiled-coil, etc.).[6]

The pioneering work by Ghadiri[7] and Zhang[8] opened the door to new strategies for the development of hydrogels out of short peptides or of the combination of peptides with polymeric or aliphatic moieties.[9]

One of the strategies used to achieve gelation using short peptide sequences has been the incorporation of N-capping groups into the sequence, such as Fmoc and Napthalene.[10,11] The aromatic interactions play an essential role in the self-assembly of those small molecules. Along with N-protected dipeptides, remarkable studies on the dipeptide phenylalanine-phenylalanine (FF) were carried out by Gazit and co-workers.[12] They reported the formation of tubular structures by the FF assembly, similar to the amyloids, through π–π interactions and hydrogen bonding between the amide groups.[12,13] Interestingly, the self-assembly of the dipeptide at high concentration in water was forming a rigid material.[14] The latter was comparable to hydrogels formed by longer peptide structures, showing higher stability through pH and temperature changes. Additionally,

Garcia *et al.*[15] have proposed the combination of D– and L– amino acids within the same peptide sequence to achieve self-assembly of ultrashort peptides, avoiding the use of N-capping aromatic groups. They used a full sequences of hydrophobic tripeptides F_D-AA-F_L to explain how chirality is mandatory to achieve net segregation between hydrophobic and hydrophilic part that lead to gel formation.[16,17]

Nonetheless, the design of peptide-based hydrogels is nontrivial as it is difficult to predict *a priori* the final mechanical properties of the gel. Ulijn, Tuttle and co-workers explored tripeptide sequences based on their aggregation behavior.[16] The results of course grained molecular dynamics simulations indicated that the self-assembly propensity is not just a result of the hydrophocity of the substrates but that it is influenced by the position of aromatic amino acids in the peptide sequence. Those results were confirmed experimentally and led to the discovery of unprotected tripeptides capable of forming hydrogel without the use of organic solvents (i.e., KYF, KFF, etc.).

4.2. Design and Synthesis of Kemptide Derivatives

In the introduction, we discussed about the evolution in the design of nanostructures based on peptide sequences for the development of nanomaterials. However, predicting *a priori* the self-assembly and the mechanical properties of the final hydrogels remains challenging because of the cooperative nature of many assembling peptides.[16] Our consensus LRRASLG sequence (also known as 'kemptide') by itself, does not form hydrogels due to its hydrophilic nature.[18]

As reported by Stupp and co-workers,[9] the specific consensus substrate recognized by the enzymes is RRXSO, where X identifies any amino acid and O a hydrophobic one. By synthetizing various sequences, they demonstrated that the serine (S) residue cannot be shifted in the amino acids sequence or phosphorylation is made impossible. Interestingly, the peptide maintains its access to the enzymatic domain even when a long hydrophobic carbon chain is introduced at the C-terminus. In the latter work, they designed and synthesized a so-called amphiphile where the head (C-terminus) is highly hydrophobic, and the tail (N-terminus) is hydrophilic.

Here, we take a simpler approach and append either a dipeptide or tripeptide to the kemptide sequence to induce the self-assembly.[12] As already discussed above, a great effort has been done in peptide combinatorial chemistry by Ulijn, Tuttle and co-workers.[16] It emerged that hydrophobic amino acids promotes the aggregation at the C-terminus position as well as positively charged amino acids induces self-assembly when present at the N-terminus.[16] For kemptide LRRASLG; R, at

the N-terminus, denotes the residue arginine that is positively charged at pH 7.5.[19] We first introduced hydrophobic linear and aromatic residues. **LRRASLGVVV (1)** and **LRRASLGFLFF (2)** were first synthesized by solid phase peptide synthesis (SPPS). The tripeptide VVV (3 x valine) is known to induce self-assembly and formation of β-sheet secondary structure.[20,21] The sequence FLFF (phenylalanine-leucine-phenylalanine-phenylalanine) was at that time the starting point for the synthesis of various sequences FFXF, FFXFF, FFFXF and etc.[15] Unfortunately, because of strict experimental conditions we are working at, namely the reaction buffer (implementation of the enzymatic network) and pH 7.5, these structures were not suitable. The main issue started already with the solubility in small volume of DMF or DMSO. Therefore, we decided to start over by inserting the well-known dipeptide FF. Again, we designed and synthesized three different sequences: **LRRASLGFF (3)**, **FFLRRASLG (4)**, **FFLRRASLFF (5)**. The dipeptide FF is a well study hydrogelator and we decided to introduce it at the C-terminus **(3)**, at the N-terminus **(4)**, or at both sides **(5)** to study the properties of the three different gels. The latter peptides were synthesized by solid phase peptide synthesis (SPPS), as shown in Scheme 4.1 and in more detail in Experimental section 4.7.

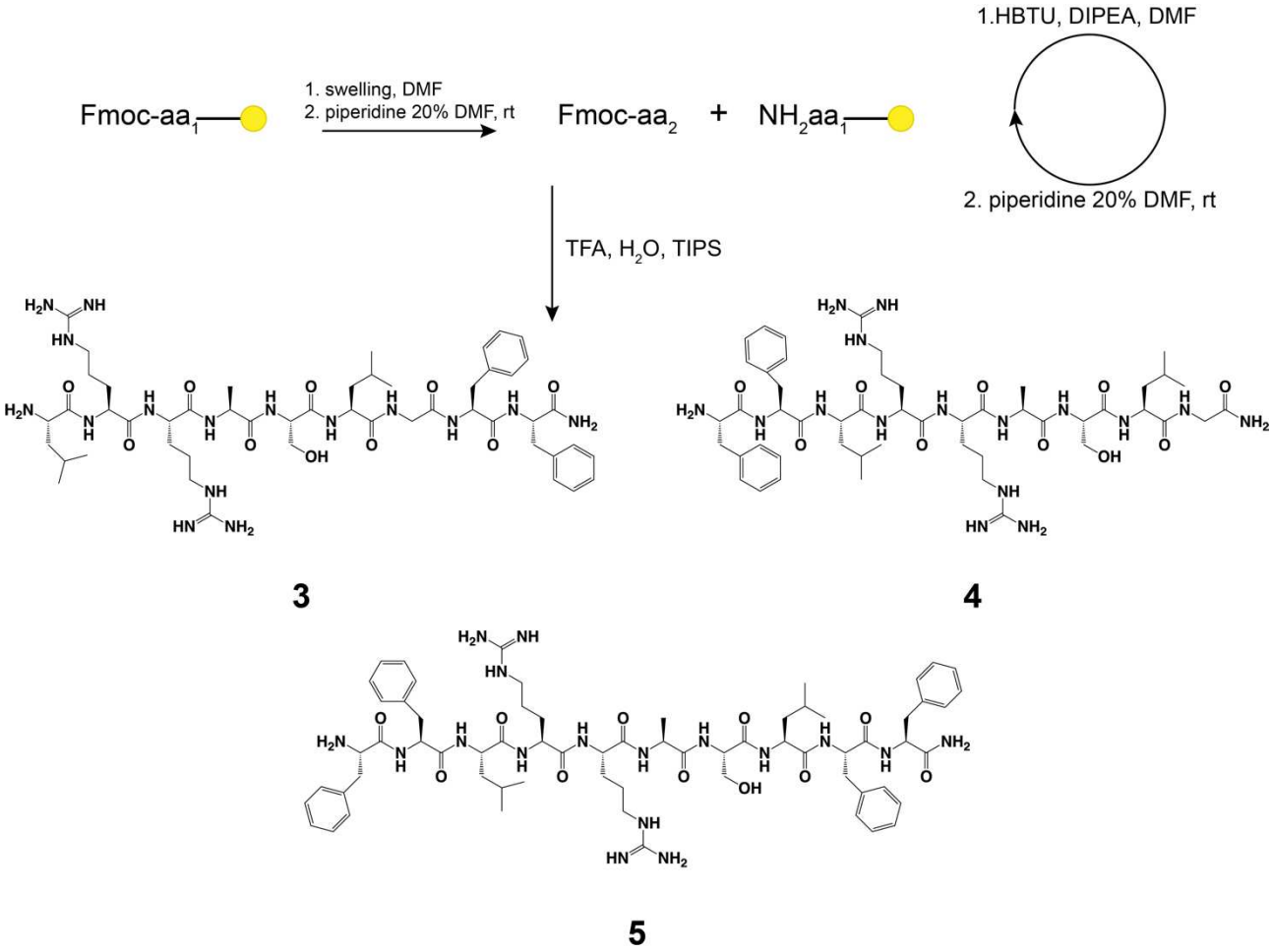

Scheme 4.1. Solid Phase Peptide Synthesis (SPPS). SPPS was carried out starting from Fmoc-protected Rink amide resin. The three peptide sequences are represented.

For all the three kemptide derivatives **3–5**, we performed the synthesis starting from the Fmoc-protected Rink amide resin, which leads the amide group at the C-terminus upon cleavage. Indeed, it has been reported that the amide induces faster self-assembly as a function of the lower solubility of the amide group in water.[4]

So far, we have discussed and shown the design and the synthesis of three different derivatives of the consensus sequence LRRASLG (kemptide). Before studying and exploring the conditions for the gelation, we need to investigate the behavior of the enzymatic network inside the gel to confirm the (de)phosphorylation cycles.

4.3. Enzymatic Network Study

In Chapter 2, we discussed the enzymatic network and the final objective of this thesis to obtain a material with its own metabolic system. This challenging achievement would have a great impact in the development of the so-called life-like materials[22]; and it would be a unique opportunity to develop a materials with its own steady-state metabolism. Moreover, it will open the door for the discovery and the study of new behavior and the investigation of structures capable of performing functions closer and closer to those of Nature (i.e., self-healing, motility).

First, we studied the phosphorylation and the dephosphorylation of the individual peptide substrates. We decided to follow the stepwise phosphorylation and dephosphorylation of substrates **3**, **4** and **5** by LC-MS. Spectra were recorded for each peptide at 100 μM, in the presence of PEP (500 μM) and ADP (500 μM) (Figure 4.1A). The spectra show the typical MS peaks of the peptides **3**, **4** and **5**, respectively. In a second step, the enzymes PKA and PK were added to the same mixture, leading to the conversion of the substrate ADP to ATP and the consequent phosphorylation of the peptides at the serine residue (red molecules in Figure 4.1B). In all the three cases, the spectra show the fully phosphorylation with peaks typical for $[M + 2H^+]$ and $[M + H^+]$. In a final step, we added λPP to induce the dephosphorylation of substrates **3**, **4** and **5** and the recovery of the initial structure (green molecules in Figure 4.1C). Figure 4.1C shows the spectra for all the sequences, confirming the full dephosphorylation with the classical mass peaks of the initial substrates.

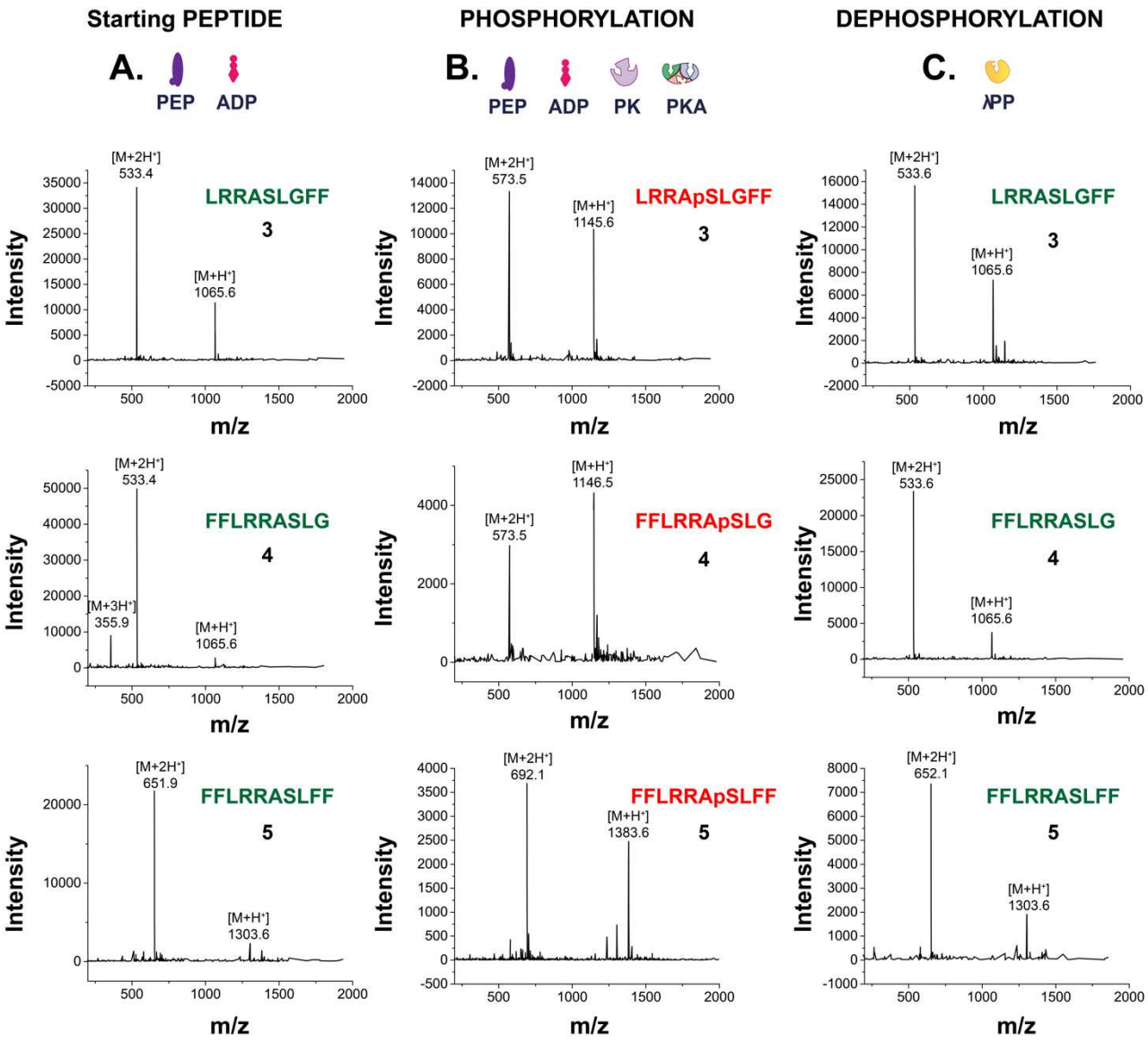

Figure 4.1. LC-MS data for the (De)Phosphorylation Cycles of substrates 3, 4 and 5. (A) LC-MS spectra of a 100 μM solution of the peptides in the reaction buffer (pH 7.5) containing PEP (500 μM) and ADP (500 μM). $[M+H^+]$ peaks for peptides **3** and **4** (MW = 1065.29 g/mol) at 1065.6 and for peptide **5** (MW = 1302.59 g/mol) at 1303.6; $[M+2H^+]$ peaks for peptides **3** and **4** at 533.4 and for peptide **5** at 651.9. (B) LC-MS spectra of a 100 μM solution of the peptides after addition of PK (0.10 μM) and PKA (0.03 μM), containing PEP (500 μM) and ADP (500 μM). $[M+H^+]$ peaks for the phosphorylated substrates **3** and **4** (MW = 1145.27 g/mol) at 1145.6 and 1146.5 respectively and for peptide **5** (MW = 1381.71 g/mol) at 1383.6; $[M+2H^+]$ peaks for peptides **3** and **4** at 573.5 and for peptide **5** at 692.1. (C) LC-MS spectra of a 100 μM solution of the peptides after addition of λPP (0.05 μM). $[M+H^+]$ peaks for peptides **3** and **4** (MW = 1065.29 g/mol) at 1065.6 and for peptide **5** (MW = 1302.59 g/mol) at 1303.6; $[M+2H^+]$ peaks for peptides **3** and **4** at 533.6 and for peptide **5** at 652.1. The LC-MS experiments were conducted in a LC-MS vial with a glass insertion (total volume of 300 μL).

Overall, these results are encouraging and in agreement with the previous studies (see Chapter 2) showing phosphorylation and dephosphorylation of **3**, **4** and **5** upon addition of the enzymatic reactions network. Interestingly, the variation of the position of the dipeptide FF within

the consensus sequence does not interfere with the recognition of the enzymatic domain, both for the kinase PKA (phosphorylation) and the phosphatase λPP (dephosphorylation).

4.4. Rheology Measurements of Peptide Self-assembly

4.4.1. Oscillatory Rheology

In order to have a better understanding of the mechanical properties of the three hydrogels, we preformed rheology studies. These properties can be investigated as a response of our material to a deformation[23], by using a parallel plate model, that is a bottom stationary plate and an upper moving plate. This allows the parameters of the viscoelastic material to be assessed. Particularly, during oscillatory shear measurements the shear storage (G') and loss (G'') moduli can be monitored over strain, frequency, time, and temperature.[24] The G' measures the elasticity of the material and, thus, its ability to store energy (i.e., the stiffness of the material); G'' represents the ability of the material to dissipate energy (i.e., how liquid-like the material is).[23] Specifically, we can consider a gel when G' is one order of magnitude higher than G'', so when the ratio of loss energy to stored energy is less than 0.1 (G''/G' < 0.1).[25]

In our specific case, to characterize the rheological properties of the hydrogels we will measure the evolution of G' and G'' in time to study the gelation kinetics. Moreover, we can determine the linear viscoelastic region (LVER) and the critical strength of the gels; the first parameter is obtained by monitoring the moduli against strain (constant frequency) and the second one represents the value of strain at which G' and G'' deviate from the linearity. All these parameters give us access to the mechanical properties of the hydrogels.

The parallel plate geometry is frequently used to study hydrogels; the sample is placed between the two plates and the measuring gap can be controlled.[26] Moreover, to have a better control during the rheological experiments, we designed and 3D printed a hollow container (Figure 4.8 in Experimental section 4.7) in which the sample was prepared for rheological measurements. The hollow container is fixed onto the stationary plate and the sample is placed inside and sandwiched between the plates.

4.4.2. Peptides Hydrogelation

Previously, we discussed boundaries that must be respected for optimal hydrogelation condition for our peptides. The reaction buffer was finely designed to permit the simultaneous activity of all the enzymes in the complex enzymatic network[19]; the buffer is prepared at pH 7.5, as specified in the Experimental section 4.7. In most cases, hydrogels are obtained with a switch in pH or solvent, or by heating/cooling cycles. In a first approach, we dissolved the substrates **3**, **4** and **5** in the reaction buffer, containing 10% DMSO, at final concentrations of 0.5, 1, 2, 10, 20, or 50 mM. We heated the solutions containing the substrates in DMSO in order to dissolve them. In a few cases, the clear DMSO solutions mixed with room temperature buffer formed transparent gels overnight, but they did not do so reliably. Better results were obtained using DMF instead of DMSO. We explored various percentages of DMF (from 2 to 10%), and we found that 10% of DMF (without heating the mixture) was ideal. In addition, we screened the peptides at the different concentrations, and we fixed the concentration to 20 mM resulting in a weak hydrogel (as we will show below). In this case, a weak gel was beneficial, since it allowed for the insertion of the enzymatic network and the investigation of the materials behavior during the (de)phosphorylation cycles.

4.4.3. Rheological studies on compound 5, FFLRRASLFF

From the three peptides that were synthesized, the sequence FFLRRASLFF (**5**) was chosen as the most promising to start rheological studies since it formed a self-supporting gel during vial inversion testing, whereas the other two peptides LRRASLFF (**3**) and FFLRRASL (**4**) did not. In section 4.4.1, we discussed about the characterization of the mechanical properties of the gel *via* kinetic experiments. Thus, we started by measuring the kinetics of gel formation from peptide **5**. The substrate was dissolved in 10% of DMF at 20 mM in the reaction buffer (50 mM Tris-HCl buffer, pH 7.5). The gelation took place *in situ* on the rheometer plate and G' and G'' were followed over time. As shown in Figure 4.2A, G' and G'' increased rapidly once the gelation started. After ~20 minutes the rate of gelation decreases, and the system reaches a plateau after 200 minutes. At this point, the network of the gel is completely formed as no further changes in the moduli are observed. There are, however, some instances where G' slightly decreases, thus deviating from linearity. The latter are likely a result of slippage between the parallel plate and the surface of the gel during

measurements. This behavior happens sometimes due to the water layer created above the gel.[27] A way to avoid wall slip effect is to use measuring geometries with a rough surface.

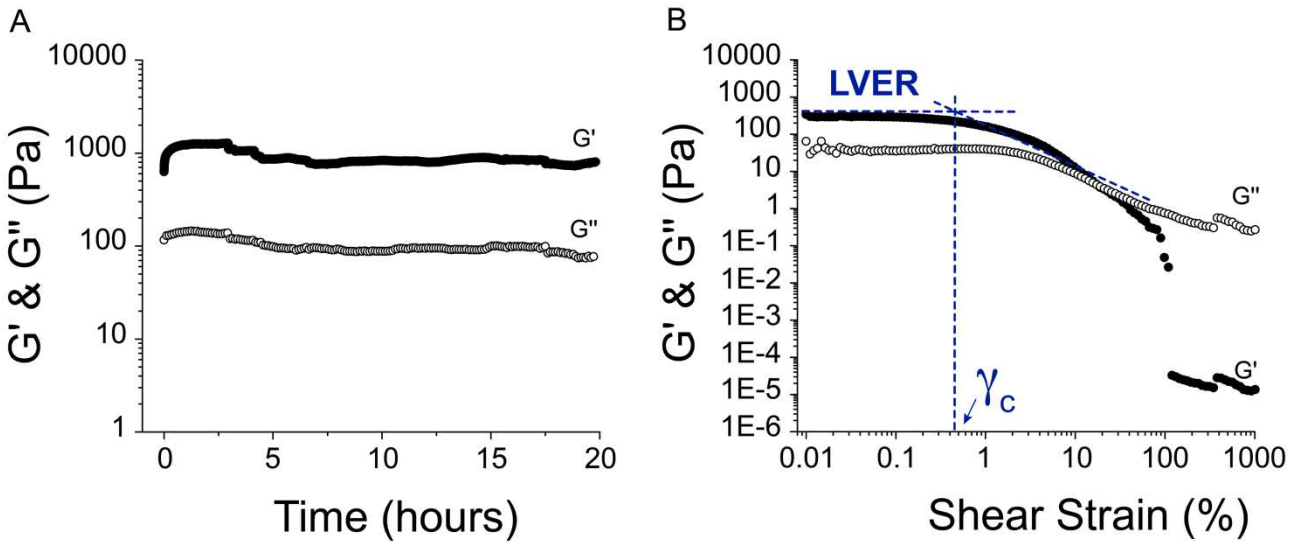

Figure 4.2. Gelation of substrate 5. (A) G' and G'' monitored over time for a sample made of **5** at a concentration of 20 mM. (B) Shear strain sweep measurement for a sample made of 5 at concentration of 20 mM. LVER and the critical strength (γ_c) are represented. Closed and open dots represent G' and G'', respectively. The experiments were carried out at 25°C.

The characterization of the mechanical parameters such as strength and stiffness are best characterized using a strain sweep. During a strain sweep, G' and G'' are evaluated as the strain is increased stepwise, while the frequency is kept constant at 10 rad s^{-1} (Figure 4.2B). The linear viscoelastic region (LVER) can be assessed as the range of strain in which G' and G'' do not deviate from linearity. That is, the properties of our gel are independent of how much deformation we are applying to our material while in the LVER. The LVER is defined by a critical strain (γ_c), beyond which the gel network starts to break. From Figure 4.2B we observe that the γ_c is around 0.4 % and this is thus the maximum shear we have applied in all following experiments, as to not disrupt the hydrogel network. Additionally, the stiffness in the LVER is in line with the final stiffness of the gel in the kinetics measurement after 20 h.

Once we characterized hydrogel **5**, we proceeded with the integration of the enzymatic network into the gel. As we have already described in section 4.3, compound **5** can be phosphorylated and dephosphorylated in the presence of the enzymes PKA, λPP and PK. In the gel state, the kinetics might be different from solution, which is why we build up our experiments step by step. First, the phosphorylation of the **5** was carried out in the presence of ATP and kinase PKA.

Interestingly, we observed a different kinetic profile when using phosphorylation compared to the hydrogel formation reported in Figure 4.2A in the absence of ATP and PKA. When we added ATP and PKA, there is sharp increase in the G' and G'' as soon as the experiment starts (region I in Figure 4.3). After ~10 minutes, the rate of gelation decreases (region II in Figure 4.3). In region II the increase in G' and G'' moduli is most likely mainly driven by the phosphorylation process. During this enzymatic reaction, ATP is consumed and hydrolyzed to ADP while the substrate is phosphorylated. As we added 2 equivalents of ATP, the fuel is still present in the system thus interacting with the self-assembly. After 5 hours, the system reaches a steady regime for about 2 hours (region III in Figure 4.3) after which G' and G'' again increase sharply (region IV in Figure 4.3) until a plateau is achieved after 12.5 hours (region V in Figure 4.3). The trend of G' and G'' in region IV could be explained as a mixture of a stabilization of the phosphorylated self-assembly network (region III in Figure 4.3) and the phosphorylation reaction still taking place. After 12.5 hours a plateau is reached (region V in Figure 4.3). At this point, no further changes are observed in the stiffness of the overall system from which we assume that all the substrate has been phosphorylated. More identical experiments, as well as experiments in which LC-MS is used to follow the degree of phosphorylation are needed to be sure of the latter hypothesis.

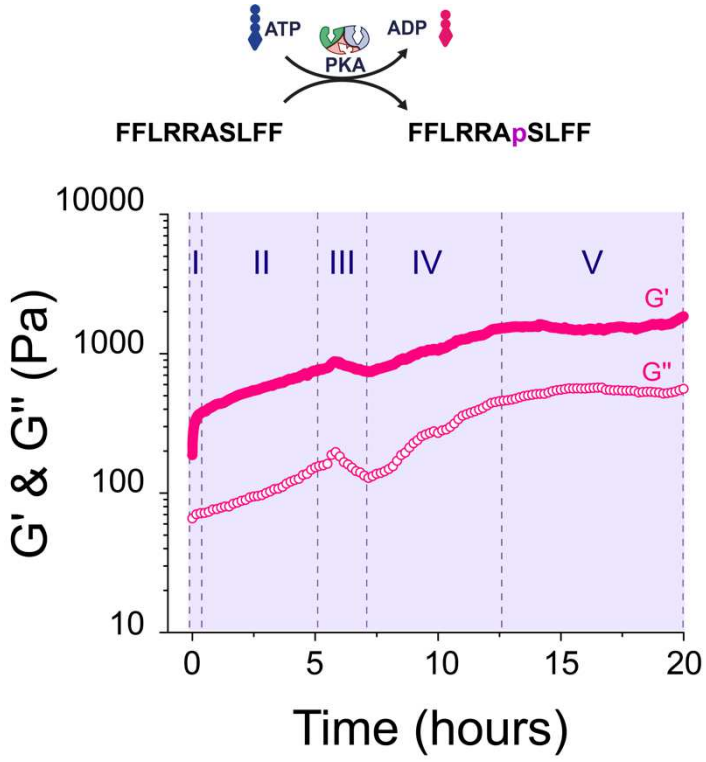

Figure 4.3. Kinetics of Gelation during Phosphorylation of substrate 5. G' and G'' monitored over time for substrate **5** at a concentration of 20 mM, containing ATP (40 mM, 2 eq.) and PKA (0.04 μM). Closed and open symbols represent G' and G'', respectively. The experiment was carried out at 25°C.

Since the final goal of this project is to obtain pseudo non-equilibrium steady states in a hydrogel system, we implemented the ATP regeneration reaction in the network. Initially, we performed the phosphorylation of substrate **5** by addition of PK, ADP, PEP and PKA for the generation of ATP *in situ* and we further compared it with the phosphorylation described earlier (Figure 4.3). In the same way, we studied the kinetics of the reaction by monitoring G' and G'' over time (Figure 4.4A).

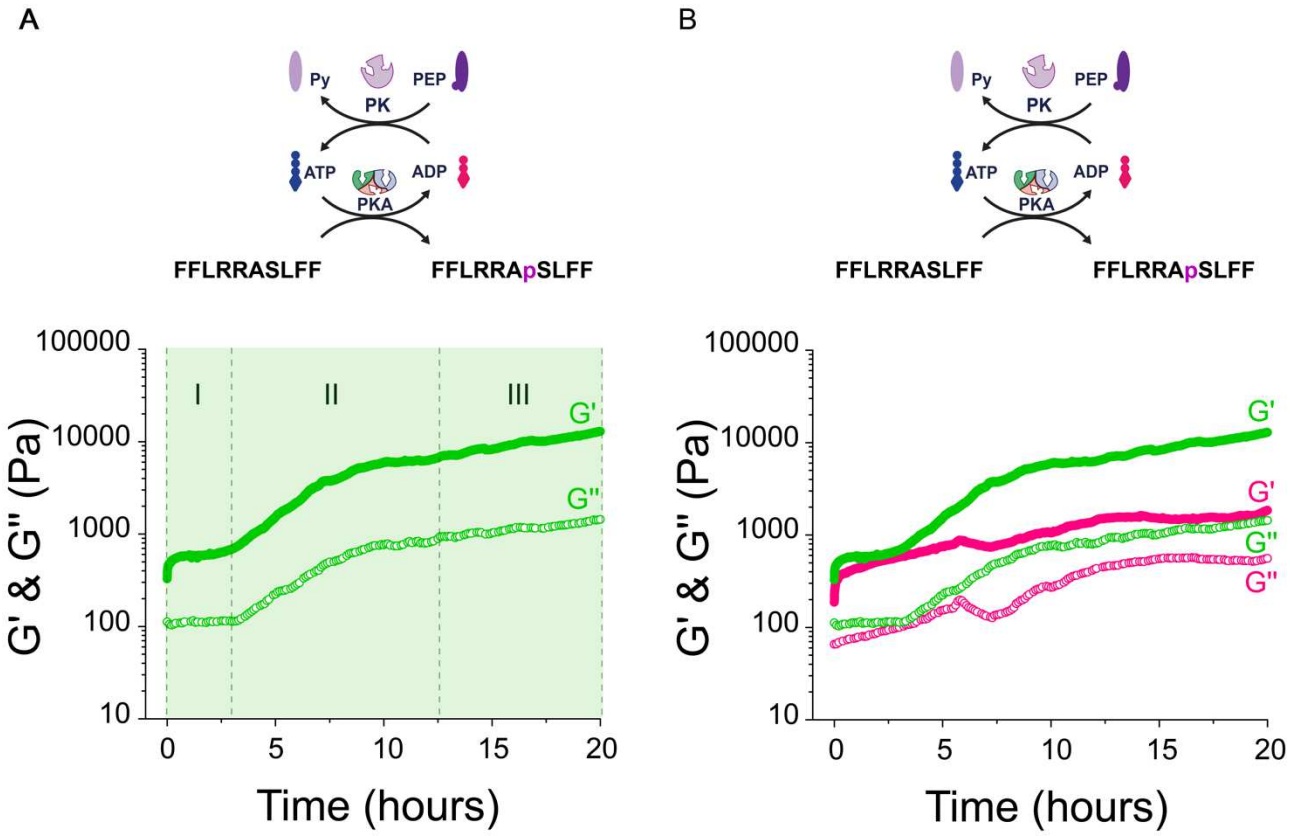

Figure 4.4. Kinetics of Gelation during Phosphorylation in the Presence of ATP Regeneration Cycle. (A) G' and G'' monitored over time for substrate **5** at a concentration of 20 mM, containing ATP (40 mM, 2 eq.), PEP (100 mM, 5 eq.), PK (0.06 μM) and PKA (0.04 μM). (B) G' monitored over time for substrate **5** during phosphorylation in the presence (green) and absence (pink) of ATP regeneration cycle. Closed and open symbols represent G' and G'', respectively. The experiments were carried out at 25°C.

In this system, where we incorporated the regeneration of ATP, we again observe the sharp increase of G' and G'' at the beginning of the experiment, as observed for region I in Figure 4.3. In region I in Figure 4.4A the G' and G'' values are similar to the ones found during phosphorylation without the ATP regeneration reaction. In this system, ATP is continuously regenerated as soon as it is consumed. Therefore, ATP is always present in the network and we believe that it affects the overall stiffness of the system. After about 10 minutes, the system reaches a plateau which lasts ~3 hours (region I in Figure 4.4A). In this region both moduli are constant. Afterwards, we observe a

continuous increase in G' and G'' (region II & III in Figure 4.4A) which presumably is a result of the continuously regenerated ATP. The latter might participate in the self-assembly process while the substrate gets phosphorylated.

In order to study the effect of ATP during gelation, we investigated the kinetics of compound **5** in the presence of 2 equivalents of ATP (Figure 4.5). If we compare the gelation in the absence of ATP (black) to the gelation in the presence of ATP (blue), it is clear that ATP affects the self-assembly process as the stiffness is very high since the onset of the gelation. ATP is a well-known multivalent binder due to its electrostatic interactions. It is reported to participate in the formation of vesicles[28] and different supramolecular structures.[29,30]

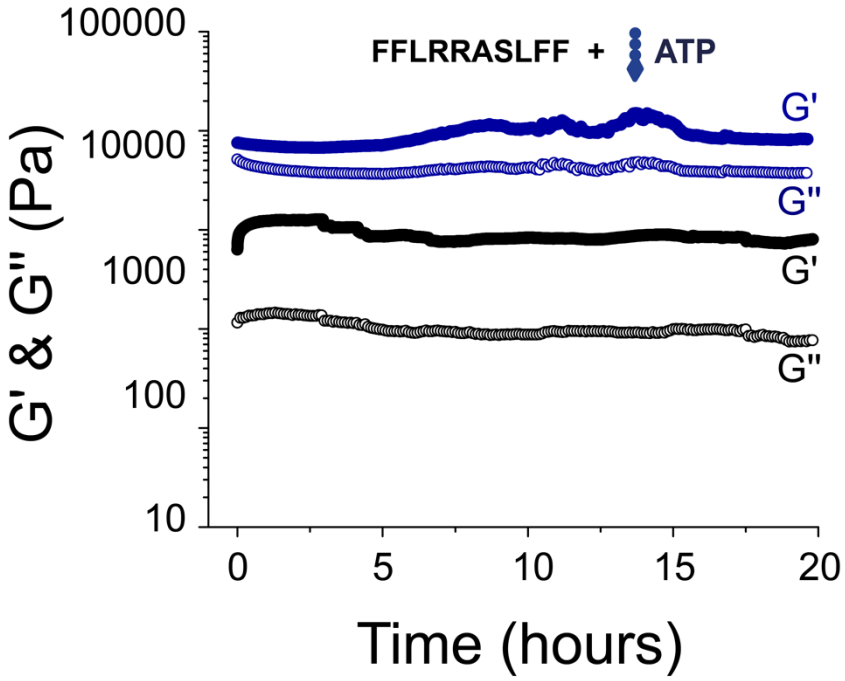

Figure 4.5. Kinetics of Gelation in the Presence and Absence of ATP. (C) G' and G'' monitored over time for substrate **5** at a concentration of 20 mM in the presence (blue) and absence (black) of ATP (40 mM, 2 eq.). Closed and open symbols represent G' and G'', respectively. The experiment was carried out at 25°C.

Then, we studied the dephosphorylation reaction catalyzed by the phosphatase λPP. Again, G' and G'' were monitored over time to follow the kinetic profile of the system. Figure 4.6 in Appendix 4.10 report the experiments performed for the phosphorylation and dephosphorylation reactions in the absence (Figure 4.6A) and presence (Figure 4.6B) of the ATP regeneration reaction. (Figure 4.18 in Appendix 4.10 shows all the kinetics of gelation studied until now).

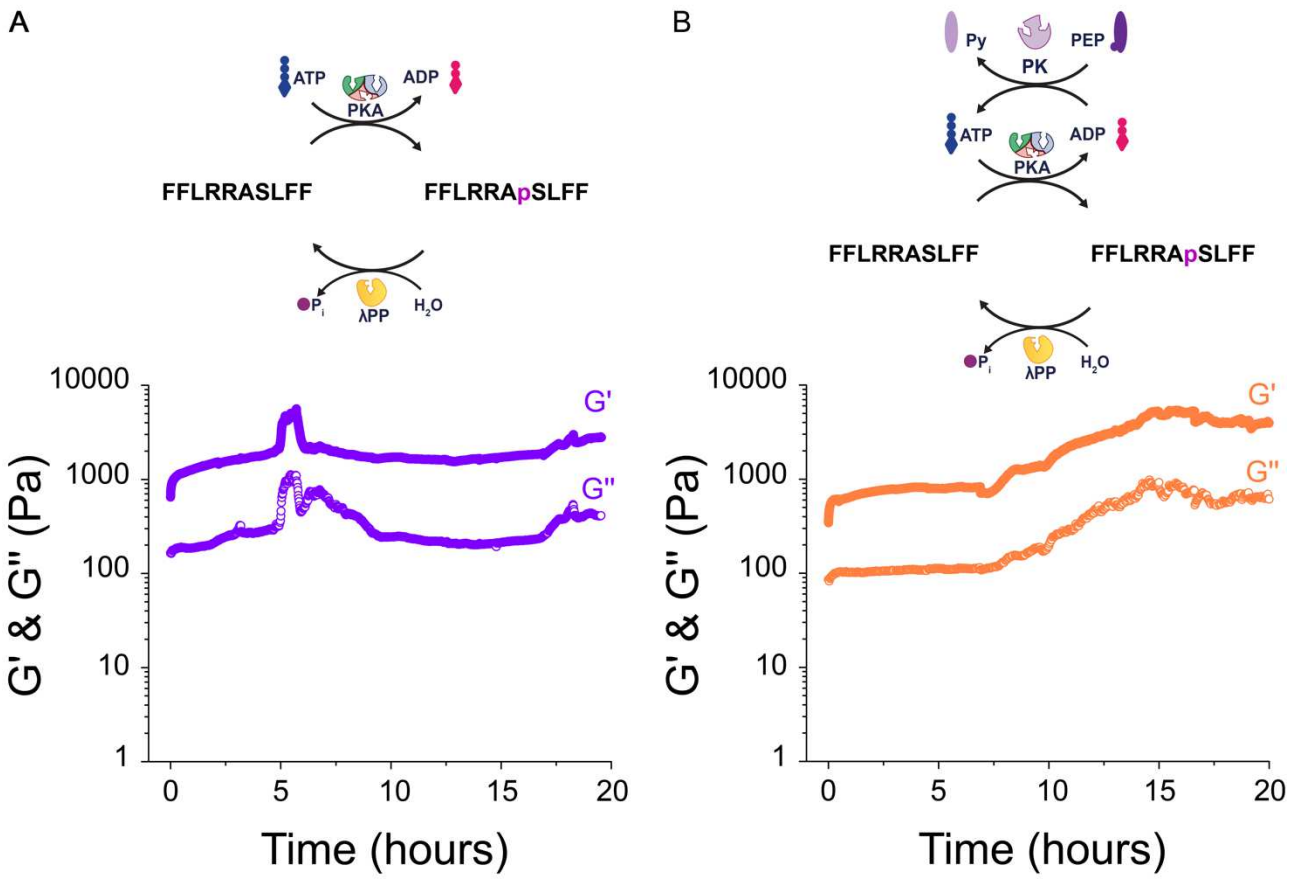

Figure 4.6. Kinetics of Gelation with Lambda Phosphatase. (A) G' and G'' monitored over time for substrate **5** at a concentration of 20 mM, containing ATP (40 mM, 2 eq.), PKA (0.04 μM) and λPP (0.02 μM). (B) (A) G' and G'' monitored over time for substrate **5** at a concentration of 20 mM, containing ATP (40 mM, 2 eq.), PKA (0.04 μM), PEP (100 mM, 5 eq.), PK (0.06 μM) and PKA (0.04 μM) and λPP (0.02 μM). Closed and open symbols represent G' and G'', respectively. The experiments were carried out at 25°C.

However, from these rheology experiments it is hard to discern the role of the peptide self-assembly, ATP, and each of the individual reactions. More experiments, and preferably in combination with other characterization techniques are required in the future. X-Ray scattering, for example, would permit the study of the system at the molecular level. This would allow to investigate how the molecules interact with each other in the continuous generation of ATP. Additionally, circular dichroism spectroscopy could permit the study of the peptides secondary structure and how it is affected during the (de)phosphorylation reactions.

4.4.3. Rheological studies on compound 4, FFLRRASLG

In the same way, rheological experiments were carried out for compound **4**. Particularly, for the latter no gel is formed at the experimental conditions, as reported in Figure 4.7A. Thus, we envisaged the formation of hydrogel induced by the phosphorylation of the kemptide derivative; the phosphorylation is indeed introducing negative charges onto the phosphoryl-accepting substrate causing an overall change in the molecular self-assembly and therefore in the structure of the gel.

Therefore, phosphorylation prompts the self-assembly of compound **4**. However, as shown in Figure 4.7B below, the differences between G' and G'' is less than one order of magnitude, thus meaning a true gel is not formed but rather a very viscous solution. To further investigate this system, we are planning to perform optical microscopy experiments to follow the formation of the self-assembled structures.

The discussion above suggests the importance and the difficulties when designing hydrogelators, as discussed in the introduction of this Chapter and previously reported.[16] Compound **4** presents the dipeptide Phe-Phe in the N-terminus, compared to compound **5** where FF is incorporated at both termini, which results in differences in the packing of the molecules and therefore, in the ability to form self-supporting structures.

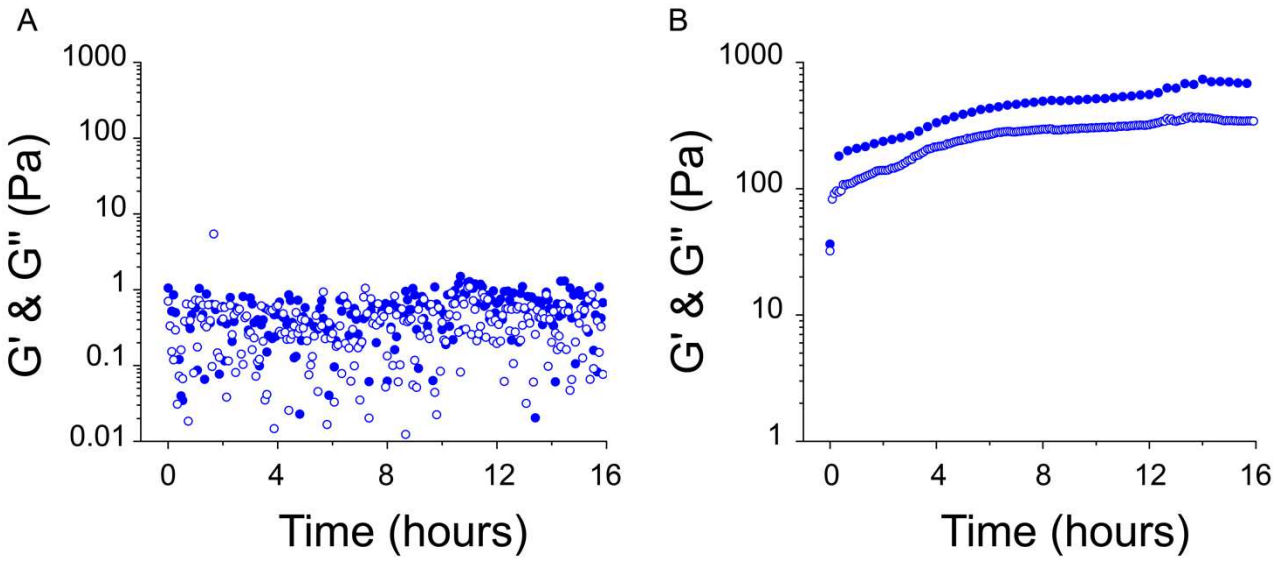

Figure 4.7. Kinetics of compound 4. (A) G' and G'' monitored over time for substrate **5** at a concentration of 20 mM (A) and (B) containing ATP (40 mM, 2 eq.) and PKA (0.04 μM). Closed and open symbols represent G' and G'', respectively. The experiments were carried out at 25°C.

4.5. Conclusions

To conclude, in Chapter 4 we have described the development of a material coupled to the enzymatic network reported in Chapter 2. In order to obtain peptide-based materials, we have designed and synthesized three different substrates containing the consensus sequence LRRASLG, namely LRRASLGFF, FFLRRASLG, and FFLRRASLFF. We have analyzed the phosphorylation and dephosphorylation reactions by LC-MS to confirm both the phosphorylation and dephosphorylation of each of the three substrates. We focused on compound **5** (FFLRRASLFF) for further studies as it had the best mechanical properties. The formation of the gel was tracked following G' and G'' values over time. These measurements were compared to ones containing: i) ATP and PKA (i.e., only phosphorylation, ii) ADP, PK, PKA, and PEP (i.e., phosphorylation and regeneration) or iii) ADP, PK, PKA, PEP, and λPP (i.e., phosphorylation, dephosphorylation, and regeneration). Both the phosphorylation as well as the presence of ATP affect the overall mechanical gel properties. Additional measurements are needed to track the chemical composition of the system during the gel changes (by LC-MS for example), in combination with (ideally *in situ*) imaging techniques. The current data does not allow for a full understanding of the system, but the fact that notable differences can be detected is encouraging in our quest for life-like materials with an in-built 'metabolism'.

4.6. Acknowledgements

Serena De Piccoli synthesized the peptide sequences and performed their characterization, she carried out the LC-MS measurements and she investigated the hydrogelation conditions. Serena De Piccoli and Ana María Fuentes Caparrós conceptualized and performed the rheological experiments. Prof. Thomas Hermans supervised the research.

4.7. Experimental Section

General. The detailed synthesis and characterization of compounds **3, 4** and **5** are described in section 4.8.

Experimental conditions. The enzymatic reactions were performed, when not differently specified, in 50 mM Tris-HCl buffer (pH 7.5) containing 10 mM $MgCl_2$, 1 mM $MnCl_2$, 2 mM dithiothreitol (DTT) and 0.1 mM EDTA, at 25°C. The addition of $MnCl_2$ was required for the activity of λPP that is a Mn^{2+}-dependent phosphatase. We refer to this buffer as the reaction buffer.

LC-MS measurements. Liquid chromatography mass spectrometry (ESI-Ion trap) was used to check qualitatively the (de)phosphorylation for compounds **3**, **4** and **5** (Figure 4.1). The experiments were run in a glass LC-MS vial with a glass insertion (final volume of 300 μL).

Rheology measurements. All rheological measurements were completed using an Anton Paar Physica MCR 302 rheometer and RheoCompass version 1.25.373 software. A parallel plate (PP) system was used throughout where 25 mm in diameter disposable plates (D-PP25/AL/S07, Anton Paar) were used to perform the different tests.

In order to ensure the dimensions of the gel being formed do not differ to those of the measuring geometry used, we designed, and 3D printed a hollow container using ABS which was used to confine our gel sample dimensions. Acetone vapor was also used to seal pores and smooth the container surface before first use. Additionally, we used a double-sided adhesive polyurethane tape, which was trimmed with exactly the same dimensions as the hollow 3D printed container, to stick the hollow container onto the rheometer stationary plate and make sure there were no leaks during measurements.

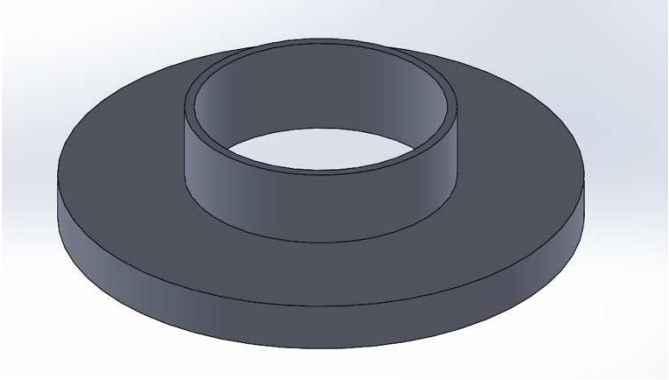

Figure 4.8. 3D-printed Holder for Rheological Measurements.

The rheological properties of the gels were investigated by means of strain and time sweeps. Strain sweeps were carried out from 0.1 % to 1000 % strain at a frequency of 10 rad s^{-1} at a pre-set temperature of 25°C. The linear viscoelastic region (LVER) was determined as the region where G' and G'' remain constant up to a strain amplitude at which the gel starts breaking (~0.4 %) and both moduli deviate from linearity. To define the critical strain (γ_c), we draw a line tangent to LVER and another line tangent to the non-linear region. The intersection of both lines will assert the value of γ_c (see Figure 4.2B). Finally, the kinetic profiles of the different tests were assessed by means of time sweep. Both G' and G'' were monitored over time at a frequency of 10 rad s^{-1} and a strain of 0.1 %.

Due to the quick gelation time for some of our gel systems, we firstly pipetted our gelator dissolved in DMF ensuring we were covering all the surface confined by the hollow container, and directly we added the buffer to trigger gelation. The position of the PP used for measurements was calculated for each specific experiment depending on the amount of sample prepared (this was normally about 1 mm for most cases). The gap time between the beginning of gelation and the start of the measurements was less than 1 min for all our samples.

4.8. Synthesis of Peptides

The peptides were synthesized following the Fmoc solid phase peptide synthesis (Fmoc-SPPS) procedure. The resin used is the Rink Amide Resin (purchased by IRIS Biotech GMBH), loading 0.72 mmol/g. SPPS was performed in a sintered column where the influx of N_2 allowed the continuous stirring of the reaction. Firstly, the resin was placed in the reaction vessel and washed twice with DMF; DMF was then added to cover all the beads and let it swell for about 1 hour. After removing DMF by vacuum filtration, we proceeded by removing the Fmoc-protecting group of the resin with a solution of 4-methyl piperidine (20%) in DMF. The solution was let it react for 20 minutes and then removed. The resin was rinsed and washed with DMF.

The first Fmoc-protected amino acid (4 eq. with respects to the resin) was activated by the addition of a solution of 0.38 M HBTU in DMF (1ml for 0.1 mmol scale) and DIPEA (6 eq.); the reaction mixture was vortex and let it react for 2 minutes. The solution was poured onto the beads and let it react for 30 minutes and continuously mixed by gentle N_2 bubbling. The mixture was then rinse and washed with DMF. To control that all the free amino group reacted, we performed the Kaiser test. Few beads were washed with EtOH (to remove DMF and avoid a false positive) and transferred in a small glass tube. 100 μL ninhydrin solution (0.5 g in 10 mL of EtOH) and 100 μL KCN solution (0.4 mL of 1 mM $KCN_{(aq.)}$ in 20 mL of pyridine) were added to the beads. The tube was placed at 115°C for 5 minutes. Afterwards, 1 mL of ethanol and 1 mL of water were added. If the solution turns blue (or does the beads), free amino groups are still present and there is a need of a second coupling; if the solution remains colorless the test is negative, and we proceeded with the Fmoc deprotection, as described above.

A series of coupling-deprotection were repeated to obtain the final peptide sequence. After the final deprotection, the resin was washed several times with DCM in order to remove all the DMF. DCM was then removed by vacuum filtration and the resin was let it dry for 1-2 hours. The resin was weighted and transfer to a round bottom flask, and the reagent cocktail (95% TFA, 2.5% TIPS, 2.5% H_2O) was poured (~1 mL per 100 mg of resin). The mixture was let it react for 2 hours. After the cleavage, -20°C diethyl ether was added (~40 mL of Et_2O for 2 mL of cocktail) to the reaction mixture leading to the precipitation of the peptide in several centrifuge tubes. The precipitation was followed by centrifugation at 4500 rpm for 3 minutes at 4°C and the precipitated was let in the freezer for few hours. The tubes were centrifuged again (4500 rpm for 3 minutes at 4°C) and the supernatant was discarded. The peptide was dissolved in a solution of ACN/H_2O (1:1) 0.1% TFA and filtered to get rid of the beads. The solution was then evaporated, and the peptides

were obtained as white powder. To remark that compound **5** was not well soluble in ACN/H_2O (1:1) 0.1% TFA, so to remove resin beads we had to dissolve it in DMF that made the work-up quite nasty. Compound **5** was obtained as a sticky powder. For all of them, HRMS, ^{1}H and ^{13}C NMR analysis were performed.

4.8.1. LRRASLGFF (3)

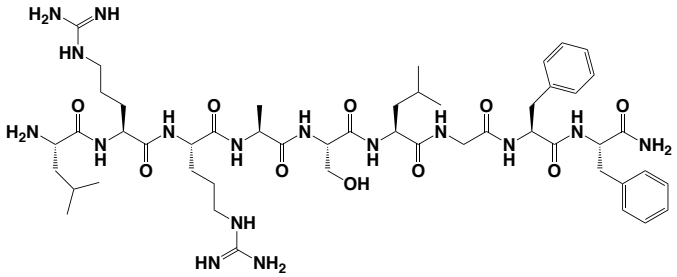

Chemical Formula: $C_{50}H_{80}N_{16}O_{10}$
Exact Mass: 1064.62
Molecular Weight: 1065.29

^{1}H NMR (500 MHz, $(CH_3)_2SO$): δ 8.67 (d, 1H), 8.15 (s, 5H), 8.10 (s, 2H), 7.98 (d, 2H), 7.66 (s, 1H), 7.58 (s, 1H), 7.24 (m, 11H), 7.18 (s, 4H), 7.11 (s, 1H), 7.04 (s, 1H), 4.29 (m, 7H), 3.82 (s, 1H), 3.66 (m, 2H), 3.58 (m, 3H), 3.20 (m, 1H), 3.03 (m, 5H), 2.95 (d, 1H), 2.89 (t, 1H), 1.51 (m, 14H), 1.27 (d, 1H), 1.20 (d, 3H), 0.88-0.81 (m, 12H).

^{13}C NMR (126 MHz, $(CH_3)_2SO$): δ 173.18, 172.75, 172.68, 171.31, 171.24, 171.13, 170.41, 169.32, 168.93, 159.32, 159.03, 158.75, 158.46, 157.19, 157.16, 138.34, 138.11, 129.67, 129.61, 128.70, 128.57, 128.50, 126.73, 117.44, 115.11, 62.06, 55.24, 54.44, 52.66, 52.59, 51.60, 51.14, 48.51, 43.68, 42.24, 41.25, 37.93, 34.78, 31.23, 29.61, 29.48, 28.56, 25.38, 24.54, 23.93, 23.56, 23.13, 22.43, 21.92, 18.74.

HRMS (ESI-MS): 533.3195 [$M+2H^+$], 355.8825 [$M+3H^+$]

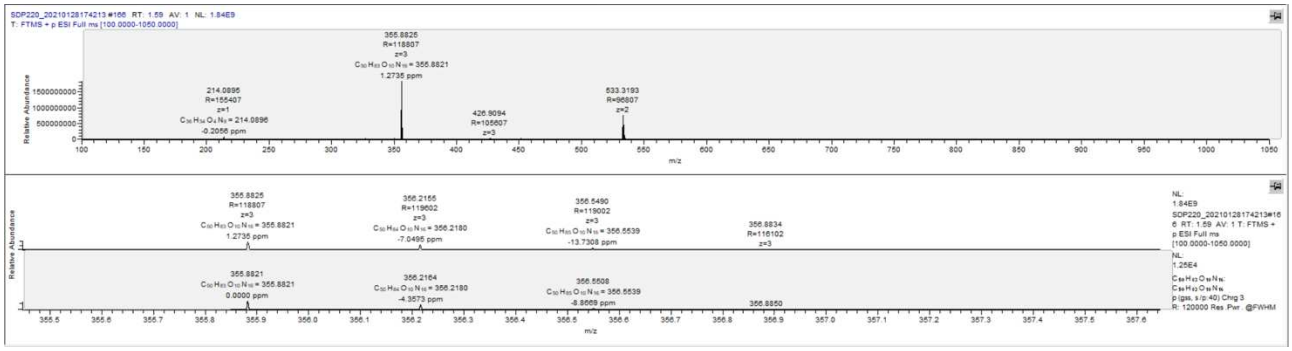

Figure 4.9. HRMS spectrum of compound 3.

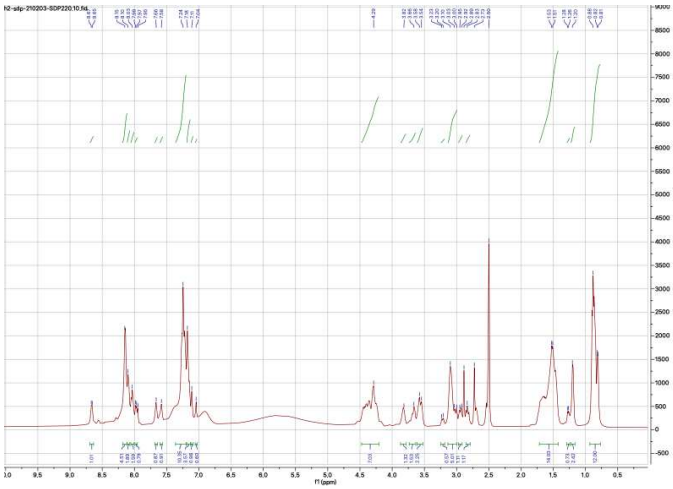

Figure 4.10. ^{1}H NMR spectrum of compound 3.

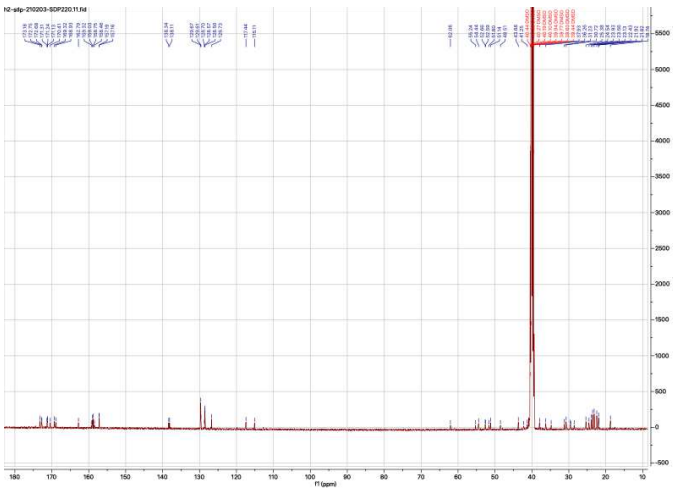

Figure 4.11. ^{13}C NMR spectrum of compound 3.

4.8.2. FFLRRASLG (4)

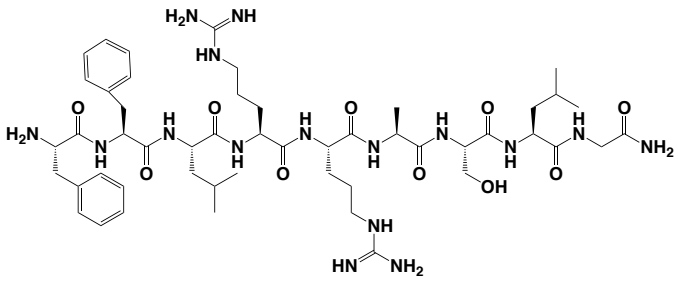

Chemical Formula: $C_{50}H_{80}N_{16}O_{10}$
Exact Mass: 1064.62
Molecular Weight: 1065.29

^{1}H NMR (500 MHz, $(CH_3)_2SO$): δ 8.84 (d, 1H), 8.42 (d, 1H), 8.26-8.25 (m, 1H), 8.10-8.03 (m, 8H), 7.66 (s, 1H), 7.60 (s, 1H), 7.33-7.24 (m, 10H), 7.22-7.15 (m, 3H), 7.09 (s, 1H), 7.06 (s, 1H), 4.65-4.60 (m, 1H), 4.39-4.35 (m, 1H), 4.31-4.22 (m, 5H), 4.01 (s, 1H), 3.73-3.70 (m, 1H), 3.6-3.54 (m, 5H), 3.15-3.03 (m, 7H), 2.92 (t, 1H), 2.82 (q, 1H), 1.69-1.58 (m, 5H), 1.49 (s, 9H), 1.2 (d, 3H), 0.88-0.86 (m, 12H).

^{13}C NMR (126 MHz, $(CH_3)_2SO$): δ 172.76, 172.54, 172.46, 171.72, 171.37, 171.26, 171.08, 170.66, 170.27, 168.46, 159.29, 159.04, 158.79, 158.54, 157.20, 157.18, 138.04, 135.09, 130.18, 129.76, 128.92, 128.61, 127.60, 126.88, 118.63, 116.26, 62.04, 55.37, 54.53, 53.44, 52.53, 52.46, 51.78, 51.48, 48.57, 42.29, 41.20, 37.94, 37.34, 29.56, 25.46, 25.35, 24.69, 24.56, 23.61, 23.58, 22.01, 21.94, 21.91, 18.64.

HRMS (ESI-MS): 533.3193 [M+2H$^+$], 355.8826 [M+3H$^+$].

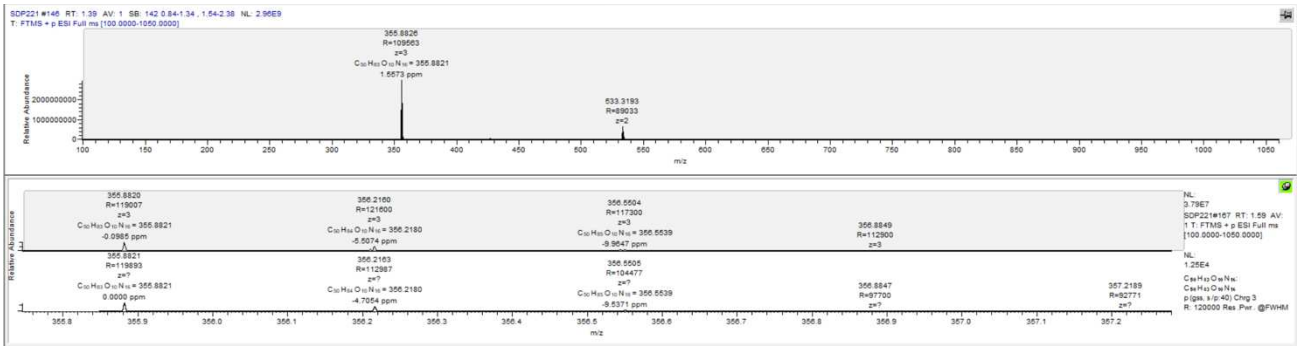

Figure 4.12. HRMS spectrum of compound 4.

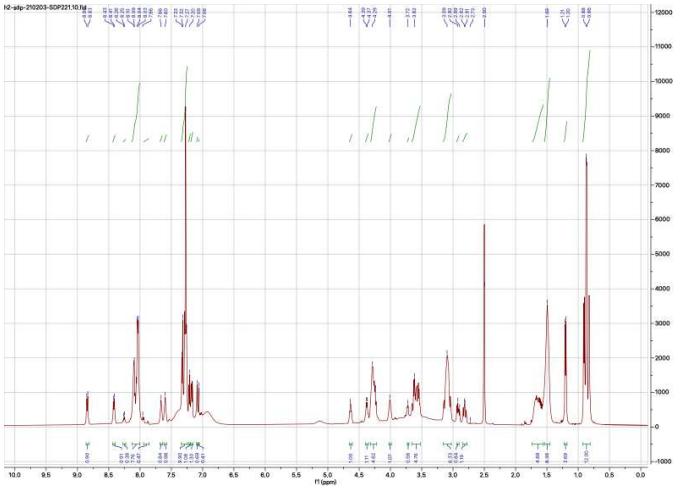

Figure 4.13. ^{1}H NMR spectrum of compound 4.

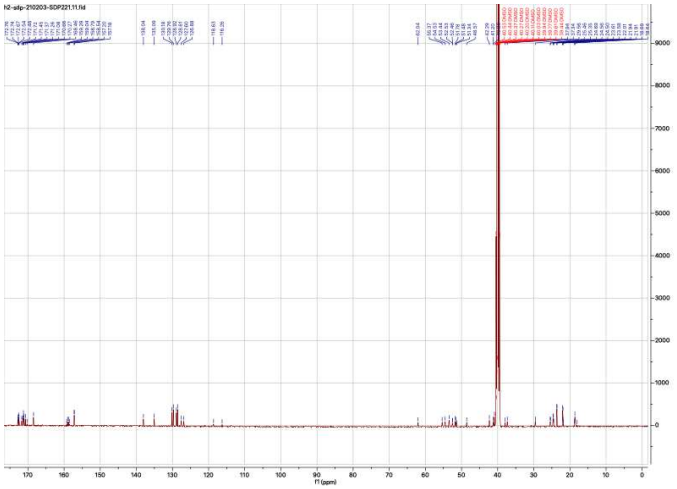

Figure 4.14. ^{13}C NMR spectrum of compound 4.

4.8.3. FFLRRASLFF (5)

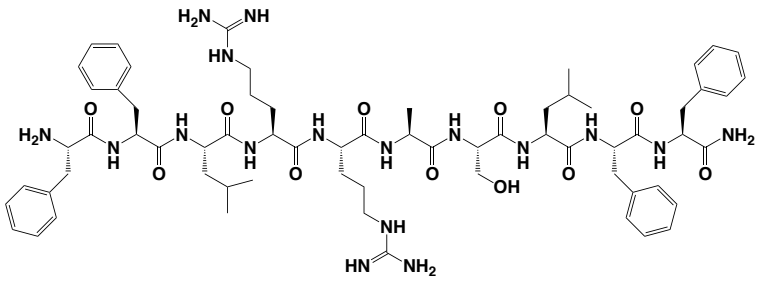

Chemical Formula: $C_{66}H_{95}N_{17}O_{11}$
Exact Mass: 1301.74
Molecular Weight: 1302.59

^{1}H NMR (500 MHz, $(CH_3)_2SO$): δ 8.77 (d, 1H), 8.10-7.96 (m, 6H), 7.94-7.90 (m, 2H), 7.86-7.80 (m, 2H), 7.73 (t, 1H), 7.66 (d, 1H), 7.26-7.11 (m, 21H), 7.06 (s, 2H), 4.62-4.56 (m, 1H), 4.52-4.49 (m, 1H), 4.40-4.18 (m, 8H), 4.15-4.08 (m, 2H), 3.96 (s, 2H), 3.55-3.49 (m, 3H), 3.05-2.91 (m, 8H), 2.88-2.84 (m, 1H), 2.80-2.74 (m, 2H), 2.67-2.63 (m, 1H), 2.36 (t, 1H), 1.67-1.64 (m, 4H), 1.47-1.43 (m, 8H), 1.30-1.26 (m, 2H), 1.16-1.14 (m, 3H), 0.86-0.69 (m, 12H).

^{13}C NMR (126 MHz, $(CH_3)_2SO$): δ 173.04, 171.09, 168.44, 159.16, 158.91, 158.66, 158.41, 157.27, 152.24, 130.15, 129.72, 129.64, 129.58, 128.91, 128.59, 128.55, 128.49, 126.71, 121.11, 118.73, 116.36, 113.98, 55.33, 54.31, 53.07, 52.55, 51.83, 51.61, 37.78, 37.47, 34.72, 25.01, 24.67, 24.45, 23.58, 23.48, 21.99, 21.88.

HRMS (ESI-MS): 618.3228 [M+2H$^+$], 434.9224 [M+3H$^+$].

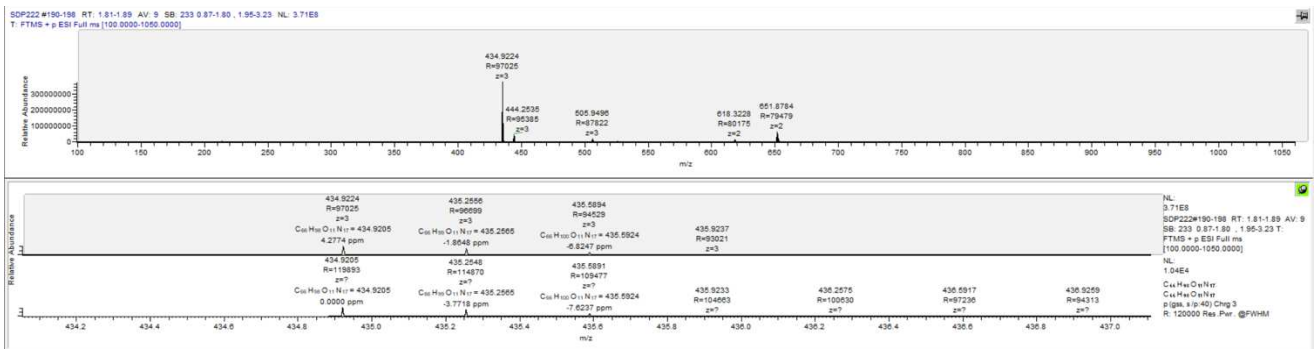

Figure 4.15. HRMS spectrum of compound 5.

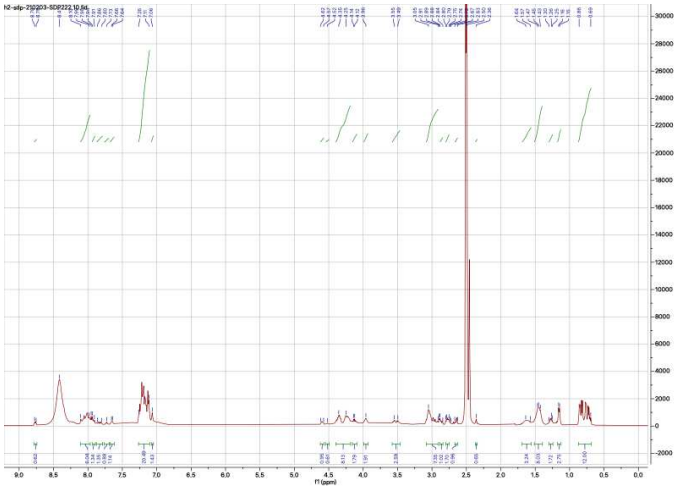

Figure 4.16. ^{1}H NMR spectrum of compound 5.

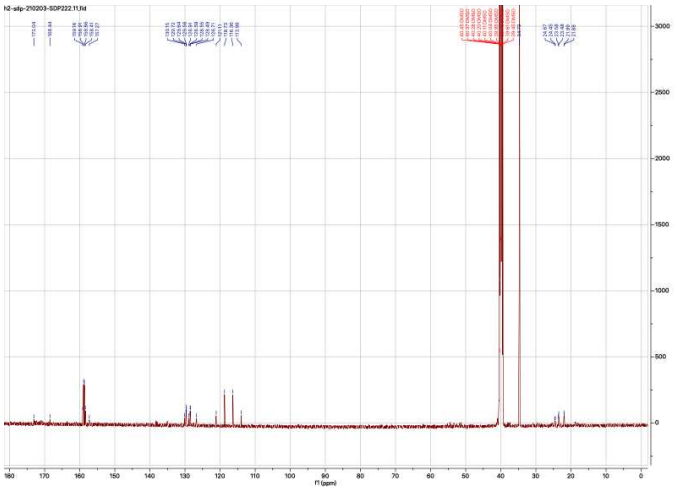

Figure 4.17. ^{13}C NMR spectrum of compound 5.

4.9. References

(1) Ulijn, R. V.; Smith, A. M. Designing Peptide Based Nanomaterials. *Chem. Soc. Rev.* **2008**, *37 (4)*, 664–675.

(2) Mart, R. J.; Osborne, R. D.; Stevens, M. M.; Ulijn, R. V. Peptide-Based Stimuli-Responsive Biomaterials. *Soft Matter* **2006**, *2* (10), 822. https://doi.org/10.1039/b607706d.

(3) Naskar, J.; Palui, G.; Banerjee, A. Tetrapeptide-Based Hydrogels: For Encapsulation and Slow Release of an Anticancer Drug at Physiological PH. *J. Phys. Chem. B* **2009**, *113* (35), 11787–11792. https://doi.org/10.1021/jp904251j.

(4) Dasgupta, A.; Mondal, J. H.; Das, D. Peptide Hydrogels. *RSC Adv.* **2013**, *3* (24), 9117. https://doi.org/10.1039/c3ra40234g.

(5) Jonker, A. M.; Löwik, D. W. P. M.; van Hest, J. C. M. Peptide- and Protein-Based Hydrogels. *Chem. Mater.* **2012**, *24* (5), 759–773. https://doi.org/10.1021/cm202640w.

(6) Fleming, S.; Ulijn, R. V. Design of Nanostructures Based on Aromatic Peptide Amphiphiles. *Chem Soc Rev* **2014**, *43* (23), 8150–8177. https://doi.org/10.1039/C4CS00247D.

(7) Ghadiri, M. R.; Granja, J. R.; Milligan, R. A.; McRee, D. E.; Khazanovich, N. Self-Assembling Organic Nanotubes Based on a Cyclic Peptide Architecture. *Nature* **1993**, *366* (6453), 324–327. https://doi.org/10.1038/366324a0.

(8) Zhang, S.; Holmes, T.; Lockshin, C.; Rich, A. Spontaneous Assembly of a Self-Complementary Oligopeptide to Form a Stable Macroscopic Membrane. *Proc Natl Acad Sci USA* **1993**, *90 (8)*, 3334–3338.

(9) Webber, M. J.; Newcomb, C. J.; Bitton, R.; Stupp, S. I. Switching of Self-Assembly in a Peptide Nanostructure with a Specific Enzyme. *Soft Matter* **2011**, *7* (20), 9665. https://doi.org/10.1039/c1sm05610g.

(10) Vegners, R.; Shestakova, I.; Kalvinsh, I.; Ezzell, R. M.; Janmey, P. A. Use of a Gel-Forming Dipeptide Derivative as a Carrier for Antigen Presentation. *J. Pept. Sci.* **1995**, *1* (6), 371–378. https://doi.org/10.1002/psc.310010604.

(11) Chen, L.; Morris, K.; Laybourn, A.; Elias, D.; Hicks, M. R.; Rodger, A.; Serpell, L.; Adams, D. J. Self-Assembly Mechanism for a Naphthalene−Dipeptide Leading to Hydrogelation. *Langmuir* **2010**, *26* (7), 5232–5242. https://doi.org/10.1021/la903694a.

(12) Reches, M. Casting Metal Nanowires Within Discrete Self-Assembled Peptide Nanotubes. *Science* **2003**, *300* (5619), 625–627. https://doi.org/10.1126/science.1082387.

(13) Reches, M.; Gazit, E. Self-Assembly of Peptide Nanotubes and Amyloid-like Structures by Charged-Termini-Capped Diphenylalanine Peptide Analogues. *Isr. J. Chem.* **2005**, *45* (3), 363–371. https://doi.org/10.1560/5MC0-V3DX-KE0B-YF3J.

(14) Mahler, A.; Reches, M.; Rechter, M.; Cohen, S.; Gazit, E. Rigid, Self-Assembled Hydrogel Composed of a Modified Aromatic Dipeptide. *Adv. Mater.* **2006**, *18* (11), 1365–1370. https://doi.org/10.1002/adma.200501765.

(15) Garcia, A. M.; Iglesias, D.; Parisi, E.; Styan, K. E.; Waddington, L. J.; Deganutti, C.; De Zorzi, R.; Grassi, M.; Melchionna, M.; Vargiu, A. V.; Marchesan, S. Chirality Effects on Peptide Self-Assembly Unraveled from Molecules to Materials. *Chem* **2018**, *4 (8)*, 1862–1876.

(16) Frederix, P. W. J. M.; Scott, G. G.; Abul-Haija, Y. M.; Kalafatovic, D.; Pappas, C. G.; Javid, N.; Hunt, N. T.; Ulijn, R. V.; Tuttle, T. Exploring the Sequence Space for (Tri-)Peptide Self-Assembly to Design and Discover New Hydrogels. *Nat. Chem.* **2015**, *7* (1), 30–37. https://doi.org/10.1038/nchem.2122.

(17) Pappas, C. G.; Shafi, R.; Sasselli, I. R.; Siccardi, H.; Wang, T.; Narang, V.; Abzalimov, R.; Wijerathne, N.; Ulijn, R. V. Dynamic Peptide Libraries for the Discovery of Supramolecular Nanomaterials. *Nat. Nanotechnol.* **2016**, *11* (11), 960–967. https://doi.org/10.1038/nnano.2016.169.

(18) Whitehouse, S.; Feramisco, J. R.; Casnellie, J. E.; Krebs, E. G.; Walsh, D. A. Studies on the Kinetic Mechanism of the Catalytic Subunit of the CAMP-Dependent Protein Kinase. *J. Biol. Chem.* **1983**, *258* (6), 3693–3701. https://doi.org/10.1016/S0021-9258(18)32720-0.

(19) Sorrenti, A.; Leira-Iglesias, J.; Sato, A.; Hermans, T. M. Non-Equilibrium Steady States in Supramolecular Polymerization. *Nat. Commun.* **2017**, *8* (1), 15899. https://doi.org/10.1038/ncomms15899.

(20) Hughes, R. M.; Waters, M. L. Model Systems for β-Hairpins and β-Sheets. *Curr. Opin. Struct. Biol.* **2006**, *16* (4), 514–524. https://doi.org/10.1016/j.sbi.2006.06.008.

(21) Narayanan, C.; Dias, C. L. Hydrophobic Interactions and Hydrogen Bonds in β-Sheet Formation. *J. Chem. Phys.* **2013**, *139* (11), 115103. https://doi.org/10.1063/1.4821596.

(22) Grzybowski, B. A.; Huck, W. T. S. The Nanotechnology of Life-Inspired Systems. *Nat. Nanotechnol.* **2016**, *11* (7), 585–592. https://doi.org/10.1038/nnano.2016.116.

(23) Megzer, T. G. *The Rheology Handbook: For Users of Rotational and Oscillatory Rheometers*, 2nd ed.; Vincentz Network GmbH & Co KG: Hannover, 2006.

(24) Macosko, C. W. *Rheology: Principles, Measurements, and Applications*; Wiley-VCH: New York, NY, 1994.

(25) Weiss, R. G. The Past, Present, and Future of Molecular Gels. What Is the Status of the Field, and Where Is It Going? *J. Am. Chem. Soc.* **2014**, *136* (21), 7519–7530. https://doi.org/10.1021/ja503363v.

(26) De Souza Mendes, P.; Alicke, A.; Thompson, R. Parallel-Plate Geometry Correction for Transient Rheometric

Experiments. *Appl. Rheol.* **2014**, *136* (24), 52721.

(27) Walter, B. L.; Pelteret, J.-P.; Kaschta, J.; Schubert, Dirk. W.; Steinmann, P. On the Wall Slip Phenomenon of Elastomers in Oscillatory Shear Measurements Using Parallel-Plate Rotational Rheometry: II. Influence of Experimental Conditions. *Polym. Test.* **2017**, *61*, 455–463.

(28) Maiti, S.; Fortunati, I.; Ferrante, C.; Scrimin, P.; Prins, L. J. Dissipative Self-Assembly of Vesicular Nanoreactors. *Nat. Chem.* **2016**, *8* (7), 725–731. https://doi.org/10.1038/nchem.2511.

(29) Kumar, M.; Brocorens, P.; Tonnelé, C.; Beljonne, D.; Surin, M.; George, S. J. A Dynamic Supramolecular Polymer with Stimuli-Responsive Handedness for in Situ Probing of Enzymatic ATP Hydrolysis. *Nat. Commun.* **2014**, *5* (1), 5793. https://doi.org/10.1038/ncomms6793.

(30) Biswas, S.; Kinbara, K.; Niwa, T.; Taguchi, H.; Ishii, N.; Watanabe, S.; Miyata, K.; Kataoka, K.; Aida, T. Biomolecular Robotics for Chemomechanically Driven Guest Delivery Fuelled by Intracellular ATP. *Nat. Chem.* **2013**, *5* (7), 613–620. https://doi.org/10.1038/nchem.1681.

4.10. Appendix

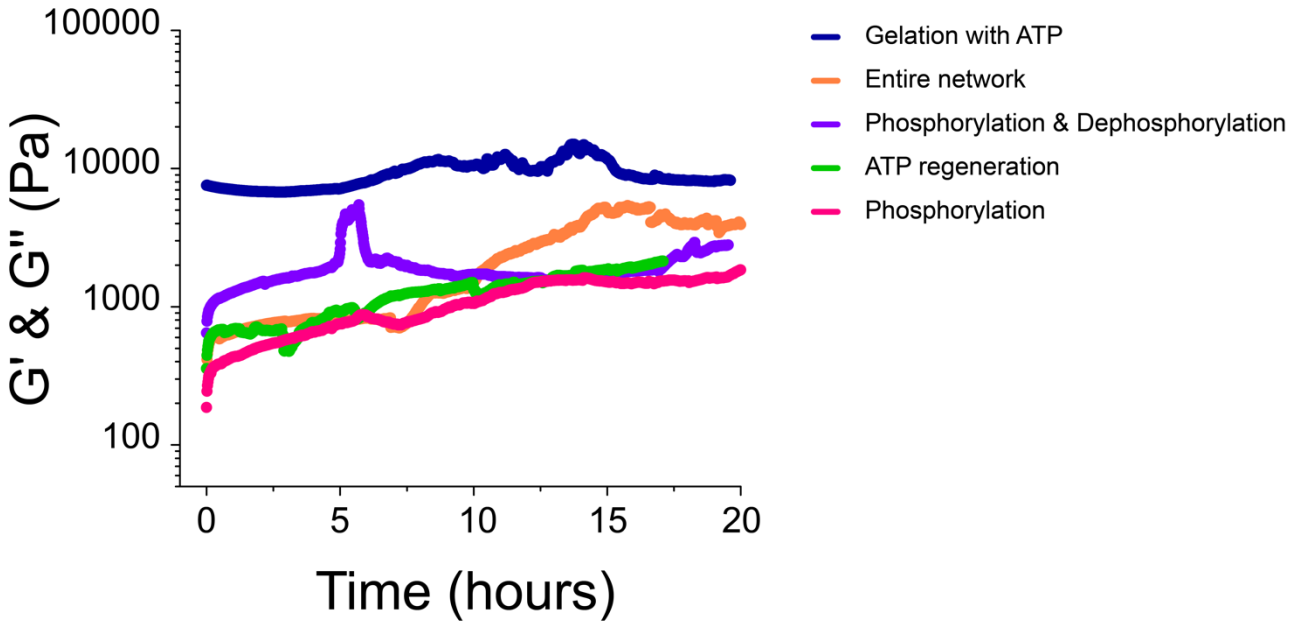

Figure 4.18. Kinetics of gelation. (A) G' monitored over time for substrate **5** at a concentration of 20 mM. The experiments were carried out at 25°C.

Chapter 5.

Re-programming Hydrogel Properties using a Fuel-Driven Reaction Cycle

Abstract

In this Chapter, we present a new chemically driven reaction cycle based on an aldehyde-appended hydrogelator. The reaction cycle is driven by dithionite, hexamine and glucono-δ-lactone to create a transient hydrogel-solution-hydrogel cycle. The aldehyde hydrogel is converted into the α-hydroxy-sulfonate upon reacting with dithionite leading to its dissolution. Delayed *in situ* release of formaldehyde by acid catalysis of hexamine using gluconolactone results in reformation of the original hydrogelator. The catalysis rate influences the kinetics of the system controlling the morphology and the mechanical properties of the hydrogel. Additionally, we show the removal of waste by syneresis and the achievement of up to thirteen cycles.

This work has been published:

Singh, N.; Lainer, B.; Formon, G. J. M.; De Piccoli, S.; and Hermans, T. M. Re-Programming Hydrogel Properties Using a Fuel-driven Reaction Cycle. *J. Am. Chem. Soc.* **2020**, 142 (9),4083-87. https://doi.org/10.1021/jacs.9b11503

5.1. Introduction

In Chapter 1, we discussed synthetic reaction cycles for non-equilibrium self-assemblies and the efforts of Systems Chemists to achieve a better control over those networks. As shown in our recent review[1], in the past decade the number of pure synthetic reaction cycles described is limited, that leaves to Systems Chemists plenty of space to investigate and explore new chemistries. However, the setting-up of complex systems remains challenging as the design of building blocks and chemical fuels is non-trivial.[2] The ultimate goal of the field in obtaining 'life-like' materials requires precise control over important steps of (dis)assembly processes, the production and the removal of the waste, and the kinetics of the system. This is why catalytically controlled reaction cycles are becoming more and more important besides the ability of the material to perform functions (i.e., motility and self-healing).[3] The classical example to simplify the concept comes from microtubules. Microtubules are perfectly organized structures capable of performing vital functions in cells where GTP/GDP turnover is catalytically controlled allowing the structure and functions to be modulated in response to the cellular environment.[4,5]

With the final purpose of exploring and expanding the chemistry applied so far, we developed a new dissipative reaction cycle. In this chapter, we investigate a chemically fueled reaction cycle based on an aldehyde-containing hydrogelator. By adding dithionite, hexamine and glucono-δ-lactone we could perform autonomous gel-sol-gel transient transformation. The catalytic hexamine hydrolysis is used to push the system out-of-equilibrium and to program the morphology and the mechanical properties of the hydrogel. The removal of waste by the process of syneresis (property allowing a gel to expel solvent from its matrix under mechanical force), permits several repetitions of the reaction cycle.

5.2. Stimuli-Responsive Hydrogel and Reaction Cycle

In 1980, Kellogg and co-authors[6] described the reduction of aldehydes to the corresponding alcohols by sodium dithionite ($Na_2S_2O_4$, DT). In the work, they performed the reaction under reflux in a mixture of dioxane-H_2O. Interestingly, under aqueous basic conditions at room temperature the reaction leads the α-hydroxy sulfonate (SO_3^-), without further reduction to its corresponding alcohol. This chemistry has been studied on a previously reported sugar-based aldehyde-containing hydrogelator(**SachCHO**) [7], that forms micron-sized fibers in water (Figure 5.1).

When treated with DT, the aldehydes react forming α-hydroxy sulfonates, **SachCHO** is converted to **SachSO$_3^-$**. As the sulfonate is soluble in water, the reduction of the hydrogel **SachCHO** leads to a clear solution within 10 minutes upon addition of dithionite (Figure 5.1). Next, using a more reactive aldehyde, such as formaldehyde, the sulfonate can be displaced from **SachSO$_3^-$** to give back the **SachCHO** hydrogelator.

Unfortunately, in the perspective of setting up an autonomous cycle, the chemicals DT and formaldehyde cannot be used simultaneously in the reaction mixture as they react quickly with each other. To avoid this, a precursor of formaldehyde -hexamine (HMTA) has been employed. HMTA dissociates into formaldehyde and ammonia under acidic conditions. We use glucono-δ-lactone (GdL) for this purpose which slowly hydrolyses into gluconic acid and releases HCHO from HMTA. By the addition of DT, HMTA and GdL to **SachCHO** hydrogel, **SachSO$_3^-$** is obtained in 5-10 minutes as a clear solution. The hydrogel is restored in 20 to 60 minutes (depending on the concentration of GdL) that is the release of formaldehyde upon catalytically driven hydrolysis of HMTA, reacts with the sulfonate giving back **SachCHO** (Figure 5.1).

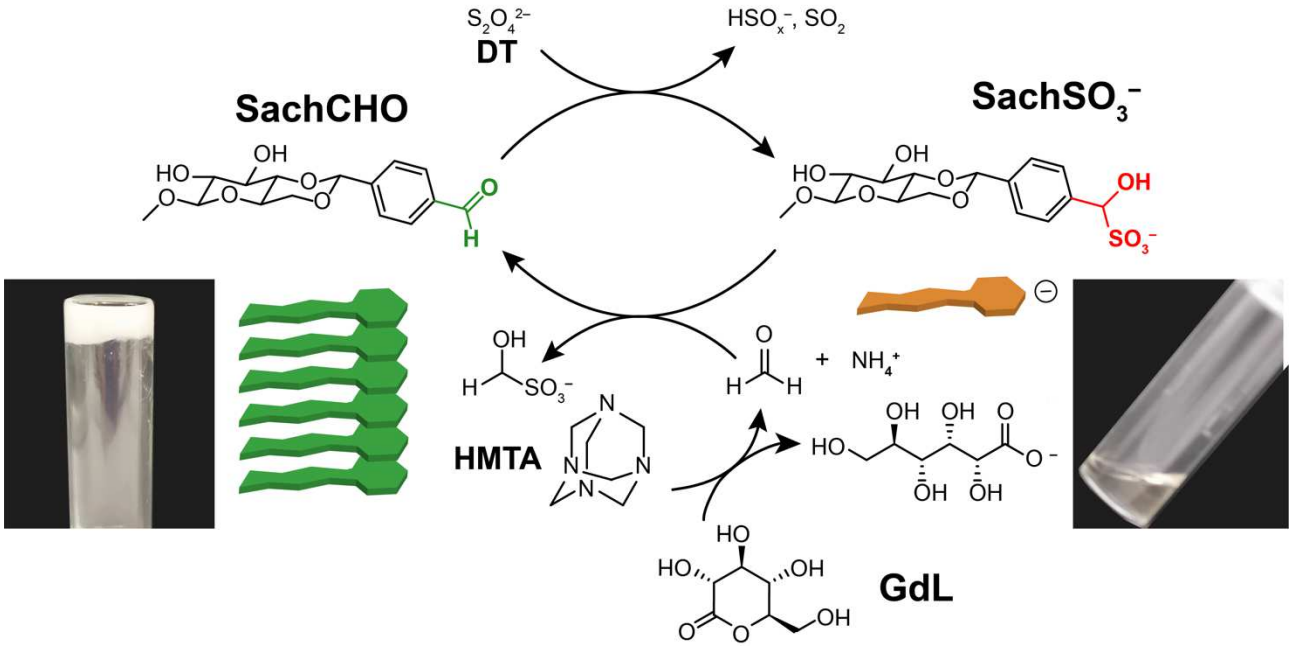

Figure 5.1. Reaction cycle targeting SachCHO. The aldehyde-containing hydrogelator is reduced to the sulfonate **SachSO$_3^-$** by dithionite (DT). Over time formaldehyde is formed, restoring **SachCHO** and the hydrogel. The production of formaldehyde from HMTA is catalytically controlled by the slowly hydrolysis of GdL into gluconic acid. Reproduced from Ref.[8]

5.3. Gelation Mechanism and Kinetics

The polymerization of **SachCHO** was investigated *via* the study of the kinetics and thermodynamics of self-assembly (hydrogelation). As discussed in Chapter 1 and 2, thermodynamic parameters of supramolecular assembly can be obtained by temperature-dependent measurements. Thus, the optical density at 500 nm was followed by UV-Vis spectroscopy as a function of temperature. The final hydrogel is opaque so we could translate the turbidity (optical density) into degree of polymerization of **SachCHO**. Heating/Cooling curves were recorded showing hysteresis (Figure 5.2A). The large hysteresis means that the polymerization of **SachCHO** is cooperative[9] which means that the self-assembly is not under thermodynamic control and that no thermodynamic parameters can be obtained.[10] Further kinetic studies on the assembly mechanism were performed. In this case, to a solution containing **SachSO$_3^-$**, 50 to 100 equivalents of formaldehyde were added to chemically trigger the conversion to **SachCHO** and the hydrogelation (Figure 5.2B). The kinetics were measured by UV-Vis spectroscopy following the change in optical density (turbidity of the sample) at 500 nm.

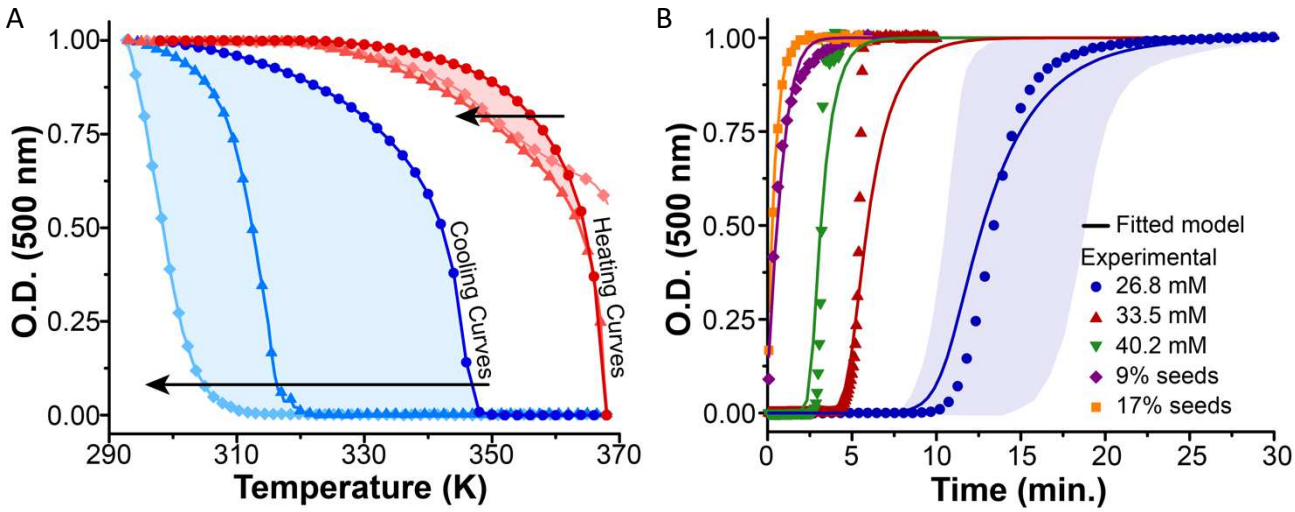

Figure 5.2. Thermodynamics and kinetics of SachCHO assembly. (A) Heating/Cooling curves of **SachCHO** following the optical density at 500 nm at different rates. 70 degree for rate 10 K/min (◆), 50 degree for rate 1 K/min (▲) and 20 degree hysteresis for 5 minutes equilibration at each temperature point (●). (B) Kinetics of the chemically triggered gelation of **SachCHO** followed by UV-Vis spectroscopy at 500 nm. Symbols represent the experimental data and the lines the global-fit of the supramolecular polymerization model. The faded blue region outlines the boundaries of triplicates experiments. Reproduced from Ref.[8]

Indeed, a lag-time followed by a fast increase in the optical density suggested that the kinetic barrier for the nucleation is high, but that elongation is fast. As shown in Figure 5.2B, the kinetics of gelation also included seeded experiments which showed the behavior nucleation-elongation aggregation. The seeding experiments confirmed the fast hydrogelation when the nucleation is overcoming. Moreover, a secondary nucleation was observed. The model was adjusted and showed a better fitting when secondary nucleation is included.[11] This behavior was observed from confocal microscopy, where new fibers are formed on top of pre-existing ones (Figure 5.13 in Appendix 5.12). The kinetic rates k_{n1}, k_{n2} and k_e are reported in the description of the mathematical model in the Experimental section 5.9.

5.4 Kinetics of the Full Reaction Cycle

Afterwards, the kinetics of the complete reaction cycle were studied by quantitative NMR experiments. **SachCHO** hydrogel was prepared by heating a suspension of the hydrogelator in water (pH 8) until dissolution and let it cool down slowly, to allow the formation of uniform long fibers. The mixture containing dithionite (3.6 equivalents), HMTA (3.5 equivalents) and GdL (0.9 to 7 equivalents) was added to the hydrogel. Considering that each hexamine molecule releases six formaldehyde equivalents, the actual formaldehyde is ~20 equivalents in relation to **SachCHO**. This is because a part of the formaldehyde will react with the excess DT present in the solution and, as the reaction between the aldehyde and the sulfonate is an equilibrium, the excess of formaldehyde will ensure the completion of the reaction.

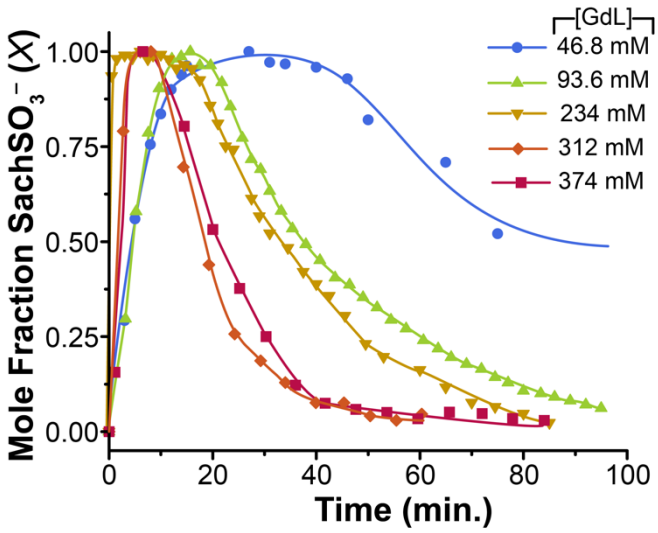

Figure 5.3. Mole fraction of $SachSO_3^-$ in function of time for different GdL concentrations. To **SachCHO** (54 mM) hydrogel, dithionite (191 mM), HMTA (190 mM) and GdL (see figure legend) are added. The kinetics data of the full reaction cycle are obtained by quantitative NMR experiments. Reproduced from Ref.[8]

As shown in Figure 5.3, **SachCHO** is fully converted in **SachSO$_3^-$** within 20 minutes, yielding a clear solution. The backward reaction, that is the degradation of HMTA to formaldehyde and ammonia, is dependent on the amount of GdL added. Higher concentrations of GdL give faster rate of hydrolysis and thus faster conversion of **SachSO$_3^-$** to **SachCHO**. However, a minimum amount of GdL is needed to complete the cycle; 46.8 mM (0.85 equivalents) is not enough to fully hydrolyze HMTA and **SachCHO** cannot be restored even after 48 hours. Increasing the concentration of GdL from 93.6 (1.7 equivalents) up to 374 mM, led the full conversion in 100 minutes down to 60 minutes for higher [GdL].

The kinetics of gelation for the full reaction cycle were obtained by UV-Vis spectroscopy, following the optical density at 500 nm (translated the turbidity of the sample). A mixture of DT (3.6 equivalents), HMTA (3.5 equivalents) and GdL (0.9 to 7 equivalents) was added to the hydrogel, prepared as described in Experimental section 5.9. The spectra were recorded for different [GdL]; the gelation takes 30 to 90 minutes (Figure 5.4). Similarly to the conversion of **SachSO$_3^-$** in the previous NMR experiments, higher concentration of glucono-δ-lactone leads to the decrease of gelation time till a plateau is reached.

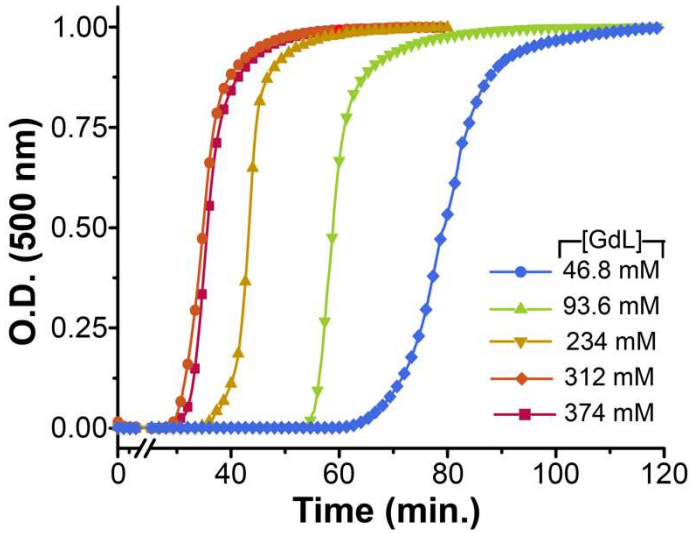

Figure 5.4. Normalized optical density in function of time for different GdL concentrations. To **SachCHO** (54 mM) hydrogel, dithionite (191 mM), HMTA (190 mM) and GdL (see figure legend) are added. Reproduced from Ref.[8]

5.5 Kinetic Control of Morphology and Mechanical Properties

The morphology of **SachCHO** fibers, prepared by heat/cool and chemically by addition of full reaction cycle, were investigated by electron and confocal microscopy (Figure 5.5). The thermogel (preparation protocol described in the Experimental section 5.9) presented long crystalline fibers hundreds of micrometers long (Figure 5.6A & 5.6B). The gel was then prepared with different amounts of GdL. In the case where a lower amount of GdL was added to the reaction cycle, the fibers observed were shorter and growing from central nuclei, forming flower-like assemblies (Figure 5.6C & 5.6D). However, when a higher concentration of GdL was used, that is 374 mM, the structures were more brunched, producing fractal aggregates (Figure 5.6E & 5.6F). Thus, the morphology of the fibers formed is strictly related to the way the hydrogel is prepared, heat/cool or chemically triggered. In the first case, we assisted to a slow nucleation and growth leading to crystalline fibers. Whereas, with the reaction cycle, the release of formaldehyde is fast and thus is the growth of the fibers.

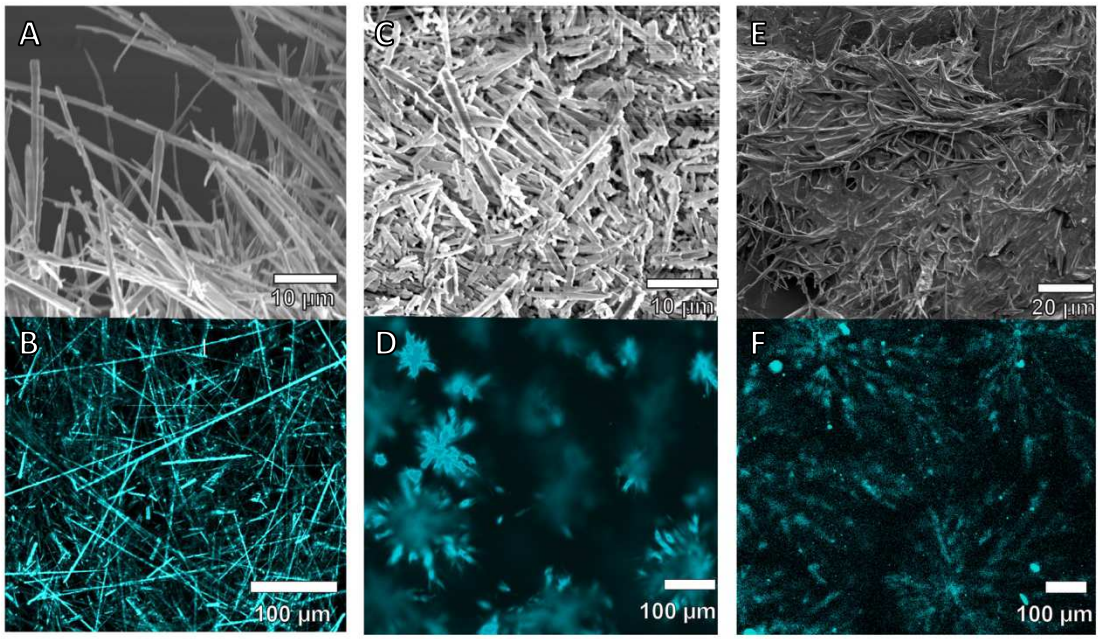

Figure 5.5. SEM (top) and confocal microscopy (bottom) photographs. (A, B) Crystalline structures formed by the hydrogel prepared by heat/cool. (C, D) Flower-like assemblies of the hydrogel obtained by the full reaction cycle using [GdL] = 234 mM. (E, F) Fractal-like assemblies of the hydrogel prepared chemically by the reaction cycle using [GdL] = 374 mM. Reproduced from Ref.[8]

Powder X-Ray Diffraction (XRD) confirmed the different morphologies deriving from the different preparation conditions used to obtain the hydrogels (Figure 5.14 in Appendix 5.12). The

XRD patterns showed no significant differences between the hydrogel obtained by heat/cool and the chemically triggered hydrogel when [GdL] = 93.6 and 234 mM. The peaks at 1.15 and 0.648 are related to inter-columnar distances whereas the one at 0.38 nm derives from the intermolecular stacking distance within the columns. Nevertheless, when the hydrogel is prepared with a higher concentration of glucono-δ-lactone (374 mM) the intermolecular packing distances is smaller, as shown by the appearance of peaks at 0.325 and 0.305. These results confirmed the direct influence of [GdL], that is the rate of catalysis, on hydrogel morphologies.[12,13]

Later, the mechanical properties of the hydrogel were investigated by rheology measurements. In Figure 5.6, the trend confirmed that the gelation time decreases at higher GdL concentrations. Moreover, by increasing the amount of GdL, the storage modulus G' increases, from ~110 Pa for [GdL] = 46.8 mM to ~2100 Pa for [GdL] = 374 mM. The thermally annealed hydrogel has a G' of ~800 Pa. Therefore, the morphological changes within the hydrogel directly influence the final mechanical properties. For instance, the branched structure obtained with 374 mM of glucono-δ-lactone leads to a tighter gel and, as a result, to a stronger material.

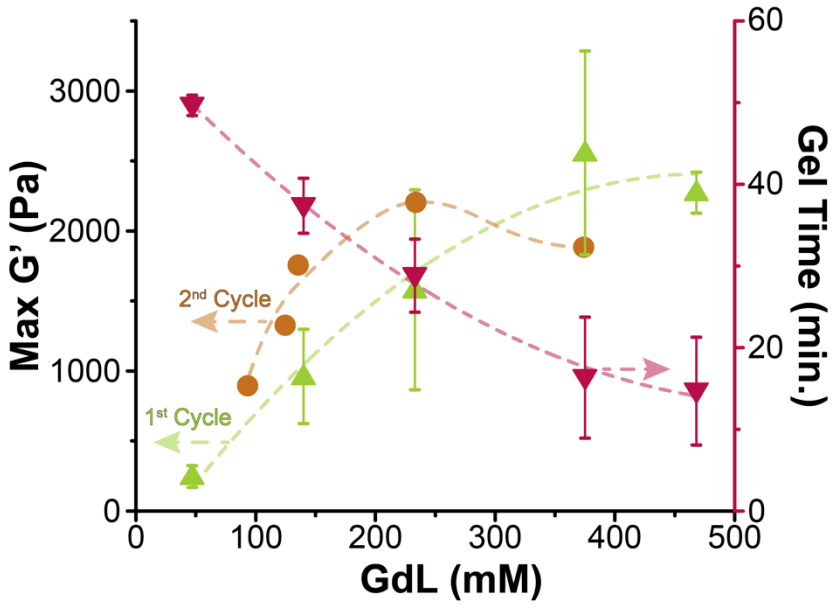

Figure 5.6. Rheology measurements at different GdL concentrations. The experiments showed the decrease in the gelation time (pink) and the increase in stiffness (G', green) with increasing [GdL]. The orange dots represent the second round of fuel addition. Error bars are the standard deviation over triplicate experiments. Reproduced from Ref.[8]

Interestingly, the system can be fueled for a second cycle (DT, HMTA and different [GdL]) when the first cycle is performed with 140 mM GdL (second cycle in orange, Figure 5.6). Once more, the G' depends on the concentration of GdL used to re-fuel the system. Unfortunately, the waste

accumulates over the two reaction cycles prevented the re-fueling of the system and the formation of the hydrogel.

5.6 Syneresis

To overcome the waste issue, we took advantage of the hydrogel property called "syneresis"[14], that is the capability of expelling the solvent from the gel matrix. Considering that fuels and waste products are water-soluble, this interesting property was investigated to remove the waste from the system and to perform multiple reaction cycles. To do that, we used a syringe, equipped with a cotton swab at the tip (Figure 5.7A). The **SachCHO** hydrogel was chemically obtained by the reaction cycle inside the syringe. After 60-70 minutes, the gel is formed and the piston of the syringe was pressed to expel the solvent and, thus, the waste products. **SachCHO** fibers were retained. However, to proceed with further cycles, 3 mg (10% of the total amount) of **SachCHO** were added along with DT (121 mM), HMTA (190 mM) and GdL (312 mM). Indeed, from NMR spectroscopy we observed that a small percentage of **SachCHO** is soluble in water that is lost during the waste removal process (Figure 5.8 in Experimental section 5.9). Once, the system was re-fueled we tracked the gel formation by UV-Vis spectroscopy at 500 nm, as shown in Figure 5.7B. The same was repeated; the gel is re-formed, and the solvent expelled. No loss of the **SachCHO** structure was observed. The cycles were repeated for 13 times with no significant variation of the kinetics of the cycle (Figure 5.7B). This method has been proved to be an efficient way to remove waste products, allowing the completion and the repetition of up to thirteen cycles, and to maintain the final structural integrity of the hydrogel (Figure 5.15 in Appendix 5.12). As widely discussed in Chapter 1 and 2, the waste removal can be a big issue to overcome in fuel-drive systems[1,15,16], and here, we solve the issue by mechanically expelling the waste and restart the cycle.

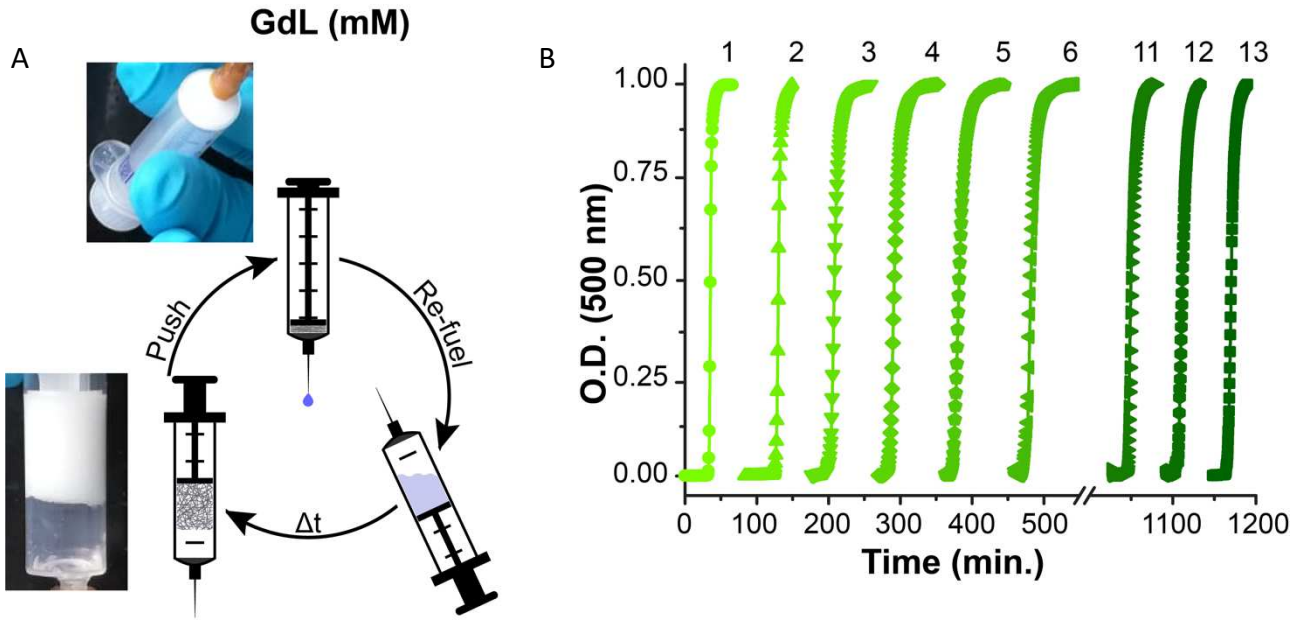

Figure 5.7. Syneresis cycles. (A) The scheme showed the waste products removal by syneresis. In clockwise direction, the chemically triggered gel is formed inside the syringe (bottom left); the water-soluble waste products are pushed out of the system; the reaction cycle is re-fueled ([DT] = 121 mM, [HMTA] = 190 mM, [GdL] = 312 mM). (B) UV-Vis spectroscopy measurements of the optical density at 500 nm. The reaction cycles were followed in a quartz cuvette (optical path 1 mm). The waste removal/re-fueling cycle was repeated up to 13 times. Reproduced from Ref.[8]

5.7 Conclusions

In this chapter, we have presented a new reaction cycle where the assembly and the disassembly of the system can be chemically controlled. The system is based on an aldehyde-containing hydrogelator; the addition of dithionite reduces the aldehyde to its α-hydroxy sulfonate derivate, leading the dissolution of the gel. The addition of hexamine and glucono-δ-lactone is necessary to re-establish the aldehyde and the formation of the hydrogel autonomously. Interestingly, by controlling the rate of catalysis, that is the acid catalysis of hexamine to formaldehyde, we could attain different morphological and mechanical properties of the final hydrogel. Additionally, taking advantage of the syneresis property of the hydrogel, we could mechanically expel the water-soluble waste products by the use of a syringe. The latter allowed us to repeat the reaction cycle up to thirteen times, removing the waste that would have caused the inhibition of the cycle completion.

5.8. Acknowledgements

Dr. Nishant Singh developed the reaction cycle and concept. Dr. Nishant Singh and Bruno Lainer synthesized **SachCHO** and **SachSO$_3^-$**, optimized the parameters and performed kinetic and rheological experiments. Dr. Georges Formon performed kinetic experiments and the numerical analysis. Serena De Piccoli performed the syneresis experiments and preliminary studies on peptide substrates (see section 5.11). Prof. Thomas Hermans and Dr. Nishant Singh supervised the research.

This chapter was written by Serena De Piccoli based on the publication: Singh, Nishant, Lainer, Bruno, Formon, Georges J. M., De Piccoli, Serena, and Hermans, Thomas M. "Re-Programming Hydrogel Properties Using a Fuel-Driven Reaction Cycle." J. Am. Chem. Soc. 142, no. 9 (2020): 4083–87. https://doi.org/10.1021/jacs.9b11503

5.9. Experimental section

Thermally annealed gel. A suspension of **SachCHO** (54 mM unless mentioned otherwise) at pH 8 in water was heated to around 80-90°C until a clear solution was formed. This solution was allowed to cool down at room temperature yielding a white gel able to support its weight when inverted.

Transient Cycles. To a thermally annealed gel of **SachCHO** (30 mg in 1.5 mL pH 8 water), the fuels: HMTA – 48 mg unless mentioned otherwise, appropriate amount of GdL (see main text), sodium dithionite (DT – 60 mg unless mentioned otherwise), dissolved in 300 μL of pH 8 water were added. The thermally annealed gel dissolves and reforms into a gel after a certain time dependent on [GdL]. This method of creating transient cycles was used for NMR kinetic experiments, UV-Vis experiments, rheology experiments (except for 2 cycle experiment).

pH experiments. A VWR Model 110 pH meter was used to record the pH measurements. The pH was recorded at different time intervals for different systems involving GdL, GdL+HMTA, DT+GdL+HMTA, DT+GdL+HMTA+**SachCHO** (full transient cycle, and for two consecutive cycles with 2 times fuels addition).

NMR experiments. (^{1}H and ^{13}C, and kinetic measurements using a coaxial tube with an external reference.) NMR spectra were recorded on a Bruker UltraShield Plus Avance III NMR instrument at 25°C.

Thermally annealed gels (10 mg in 500 μL D_2O pH 8) were made in a NMR tube. To this tube was introduced a co-axial tube containing p-toluidine as an external reference (0.97 mg in 200 μL). The fuels dissolved in 100 μl (HMTA-16 mg, GdL appropriate amounts, DT-20 mg) D_2O pH 8 were added to the NMR tube and spectra were recorded for specified time intervals.

Rheology experiments. Rheology experiments were performed on a Thermofischer Scientific MARS 40 rheometer using parallel plate geometry with plate distance of 1.8 mm, γ = 0.08%, ν = 1Hz at 25°C.

Fuels (dissolved in 300 μL) were added to thermally annealed gels (1.5 mL) and upon dissolution the solution was transferred to the bottom plate of the rheometer and measurements were recorded until the values plateaued. Time points reflecting ~50% of G' max values were considered as gelation time. G' and G'' crossover was seen early during the measurements in the experiments.

DT degrades rapidly in acidic environment. This is bound to happen when DT, HMTA and GdL are all mixed together in a solution before addition to the thermal gel. Thus, to attain complete transient cycles while using lesser amount of fuels and thus generating lesser wastes we add all the fuels directly in powder form to 1.8 mL thermally annealed gel. This method was used for rheology experiments involving two consecutive cycles. The fuels used for the 1st cycle were **SachCHO** (30 mg in 1.8 ml pH 8 water), DT (40 mg), HMTA (24 mg), GdL (30 mg) and for the 2nd cycle DT (40 mg), HMTA (48 mg), GdL (different concentrations). The pH was not readjusted after each cycle. Only the first solution is adjusted to pH 8 by addition of a solution of NaOH (aq.; 0.1 M).

UV-Vis experiments. UV-Vis experiments were performed on Agilent CARY 8454-UV spectrometer in 1 mm cuvettes. Results found in Figure 5.2B are UV-Vis normalized absorbance at 500 nm of seeded and unseeded chemical gel formation with the addition of the same large amount of Formaldehyde solution (50 to 100 equivalents) to a **SachSO_3^-** solution, to ensure rapid conversion of the α-hydroxy sulfonate to aldehyde.

In a typical reaction cycle experiment, Figure 5.4, the fuels were added to the gel in a vial. Once the gel turned to solution, the solution was transferred to the cuvette. The measurement started with a delay of 6 minutes from fuel addition.

The fibers formed by **SachCHO** are big enough to be visible by naked eye and they are opaque, so gelation can be easily followed by the increase in 'absorbance' followed by UV-Vis. We assume that the increase in opacity is proportional to the gelation process.

Syneresis experiments. For utilizing syneresis to extrude the dissolved waste products we made a simple set up comprising of a syringe and a needle. The needle was stuffed with cotton so as to avoid seeping out of any fibers which are several micrometers in length and width. A thermally annealed gel was transferred to the syringe using a spatula to which the fuels were added in powder form. After each transient cycle the plunger was pushed slowly so as to compress the gel and allow solvent + waste to be expelled via the outlet of the needle. For the next cycle the solvent (1.8 mL) and fuels were added. Importantly, for each cycle an extra 3 mg of **SachCHO** was added along with the fuels to compensate the amount of soluble **SachCHO** coming out during syneresis. This amount of replenished SachCHO was calculated based on the concentration of soluble **SachCHO** (10% of the total amount) evident by NMR in the hydrogel using the ERECTIC NMR method as described before (Figure 5.8). After syneresis we could confirm the amount of **SachCHO** coming out with the waste products, which was 2.96 ± 0.68 mg (10% of the total amount).

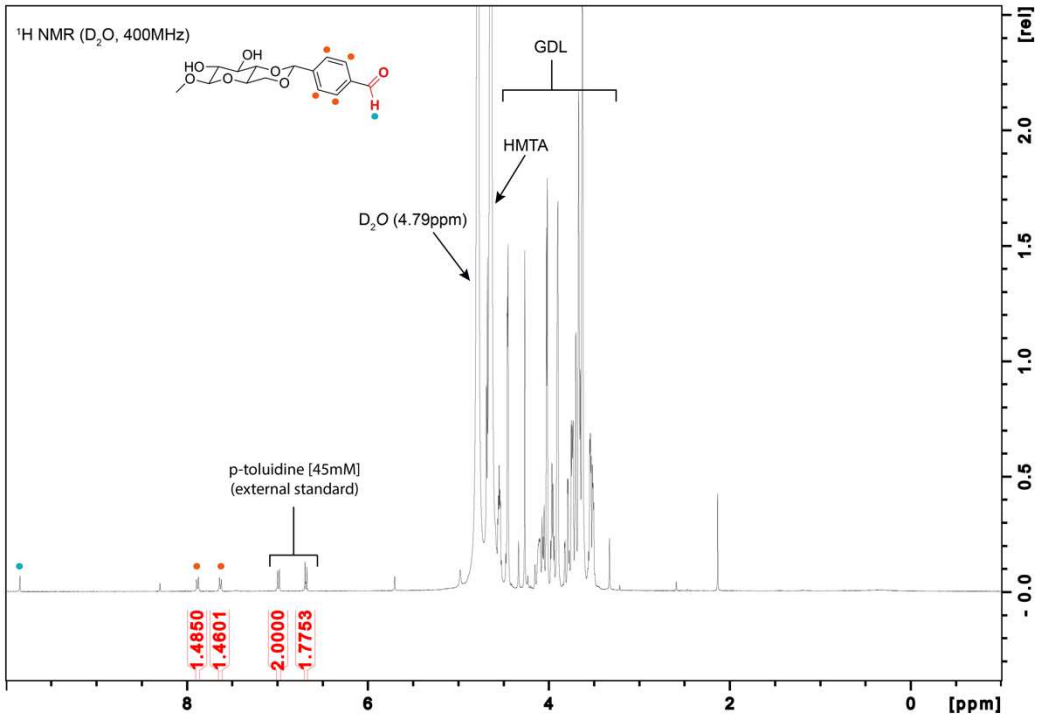

Figure 5.8. ^{1}H NMR spectrum extruded from Syneresis experiments. The amount of **SachCHO** in the solution was calculated by comparing it with the known concentration of the internal standard and is comparable to the soluble **SachCHO** molecules present in the original hydrogel. Reproduced from Ref.[8]

Confocal Microscopy. Images were acquired using a ZEISS LSM 710 confocal microscope. No fluorescent markers were used.

Powder X-Ray diffraction. Powder X-ray diffraction measurements were performed on a Bruker D2 Phaser diffractometer (Source: Standard ceramic sealed tube CuKa 1.54184 Å. Detector: Bruker 1D-LYNXEYE). The lyophilized hydrogels were washed repeatedly with water to remove the salts and wastes, and then mounted on a silicon wafer for measurements. The measurements were done at 25°C.

Scanning Electron Microscopy. SEM images were taken using a FEI Quanta FEG 450 microscope. Using a 5.0 kV High Voltage and dwell time of 50 μs. The lyophilized hydrogels were washed repeatedly with water to remove the salts and wastes, mounted on a silicon wafer and sputtered with 10 to 15 nm of gold.

5.10. Synthesis SachCHO & $SachSO_3^-$

SachCHO was synthesized following a previously reported method.[7] UV/Vis λ_{max} = 250 nm (Figure 5.9).

$SachSO_3^-$ was prepared by adding the required amount of Dithionite (typically 3.6 equivalents, 85% pure) to **SachCHO**. NMR spectra were recorded in D_2O (Figure 5.10).

^{1}H NMR 400MHz (D_2O, ppm): δ 3.46 (3H, s) 3.67-3.74 (2H, m) 3.90-3.91 (3H, m) 4.35 (1H, q, J= 10.7 Hz) 4.90 (1H, d, J= 3.25 Hz) 5.57 (1H, s) 5.77 (1H, s) 7.60 (4H, q, J = 7.94 Hz)

^{13}C NMR 100MHz (D_2O, ppm): δ 55.3, 62.3, 68.1, 70.1, 71.7, 80.4, 85.2, 100.1, 101.4, 126.2, 127.9, 136.8, 137.0

UV/Vis λ_{max} = 218 nm (Figure 5.9).

Calculated mass (m/z): 391.0704, Mass found (m/z): 391.0703.

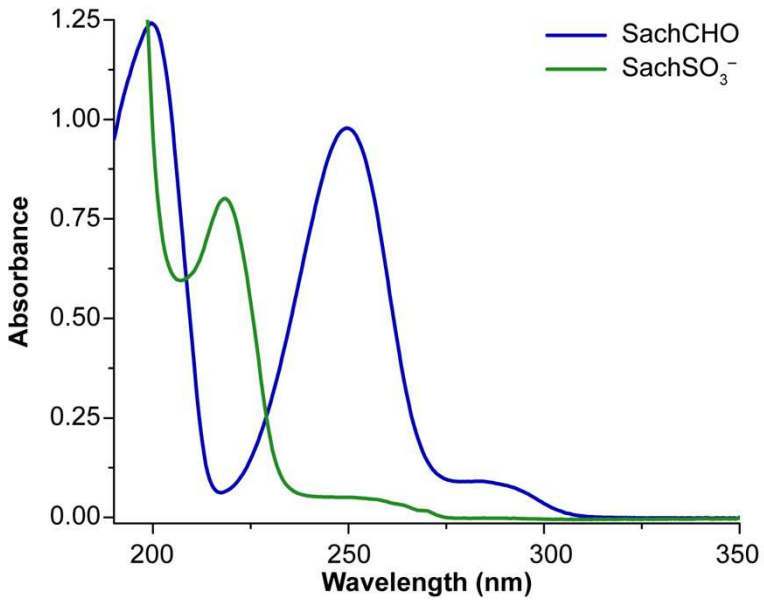

Figure 5.9. UV-Vis spectra of SachCHO and $SachSO_3^-$. The blue line is the spectrum of **SachCHO** at 500 μM. The green line is the same solution with 3.6 equivalents of dithionite, the same proportion used in the reaction cycles. Reproduced from Ref.[8]

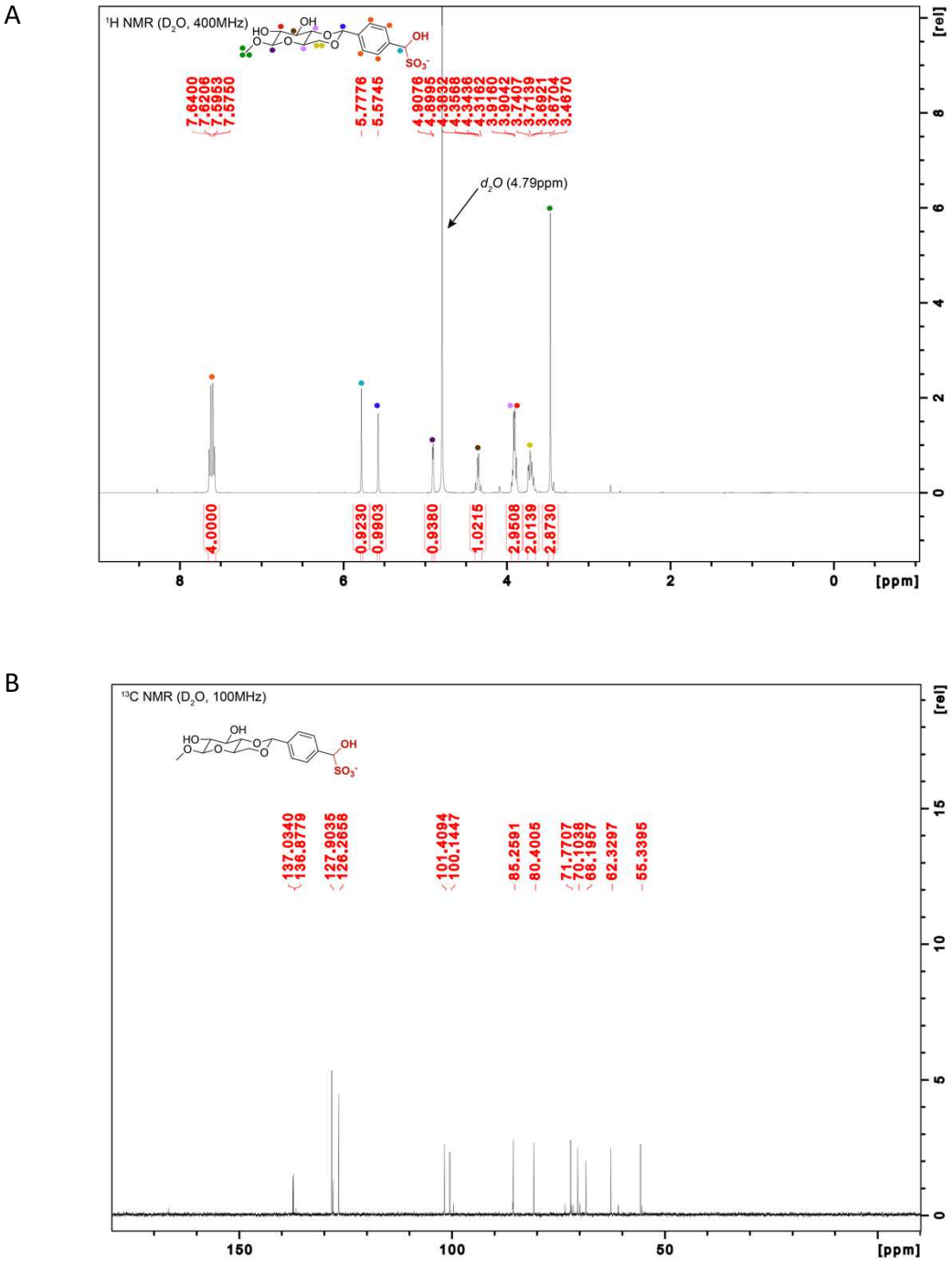

Figure 5.10. NMR (A) ^{1}H (D_2O, 400MHz), (B) ^{13}C (D_2O, 100MHz) NMR spectra of SachSO_3^-. Reproduced from Ref.[8]

Mathematical model. The model chosen to be fitted to the experimental supramolecular polymerization kinetic data was the analytical solution of the nucleation-elongation moments model derived by T. Knowles *et al.*[17], including secondary nucleation.[18,19] This particular mechanism (nucleation, elongation and secondary nucleation) was chosen after the analysis of the half-times of nucleation as a function of monomer initial concentration, discussion in the caption of Figure 5.12, and because of microscopy data evidencing the phenomenon of secondary nucleation (Figure 5.13 in Appendix 5.12). The original differential equations for the moments model are as follows:

$$\frac{dP(t)}{dt} = k_{n1}m(t)^{n1} + k_{n2}m(t)^{n2}M(t) \quad \text{Eq.1}$$

$$\frac{dM(t)}{dt} = 2\big(m(t)k_e - k_{off}\big)P(t) + n1k_{n1}m(t)^{n1} + n2k_{n2}M(t)m(t)^{n2} \quad \text{Eq.2}$$

Where $P(t)$ is the supramolecular polymer concentration at a given time (number of fibers in solution), $M(t)$ is the concentration of molecules in the polymeric form (number of molecules in fibers), $m(t)$ is the free monomer molar concentration, k_{n1} is the primary nucleation rate constant, k_{n2} is the secondary nucleation rate constant, k_e is the elongation rate constant, k_{off} is the depolymerization rate constant, $n1$ is the primary nucleus size and $n2$ is the secondary nucleus size.

The analytical solution of coupled differential equations for the calculation of $M(t)$ is:

$$\frac{M(t)}{M(\infty)} = 1 - \left(1 - \frac{M(0)}{M(\infty)}\right) \times \left(\frac{B_+ + C_+}{B_+ + C_+ e^{kt}} \frac{B_- + C_+ e^{kt}}{B_- + C_+}\right)^{\frac{k_\infty^2}{\kappa k_\infty}} e^{-k_\infty t} \quad \text{Eq.3}$$

Where $M(0)$ is the initial concentration of molecules in the polymeric form, $M(\infty)$ is the final concentration of molecules in the polymeric form, and the other parameters are:

$$\kappa = \sqrt{2k_{n2}m(0)^{n2}(m(0)k_e - k_{off})} \quad \text{Eq.4}$$

$$\lambda = \sqrt{2k_e k_{n1}m(0)^{n1}} \quad \text{Eq.5}$$

$$C_\pm = \frac{k_e P(0)}{\kappa} \pm \frac{k_e M(0)}{[2(m(0)k_e - k_{off})]} \pm \frac{\lambda^2}{2\kappa^2} \quad \text{Eq.6}$$

$$k_{\infty} = \kappa\sqrt{\frac{2}{n2(n2+1)} + \frac{2\lambda^2}{n1\kappa^2} + \frac{2M(0)}{n2m(0)} + (\frac{2k_eP(0)}{\kappa})^2} \quad \text{Eq.7}$$

$$\tilde{k}_{\infty} = \sqrt{k_{\infty}^2 - 4C_+C_-\kappa^2} \quad \text{Eq.8}$$

$$B_{\pm} = \frac{k_{\infty} \pm \tilde{k}_{\infty}}{2\kappa} \quad \text{Eq.9}$$

Where $P(0)$ is the initial supramolecular polymer concentration and $m(0)$ is the initial free monomer molar concentration.

Practically, the equations (3) to (9) were used to perform the fitting. The fitting is done by comparing the results of Equation (3) to the experimental data set and using the kinetic rate constants as free parameters.

The supramolecular polymerization model, described above, was fitted to match the normalized Optical Density experimental data present in Figure 1c. It is assumed that Optical Density is linearly related to $M(t)$, because the opacity of the sample is directly proportional to gelation. This is not to be confused with actual light scattering experiments where intensity is changed by the number of scatterers (linearly) and by the size of the aggregates (nonlinearly).

To perform the fitting the values $n1$ and $n2$ (primary and secondary nucleus size) were set as global constants with a value of 6. For the model to be applicable, k_{off} (depolymerization rate constant) must be negligible when compared to the elongation rate constant, so in this case it is set as a global constant with a value of 10^{-9} s^{-1}. For seeded experiments, the value of $P(0)$ is a needed parameter, but it is a very difficult value to measure or estimate since it is almost impossible to count the number of fibers injected in solution.[11] Those values were set as arbitrary small values (two orders of magnitude smaller than $M(0)$): $P(0)$ = 10^{-5} $mol\ L^{-1}$ for the experiments with 9% seeds; $P(0)$ = 2x10^{-5} $mol\ L^{-1}$ for the experiments with 16% seeds. The only free parameters for fitting were: Primary nucleation rate constant, k_{n1}; Elongation rate constant, k_e; Secondary nucleation rate constant, k_{n2}. Global fitting was performed, using online application amylofit.ch.cam.ac.uk, over triplicate experiments for unseeded experiments and duplicates for seeded - Mean squared error = 0.0271.

The following numerical results were obtained (numbers between brackets represent asymmetrical error to the fit):

- Primary nucleation rate constant: $k_{n1} = 4.79\ \binom{+0.59}{-1.99} \cdot 10^{-5}\ L^5 mol^{-5} s^{-1}$

- Elongation rate constant: $k_e = 1.67\ \binom{+0.12}{-0.16} \cdot 10^{3}\ L\ mol^{-1} s^{-1}$

- Secondary nucleation rate constant: $k_{n2} = 1.75\ \binom{+0.19}{-0.15} \cdot 10^{4}\ L^6 mol^{-6} s^{-1}$

5.11. Synthesis of aldehyde-containing hydrogelators (Preliminary studies)

During preliminary studies, few different aldehyde-containing peptide sequences were synthesized. Fmoc-RGDF-OH, Fmoc-GFFY-OH and Fmoc-FF-OH were synthesized by solid phase peptide synthesis (SPPS).[20] The sequence 2-Naphtylacetic acid-GFFY-OH was provided by Ontores Biotechnologies (90% purity, white powder). For all the peptide sequence the C-terminus was modified, following the procedure reported in literature.[21] The final Fmoc-RGDF-ONHCHO, Fmoc-GFFY-ONHCHO and Fmoc-FF-ONHCHO were tested. Unfortunately, only a slightly change in the self-assembly (by primary optical microscopy studies) was observed. However, Naph-GFFY-ONHCHO (**ChinCHO**) was indeed a strong hydrogelator and has been further characterized (MALDI, HRMS in Figure 5.11) and explored. **ChinCHO** demonstrated to form hydrogels at very low concentration that turned out to be an issue for the reaction cycle developed, as a huge amount of DT was needed to hydrolyze the aldehyde.

General SPPS procedure. The resin (preloaded resin, 2-H-chlorotrytil resin 200-400 mesh) was washed with DMF and then let it swell for 30 minutes, gently stirred once in a time.

The Fmoc-amino acid (4 eq, 0.4 mmol) was dissolved in 1 mL of a solution of HBTU dissolved at conc. 0.38 M in DMF (3.8 eq). For preactivation the 110 µL of DIPEA (6 eq) were added, then the reaction mixture was vortexed and let to react for 2 minutes. The resulting solution was poured onto the resin beads. The coupling reaction lasted 30 minutes with stirring every 5 minutes. The beads were rinsed and washed with DMF. The completion of the coupling was monitored by Kaiser test.

The resin was rinsed twice with a solution of 20 % of 4-methyl piperidine in DMF. The beads were let to react for 20 minutes with stirring every 5 minutes. The piperidine was removed and the beads were washed four times with DMF. The coupling and deprotection were repeated for each amino acid in the sequence of a peptide following from C-terminus to N-terminus.

The resin was washed with DCM and dried by air flow using a vacuum filtration setup for 20 minutes. The resin was weighted: for 100 mg of resin, 1 mL of cleavage cocktail (95 % TFA, 2.5 % TIPS, 2.5 % H_2O). The resulting mixture was stirred for 2 hours at room temperature.

The cleavage mixture was transferred into several 50 mL centrifuge tubes and chilled diethyl ether (-20 °C) was added to reach a total volume of 40 mL. Afterwards, crude peptide product precipitated and was centrifuged at 4500 rpm for 3 minutes, at -4°C. Falcons were then let in the freezer at -20°C for 1 hour and centrifuge again. The supernatant was discarded and the peptide was dissolved in 15 mL of a 1 : 1 mixture ACN/H_2O, 0.1 % TFA. The solution was filtered to remove the resin beads. The peptide solution was lyophilized to obtain a white powder.

General CHO peptide derivates procedure. In order to obtain the aldehyde peptide derivatives, DIPEA (2 eq.), PyBOP (1.3 eq.) and aminoacetal (10 eq.) were added to a solution of peptide in DMF. The reaction mixture was stirred at room temperature for 2 hours. The addition of 0.5 mM $HCl_{(aq.)}$ led to the precipitation of the product. The supernatant was removed by filtration over a glass sintered filter. Then, the powder obtained was let it stir for 2 hours in the presence of an excess of TFA. The final aldehyde-containing compound was obtained after precipitation by the addition of H_2O.

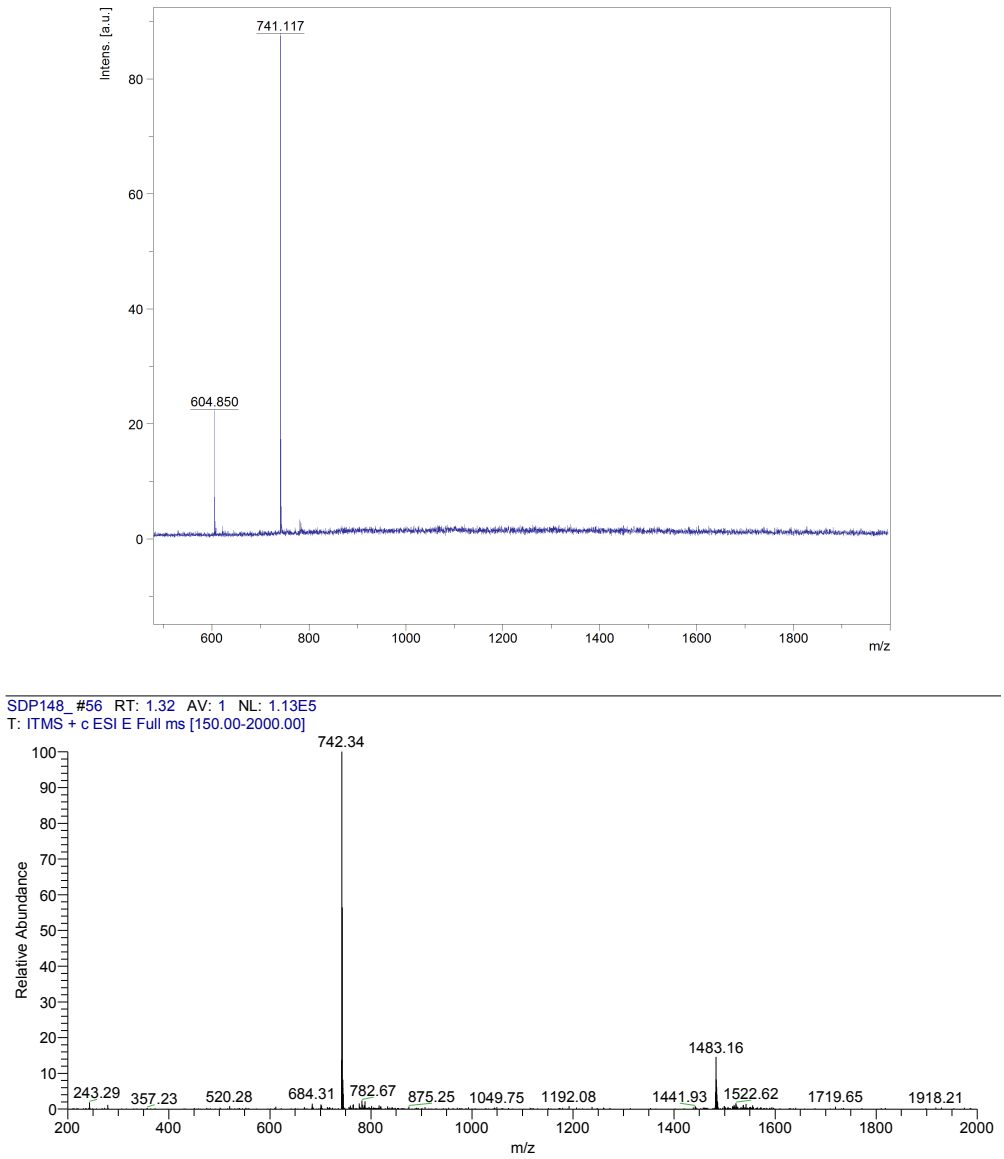

Figure 5.11. Characterization of ChinCHO. MALDI-TOF and HRMS (ESI^+) spectra of **ChinCHO**. $C_{43}H_{43}N_5O_7$ [M+2H$^+$]: calculated 1482.64; found 1483.16 [M+H$^+$]: calculated 741.32; found 742.34.

5.11. References

(1) Singh, N.; Formon, G. J. M.; De Piccoli, S.; Hermans, T. M. Devising Synthetic Reaction Cycles for Dissipative Nonequilibrium Self-Assembly. *Adv. Mater.* **2020**, *32* (20), 1906834. https://doi.org/10.1002/adma.201906834.

(2) Fan, B.; Men, Y.; van Rossum, S.; Li, G.; Eelkema, R. A Fuel-Driven Chemical Reaction Network Based on Conjugate Addition and Elimination Chemistry. *ChemSystemsChem* **2020**, 2 (1), e1900028. https://doi.org/10.26434/chemrxiv.9114659.v1.

(3) Grzybowski, B. A.; Huck, W. T. S. The Nanotechnology of Life-Inspired Systems. *Nat. Nanotechnol.* **2016**, *11* (7), 585–592. https://doi.org/10.1038/nnano.2016.116.

(4) Alberts, B. *Molecular Biology of the Cell*, Sixth edition.; Garland Science, Taylor and Francis Group: New York, NY, 2015.

(5) Brouhard, G. J.; Rice, L. M. Microtubule Dynamics: An Interplay of Biochemistry and Mechanics. *Nat. Rev. Mol. Cell Biol.* **2018**, *19* (7), 451–463. https://doi.org/10.1038/s41580-018-0009-y.

(6) De Vries, J. G.; Kellogg, R. M. Reduction of Aldehydes and Ketones by Sodium Dithionite. *J. Org. Chem.* **1980**, *45* (21), 4126–4129. https://doi.org/10.1021/jo01309a011.

(7) Chen, Q.; Lv, Y.; Zhang, D.; Zhang, G.; Liu, C.; Zhu, D. Cysteine and PH-Responsive Hydrogel Based on a Saccharide Derivative with an Aldehyde Group. *Langmuir* **2010**, *26* (5), 3165–3168. https://doi.org/10.1021/la903102z.

(8) Singh, N.; Lainer, B.; Formon, G. J. M.; De Piccoli, S.; Hermans, T. M. Re-Programming Hydrogel Properties Using a Fuel-Driven Reaction Cycle. *J. Am. Chem. Soc.* **2020**, *142* (9), 4083–4087. https://doi.org/10.1021/jacs.9b11503.

(9) De Greef, T. F. A.; Smulders, M. M. J.; Wolffs, M.; Schenning, A. P. H. J.; Sijbesma, R. P.; Meijer, E. W. Supramolecular Polymerization. *Chem. Rev.* **2009**, *109* (11), 5687–5754. https://doi.org/10.1021/cr900181u.

(10) Kulkarni, C.; Meijer, E. W.; Palmans, A. R. A. Cooperativity Scale: A Structure−Mechanism Correlation in the Self-Assembly of Benzene-1,3,5-Tricarboxamides. *Acc Chem Res* **2017**, *50*, 1928–1936.

(11) Meisl, G.; Kirkegaard, J. B.; Arosio, P.; Michaels, T. C. T.; Vendruscolo, M.; Dobson, C. M.; Linse, S.; Knowles, T. P. J. Molecular Mechanisms of Protein Aggregation from Global Fitting of Kinetic Models. *Nat. Protoc.* **2016**, *11* (2), 252–272. https://doi.org/10.1038/nprot.2016.010.

(12) Hirst, A. R. Biocatalytic Induction of Supramolecular Order. *Nat. Chem.* **2010**, *2*, 1089-1094.

(13) Boekhoven, J.; Poolman, J. M.; Maity, C.; Li, F.; van der Mee, L.; Minkenberg, C. B.; Mendes, E.; van Esch, J. H.; Eelkema, R. Catalytic Control over Supramolecular Gel Formation. *Nat. Chem.* **2013**, *5* (5), 433–437. https://doi.org/10.1038/nchem.1617.

(14) Conte, M. P.; Singh, N.; Sasselli, I. R.; Escuder, B.; Ulijn, R. V. Metastable Hydrogels from Aromatic Dipeptides. **2016**, *52*, 13889–13893.

(15) Sorrenti, A.; Leira-Iglesias, J.; Sato, A.; Hermans, T. M. Non-Equilibrium Steady States in Supramolecular Polymerization. *Nat. Commun.* **2017**, *8* (1), 15899. https://doi.org/10.1038/ncomms15899.

(16) Mukhopadhyay, R. D.; Choi, S.; Sen, S. K.; Hwang, I.; Kim, K. Transient Self-assembly Processes Operated by Gaseous Fuels under Out-of-Equilibrium Conditions. *Chem Asian J* **2020**, *15* (23), 4118-4123. https://doi.org/10.1002/asia.202001183.

(17) Knowles, T. P. J.; Waudby, C. A.; Devlin, G. L.; Cohen, S. I. A.; Aguzzi, A.; Vendruscolo, M.; Terentjev, E. M.; Welland, M. E.; Dobson, C. M. An Analytical Solution to the Kinetics of Breakable Filament Assembly. *Science* **2009**, *326* (5959), 1533–1537. https://doi.org/10.1126/science.1178250.

(18) Cohen, S. I. A.; Vendruscolo, M.; Dobson, C. M.; Knowles, T. P. J. Nucleated Polymerization with Secondary Pathways. II. Determination of Self-Consistent Solutions to Growth Processes Described by Non-Linear Master Equations. *J. Chem. Phys.* **2011**, *135* (6), 065106. https://doi.org/10.1063/1.3608917.

(19) Cohen, S. I. A.; Linse, S.; Luheshi, L. M.; Hellstrand, E.; White, D. A.; Rajah, L.; Otzen, D. E.; Vendruscolo, M.; Dobson, C. M.; Knowles, T. P. J. Proliferation of Amyloid- 42 Aggregates Occurs through a Secondary Nucleation Mechanism. *Proc. Natl. Acad. Sci.* **2013**, *110* (24), 9758–9763. https://doi.org/10.1073/pnas.1218402110.

(20) Orbach, R.; Adler-Abramovich, L.; Zigerson, S.; Mironi-Harpaz, I.; Seliktar, D.; Gazit, E. Self-Assembled Fmoc-Peptides as a Platform for the Formation of Nanostructures and Hydrogels. *Biomacromolecules* **2009**, *10* (9), 2646–2651. https://doi.org/10.1021/bm900584m.

(21) Wang, Y.; Zhang, Y.; Li, X.; Li, C.; Yang, Z.; Wang, L. A Peptide-Based Supramolecular Hydrogel for Controlled Delivery of Amine Drugs. *Chem. - Asian J.* **2018**, *13* (22), 3460–3463. https://doi.org/10.1002/asia.201800708.

5.12. Appendix

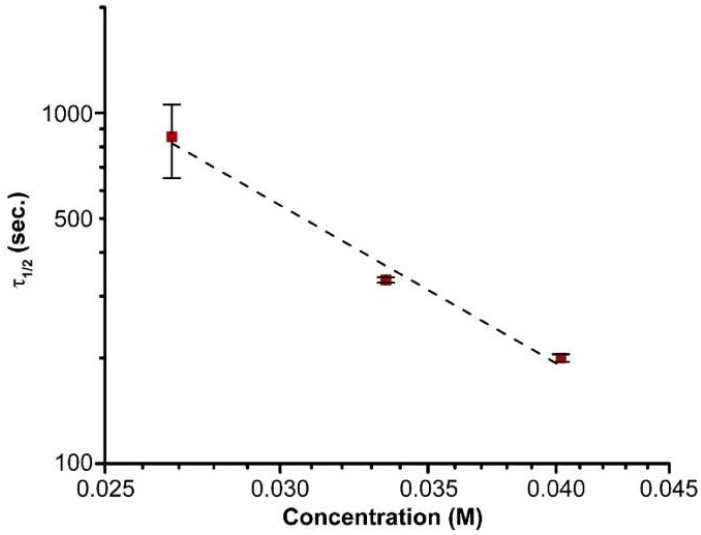

Figure 5.12. log-log plot of the half-times of gelation versus original concentration of $SachSO_3^-$ (before formaldehyde addition). Symbols represent the experimental data, solid line is a power law fit. The fit is as follows (with the errors to the fit between parentheses): $\tau_{1/2}$ = 1.77 x 10^{-3} [**SachCHO**] ^ –3.61. According to Meisl *et al.*[11] the exponent of this fit gives the parameter called scaling exponent, γ. This constant is indicative of the mechanism taking place during supramolecular polymerization. Such a scaling exponent, γ~3.5, means that there is a secondary nucleation phenomenon taking place with nucleus size of 6. Each point corresponds to the average over triplicate experiments, the error bars are the standard deviation. Reproduced from Ref.[8]

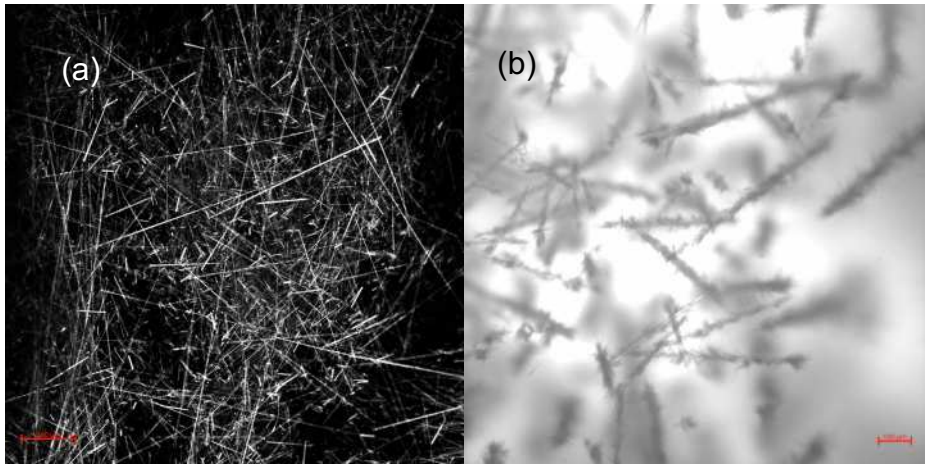

Figure 5.13. Confocal images. Confocal image proving the secondary nucleation phenomenon by formation of new fibers on top of already existing fibers giving brush-like morphology. Scale bar-100µm (a) Straight needle like fibers present in the thermally annealed gel, (b) brush like assemblies formed after a reaction cycle chemically fueled with dithionate (insufficient to dissolve all the primary fibers of the thermally annealed gel), HMTA and GdL. Insufficient DT concentration leaves some of the primary fibers from the thermally annealed gel intact which act as nuclei for the formation of new fibers on them once the **$SachSO_3^-$** is converted back to **SachCHO** giving brush like morphologies. Reproduced from Ref.[8]

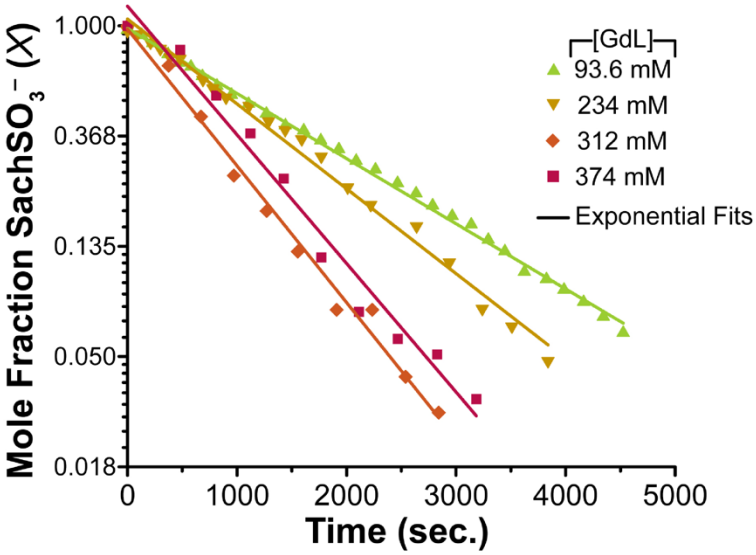

Figure 5.14. Semi-log plot of the mole fraction $SachSO_3^-$ as function of time (from quantitative NMR experiments). Apparent first order rates could be extracted. Symbols represent the experimental data, solid lines are the linear fits from the semi-ln plot. Results of the linear fits are as follows (with the errors to the fit between parentheses): [GdL] = 93.6 mM, ln[**$SachSO_3^-$**] = -5.91×10^{-4} ($\pm$ 0.05×10^{-4}) x t – 0.0225($\pm$ 0.0138); [GdL] = 234 mM, ln[**$SachSO_3^-$**] = -7.70×10^{-4} ($\pm$ 0.17×10^{-4}) x t – 0.0614($\pm$ 0.03); [GdL] = 312 mM, ln[$SachSO_3^-$]=-1.24×10^{-3} ($\pm$ 0.04×10^{-3}) x t– 0.0302 ($\pm$ 0.0770) ; [GdL] = 374 mM, ln[$SachSO_3^-$] = -1.17×10^{-3} ($\pm$ 0.06×10^{-3}) x t – 0.179 ($\pm$ 0.120). The fits were performed for the following time ranges: for [GdL] = 93.6 mM from 1175 s to 5700 s; for [GdL] = 234 mM from 960 s to 4800 s; for [GdL] = 312 mM from 485 s to 3325 s; for [GdL] = 374 mM from 390 s to 3575 s. Reproduced from Ref.[8]

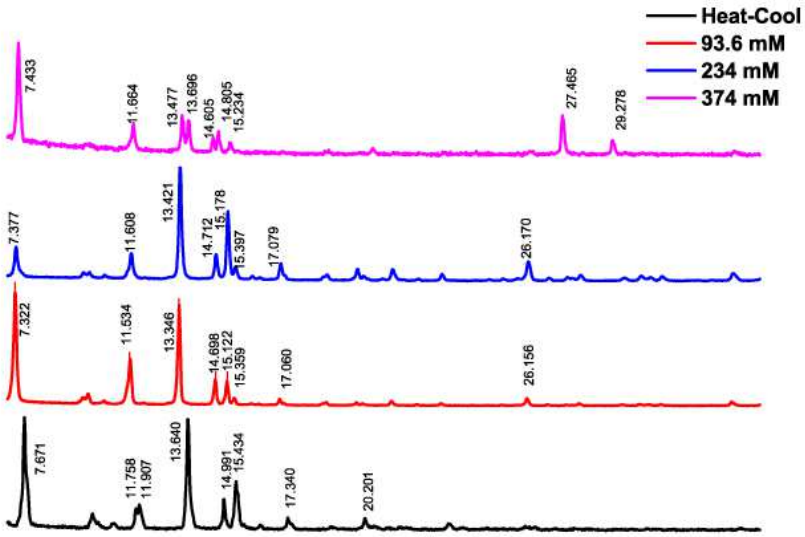

	Heat-Cool		93.6 mM		234 mM		374 mM	
Peak #	2θ	d (nm)	2θ	d (nm)	2θ	d (nm)	2θ	d (nm)
1	7.671	1.153	7.322	1.208	7.377	1.199	7.433	1.190
2	11.758	0.753	11.534	0.768	11.608	0.763	11.664	0.759
3	11.907	0.744	13.346	0.664	13.421	0.660	13.477	0.657
4	13.640	0.650	14.698	0.603	14.712	0.603	13.696	0.647
5	14.991	0.591	15.122	0.586	15.178	0.584	14.605	0.607
6	15.434	0.574	15.359	0.577	15.397	0.576	14.805	0.599
7	17.340	0.512	17.060	0.520	17.079	0.519	15.234	0.582
8	20.201	0.440	26.156	0.341	26.170	0.341	27.465	0.325
9							29.278	0.305

Figure 5.15. Powder X-Ray Diffraction (XRD) patterns. Comparison of XRD diffraction patterns obtained from xerogels (lyophilized). Reproduced from Ref.[8]

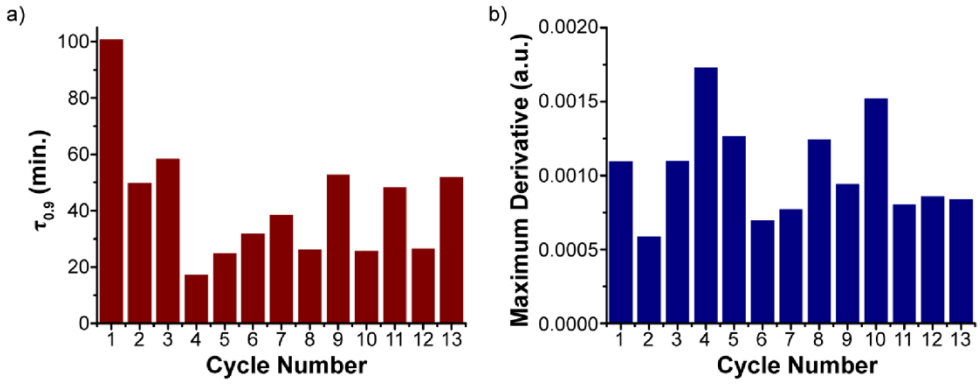

Figure 5.16. (a) Times of gelation for each syneresis recycling cycle, τ0.9 indicates the time where we reach 90% of maximum Optical Density at 500 nm. The gelation times remain similar for every cycle after the first. (b) Maximum derivative (or slope) of the gelation curves for each syneresis cycle. The gelation rate remains similar for every cycle. Reproduced from Ref.[8]

Chapter 6.

Conclusions and Outlook

In the past decade, researchers in the field of Systems Chemistry have developed increasingly complex bottom-up systems, in an attempt to better control the spatiotemporal behavior of 'life-like' materials.[1] Such materials, one day, should reproduce functions performed by the cellular processes network. As such, living systems use designed features to self-reproduce, communicate and move. These properties are: i) Molecular recognition, ii) Non-equilibrium conditions, iii) Compartmentalization and communication, iv) Feedback loops, and v) Reaction-diffusion.[1]

As we have repeatedly pointed out, microtubules are incredible interesting materials because they are both stiff and dynamic as a result of a so-called 'dynamic instability'.[2,3] Microtubules accomplish these features to allow for motility, mitosis and self-healing of cells.[4] The latter are processes that microtubules carry out under dissipative non-equilibrium conditions. Indeed, they need a continuous flow of fuel to be kept in such dissipative state.

The development of synthetic materials reproducing these processes is an important goal for the field of Systems Chemistry because it will open access to new material behaviors unlike those explored so far.[1,5,6] Nevertheless, the engineering of such complex networks is nontrivial because of issues mainly deriving from waste production, toxicity of fuels and/or solvents, lack of catalytic control, and products cross-inhibition.[7]

In this thesis, we have used different approaches to better control kinetics, morphologies and mechanical properties of materials. Living systems do not perform their work at the thermodynamic equilibrium, instead they need a flow of matter and energy to be constantly at a dissipative steady state. Herein, pseudo non-equilibrium steady states were achieved in an enzymatic network. In Chapter 2, the waste issue, which was previously hindering non-equilibrium conditions[8], was solved by coupling a third reaction. The latter recycles waste, and produces fuel *in situ*. In this manner, natural processes are the result of complex cascades where a fuel molecule is continuously

regenerated. Another way the cell solves waste and product cross-inhibition is by compartmentalizing the reactions. Increasingly, effort has been taken to reach the high level of organization as in eukaryotic cells in synthetic systems. For instance, interesting new possibilities are arising due to the use of vesicles[9,10], coacervates[11], etc.

Interestingly, the study of non-equilibrium conditions brought about the emergence of an oscillatory behavior from our enzymatic network. Temporal phenomena are well-established in living organisms like in circadian rhythms[12], or in signaling processes. For example, MAPK signaling leads to oscillations induced by multisite phosphorylation.[13] At first glance, this explanation fit our system since the substrate, **PDI**, has two phosphorylation sites. However, detailed experiments demonstrated that the enzymatic network is more complex than expected, since oscillations were also observed in a single phosphorylation-site substrate (see Chapter 2). The fact that we maintained pseudo NESS conditions was crucial to find such an interesting oscillatory behavior. Only when steady state conditions are maintained for long enough, can we start to find more complex emergent features.

As stated before, one of the properties used by natural systems to perform their functions is by using feedback loops. Chapter 3 shows a way to introduce feedback into an enzymatic network by the use of a competitive inhibitor. Positive and/or negative feedback are essential processes in living systems as they control metabolite production, signaling, and body temperature.[14] In the long-term, direction of synthesizing life-like materials, the ability of the entire hydrogel to respond to a local stimulus *via* a complex reactions network is promising to design more complex biomimetic functions. We hope that a supramolecular approach will contribute to mechanochemical feedback.

Next, in Chapter 4 we combined a peptide-based hydrogelator with our previously established enzymatic network (cf. Chapter 2). The general idea is to study non-equilibrium conditions in a material. As such, the resulting hydrogel properties in an out-of-equilibrium steady state differ from the ones observed at the thermodynamic equilibrium or in a transient self-assembly.

In the literature there are examples where scientists have obtained active gels consisted of bundles of microtubules and actin filaments.[15,16] Dogic and co-workers investigated the dynamics of a material of microtubules driven by kinesin molecular motors.[15] The fuel used is ATP and in the network is present a cycle of regeneration of fuel. Thus, they showed dynamic instabilities, typical of microtubule structures. These properties and functions were maintained as long as the system were driven out-of-equilibrium by the presence of chemical fuel. This work is inspiring as the goal is

the investigation of new behaviors when the material is pushed and maintained in a dissipative non-equilibrium steady state.[17]

Besides the enzymatic network, Chapter 5 presents a non-equilibrium chemically-fueled reaction cycle.[18] The system is based on a hydrogelator where the gel-sol-gel transition is catalyzed by an acid. The catalysis control allows the programming of the morphological and mechanical properties of the gel. Catalysis has been revealed to be an important tool to control molecular self-assembly as well as the properties of the material. Particular important is the design of a kinetic asymmetry in the system.[19,20] The latter is driving the cycle in a fuel-to-waste direction, allowing the investigation of supramolecular structures at dissipative states.

The work presented in this thesis provides a few solutions to currently open problems in Systems Chemistry and the progress that has been made so far to develop life-like materials. Each chapter represents a step forward to achieve active materials able to mimic nature and interact with it.

References

(1) Grzybowski, B. A.; Huck, W. T. S. The Nanotechnology of Life-Inspired Systems. *Nat. Nanotechnol.* **2016**, *11* (7), 585–592. https://doi.org/10.1038/nnano.2016.116.

(2) Brouhard, G. J.; Rice, L. M. Microtubule Dynamics: An Interplay of Biochemistry and Mechanics. *Nat. Rev. Mol. Cell Biol.* **2018**, *19* (7), 451–463. https://doi.org/10.1038/s41580-018-0009-y.

(3) Katrukha, K. A.; Guriya, G. T. Dynamic Instabilities in the Microtubule Cytoskeleton: A State Diagram. *Biophysics* **2006**, *51* (5), 781–788.

(4) Alberts, B. *Molecular Biology of the Cell*, Sixth edition.; Garland Science, Taylor and Francis Group: New York, NY, 2015.

(5) Ashkenasy, G.; Hermans, T. M.; Otto, S.; Taylor, A. F. Systems Chemistry. *Chem. Soc. Rev.* **2017**, *46* (9), 2543–2554. https://doi.org/10.1039/C7CS00117G.

(6) Mattia, E.; Otto, S. Supramolecular Systems Chemistry. *Nat. Nanotechnol.* **2015**, *10* (2), 111–119. https://doi.org/10.1038/nnano.2014.337.

(7) Singh, N.; Formon, G. J. M.; De Piccoli, S.; Hermans, T. M. Devising Synthetic Reaction Cycles for Dissipative Nonequilibrium Self-Assembly. *Adv. Mater.* **2020**, *32* (20), 1906834. https://doi.org/10.1002/adma.201906834.

(8) Sorrenti, A.; Leira-Iglesias, J.; Sato, A.; Hermans, T. M. Non-Equilibrium Steady States in Supramolecular Polymerization. *Nat. Commun.* **2017**, *8* (1), 15899. https://doi.org/10.1038/ncomms15899.

(9) Wanzke, C.; Jussupow, A.; Kohler, F.; Dietz, H.; Kaila, V. R. I.; Boekhoven, J. Dynamic Vesicles Formed By Dissipative Self-Assembly. *ChemSystemsChem* **2020**, *2* (1), e1900044. https://doi.org/10.1002/syst.201900044.

(10) Maiti, S.; Fortunati, I.; Ferrante, C.; Scrimin, P.; Prins, L. J. Dissipative Self-Assembly of Vesicular Nanoreactors. *Nat. Chem.* **2016**, *8* (7), 725–731. https://doi.org/10.1038/nchem.2511.

(11) Nakashima, K. K.; Baaij, J. F.; Spruijt, E. Reversible Generation of Coacervate Droplets in an Enzymatic Network. *Soft Matter* **2018**, *14* (3), 361–367. https://doi.org/10.1039/C7SM01897E.

(12) Novák, B.; Tyson, J. J. Design Principles of Biochemical Oscillators. *Nat. Rev. Mol. Cell Biol.* **2008**, *9* (12), 981–991. https://doi.org/10.1038/nrm2530.

(13) Suwanmajo, T.; Krishnan, J. Mixed Mechanisms of Multi-Site Phosphorylation. *J. R. Soc. Interface* **2015**, *12* (107), 20141405. https://doi.org/10.1098/rsif.2014.1405.

(14) Cannon, W. B. Organization for Physiological Homeostasis. *Physiol. Rev.* **1929**, *9* (3), 399–431. https://doi.org/10.1152/physrev.1929.9.3.399.

(15) Henkin, G.; DeCamp, S. J.; Chen, D. T. N.; Sanchez, T.; Dogic, Z. Tunable Dynamics of Microtubule-Based Active Isotropic Gels. *Philos. Trans. R. Soc. Math. Phys. Eng. Sci.* **2014**, *372* (2029), 20140142. https://doi.org/10.1098/rsta.2014.0142.

(16) Backouche, F.; Haviv, L.; Groswasser, D.; Bernheim-Groswasser, A. Active Gels: Dynamics of Patterning and Self-Organization. *Phys. Biol.* **2006**, *3* (4), 264–273. https://doi.org/10.1088/1478-3975/3/4/004.

(17) Dou, Y.; Dhatt-Gauthier, K.; Bishop, K. J. M. Thermodynamic Costs of Dynamic Function in Active Soft Matter. *Curr. Opin. Solid State Mater. Sci.* **2019**, *23* (1), 28–40. https://doi.org/10.1016/j.cossms.2018.11.002.

(18) Singh, N.; Lainer, B.; Formon, G. J. M.; De Piccoli, S.; Hermans, T. M. Re-Programming Hydrogel Properties Using a Fuel-Driven Reaction Cycle. *J. Am. Chem. Soc.* **2020**, *142* (9), 4083–4087. https://doi.org/10.1021/jacs.9b11503.

(19) Ragazzon, G.; Prins, L. J. Energy Consumption in Chemical Fuel-Driven Self-Assembly. *Nat. Nanotechnol.* **2018**, *13* (10), 882–889. https://doi.org/10.1038/s41565-018-0250-8.

(20) Astumian, R. D. Kinetic Asymmetry Allows Macromolecular Catalysts to Drive an Information Ratchet. *Nat. Commun.* **2019**, *10* (1), 3837. https://doi.org/10.1038/s41467-019-11402-7.

Serena DE PICCOLI

Chemically-fueled reaction networks to control supramolecular polymers

Résumé

Le but de cette thèse était de développer des systèmes complexes pour contrôler les polymères supramoléculaires. Pour cela, deux systèmes principaux ont été étudiés. D'une part, des états pseudo stables hors équilibre (pNESS) ont été atteints dans un réseau enzymatique. Le système était constamment maintenu hors équilibre en présence de carburant. De plus, un comportement oscillatoire est observé à la suite d'un réseau complexe de (dé)phosphorylation. Ensuite, une boucle de feedback a été mise en place afin de réguler les processus enzymatiques. Enfin, un matériau à base de peptides a été développé. Le réseau enzymatique a été inséré pour contrôler les propriétés mécaniques du gel à des états hors équilibre. D'autre part, un cycle de réaction hors équilibre a été exploité pour obtenir le contrôle temporel et mécanique d'un hydrogel contenant de l'aldéhyde. Ces résultats représentent un progrès vers l'étude des conditions non équilibrées dans la chimie des systèmes complexes et le développement de matériaux mimant la vie.

Mots-clés : polymères supramoléculaires, réseau enzymatique, états stables hors équilibre, oscillations, matériaux mimant la vie.

Résumé en anglais

The aim of this thesis was to develop complex reaction networks to control supramolecular polymers. For this, two main systems were investigated. On the one hand, pseudo non-equilibrium steady states (pNESS) were achieved in an enzymatic network. The system was continuously maintained at pNESS as fuel was present. In addition, an oscillatory behavior emerged as result of a complex net of (de)phosphorylation reactions involving substrates and enzymes. Then, a feedback loop was implemented in order to regulate the enzymatic processes. Last, a peptide-based material was developed. The enzymatic network was inserted to control the mechanical properties of the gel at non-equilibrium. On the other hand, an out-of-equilibrium reaction cycle was exploited to obtain temporal and mechanical control of an aldehyde-containing hydrogel. These results represent an advancement towards the study of non-equilibrium conditions in Systems Chemistry and the development of 'life-like' materials.

Keywords: supramolecular polymers, enzymatic network, non-equilibrium steady states, oscillations, life-like materials.